



UNIVERSITY OF

LIVERPOOL

**Role of cell-surface receptor LRP1 in the
development of lung fibrosis**

Thesis submitted in accordance with the requirements of the
University of Liverpool for the degree of Doctor in Philosophy

By

Maria Martina Meschis

November 2022

Acknowledgments

Firstly, I would like to express my gratitude to my primary supervisor Dr Kazuhiro Yamamoto for the important opportunity and great help to undertake this PhD project. My sincere thanks also go to my secondary supervisor Professor George Bou-Gharios for his contagious scientific enthusiasm and his door always being open. It has been a pleasure to work with both of you over the last 4 years. I want to also thank my third supervisor Dr Sonya Craig for her support in this PhD project. I would like to thank the Crossley Barnes Bequest studentship that funded my project. This project would not have been possible without the histology team who helped me during my second and third year of PhD. In particular, I would like to thank Gemma Charlesworth and Mandy Prior for their help and support. I want to thank also Prof Rob van't Hoff who guided me with his knowledge in my PhD. I would also like to express my gratitude to the incredible team at the BSU that helped me for my PhD project. I want to thank Rees and Steve for being amazing supporters and helping me during this time.

Doing a PhD in the middle of a global pandemic situation has been definitely challenging, and I am deeply grateful to all the people who constantly helped me to pursue until the end. I had the chance to meet incredible people in the Institute. These people have filled my life with love and have helped me along the way in and outside the lab. I would like to thank the Italian group: Niccolo', Maria, Giulio, Bernadette, Alice, Elena, Tommy, and Davide. Thank you Niccolo and Giulio for our daily philosophic conversations over a coffee. Thanks to Maria, Bernadette and the sweet Alice. Your affection warmed me up during this year. I felt like home with all of you guys. I don't know how I would have coped with this last stage of my PhD without friends like you. It was a breath of fresh air having you here for me.

I could never forget to thank Anders who listened to me trying to repeat me how good I am. I will always be eternally grateful to your huge support as lab mate and true friend.

I want to thank my family and friends back home who demonstrated me that distance is not a problem when there is love. To my dad and mum, who always pushed me to do better in this journey. You never doubted that I would make it. So, thank you for always being my biggest supporters. I want to thank my brother, Davide for being my lighthouse when I felt lost. To my grandma, her constant blessings through video calls meant a lot to me.

A big thank you to my best friends. To Zan, my person. You have always been my certainty, my rock. To Ale, my precious supporter and friend. To Emi, thank you for being the best motivator and partner in laughter.

Lastly, thank you to Micky mouse. You were there in my worst moments reminding me to breathe. Thank you for being my peace of mind.

I want to dedicate these last thanks to Elena, forever my beloved little sister. You enormously supported me during my first year. I will never forget when you used to send me interesting papers to read. I feel that there is also a little bit of you in this thesis. Even though you are no longer with us, you always find a way to tell me “I'm with you”. Thank you.

Abstract

Idiopathic pulmonary fibrosis (IPF) is a chronic lung disease leading to a reduction of lung function, respiratory failure, and death. Around 3 million people are affected by IPF with a median survival after diagnosis of approximately 3 years. Currently there are no effective treatments available partly due to the incomplete understanding of molecular mechanisms that drive fibrosis through excessive accumulation of collagens, the hallmark of IPF.

Low-density lipoprotein receptor-related protein 1 (LRP1) is a ubiquitously expressed cell-surface receptor that is involved in many physiological roles. LRP1 mediates clathrin-dependent endocytosis of various molecules (LRP1 ligands) and modulates cellular signalling pathways. The relevance of *LRP1* gene to lung function was discovered by a large genome-wide association study. However, little is known about its role in lung health and disease *in vitro*.

In this study, the role of LRP1 in lung tissue *in vivo* was investigated using conditional *Lrp1* knockout (KO) mice models. Since lung tissue consists of a variety of cell types, I first deleted *Lrp1* in the whole body. Global deletion of *Lrp1* gene in adulthood caused a rapid weight loss (>20%) and gastrointestinal abnormalities, suggesting a crucial role of LRP1 in the digestion system and difficulty to use this mouse model to investigate the respiratory system. Among various lung cells, fibroblasts play a major role in collagen deposition. I thus specifically deleted *Lrp1* in lung fibroblasts and challenged the mice with bleomycin to induce lung fibrosis. I discovered that excess collagen deposition was observed in control mice, whereas almost no collagen accumulation was detected in fibroblast-selective *Lrp1* knockout mice. I also found that the inhibition of LRP1-mediated endocytosis induces cell death of various types of cells *in vitro*, highlighting the cytotoxicity of prolonged presence of LRP1 ligands. Finally, I identified molecules regulated by LRP1 in lung tissue by proteomics analysis.

These findings shed light on novel *in vivo* roles of LRP1 that play a major role in the digestive system. Moreover, fibroblast LRP1 plays a crucial role in excess collagen deposition during the development of lung fibrosis. Identifying molecular mechanisms behind LRP1 function in collagen deposition may uncover new therapeutic approaches for lung fibrosis disease.

Table of Contents

CHAPTER 1 INTRODUCTION	1
Summary	1
1.1 Respiratory system and lungs	1
1.1.1 Biogenesis and development of lungs	2
1.1.2 Lung parenchyma.....	3
1.1.3 Alveolus	4
1.2 Lung cells	6
1.2.1 Lung epithelial cells.....	8
1.2.2 Alveolar cells	8
1.2.3 Pulmonary macrophages	9
1.2.4 Lung fibroblasts	10
1.3 Lung diseases	11
1.3.1 Idiopathic pulmonary fibrosis (IPF)	14
1.4 Bleomycin-induced lung fibrosis	18
1.5 Extracellular matrix (ECM)	19
1.5.1 Structure and function of ECM	20
1.5.2 Collagen.....	22
1.5.3 ECM-cell communication.....	23
1.5.4 ECM in lung diseases	25
1.6 Low-density lipoprotein receptor-related protein 1 (LRP1)	26
1.6.1 Endocytosis	29
1.6.2 LRP1-mediated endocytosis.....	30
1.6.3 LRP1 in cell signalling.....	31
1.6.4 Proteolytic shedding of LRP1 ectodomain.....	34
1.6.5 Genome-wide association studies (GWAS) - LRP1.....	35

1.7	General aims and objectives	35
1.8	Initial hypothesis	36
CHAPTER 2 MATERIALS AND METHODS		37
2.1	List of general reagents	37
2.2	List of antibodies	38
2.3	Transgenic mouse models	39
2.3.1	Declaration of Ethics	39
2.3.2	Mouse colony establishment and <i>Cre/loxP</i> -based system for LRP1 deletion <i>in vivo</i> 39	
2.3.3	Inducible knockout of LRP1 in fibroblasts (COL1A2-LRP1fl) and pan tissue (ROSA-LRP1fl).....	41
2.3.4	COL1A2-R26TmG fibroblast-specific Cre reporter mice	42
2.4	Mouse genotyping	42
2.4.1	Protein K based DNA extraction	42
2.4.2	Polymerase Chain Reaction (PCR)	43
2.4.3	Agarose Gel Electrophoresis	44
2.5	Animal Research Sample Size Calculation	44
2.6	Tamoxifen preparation	45
2.6.1	Tamoxifen - COL1A2-LRP1fl, ROSA-LRP1fl and COL1A2-R26tdTomato mice ..	45
2.7	Histological examination	46
2.7.1	Paraffin wax histology	46
2.7.2	Tissue Sectioning	46
2.7.3	Preparation for slides staining: dewax.....	46
2.7.4	Haematoxylin Eosin Stain (H&E)	47
2.7.5	Immunohistochemistry (IHC)	47
2.7.6	Histology imaging acquisition	48
2.8	Cell culture	49

2.8.1	Isolation and maintenance of murine primary lung fibroblasts	49
2.8.2	Maintenance of human primary lung cells	49
2.9	Statistical Analysis	49

CHAPTER 3 DETRIMENTAL EFFECT OF GLOBAL *LRP1* DELETION IN ADULT MICE **51**

Summary	51
3.1 Introduction	51
3.2 Aim and objectives	52
3.3 Chapter-specific methods	53
3.3.1 Transgenic mice and tamoxifen administration routes	53
3.3.2 Quantitative reverse transcriptase (qRT)-PCR	55
3.4 Results	56
3.4.1 Global LRP1 loss leads to rapid weight loss of adult mice.....	56
3.4.2 Assessment of LRP1 depletion in adult mice tissues	57
3.4.3 Evaluation of LRP1 deletion in tissue by IHC analysis	59
3.4.4 Global LRP1 loss results in gastrointestinal dysfunction and impairs digestive system	59
3.4.5 Histological abnormalities in the gastro-intestinal tract of tamoxifen-treated LRP1-KO mice.....	61
3.5 Discussion	73
3.5.1 Why does global deletion of LRP1 in adult mice cause rapid weight loss?	73
3.5.2 Does <i>LRP1</i> loss affect liver and kidneys?	74
3.5.3 Limitations.....	75
3.5.4 Conclusions and future plans	76

CHAPTER 4 MAJOR CONTRIBUTION OF FIBROBLAST LRP1 TO EXCESSIVE ACCUMULATION OF COLLAGEN IN LUNG FIBROSIS **77**

Summary	77
4.1 Introduction	78
4.2 Aims and objectives	79
4.3 Chapter-specific methods	81
4.3.1 Bleomycin Administration: oropharyngeal route (OA)	81
4.3.2 Bleomycin dose	82
4.3.3 Bleomycin administration in transgenic mice	83
4.3.4 <i>In vivo</i> micro computed tomography (μ Ct) live imaging of the lungs	84
4.3.5 Inflation and isolation of lungs	85
4.3.6 Histological examination	86
4.3.7 Masson-Goldner's Trichrome Stain	86
4.3.8 Picrosirius red staining	87
4.3.9 Collagen quantification on lung tissue	88
4.3.10 Immunohistochemistry	91
4.3.11 Cryosectioning	91
4.3.12 Inducible COL1A2-Cre/tdTomato mice	91
4.3.13 TGF- β 1 treatments on WT and LRP1 ^{-/-} MEF cells and western blotting	93
4.4 Results	94
4.4.1 Establishing the dose-response effects of bleomycin-induced lung fibrosis <i>in vivo</i> 94	
4.4.2 <i>In vivo</i> μ CT: a preliminary densitometric analysis of the lungs	97
4.4.3 Bleomycin-induced lung fibrosis is markedly reduced in COL1A2-selective LRP1 KO mice	99
4.4.4 Reduced deposition of collagen type I and III in COL1A2 LRP1 KO mice upon bleomycin injury	106
4.4.5 Detection of COL1A2-expressing cells in the bleomycin-induced lung fibrosis model using a COL1A2-R26tdTomato reporter mice	109
4.4.6 Spatial distribution of fibroblast cells in lung tissue by Immunohistochemistry ...	114
4.4.7 LRP1 involvement upon TGF- β 1 presence	118
4.5 Discussion	120

4.5.1	Why is LRP1 important for collagen deposition upon bleomycin injury?	121
4.5.2	Is LRP1 involved in the vascular integrity?	122
4.5.3	Are we sure that only fibroblast express COL1A2?	123
4.5.4	Molecular mechanisms of LRP1 in lung fibrosis development	126
4.5.5	Molecules with anti-fibrotic effects on bleomycin-induced lung fibrosis model ...	126
4.5.6	Limitations.....	127
4.5.7	Conclusions and future plans	127

CHAPTER 5 IDENTIFICATION OF LRP1 LIGANDS IN LUNG TISSUE 129

Summary	129
5.1 Introduction.....	129
5.2 General aims and objectives.....	130
5.3 Chapter-specific methods	130
5.3.1 Endocytosis Assays	130
5.3.2 Protein purification of sLRP1-2 and RAP.....	131
5.3.3 Silver staining.....	132
5.3.4 Mass-spectrometry analysis	133
5.3.5 Cell survival assay human primary lung cells	134
5.3.6 Cell survival assay of murine lung cells after isolation.....	135
5.3.7 siRNA-mediated gene silencing of LRP1.....	135
5.4 Results	136
5.4.1 LRP1 is highly expressed in human and murine primary lung cells	136
5.4.2 Rapid clearance of ADAMTS-5 by human and murine lung cells	137
5.4.3 Novel LRP1 ligands candidates in human and murine lung cells	139
5.4.4 Blockade of LRP1 effects on lung cells.....	142
5.4.5 siRNA-mediated knockdown of LRP1 in human lung cells	147
5.4.6 Cell survival assay of LRP1-expressing and LRP1 KO murine lung cells	148
5.4.7 Investigation of the dose-dependent response of sLRP1-2 on lung cells.....	150
5.4.8 Co-purified molecules can induce cell death and detachment	152

5.5	Discussion.....	155
5.5.1	Biological functions of LRP1 ligands detected in lung cells	155
5.5.2	Why the suppression of LRP1-mediated endocytosis induces cell death?	156
5.5.3	Limitations.....	157
5.5.4	Conclusions and future plans	157
 CHAPTER 6 GENERAL DISCUSSION		 159
6.1	Final thoughts.....	160
 CHAPTER 7 BIBLIOGRAPHY		 162

Abbreviations

A2M	alpha -2- macroglobulin
ADAM	A disintegrin and Metalloproteinase with Thrombospondin motif
AECs	alveolar epithelial cells
ARDS	Acute respiratory distress syndrome
AT1	Alveolar type I
AT2	Alveolar type II
BLM	bleomycin
BM	Basement membrane
CD146	cluster of differentiation 146
cDNA	Complementary cDNA
Col I-II	Collagen I-II
COPD	chronic obstructive pulmonary disease
CRs	cysteine-rich complement-like repeats
CT	computer tomography
C-terminus	Carboxyl-terminus
DAPI	4',6-diamidino-2-phenylindole
DG	Dystroglycan
DMEM	Dulbecco's Modified Eagle Medium
ECM	Extracellular matrix
EDTA	Ethylenediaminetetraacetic acid
EGF	Epidermal growth factor
EMT	Epithelial-mesenchymal transition
FLOX	Flanked by the LoxP sequences
FMT	Fibroblast to myofibroblast transition
GBM	Glomerular basement membrane
GFP	Green fluorescent protein
H&E	haematoxylin and eosin

ILD	interstitial lung disease
IN	intranasal
IP	intraperitoneal
IPF	idiopathic pulmonary fibrosis
IT	intratracheal
IV	intravenous
kDa	Kilodaltons
KO	knockout
LM	Laminin
LN	Laminin N-terminal
LoxP	locus of x-over, P1
LRP1	Low-density lipoprotein receptor-related protein 1
M1	macrophage type 1
M2	macrophage type 2
MEF	murine embryonic fibroblast
MMPs	matrix metalloproteinases
mRNA	Messenger RNA
MSCs	mesenchymal stem cells
NMDAR	N-methyl-D-aspartate receptor
NSCLC	non-small cell lung carcinomas
OA	osteoarthritis
OA	oropharyngeal aspiration
OCT	Optimal cutting temperature compound
OG	oral gavage
PAGE	Polyacrylamide gel electrophoresis
PBS	Phosphate buffered saline
PBS-T	Phosphate buffered saline- tween 20
PCR	Polymerase chain reaction

PDGFR	Platelet-derived growth factor receptors
PGs	Proteoglycans
PI3K	phosphoinositide 3-kinase
polyA	Polyadenylation signal
PSD95	adaptor protein postsynaptic density protein-95
R26	Rosa26
RAP	receptor associated protein
Rbt	Rabbit
SC	subcutaneous
SCLC	small-cell lung carcinomas
SD	Standard deviation
SDS	Sodium dodecyl sulfate
tdTomato	Tandem dimer tomato protein
TGF- β	Transforming growth factor beta
TIMP	Tissue inhibitor metalloproteinase protein
TNF	alpha - tumour necrosis factor alpha
tPA	Tissue plasminogen activator
TX	tamoxifen
TYR	tyrosine
WHO	World Health Organisation
WNT	Wingless-related integration site
WT	wild type

List of Tables

Table 1.1 Collagen subtypes cover different roles in airway	23
Table 2.1 Lysis buffer reagents.	43
Table 2.2 Primer pairs for genotyping	43
Table 2.3 Power calculation.	45
Table 2.4 Paraffin-embedding protocol.	46
Table 2.5 Dewaxing protocol.	47
Table 2.6 Haematoxylin Eosin Staining protocol.	47
Table 3.1 Tamoxifen administration by intraperitoneal (IP) injection (2mg/mL).	54
Table 3.2 Tamoxifen administration by oral gavage (OG).	55
Table 4.1 Initial optimisation Bleomycin dose.	83
Table 4.2 Masson's trichrome staining steps and reagents details.	87
Table 4.3 Panel of fibroblast marker tested in lung tissue.	91
Table 4.4 The table displays the experiment's plan at different time points.	92
Table 5.1 Novel LRP1 ligands candidates identified in Human primary lung fibroblast cells (MRC-5).	140
Table 5.2 Novel LRP1 ligands candidates identified in primary murine lung cells.	141
Table 5.3 List of LRP1 ligands in both human and murine lung cells	142
Table 5.4 co-purified molecules with sLRP1-2 from conditioned medium of HEK293 cells.	153
Table 5.5 List of molecules identified by mass-spectrometry analysis in R&D sample.	154

List of Figures

Figure 1.1 Respiratory system.	2
Figure 1.2 Cast of human bronchial tree.	4
Figure 1.3 Various cell types in distal airways and alveolus in human and murine lung tissue	7
Figure 1.4 Percentage of UK death from IPF.	14
Figure 1.5 Axial computed tomography (CT) image of a patient with IPF.	15
Figure 1.6 Schematic illustration of pathological mechanism of bleomycin-induced pulmonary fibrosis.	17
Figure 1.7 Schematic overview of ECM and its major components.	21
Figure 1.8 Pathological changes in ECM and lung disease.	26
Figure 1.9 Structure of LRP1 protein.	28
Figure 1.10 Outline of the currently proposed hypothesis of LRP1-mediated endocytosis. .	31
Figure 1.11 Schematic representation of LRP1 involved in cell signalling pathways.	33
Figure 2.1 Tamoxifen-dependent gene deletion system.	41
Figure 3.1 Flowchart of generating conditional knockout mice: LRP1 (flox/flox) / ROSA26 (cre/ERT2) (KO).	53
Figure 3.2 Global deletion of Lrp1 induces rapid weight loss in adult mice.	57
Figure 3.3 Reduced gene expression level of LRP1 in total KO mice.	58
Figure 3.4 Reduced protein expression level of LRP1 in total KO mice.	58
Figure 3.5 LRP1 deletion in lung and muscle tissues.	59
Figure 3.6 Abnormalities of gastro-intestinal tract observed during gross examination.	60
Figure 3.7 Enlarged intestine and stomach in LRP1 KO mice.	60

Figure 3.8 LRP1 is expressed in intestine and stomach.	61
Figure 3.9 LRP1 loss causes abnormalities in stomach and intestine.	63
Figure 3.10 Representative H&E of intestine of WT and LRP1 KO treated mice by IP injection.	64
Figure 3.11 Representative images of intestine of mice by OG administration.	65
Figure 3.12 H&E of stomach of WT and KO treated mice by IP injection.	66
Figure 3.13 Adipocytes in liver and inflammatory cells infiltration in kidneys of LRP1 KO mice.	67
Figure 3.14 Representative H&E stained autoscanned sections of stomach of WT mice.	68
Figure 3.15 Representative H&E stained autoscanned sections of stomach of LRP1 KO mice.	69
Figure 3.16 Representative H&E stained autoscanned sections of intestine of WT mice	70
Figure 3.17 Representative H&E stained autoscanned sections of intestine of LRP1 KO mice.	71
Figure 3.18 Summary of the key findings in LRP1 total KO mice in adult stage.	72
Figure 4.1 Initial hypothesis: LRP1 prevents collagen deposition and is protective in lung fibrosis	78
Figure 4.2 Illustration of OA administration route in mice.	82
Figure 4.3 Lung fibrosis development upon bleomycin injury.	83
Figure 4.4 Quantum GX μ-CT machine	85
Figure 4.5 First step of the collagen quantification analysis showing the selection of the area of interest.	88
Figure 4.6 Adjustment of the parameters threshold for the identification of the air spaces in the lung tissue.	89
Figure 4.7 Highlighting selection of air space in the lung	90

Figure 4.8 Air space selection removing the blood vessels.	90
Figure 4.9 Final tracking of the collagen in “pink” to be quantified.	90
Figure 4.10 Results obtained by quantification analysis.	91
Figure 4.11 Characterization of Mesenchymal-Fibroblast Cells Using the Col1a2 Promoter/Enhancer.	92
Figure 4.12 Lung fibrosis development observed by Masson’s trichrome staining.	95
Figure 4.13 Collagen fibers detected under polarized light by Picrosirius red staining.	96
Figure 4.14 Cell infiltration observed in pulmonary fibrosis by H&E staining.	96
Figure 4.15 Lung fibrosis observed by <i>in vivo</i> μCT.	98
Figure 4.16 Negligible collagen deposition is observed in LRP1 COL1A2 KO mice compared to WT.	100
Figure 4.17 Lung fibrosis in a WT mouse 4 weeks after OA bleomycin administration.	101
Figure 4.18 Lung fibrosis in to LRP1 COL1A2 KO 4 weeks after OA bleomycin administration.	102
Figure 4.19 Histological examination by Masson’s trichrome staining of WT mice after bleomycin administration.	103
Figure 4.20 Negligible collagen deposition and less cell infiltration in COL1A2 LRP1 KO mice after bleomycin administration by Masson’s trichrome staining.	104
Figure 4.21 Representative lung fibrosis in COL1A2 LRP1 KO.	105
Figure 4.22 Quantification analysis of ctrl lung tissue (no bleomycin), WT mice-treated and COL1A2 LRP1 KO mice.	105
Figure 4.23 Representative collagen fibres deposition by Picrosirius Red staining of WT fibrotic lung samples.	107
Figure 4.24 No excessive collagen deposition was detected by Picrosirius Red staining in COL1A2 fibrotic lung samples.	108

Figure 4.25 Lower collagen birefringence is detected in COL1A2 LRP1 KO mice upon bleomycin injury.	109
Figure 4.26 COL1A2-expressing cells and nuclei visualisation.	111
Figure 4.27 Lung tissue treated with bleomycin shows collagen-producing cells.	112
Figure 4.28 Visualisation of COL1A2-expressing cells.	113
Figure 4.29 Representative LRP1 staining of WT fibrotic lung samples.	114
Figure 4.30 Representative LRP1 staining of COL1A2 KO fibrotic lung sample.	115
Figure 4.31 Representative optimisation of fibroblast staining on lung samples.	116
Figure 4.32 Representative LRP1 and fibroblast staining comparison on fibrotic lung tissue.	117
Figure 4.33 Immunostaining for vimentin protein in normal and fibrotic lung tissue.	118
Figure 4.34 TGFβ1 treatments of MEFs cells are accompanied by expression and activation of SMAD2/3, FAK and p-FAK proteins.	119
Figure 4.35 Possible involvement of LRP1 in collagen internalization for its maturation and release to the ECM	122
Figure 4.36 Distinct Localisation of fibroblast subpopulation in respiratory tissue	125
Figure 4.37 LRP1 loss in COL1A2-expressing cells is preventing fibrosis development.	128
Figure 5.1 Schematic experiment's design for the endocytosis assay.	131
Figure 5.2 LRP1 and its soluble receptor domains.	132
Figure 5.3 Schematic diagram of the experiment's plan for the mass spectrometry analysis.	134
Figure 5.4 LRP1 is highly expressed in lung cells.	137

Figure 5.5 ADAMTS-5 is rapidly internalised by LRP1 in lung cells	138
Figure 5.6 Pie chart showing number of secreted, transmembrane, and intracellular proteins found by mass-spectrometry analysis in human and murine lung cells.	139
Figure 5.7 Human primary lung fibroblast cells (MRC-5) and Murine Lung	143
Figure 5.8 Representative with or without treatment at 24 and 48 hours.	144
Figure 5.9 Cell death in the presence of sLRP1-2 and RAP in the media of lung cells.	145
Figure 5.10 Reduction of cell survival upon treatment with sLRP1-2 and RAP.	146
Figure 5.11 Reduced cell number in siRNA-mediated knockdown of LRP1 in human primary lung fibroblast cells (MRC-5).	147
Figure 5.12 Reduced protein level of LRP1 in siRNA-mediated knockdown human lung fibroblasts cells.	148
Figure 5.13 Reduction in cell number in LRP1 KO cells compared to WT.	149
Figure 5.14 Reduction of cell number and survival in LRP1-mediated endocytosis blockade.	151
Figure 5.15 Inhibition of LRP1-mediated endocytosis by sLRP1-2 induces a cell death at 10nM concentration.	152
Figure 5.16 A2M co-purified in sLRP1-2 from commercial R&D is higher than sLRP1-2 home purified.	155

Chapter 1 Introduction

Summary

The introduction is to give an overview of respiratory system in healthy and pathological conditions and provide a rationale for the studies carried out in this research project. The first part of the chapter will describe the anatomical and biological functions of the lungs, including the role of extracellular matrix (ECM) remodelling and the lung fibroblast cells in the collagen deposition during lung fibrosis development. Next, I will highlight the role of the endocytic receptor LRP1 in regulation of signalling events and uptake of cellular molecules in a tissue-specific manner. Finally, undefined molecular mechanisms and the potential involvement of LRP1 in pulmonary fibrosis disease are discussed.

1.1 Respiratory system and lungs

The respiratory system is an elaborate biological structure composed of specialised organs, which are responsible for constant supply and exchange of oxygen between the air, blood, and cells. In humans, this complex system is anatomically divided into an upper and a lower network of different organs, which are essential for inspiration (inhalation) and expiration (exhalation) process. The lungs are the major organs of the respiratory system and are situated in the thoracic cavity and surrounded by the sternum and ribcage on the anterior side and the backbones on the posterior side. In 1942, the Danish anatomist A. Kroug described the lungs as “the most evolutionary unique organs” where gas exchange takes place. The human lungs consist of the right lung and left lung, which are divided into three and two lobes, respectively (George, et al., 2014). The lungs consist of a well-defined anatomical structure to facilitate two vital functions: a balance exchange of oxygen entering and carbon dioxide leaving the body, and a host defence mechanism against foreign particles and pathogens during respiration (Figure 1.1) (Nomellini &

Chen, 2012). The capacity of a lung ranges from 2.5-6L and 50% of the overall weight of a single lung cell can be contributed to oxygen/CO₂. The efficiency of the gas exchange process is determined by the presence of the “alveolar parenchyma”, where air and blood are conducted via the diffusion of the airway tree. The human lungs consist of 80% air and about 10% blood. The remaining part (100g) is made of “physical” tissue (Effros, 2006).

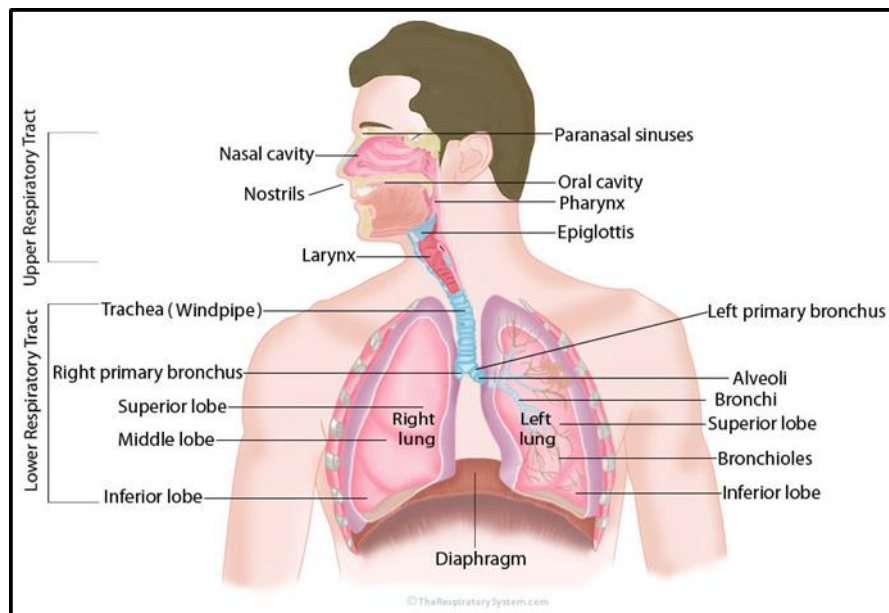


Figure 1.1 Respiratory system. Respiratory system consists of the airways, the lungs, and the respiratory muscles that mediate the movement of air into and out of the body (Public domain, <https://quizlet.com/372457089/respiratory-system-diagram/>).

1.1.1 Biogenesis and development of lungs

Lung morphogenesis occurs in a sequential process and can be separated into defined stages. The process begins during the embryonic stage where evaginations appear from the primitive gut, which invade the surrounding mesenchyme and continues up to branching of airways. The lung bud is made predominantly of epithelium and mesenchyme, which initiate a series of dichotomous separations up to the conducting airways and a total of five primordial lung lobes in human, two on left and three on right. During this stage, the major airways are conveyed by the tight pulmonary vasculature. A

progressive and complete division of the airways follows this stage into smaller branches, a complete formation of the diaphragm and a development of pulmonary “acini” (Hsia, et al., 2016). Postnatal lung development occurs into additional stages (Burri, 2006). Interestingly, alveolarization has been shown to occur in the latest stage of life, suggesting that lung development goes on until the adult age (Yammine, et al., 2015). For instance, branching of the respiratory organs endures into the pseudoglandular stage of the development. Microvascular maturation, also known as postnatal lung development phase, occurs through 3 years of age. In fact, during the first 2 years of age to adulthood, the lung volume proportionately expands to the body-weight (Fraga & Guttentag, 2012).

The amount of information to which all these programmed mechanisms take place during the prenatal and postnatal lung development, is still limited for pulmonary researchers.

1.1.2 Lung parenchyma

As the airway tree grows, the pulmonary arteries and veins form an integrated system of three interdigitating trees with their stems in the hilar region and their terminal branches converging in the gas-exchanging distal region (Hsia, et al., 2016) (Figure 1.2). The lung parenchyma is where the gas exchange occurs and consists of alveoli, alveolar ducts, bronchioles, capillaries, and other respiratory interstitial tissues.

The most important functional unit of the lung parenchyma is the alveolus. Each alveolus directly expands to an alveolar duct and into a respiratory bronchiole. These structures are mainly composed of a connective tissue, called “parenchymal interstitium” consisting of ECM proteins such as collagen, elastin, proteoglycans and reticulin. The entire lung parenchyma covers a large number of alveoli, where the majority of gas exchange takes place. The alveoli experience mechanical stress during inspiration and expiration by the expansion tensions generated from surrounding tissues and

adherent cells (Bates & Suki, 2008). Thus, the ECM proteins determine the mechanical properties, lung function and biology. Therefore, the biomechanical forces in the lung are critical determinants for the activation of cell signalling pathways in different stage of the lung development such as branching, surfactant production by alveolar epithelial cells (Wirtz & Dobbs, 2000), contraction of airway smooth muscle cells (Fredberg, et al., 1997) and ECM remodelling (Burgstaller, et al., 2017)

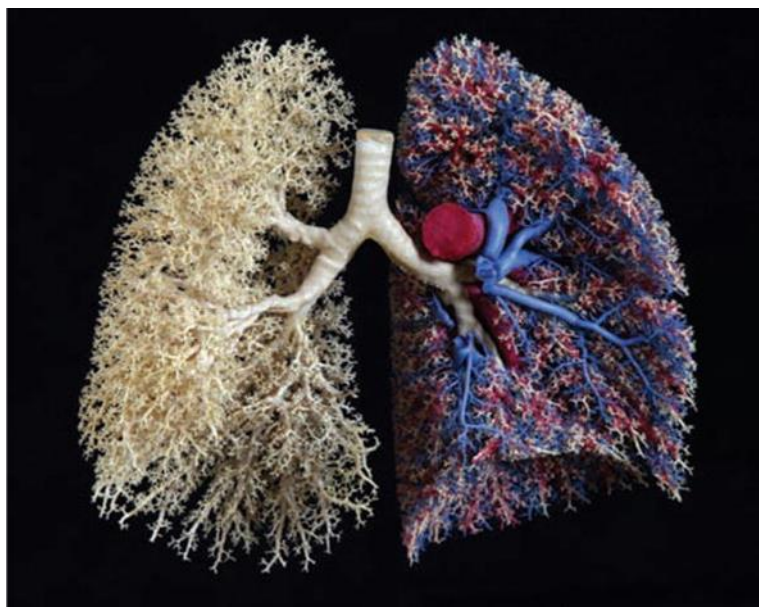


Figure 1.2 Cast of human bronchial tree. Airways (yellow), pulmonary arteries (red), and pulmonary veins (blue) (Hsia, et al., 2016).

1.1.3 Alveolus

The alveoli are the primary and smallest lung structures where gas-exchange between lungs and bloodstream taken place and account for approximately 90% of total pulmonary volume. Each alveolus is balloon-shaped with a very thin wall where the remaining non-parenchyma section consists of conducting airways and vessels. The most distal part of the alveoli is connected to the airways. Alveoli can be considered as largely abundant respiratory sacs, which are sited at the side-line of bronchioles and are surrounded by a vast network of pulmonary capillaries (Khan et al., 2021). The

surface of the inner respiratory membrane in each alveolus is covered with a fluid surfactant produced by alveolar cells localised on the alveolar walls. Alveoli are organised in clusters throughout the lungs and localised at the ends of the branches of the respiratory tract. The inter-alveolar septum facilitates the gas exchange in the lung and is essential for separating the alveolar space (air) from the capillary space (blood) (Powers & Dhamoon, 2021).

In the alveoli two types of cells can be distinguished: alveolar type I (AT1), responsible for the oxygen and CO₂ exchange, and type II (AT2), involved in the production of surfactant and in the repair process by differentiating into type I cells. The ratio of type I to type II is approximately 1:2 (Crapo, et al., 1982). The alveoli also consist of immune cells such as alveolar and interstitial macrophage cells. The alveolar macrophages represent the first line of defence in the air spaces from infectious and toxic particles. Clusters of alveoli are organised into larger functional units called acini and human lungs consist of approximately 30,000 acini. An acinus is considered the beginning of the bronchiole structure (Basil, et al., 2020). Under normal conditions, the entire lung parenchyma is continuously subjected to volume changes of the alveolar spaces for the respiratory cycle. For instance, the inter-alveolar septum covers a secondary functional role to maintain stability and flexibility during the movements of the thorax for the respiration process. Physical or chemical damage of the alveolus frequently occurs throughout life and the wound repair process is tightly regulated by cellular mechanisms orchestrated for the maintenance of lung tissue homeostasis. However, when these repair mechanisms fail to reconstruct the alveolar structure, detrimental consequences occur in the lung parenchyma (Basil, et al., 2020). The disruption of the alveoli structures, therefore, is recognised as one of the earliest events that leads to the development of many lung diseases such as lung cancer, pulmonary fibrosis (Maher, et al., 2008; Chambers, et al., 2008; Datta, et al., 2011), chronic obstructive pulmonary disease (COPD) (Chilosi, et

al., 2012), emphysema (Rennard & Vestbo, 2006) and asthma (Shifren, et al., 2012).

1.2 Lung cells

In 2020, a study by Travaglini et al., used droplet and plate-based single cell RNA sequencing of 75,000 human cells to identify in total 58 transcriptionally exclusive cell populations in human lungs. Among these 58 cells types 15 epithelial, 9 endothelial, 9 stromal and 25 immune populations have been identified (Travaglini, et al., 2020). Resident cells of the respiratory tract composition are different between large airways and alveoli. Large airways consist of many cells such as ciliated, basal, secretory, neuroendocrine, and goblet. The self-renewal and differentiation of lung epithelial cells are modulated by other neighbouring cells, such as epithelial cells, mesenchymal cells, airway smooth muscle, neurons and neuroendocrine cells, endothelium, and various leukocyte populations (Barkauskas, et al., 2013; Cao, et al., 2017; Lechner, et al., 2017; Lee, et al., 2017; Rafii, et al., 2015; Zepp, et al., 2017). Pulmonary alveolar epithelium is composed of AT1 and AT2, which are in close contact with alveolar macrophages and fibroblasts (Barron, et al., 2016; Basil, et al., 2020). Studies of comparative biology of human lung tissue has found cellular and structural differences that make it unique from its murine counterparts. The mouse consists of 13 generations of airways, compared to an average of 23 generations in the more branched human lung. The terminal end of the airways in human lung contains respiratory bronchioles interspersed with alveoli while the murine conducting airways terminate into alveolar sacs. Overall, these structural differences reflect the complexity of the respiratory system in large mammals. While there are differences across the anatomical structure, the fundamental cellular composition of the alveolus appears to be relatively similar. For example, AT2 cells population has been identified in both mouse and human lungs and display a similar response to injuries (Beers & Moodley, 2017) (Figure 1.3).

Furthermore, non-functional epithelial cells have been shown in both murine and human lung in a maladaptive repair respiratory response (Vaughan et al., 2015). Recently, ionocyte cells have been identified as one of the newest members of lung epithelial cell, in both mouse and human pulmonary tissue, but the functional role is still unclear (Montoro et al., 2018).

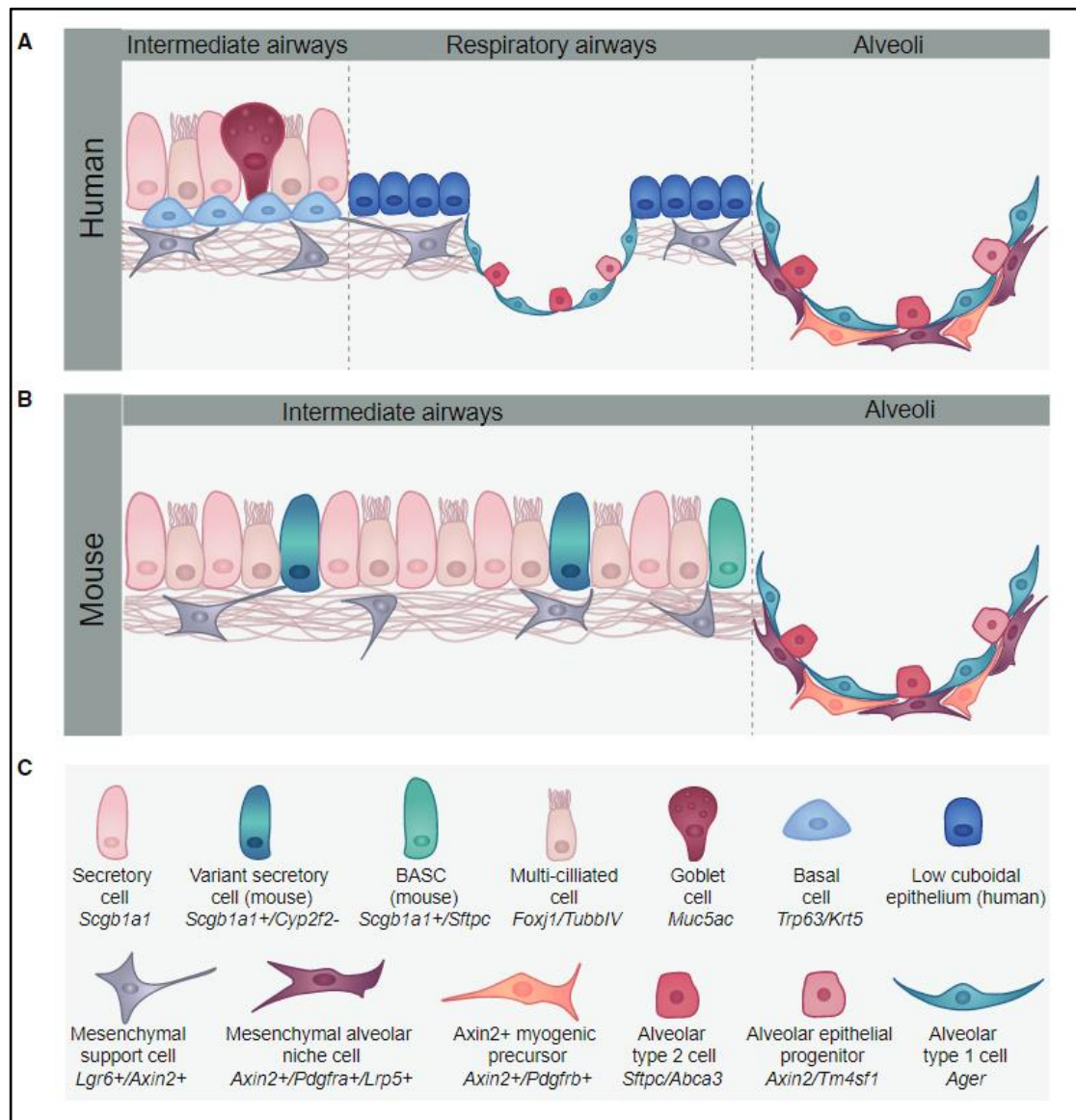


Figure 1.3 Various cell types in distal airways and alveolus in human and murine lung tissue. (A) Intermediate human airways contain a basal cell layer and significant numbers of goblet cells whereas the mouse intermediate airways (B) lack extensive numbers of goblet cells and also lack basal cells. (C) Table of cell types found in human and/or mouse airways (Basil, et al., 2020).

1.2.1 Lung epithelial cells

The respiratory epithelium consists of cells that function to moisten the outer surface of the lungs and provide a shield against toxins, pathogens, and tissue injury. In this context, epithelial cells are also involved in mucociliary clearance and resistance of mechanical tensions in the alveoli (Whitsett & Alenghat, 2015). The bronchial epithelium plays a key role in the immune response in the whole airway surface, by the presence of inflammatory mediators such as cytokines, chemokines, growth factors, and arachidonic acid metabolites (Van Der Weijden, et al., 1998). The respiratory epithelium is a pseudostratified layer consisting of three cell types. Firstly, goblet cells, which contribute to the secretion of mucus and maintain the epithelial moisture. Secondly, basal cells, which can differentiate into other cells to activate the repair process and restore healthy tissue. Finally, cilium cells are responsible for the movement of microbes and debris out of the respiratory tract (Kia'i & Bajaj, 2022).

1.2.2 Alveolar cells

AT1 cells cover more than 95% of alveolar surface and are important for facilitating the passive gas diffusion between alveoli and capillaries. AT1 cells create a pseudobarrier, which facilitates gas exchange (Crapo, et al., 1982; Williams, et al., 2003). Electron microscopy have been previously used to show that AT1 cells have a thin diameter less than $<0.1 \mu\text{m}$ with a complex morphology in the formation of numerous alveoli (Weibel, 2015; Stone & Marietta, 1994). During alveologenesis, AT1 cells expand their surface area to accommodate postnatal lung growth retaining an important cellular plasticity property (Yang, et al., 2016). AT2 cells comprise a small part of the total alveoli surface (around 5%) in comparison to AT1 (95%) and they constitute around 60% of alveolar epithelial cells and 15% of all lung cells. AT2 are cuboidal cells involved in the production of lung surfactants, a mixture of phospholipids and

surfactant proteins, to maintain mechanical tension in the alveoli structure (Fehrenbach, 2001; Beers & Moodley, 2017) and the level of surface tension in the alveoli structures, which prevents tissue collapse (Zhao, et al., 2010). In the normal lung, AT2 cells are considered as stem cells for the ability to self-renew and differentiate into AT1 cells at a very low turnover rate (Barkauskas, et al., 2013; Desai, et al., 2014; Wu & Song, 2020). Additionally, AT2 cells provide a fluid layer on the alveolar surface by sodium transporters that regulate apical to basolateral fluid transport (Eaton, et al., 2004; Selman & Pardo, 2006; Shannon & Hyatt, 2004).

1.2.3 Pulmonary macrophages

Pulmonary macrophages are a heterogeneous cell population with different functions, such as phagocytic, antigen processing, immune surveillance, and resolution of inflammation (Gordon & Read, 2002).

In the lung tissue, there are two different types of macrophages: alveolar and interstitial. Therefore, lung macrophages throughout the respiratory system are key effector cells involved in the first line of defence against pathogens by modulating the immune response (Busse & Lemanske, 2001). The precursor cells of lung macrophages originate from haemopoietic organs and are recruited to the lung via blood or lymph as monocytes. As monocytes enter to the lung, they shift their phenotype to macrophage, strictly depending on the site and state of activation. The process of differentiation from monocytes to macrophages is regulated by the release of cytokines from respiratory cells (Hussell & Bell, 2014).

Alveolar macrophages can migrate from bronchioles to the pulmonary interstitium, where they are in close contact with the type I and II epithelial cells. Respiratory macrophages modulate the interaction with other cells of the immune system to orchestrate a response that maintains immunologic and tissue homeostasis in the body (Lambrecht, 2006). Two distinct phenotypes of alveolar macrophages have been found: macrophages type 1 (M1) are

activated via classical pathways and macrophages type 2 (M2) are macrophages activated via alternative pathways. The M1 phenotype is involved in the release of inflammatory cytokines and the M2 phenotype is involved also in phagocytosis and collagen deposition (Viola, et al., 2019; Xue, et al., 2014).

1.2.4 Lung fibroblasts

Fibroblasts are the most abundant cell type in connective tissues throughout the whole body and constitute the bulk of the widely spaced ECM (Wight & Potter-Perigo, 2011). Fibroblasts generate an interconnecting network of ECM proteins such as collagen, elastin, laminins, fibronectin (FN), and other glycoproteins (Kalluri, 2016). Fibroblasts provide additional biological functions for the cells beyond the production of a robust repertoire of ECM proteins. In fact, they are involved in wound healing, inflammation, angiogenesis, cancer progression and fibrosis development (Kendall & Feghali-Bostwick, 2014). Lung fibroblasts are crucial for the maintenance of alveolar structure integrity, response of damage, recruiting inflammatory cells, airway remodelling and disease (Kendall & Feghali-Bostwick, 2014). They consist of a large, flat, elongated shape with an extending protrusion from the ends of the cell. Fibroblasts are plastic-adherent mesenchymal cells (MSCs) derived from non-differentiated embryonic mesoderm tissue (Aronson, 1983; Barry & Murphy, 2004; Javazon, et al., 2004). Furthermore, lung fibroblast cells are the major source of ECM proteins in the respiratory system, such as collagen I and III which are important to maintain a stable framework in the tissue and to control the ECM degradation through the production of matrix metalloproteinases (MMPs) (Greenlee, et al., 2007). As part of the self-repair mechanism upon injury, fibroblasts interact with ECM proteins through chemical signals from inflammatory mediators and promote their proliferation and cellular differentiation to myofibroblasts cells (Royce, et al., 2012). Lung fibroblasts constitute 10%-20% of all lung cells, which has complicated their

study and understanding of their specific functions in pulmonary fibrosis (Barron, et al., 2016). Normal resident lung fibroblasts can be identified by their expression of many markers such as, platelet-derived growth factor receptor (PDGFR) α , cluster of differentiation 146 (CD146), collagen type I, vimentin, and desmin (Marriott, et al., 2014). Fibroblasts cells show a different phenotype across sites of the same organ as shown in skin (Jelaska & Korn, 2000) and lung (Pechkovsky, et al., 2010). Cell signalling modulators such Wnt (Liu, et al., 2013), Neurogenic locus notch homolog protein (Notch) (Kavian, et al., 2012), and Sonic hedgehog ligands (Stewart, et al., 2003; Petrova & Joyner, 2014) are involved in the myofibroblasts differentiation from precursor fibroblast cells *in vivo* and *in vitro* after cytokine stimulation. A variety of cells have been identified as myofibroblasts precursors such as epithelial cells, smooth muscle cells, perivascular adventitial cells, pericytes and fibrocytes (Kendall & Feghali-Bostwick, 2014). A study by Rock et al. showed focal presence of fibroblasts from stromal cells using a murine model of a recombinant td-Tomato and f-GFP tags (Rock & Hogan, 2011). Another source of myofibroblasts during fibrosis has been hypothesised to originate from endothelial cells (Piera-Velazquez, et al., 2011). All these biological processes of fibroblasts including wound healing, inflammation, fibrosis, angiogenesis, play critical roles in cancer by regulating the tumour-environment, tumour size, and tumour metastasis (Mueller & Fusenig, 2004). Since fibroblasts are the main cells involved in the fibrosis development, they are the most studied candidates in the therapy and treatment of pulmonary fibrosis diseases.

1.3 Lung diseases

Lung diseases are the most common medical conditions and highest causes of death worldwide (Soriano, et al., 2020). As a result of their frequency, respiratory diseases inflict an enormous worldwide health burden. Five of the 30 total recognised respiratory diseases are some of the most common causes of death: asthma, chronic obstructive pulmonary disease (COPD), pulmonary

fibrosis, acute respiratory distress syndrome (ARDS) and lung cancer (Figure 1.4) (Wang, et al., 2016).

An estimated 65 million people are affected by COPD making it the third leading cause of death worldwide (Quaderi & Hurst, 2018). Hallmarks of COPD are irreversible lung damage followed by a consistent impairment of the respiratory capacity due to a restriction of the airflow through the bronchi and lungs (Devine, 2008). COPD patients are typically characterised by chronic obstructive bronchitis, pulmonary emphysema, and mucus plugging (Barnes, 2000). It has been reported a genetic risk due to alpha-1-antitrypsin enzyme deficiency in less than 1% of patients (around 1 in 100) affected by COPD (Brode, et al., 2012). Cigarette smoke and other irritant substances are able to activate alveolar macrophage and epithelial lung cells to stimulate neutrophils to release proteases such as cathepsins, elastase and other MMPs resulting in an excessive mucus hypersecretion and emphysema (Keating, 2012; Stockley, 1999). Activated lung epithelial cells further activate cytotoxic T cells involved in the inflammatory cascade (Liu, et al., 2011). Previous findings have highlighted the presence of apoptosis in alveolar and bronchial epithelial cells in the lung parenchyma of patients suffering from COPD (Henson, et al., 2006). Although there is improved research behind the molecular pathophysiology of the COPD, little is known about the cellular mechanisms and there have been few advances in the therapy treatments, which target underlying mechanism of the disease.

Globally, ARDS affects more than 3 million people a year and is known to impact a wide range of ages (Bellani, et al., 2016; Fan, et al., 2020). ARDS may resolve completely after an initial acute phase or progress to fibroproliferative stage with the development of pathologic tissue in a chronic inflammation context. ARDS is characterised by a diffuse inflammation of lung tissue with an increased permeability to liquid across the lung endothelium, which causes oedema in the lung interstitium. The global COVID-19 pandemic has seen a consistent number of patients with ARDS. Observational studies

suggest a similarity in the molecular mechanisms of ARDS between patients with COVID-19 and patients with ARDS from other causes (Fan, et al., 2020). An early recognition of ARDS and an ongoing effort to better understand the mechanisms of lung injury could improve clinical outcomes and design new therapeutic treatments.

Lung cancer is the leading cause of cancer-related deaths worldwide with a relatively high rate of mortality compared with other types of cancer. More than 1.76 million deaths globally have been attributed to lung cancer and around 47,000 people are diagnosed every year in the UK alone (WHO, 2020) (Thai, et al., 2021). It is commonly classified in two groups: non-small cell lung carcinomas (NSCLC) or small-cell lung carcinomas (SCLC) (Travis, et al., 2015). In 2019, an estimated 80% of all deaths from lung, tracheal and bronchus cancer were linked to risk factor exposure. Smoking was identified as the leading risk factor of lung cancer contributing to 64% of total deaths for both sexes (Ebrahimi, et al., 2021).

Many other lung diseases, such as smoking-associated and interstitial lung diseases (ILDs) can involve a combination of all these conditions. ILDs is a group of lung diseases, which consist of a mixture of fibrosis and inflammation of the lung parenchyma. Among the ILDs, the idiopathic pulmonary fibrosis (IPF) is the most common with an elusive aetiology (Kalchiem-Dekel, et al., 2018).

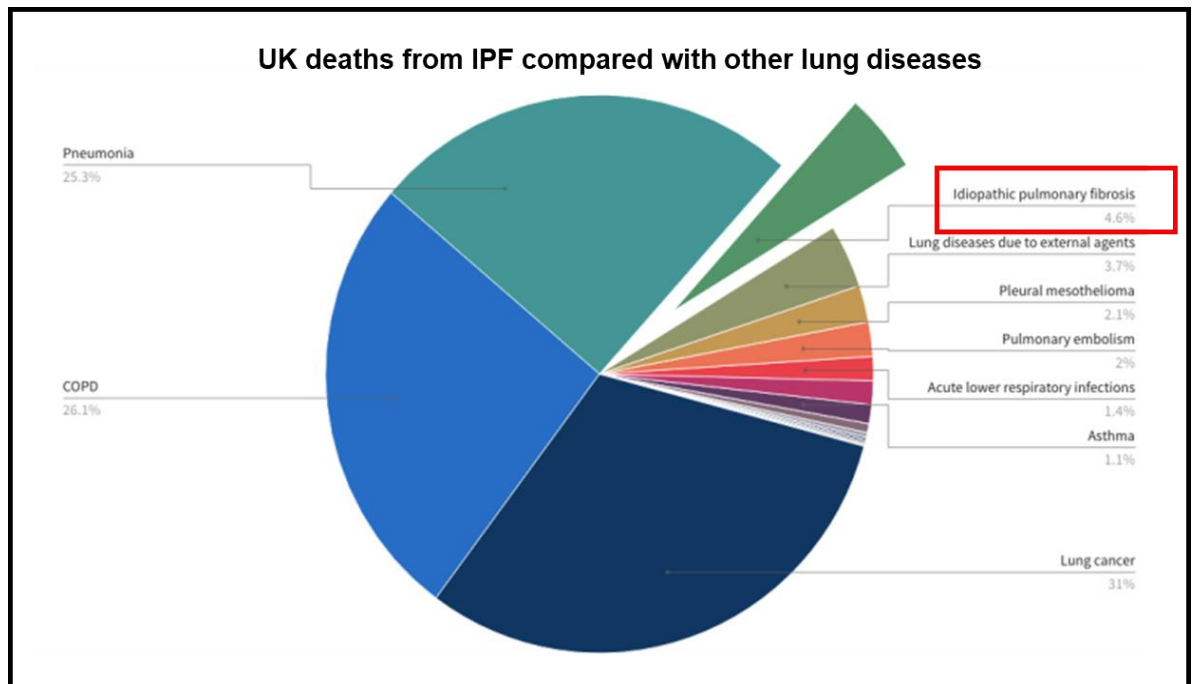


Figure 1.4 Percentage of UK death from IPF. Figure revised from British Lung Foundation (BLF): <http://www.statistics.blf.org.uk/pulmonary-fibrosis>.

1.3.1 Idiopathic pulmonary fibrosis (IPF)

IPF is a pathological condition in which the lungs are damaged by the formation of scar tissue over time and a slower oxygen flow through the respiratory tracts to the blood. It is frequently associated to the end-result and effect of other ILDs. IPF is one of the most common ILDs, and a prototype of chronic, progressive and fibrotic lung disease (Richeldi, et al., 2017). Epidemiology studies observed a rising number of patients affected by pulmonary fibrosis, which affects 3 million people worldwide (Nalysnyk, et al., 2012). The most common clinical features in the pathophysiology of IPF include ages between 50-70, dry cough, insidious onset of shortness of breath on exertion, chronic hypoxemia with a consequent abnormal pulmonary function test result (Flaherty, et al., 2019; Maher, et al., 2020). The prognosis of IPF is poor with a median survival of 3 years after diagnosis, and currently nintedanib and pirfenidone were approved as treatments in slowing the

progression of IPF (Walters & Kleeberger, 2008) (Wollin, et al., 2014). Although IPF has been considered rare within the context of other the lung diseases, the incidence of IPF has consistently risen over the last century. In fact, it has been registered in 5 million people worldwide per year (Maher, et al., 2021) (Figure 1.5).

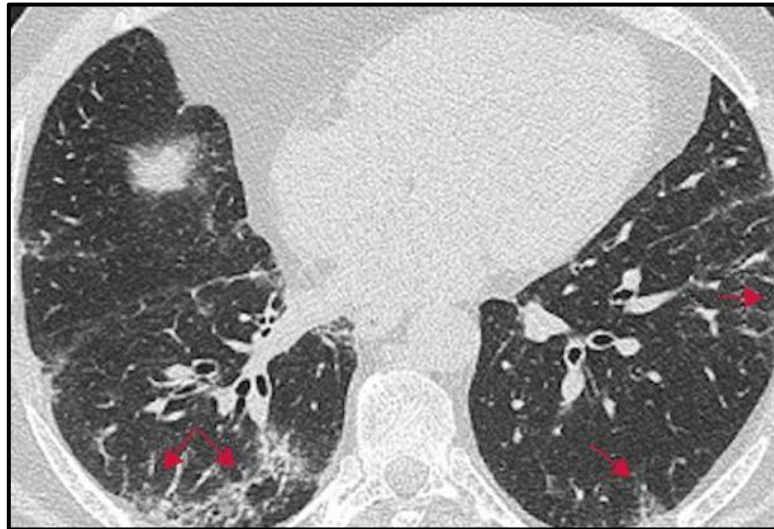


Figure 1.5 Axial computed tomography (CT) image of a patient with IPF. Note the progressive ECM deposition in the lung parenchyma indicated with red arrows (Robbie et al., 2017).

Environmental and genetic factors play an important role in the pathogenesis of IPF but the identification of the molecular mechanisms behind the IPF development has been challenging. For instance, cigarette smoking has been associated as risk factor for the development of IPF in patients. (Baumgartner, et al., 1997). Since 1990, cumulative sources of evidence support the hypothesis that environmental agents may play an etiologic role in IPF including virus, wood dusts, metal, silica, and stone (Raghu, et al., 2011; Hubbard, et al., 2000; Taskar & Coultas, 2006). Increasing data associate genetic predispositions to IPF development within the presence of rare genetic variants in genes responsible for surfactant production (*SFTPC*, *SFTPA2*) and telomere activity (*TERT*, *TERC*, *PARN*) (Armanios, et al., 2007; Wang, et al., 2009; Richeldi, et al., 2017).

Repetitive microinjuries in the alveolar epithelium leads to basement membrane disruption with the activation of a strong immune response and consequent dysregulated repair signalling. Myofibroblasts recruitment, epithelial mesenchymal transition, and fibroblast to myofibroblasts transition are responsible for the activation of a positive feedback loop where an increased deposit and over production of ECM (collagen I and III) occur and finally lead to an altered tissue stiffness in the lungs (Figure 1.6). IPF is currently considered an epithelium-driven disease where an aberrant epithelial-mesenchymal crosstalk causes a dysregulated ECM remodelling. Concurrently, the replacement of normal wound healing repair system with chronic fibrosis and the deposition of ECM creates an unbalanced level between profibrotic and fibrotic mediators (Richeldi, et al., 2017; Todd, et al., 2012). Tissue repair consists of three distinct cellular processes: immune recruitment after damage, activation of immune cells and myofibroblasts, and myofibroblast renewal of ECM (Jun & Lau, 2018). In this context, macrophages play a key role in inflammatory response during fibrosis development. Macrophages have been found in proximity with collagen-producing myofibroblasts and to shift their cytokine pattern profile to pro-fibrotic mediators including transforming growth factor- β (TGF- β) (Wynn & Barron, 2010).

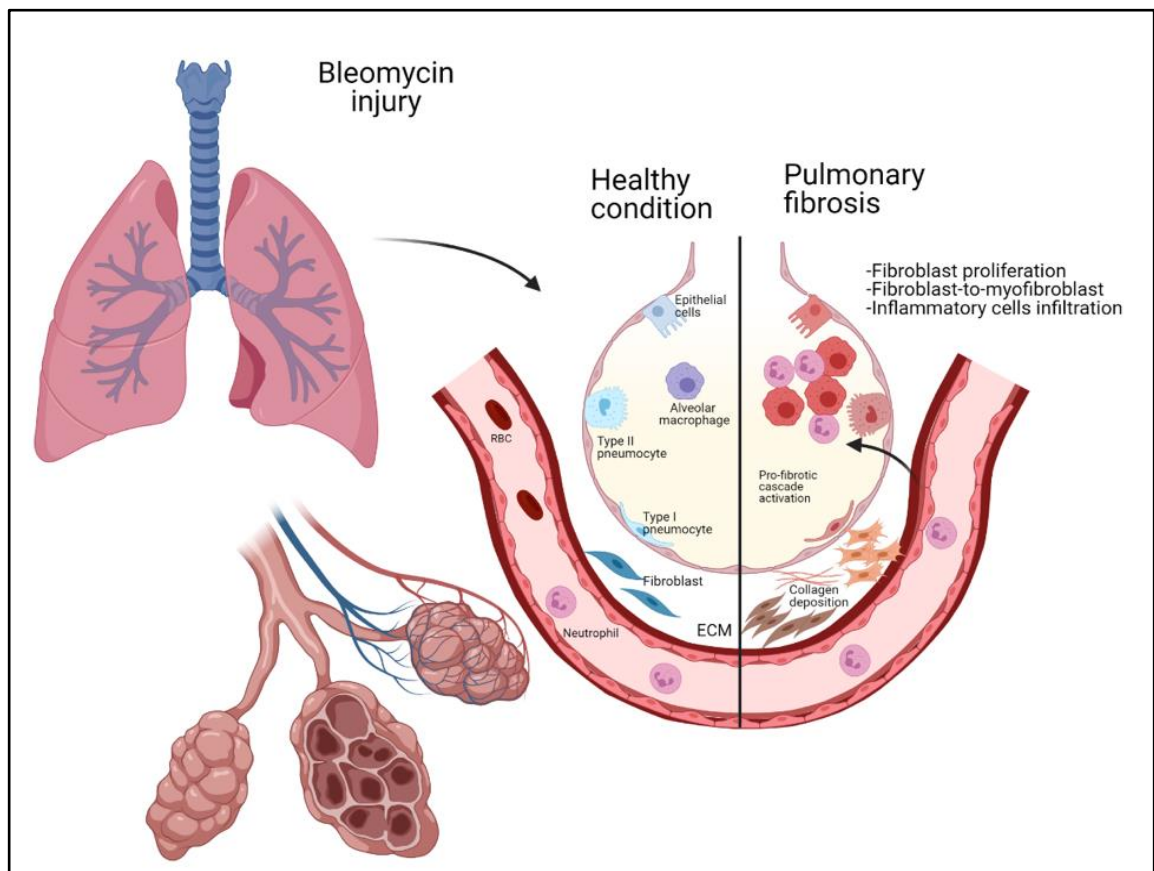


Figure 1.6 Schematic illustration of pathological mechanism of bleomycin-induced pulmonary fibrosis. A comparison between healthy and fibrotic lung tissue is shown. Figure created in biorender.com

TGF- β is one of the most important fibrogenic inducer of ECM production, such as collagen and other matrix proteins (Yue, et al., 2010). The major cellular sources of TGF- β overproduction during the development of lung fibrosis are fibroblasts, alveolar macrophages and alveolar epithelial cells (AECs) (Broekelmann, et al., 1991; Khalil, et al., 1991). In animal models, it has been demonstrated that the overexpression of TGF- β leads to the excess synthesis and collagen deposition. Although it has been demonstrated that all three TGF- β isoforms stimulate fibroblasts to produce collagen *in vitro*, TGF- β 1 is the most expressed isoform during lung fibrosis and induces the differentiation of fibroblasts to myofibroblasts (Baecher-Allan, et al., 2018; Yue, et al., 2010). By contrast, it has been demonstrated that TGF- β 1 is able to

suppress an inflammatory process when released by regulatory T-cells by Interleukin-10 (IL-10) stimulation. Taken together, these findings explain that TGF- β 1 could simultaneously suppress inflammation and activate collagen synthesis responses in myofibroblasts (Kitani, et al., 2003). For this purpose, a better understanding of this cytokine could provide advantages not only in relation to a suppression of inflammatory response, but also in relation to the capacity of TGF- β 1 to mediate fibrosis.

1.4 Bleomycin-induced lung fibrosis

Animal models are an indispensable scientific tool for the investigation of many diseases. They are employed for the study of the pathophysiological mechanisms and in the development of potential therapeutic strategies. Chronic diseases are more difficult to model mainly due to complex pathogenesis with a full range of features. Animal models remain the most used approaches available for exploring key traits of IPF disease. Historically, the first to be developed and used widely is the bleomycin model, which is currently well-characterised due to its capacity to reproduce and mimic many aspects of IPF condition (Figure 1.6). Bleomycin is an antibiotic, which was discovered and isolated from culture of the bacterium *Streptomyces verticillus* in 1962 by the Japanese scientist Hamao Umezawa (Adamson, 1976; Umezawa, et al., 1967). It is typically employed in chemotherapy due to its anti-cancer properties, to treat lymphoma, squamous cell cancers, sarcoma, testicular cancer, ovarian cancer, and lung cancer (<https://www.drugs.com/monograph/bleomycin.html>). The bleomycin is a non-ribosomal peptide which induces single and double DNA breaks with a potency to stop the cell cycle during the progression of cancer. Along with its therapeutic effects in the cancer treatment area, several side effects have been reported. (Williamson, et al., 2015). Although bleomycin is effective as an anti-cancer agent, its therapeutic use is limited due to pulmonary toxicity. For instance, one of the reported side effects is the development of lung

fibrosis due to the lack of the bleomycin hydrolase (BLMH). Whilst BLMH is known to be expressed in the entire human body, its physiological role in lungs is still not clearly understood. BLMH is a well-conserved cysteine protease widely expressed in several mammalian tissues and is able to inactivate bleomycin activity. Although the bleomycin model of lung fibrosis is reproducible, it presents limitations due to the lack of hyperplastic alveolar type II cells, usually induced by chronic damage (Mouratis & Aidinis, 2011). Nevertheless, the bleomycin model of lung fibrosis remains a fundamental tool in this field of research.

1.5 Extracellular matrix (ECM)

ECM is a three-dimensional network consisting of a non-cellular component and macromolecules, such as proteoglycans (PGs) and other fibrous proteins that provide structural support to organs, tissues, and surrounding cells (Theocharis, et al., 2016; Bonnans, et al., 2014). The ECM is responsible not only for supporting the cellular constituents but is also required for many biological functions such as tissue morphogenesis, development, homeostasis, and differentiation (Frantz, et al., 2010). In 2012, the “matrisome project” has been established for the development of an inventory of ECM, identifying ~300 proteins as core components of the ECM within a mixture of previously identified proteins (Hynes & Naba, 2012). Comparative and genome sequencing analysis identified two key components of the ECM: the interstitial connective tissue, involved in the structural scaffolding for tissues surrounding the cells, and the pericellular matrices such as the basement membrane (BM), which is adjacent with the cells (Bonnans, et al., 2014). All cells including epithelial, fibroblasts, immune cells and endothelial cells, produce and secrete matrix macromolecules thus contributing to the composition of ECM compartment (Theocharis, et al., 2016). Although the ECM is composed of water, proteins and polysaccharides, each tissue has a unique and specific ECM composition, which is generated

during tissue development. Moreover, the ECM is constantly remodelled, deposited, and degraded for the maintenance of tissue homeostasis (Zhang & Newton, 2021). The composition and organisation of ECM are tightly and spatiotemporally regulated to drive cell behaviour during the cellular differentiation stage (Walker, et al., 2018). Dysregulation of its remodelling alters the composition and structure of the ECM components, leading to the development and progression of pathological conditions such as osteoarthritis, cardiovascular disease and tissue fibrosis, commonly characterised by an excessive degradation and accumulation of the ECM- (Cox & Erler, 2011; Bonnans, et al., 2014; Selman & Pardo, 2006).

1.5.1 Structure and function of ECM

The ECM is predominantly composed of PGs and fibrous proteins (Järveläinen, et al., 2009; Schaefer, 2010). Together these macromolecules produce the highly specialised polymeric BM, the scaffold for mechanical interactions with integrins and other receptors required for cell signalling (Breitkreutz, et al., 2009), and interstitial matrix, the porous three-dimensional networks (Harburger & Calderwood, 2009). The interstitial matrix controls the structural integrity of tissues but also regulates cell differentiation and migration (Winkler, et al., 2020). The protein composition of the interstitial matrix mainly includes collagens I, III, V, fibronectin, and elastin (Frantz, et al., 2010) (Figure 1.7). The BM consists mainly of collagen IV and laminins, which are interconnected through different network-bridging proteins such as heparan sulphate proteoglycans (HSPGs) (Winkler, et al., 2020). BMs-cell association is essential for establishing cell polarity and is crucial for many developmental processes (Jayadev & Sherwood, 2017). In fact, BM is anchored to cell surfaces through interactions with adhesion receptors and sulphated glycolipids. ECM remodelling involves over 700 proteins and changes overall abundance, concentration, structure, and organisation of individual ECM components. Such remodelling affects the three-dimensional

spatial topology of the matrix around cells, its biochemical and biophysical properties and consequently its effect on cell fate (Naba et al., 2016).

The composition and topology of the ECM is different from one tissue to another and even within the same organs, as well as from a normal to pathological tissue (Frantz, et al., 2010). Different quantities and types of collagens, adhesion molecules, proteoglycans, growth factors and cytokines or chemokines are present in ECM in the different tissues (Kleinman, et al., 2003). For example, cartilage ECM is rich in collagen II and proteoglycans for resisting functions, and the BM is mainly made of laminin and non-fibrillar collagen forming a separating interface between different tissue layers, and ECM acts as a molecular filter in the kidney (Breitkreutz, et al., 2009; Kuure, et al., 2000).

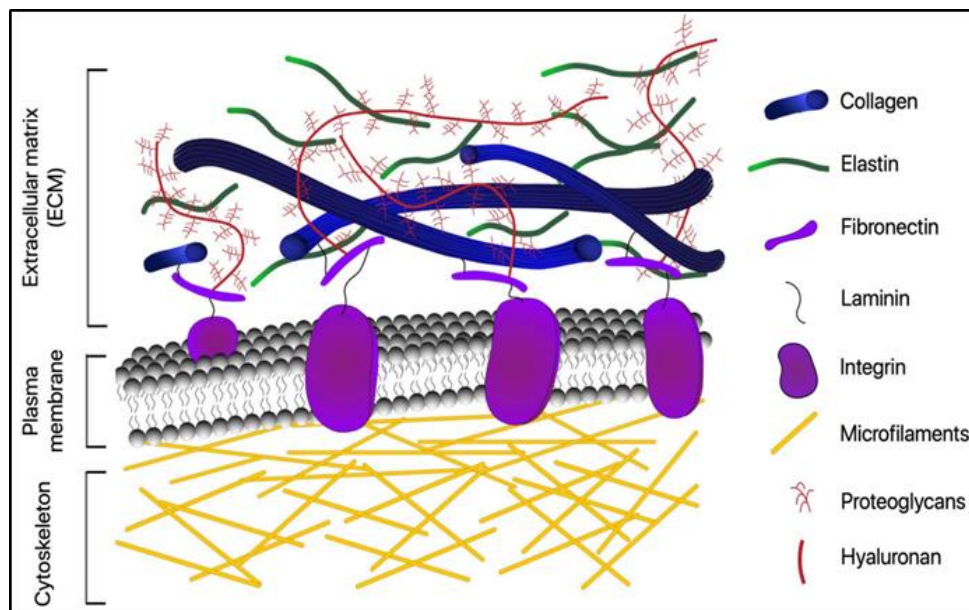


Figure 1.7 Schematic overview of ECM and its major components. Although the ECM composition varies depending on the tissue, the matrix is mainly composed of collagen, elastin, fibronectin, and laminin proteins assembled into an organised meshwork (Poole & Mostaço-guidolin, 2021).

Although the ECM represents an evolutionarily conserved composition of molecules and non-cellular components, the characterisation of its composition is currently revealing new insights into ECM structure and

function. However, the total identification of extracellular proteins still represents a challenging process due to the insolubility nature of these macromolecules (Byron, et al., 2013).

1.5.2 Collagen

Collagens are the most abundant proteins in mammals. Since their discovery, 28 collagen types have been identified and subclassified into subfamilies (Ricard-Blum, 2011). Collagen proteins conserve all the same trimeric structure: a right-handed triple helix with three separate collagen chains ranging between 662–3152 amino acids twisted around each other (Ottani, et al., 2002). The typical tropocollagen subunit is a rod of approximately 300 nm long and 1.5 nm in diameter, made up of three polypeptide strands, each of which is a left-handed helix (note that the α -helix is right-handed). The distinct quaternary structure of collagens is stabilised by hydrogen bonds among neighbouring molecules (Gordon & Hahn, 2010). One of the collagen subfamilies are the fibrillar collagens that have been described in almost all animals and are the components of striated fibrils (Exposito, et al., 2010). This family includes fibrillar collagens types I, II, III, V, XI, XXIV and XXVII. Recent proteomic data on mouse models of lung ageing identified specific changes in levels of type IV and type VI as well as the two fibril-associated collagens with interrupted triple helices (FACIT), namely type XIV and type XVI collagens (Onursal, et al., 2021). In addition, levels of the extracellular collagen crosslinking enzyme lysyl oxidase are decreased, indicating less enzymatically mediated collagen crosslinking upon ageing (van Huizen, et al., 2019; Onursal, et al., 2021). Collagens I and III are both classified as fibril-forming interstitial collagens. Both are predominantly found in tissues with elastic properties such as skin, vasculature and lung (Hulmes, 2008). The collagen fibrillar family is the most abundant component of the airway ECM. In fact, the lung consists mainly of collagen types I and III, accounting for 90 % of total lung collagen proteins (Bates & Suki, 2008). These

collagens are localised in the alveolar wall and respiratory septa while type IV collagen is accumulated in the BM and type II collagen is present in most airway cartilage structures (Ito, et al., 2019). Type I collagen is responsible for mechanical stability and structure of the airways ECM (Liu, et al., 2009; Liu, et al., 2021). Type II collagen is the major component of airway cartilage (95% of total collagen), facilitating chondrocyte synthesis of ECM (Pieper, et al., 2002; Borgia, et al., 2018). Both molecules also provide a structural framework in the bronchi, interstitium, and alveolar wall (Sobin, et al., 1988; Davidson, et al., 1993). The ratio type I/type III determines the resistance of collagen fibres under mechanical forces during tissue stretching (Table 1.1) (Bates & Suki, 2008).

Table 1.1 Collagen subtypes cover different roles in airway (Liu et al. 2021).

Collagen Subtype	Collagen's Role
Type I collagen	<ul style="list-style-type: none"> • a primary contributor to lung mechanics • provides mechanical stability and structure • provides a structural framework in the bronchi, interstitium, and alveolar wall
Type II collagen	<ul style="list-style-type: none"> • the major component of airway cartilage (95% of total collagen) • facilitates chondrocyte synthesis of extracellular matrix (ECM)
Type III collagen	<ul style="list-style-type: none"> • a primary contributor to lung mechanics • provides a structural framework in the bronchi, interstitium, and alveolar wall
Type IV collagen	<ul style="list-style-type: none"> • fundamental for maintaining the strength and function of the basement membranes
Collagen type I/type III ratio	<ul style="list-style-type: none"> • determines the resistance of collagen fibers to breakdown under mechanical forces during stretching

1.5.3 ECM-cell communication

The ECM plays an important role in the cell adhesion function and mediates direct interactions of the cell with its extracellular environment. In

fact, it is considered to provide a substrate to cell-cell communication that is assisted by cell adhesion molecules (CAMs). ECM proteins and structures can determine the cell behaviour, migration, proliferation and survival by communicating with the intracellular cytoskeleton and transmission of growth factor signals (Kim, et al., 2011). Integrins and proteoglycans are the major ECM adhesion receptors which cooperate in signalling events, determining the signalling outcomes, and thus the cell fate (Schwartz, 2010). The cells can physically attach transitory or permanently to the ECM via these adhesion receptors (Berrier, et al., 2007).

Two types of ECM receptors can be distinguished in non-integrin and integrin receptors. However, their role in homeostasis and fibrosis are partially understood. The regulation of cell signalling by the ECM macromolecules takes place either directly or indirectly. In direct regulation, the ECM macromolecules interact via integrins (O'Toole, et al., 1994) or other types of cell receptors such as a receptor for hyaluronan (HA), namely CD44, and syndecans (Radotra, et al., 1994; Afratis, et al., 2017). In indirect regulation, ECM macromolecules co-operate concurrently with several receptor molecules and GFs (Kim, et al., 2011). It has been demonstrated that cells respond to mechanical forces by remodelling of the ECM. For example, stretching of fibroblasts activates expression of genes for collagens, fibronectin, and MMPs contributing to the repertoire of ECM (Chiquet, et al., 2003). This function is important for the maintenance of tissue organisation and a dynamic dialogue with a surrounding stroma (Rønnov-Jessen & Petersen, 1996). Another important receptor for ECM proteins is dystroglycan, which binds to laminin, agrin, and perlecan in BM as well as to transmembrane neuroligins (Barresi & Campbell, 2006). The best-developed theory regarding growth factors and ECM concerns the roles of diverse ECM proteins and their receptors in binding and regulation of TGF- β . In addition, other surface receptors can bind ECM components and induce signalling, including the syndecans (Bernfield, et al., 1999) and the receptor tyrosine kinases discoidin

domain receptors (DDR) (Yoshimura, et al., 2005). Therefore, disruption of the balance of ECM proteins or their interactions has important impacts for the behaviour and the fate of cells within that tissue leading to the development of pathological conditions.

1.5.4 ECM in lung diseases

The pulmonary ECM dictates the whole tissue lung's structure and provides functional support for the respiratory process which is crucial for lung function (Hynes, 2009). Pulmonary tissue is characterised by a unique and peculiar ECM composition to provide three important biological functions: homeostasis, tissue morphogenesis and injury-repair responses (Zhou et al., 2018). It has been previously recognised that the pulmonary ECM changes dynamically and temporally in the lung tissue during the foetal, neonatal, and adult stages (Coraux, et al., 2003). Dynamic changes and alterations within the ECM that occur upon injury or with ageing, lead to either an aberrant expression or turnover of matrix components, or an altered post-translational modification and proteolytic matrix degradation. These mechanisms can markedly disrupt ECM function and lead to the development of many lung diseases (Figure 1.8) (Burgstaller, et al., 2017). Proteolytic enzymes in the lung ECM, such as MMPs, and their inhibitors, tissue inhibitors of metalloproteinases (TIMPs), orchestrate lung development. However, the dysregulation of those molecules can contribute to the pathogenesis of lung disease.

Only recently, structural changes of the ECM have been addressed to the development of chronic lung diseases such as asthma, COPD, and IPF (Burgess, et al., 2016).

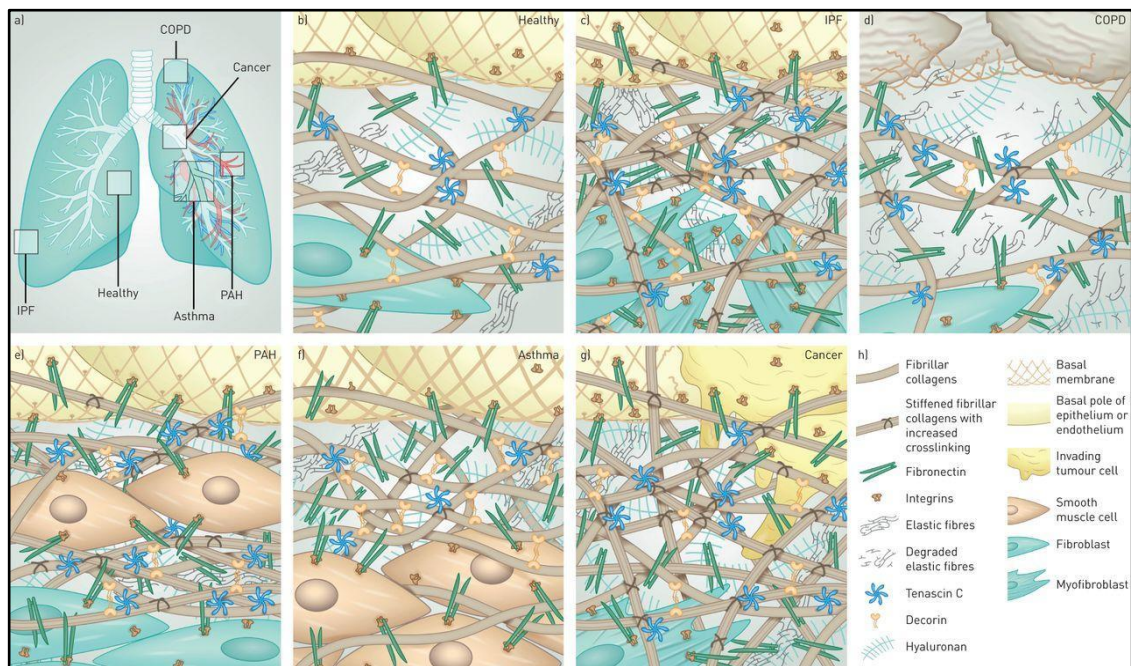


Figure 1.8 Pathological changes in ECM and lung disease. a) Overview lung tissue. b) Healthy interstitial ECM with resident fibroblasts and a meshwork of collagens, elastin and fibronectin. c) In IPF myofibroblasts deposit high levels of ECM molecules into the interstitium. d) COPD is characterised by destruction of elastic fibres by ECM-degrading enzymes and elevated levels of hyaluronan and tenascin C, and decreased deposition of decorin. e) In pulmonary arterial hypertension (PAH), is characterised by an increase in elastin and collagen fibres, fibronectin, and tenascin C, and hyperplasia of smooth muscle cells. f) In asthma, the ECM changes cause less bronchial epithelium and thickened basal membrane. g) In cancer, an extensive stiff stroma contains highly crosslinked collagens, and fibronectin, and hyaluronan. h) Legend describing molecules and cell types (Burgstaller, et al., 2017).

1.6 Low-density lipoprotein receptor-related protein 1 (LRP1)

In 1974 Brown and Goldstein discovered that the LDL receptor superfamily as responsible for the transport of molecules into the cellular endosomal compartments (Brown & Goldstein, 1976). LRP1 (also known as CD91 and α_2 -macroglobulin (α_2 M) receptor (Hanover, et al., 1983) is an endocytic transmembrane receptor that mediates clathrin-dependent endocytosis of many ligands and regulates a number of cell-signalling pathways (Strickland, et al., 2002). LRP1 is ubiquitously and abundantly expressed in hepatocytes, neurons, adipocytes, muscle, fibroblasts, chondrocytes and macrophages (Gaultier, et al., 2009; Gonias & Campana, 2014; Pflanzner, et al., 2011). It is

synthesised as a 600 kDa precursor which is processed in Golgi by a furin protease resulting in a non-covalently associated receptor of an extracellular α -chain (515 kDa) and, transmembrane and intracellular β -chain (85 kDa) subunits, respectively (Willnow, et al., 1995). The extracellular α -subunit contains four different cluster binding domains with complement-like repeats that can bind LRP1 ligands and mediate their endocytosis. The intracellular and transmembrane β -subunit contains a YxxL, di-Leucine (LL), and NPxY motifs, responsible for the activation of cell signalling pathway and regulation of gene expression (Figure 1.9) (Strickland & Dudley, 2001). Ligand interactions with LRP1 can be antagonised by the presence of a receptor-associated protein (RAP). Endogenous RAP acts as an LRP1 chaperone to assist its correct folding in the maturation process and prevent any premature binding to intracellular ligands during receptor trafficking (Willnow, et al., 1995). Following endocytosis, RAP dissociates in the acidic endosome, allowing LRP1 to recycle back to the cell surface (Marakasova, et al., 2021).

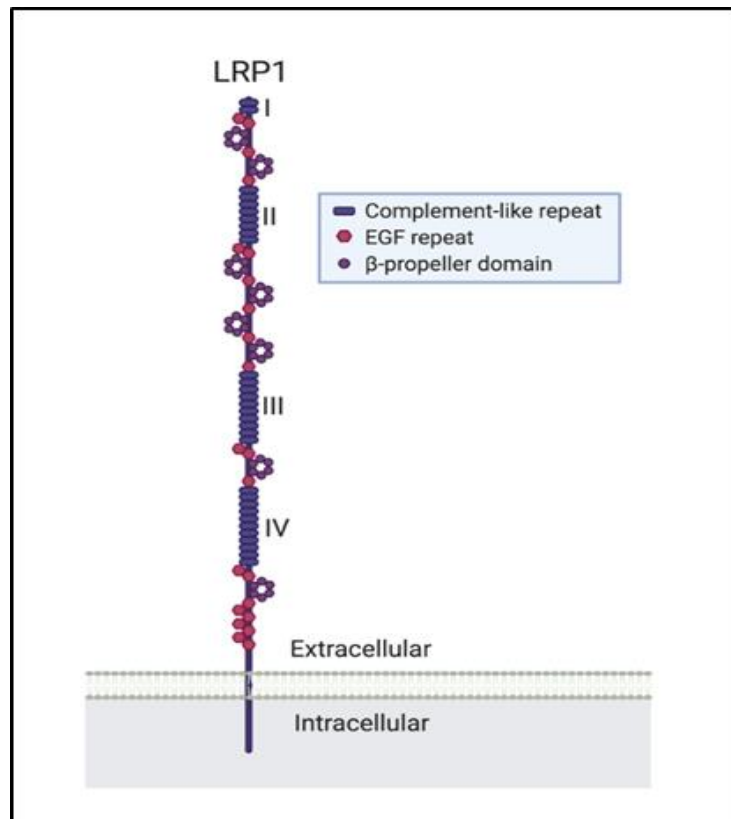


Figure 1.9 Structure of LRP1 protein. LRP1 binds many extracellular and intracellular ligands. It contains an α -chain (515 kDa), acidic cysteine-rich complement-like repeats (CRs), along with epidermal growth factor (EGF)-like domains and β -propeller domains. It consists of four ligand-binding domains (I, II, III, VI), which are constituted of 2, 8, 10, and 11 CRs, respectively. The intracellular portion is responsible for the endocytosis and cell signalling process. Figure created in biorender.com and revised from Yamamoto, et al., 2022.

Embryonic lethality has been described in a murine global LRP1 deletion due to a failure of the blastocyst's implant, revealing a fundamental role in the development stage (Herz, et al., 1992).

In addition to the membrane-associated protein, LRP1 also exists in a soluble form (sLRP1) which is composed of the α -chain and a fragment of the β chain. LRP1 is subject to proteolytic shedding at the cell surface by the sheddases, which prevents endocytic transport of ligands. However, this circulating soluble form still covers the capacity to bind LRP1 ligands increasing their extracellular half-life by preventing membrane LRP1-mediated endocytosis (Quinn, et al., 1997; Strickland & Dudley, 2001; Etique, et al.,

2013). Expression of LRP1 gene is activated by sterol regulatory element binding protein 2 (SREBP2), hypoxia-induced factor 1 α (HIF1 α), and nitric oxide-dependent transcription factors and can be blocked by an antisense RNA that is transcribed from LRP1 gene exons 5 and 6 (Myklebost, et al., 1989; Auderset, et al., 2016). Considerable work has been focussing on the functions of LRPs in vascular biology, neurobiology and cancer, including LRP1b, LRP2/megalin, LRP3, LRP5, LRP6, LRP8/apolipoprotein E receptor 2, LRP10, which also has been referred to as LRP9 (Sugiyama, et al., 2000; Lillis, et al., 2009). Among those receptors LRP1 has been identified to play many functions in several organs including lungs (Artigas, et al., 2011).

1.6.1 Endocytosis

Endocytosis is a fundamental cellular process by which cells can generate very small membrane vesicle structures to transport and internalise a wide range of molecules from the extracellular milieu to the cytoplasm. This process covers many physiological processes such as antigen presentation, the maintenance of protein homeostasis, cell migration, nutrient uptake, signalling pathways by cell-surface receptors, junction formation and removal of apoptotic bodies. (Marsh & McMahon, 1999). In this process, the small membrane vesicles are between 60-120 nm and they are able to transport ECM proteins and their ligands (Figure1.13). Proteins can be endocytosed through several different endocytic pathways. In mammalian cells, multiple endocytic pathways have been identified, but generally can be categorised in: clathrin dependent and clathrin-independent (Mayor & Pagano, 2007; Bitsikas, et al., 2014). Receptor for low-density lipoproteins (LDLRs) is a classic example of cargo protein that undergo clathrin-coated pits mediated endocytosis pathway (Doherty & McMahon, 2009). This family of receptors consist of a cytoplasmic tail that contains sequences recognized by adaptor proteins that facilitate the polymerization of a clathrin coat around the membrane vesicle structures.

Overall, the endocytosis process occurs in sequential events: the internalised molecules are transported to the early endosome, where some of them are routed for the degradation to late endosomes and lysosomes compartments, while others clathrin-dependent cargoes are rapidly recycled back to the cell membrane surface and eventually selected ligands are re-exocytosed to the extracellular milieu (Grant & Donaldson, 2009). Among all the LDLRs, LRP1 is the most representative member of this endocytic pathway (Lillis, et al., 2015).

1.6.2 LRP1-mediated endocytosis

LRP1 mediates clathrin-dependent endocytosis for more than 80 ligands from the extracellular matrix environment (Figure 1.10) (Wu & Gonias, 2005; Lin & Hu, 2014; Yamamoto, et al., 2022). The first identified LRP1 ligand was apolipoprotein E-containing β -VLDL (Kowal, et al., 1989). Apart from α 2M, LRP1 has been shown to bind and internalise a large number of other structurally distinct ligands, such as β -amyloid, apolipoprotein E (APOE) (Kowal, et al., 1989); CTGF, also known as CCN2 or connective tissue growth factor, fibronectin, elastase, MMP-13, MMP-2, MMP-9, TIMP-1; TIMP-2 and TIMP-3 (Lillis, et al., 2005). LRP1-mediated endocytosis is essential to modulate protein level of the plasma membrane and the ECM environments (Strickland, et al., 2002).

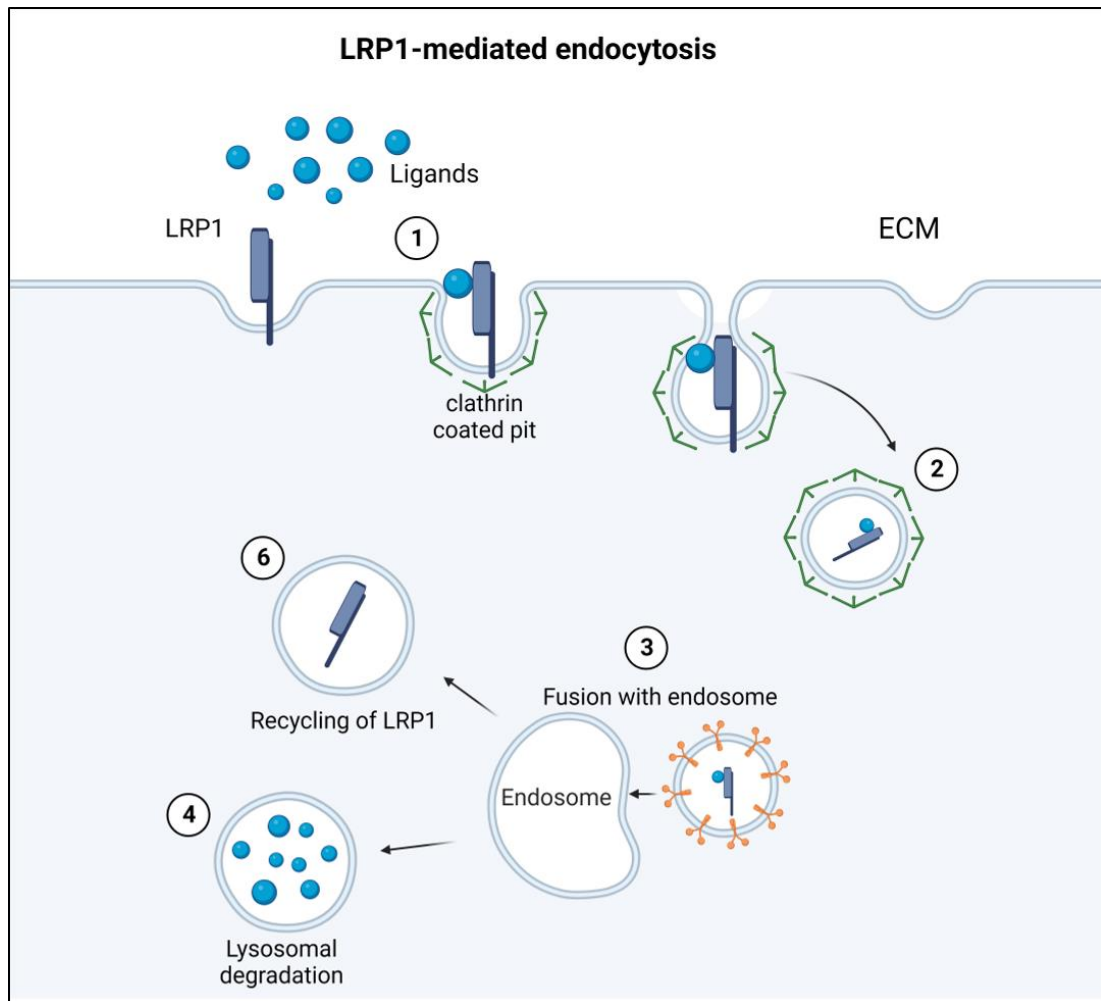


Figure 1.10 Outline of the currently proposed hypothesis of LRP1-mediated endocytosis. Ligands bound to the extracellular domain of LRP1 are internalised and degraded in the lysosome; LRP1 can be recycled back to the cell-surface. Figure realised using Biorender.com.

1.6.3 LRP1 in cell signalling

In addition to its endocytic function, LRP1 is also important in the modulation of cell signalling pathways involved in cell proliferation, adhesion, differentiation, proliferation, morphogenesis, and development. Two different models have been proposed for signalling transduction by LRP1. The first model depends entirely on the homodimerization within its cytoplasmic domains and all the proteins involved can directly or indirectly interact with this domain mediating signal transduction. The second model proposes a

heterodimerization between LRP1 and unrelated receptors. For example, it has been reported that if heterodimerization takes place with a receptor with kinase activity, LRP1 phosphorylation could result on tyrosine residues in NPxY motifs (Betts, et al., 2008; Van Der Geer, 2002). For example, LRP1 phosphorylation occurs with the association of proteins, such as FE65, Shc, Disabled, suggesting that it also covers a role as signalling receptor (Lilias, et al., 2009). This idea is supported by previous studies that show other members of the LDLR family are involved in signalling pathways. As previously described, the YxxL and dileucine motifs function as principal endocytosis signals, whereas the NPxY motifs work as binding sites for other adapter proteins modulating the cell signalling pathways (Herz, et al., 1990). Recently, it has been established that tissue plasminogen activator (tPA) induces LRP1-mitogenic signalling through the phosphorylation of the tyrosine (Tyr) 4507 in the cytoplasmic portion (Lin, et al., 2010). Previous results show platelet-derived growth factor (PDGF) binds to LRP1 and with the PDGF-receptor induces a transient phosphorylation of the intracellular domain of LRP1 (Loukinova, et al., 2002). Another signalling system includes the N-methyl-D-aspartate receptor (NMDAR) in neurons by the interaction of the adaptor protein postsynaptic density protein-95 (PSD95) with the LRP1 cytoplasmic tail, which arbitrates the neuronal calcium flux through the cell membrane (Mantuano, et al., 2013). Convergent signalling pathways have been shown to be tightly controlled by LRP1 on TGF β and Wnt5a. In this study, it has been demonstrated that TGF β positively regulates a canonical Wnt5a signalling pathway through the interaction with LRP1 extracellular domain while the second NPXY motif tail of LRP1 is bound to Erk2 stopping the cholesterol accumulation. The whole synergy of these signalling pathways involves both extracellular and cytoplasmic LRP1 domains (Figure 1.11) (El Asmar, et al., 2016). In cartilage, LRP1 controls not only ECM-degrading proteases but also the Wnt/ β -catenin signalling pathway by interacting with Frizzled-1 (Zilberberg, et al., 2004) and CCN2. Both pathways regulate endochondral ossification

and articular cartilage regeneration highlighting the importance of LRP1 during skeletal development and maintenance of cartilage homeostasis (Kawata, et al., 2012).

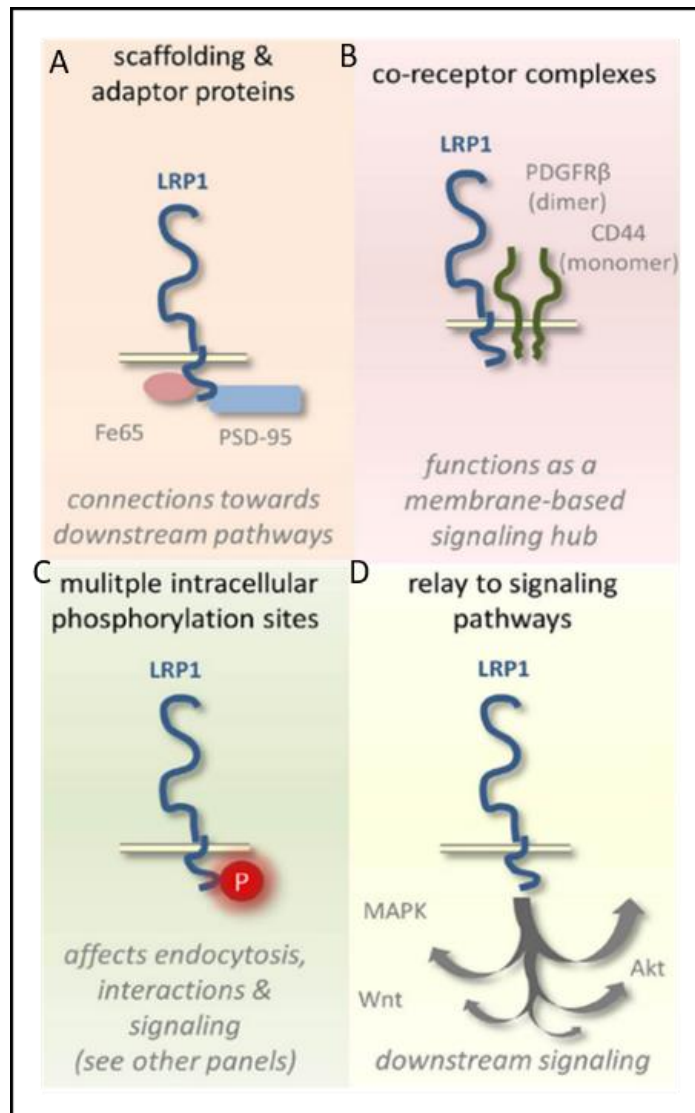


Figure 1.11 Schematic representation of LRP1 involved in cell signalling pathways. (A) The intracellular LRP1 domain interacts with several adaptor and scaffolding proteins. (B) The formation of co-receptor complexes with LRP1 influences signalling. (C) The phosphorylation of its intracellular domain influences signaling and regulates endocytosis. (D) LRP1-mediated signaling affects several well-known pathways linked to diseases. Figure revised from Gool et al., 2015.

1.6.4 Proteolytic shedding of LRP1 ectodomain

After shedding of LRP1, sLRP1 is produced and released from the cell membrane surface to the ECM (Quinn, et al., 1999). The physiological function of LRP1 ectodomain shedding remains still undefined. Many evidence suggests that LRP1 is a receptor target for numerous proteinases. Several sheddases have been identified in the proteolytic cleavage of LRP1 such as a disintegrin and metalloproteinase with thrombospondin motifs-10 (ADAM-10) (Shackleton, et al., 2016), a disintegrin and metalloproteinase with thrombospondin motifs-12 (ADAM-12) (Selvais, et al., 2011), a disintegrin and metalloproteinase with thrombospondin motifs-17 (ADAM-17) and MMP-14 also known as type 1 matrix metalloproteinase (MT1-MMP) (Liu, et al., 2009). However, shedding of LRP1 is not restricted to only the extracellular portion but also to the trans and intracellular domain. This portion can be proteolytically cleaved generating an LRP1 intracytoplasmic domain (ICD) which is able to regulate gene expression at the nuclear level (Zurhove, et al., 2008). LRP1 shedding has been detected in human plasma and serum (Quinn, et al., 1997). Other studies found the presence of sLRP1 in cerebral spinal fluid (Fuentealba, et al., 2009); in the conditioned medium of HT1080 cultured cells (Selvais, et al., 2011); in osteoarthritis (OA) human cartilage (Yamamoto, et al., 2017) and in bronchoalveolar lavage fluids of patients affected by ARDS (Wygrecka, et al., 2011). In recent work, it has been shown that ADAM-17 and MMP-14, were identified as the LRP1 sheddases in cartilage and their inhibition can reverse the degradation of ECM in OA cartilage (Yamamoto, et al., 2017). Overall, the ectodomain shedding of LRP1 plays an important role in both physiological and pathological conditions. In fact, it has been hypothesised that the impairment of LRP1 function and shedding can affect the ECM turnover and disrupt the cell homeostasis (Yamamoto, et al., 2017) . This has been linked to the development of a large number of conditions such as Alzheimer's diseases, OA, cancer and inflammation. However, the pathological mechanisms behind this process have not been clarified yet.

1.6.5 Genome-wide association studies (GWAS) - LRP1

A total number of 61 GWAS studies have identified *LRP1* gene involved in different physiological and pathological conditions. The first GWAS study revealed *LRP1* modulates neuronal glutamate signalling, linking to migraine pathophysiology (Chasman, et al., 2011). Many other studies were carried out finding an involvement of *LRP1* gene in coronary artery disease and aortic aneurysm (Brown, 2011; Sakaue, et al., 2021; Pirruccello, et al., 2021; Francis, et al., 2022; Jones, et al., 2016).

Pulmonary function has been considered as a heritable trait able to determine the physiological state of airways and lungs and able to identify any pulmonary impairment. Cumulative evidence suggests that specific genes can influence the pulmonary function (Wilk, et al., 2000). In 2011, Artigas et al. identified *LRP1* gene in a large GWAS as relevant for the pulmonary function (Artigas, et al., 2011). Later, Shrine et al. in 2019 performed another GWAS study, defined a new association of *LRP1* and risk of developing COPD (Shrine et al., 2019). Based on these findings, it could be useful to elucidate the mechanisms through which the *LRP1* gene can influence pulmonary function. This could contribute to gaining a more complete insight into the pathophysiological understanding of lung diseases such as COPD, lung cancer and lung fibrosis.

1.7 General aims and objectives

Lung fibrosis is considered one of the most severe forms of lung disease and it eventually leads to death. Despite the fact that no cure is available and the biological mechanisms that lead to the development of fibrosis in most cases remains elusive, three pathological processes have been identified: excessive ECM deposition, fibroblast to myofibroblast differentiation and inflammation. A large genome-wide association study identified the *LRP1* gene as relevant in lung function (Artigas, et al., 2011). Therefore, it is of interest to test how the loss of *LRP1* could affect the lung tissue *in vivo* and to

explore the molecular mechanisms behind the respiratory homeostasis and its role in lung disease.

Herein, the major aim of my PhD project was to investigate the pathophysiological function of LRP1 in lung tissue during the pulmonary fibrosis. The specific aims were as following:

- i. Determine a role of LRP1 in lung fibrosis development. The first objective of this aim was to test the effects of LRP1 global deletion and the second objective was to use specific deletion of LRP1 in COL1A2-expressing cells in the bleomycin-induced fibrosis model.
- ii. To investigate the molecular basis behind the function of LRP1 in lung fibrosis. The first objective was to assess a ligandome assay by mass-spectrometry analysis and the second objective was the characterisation of the effects of the accumulation of LRP1 ligands *in vitro*.

1.8 Initial hypothesis

In this thesis, a series of experiments were performed to address the initial hypothesis: “LRP1 plays a key physiological role in healthy lung and its dysregulation leads to pathological lung conditions”.

Chapter 2 Materials and Methods

2.1 List of general reagents

Reagent	Catalogue number	Supplier
DMEM F-12	D9785	Sigma Aldrich
DMSO	231	VWR
Fetal Bovine Serum	A3160401	ThermoFisher
EDTA	E6758	Sigma
Ethanol (histology)	E7023	Honeywell
Glacial acetic acid	305238	Scientific Laboratory Supplies
HBSS	14025	Life Technology
Isopropanol	278475	Sigma Aldrich
Lipofectamine 2000	11668019	ThermoFisher
Neutral buffer formalin	HT501128	Leica
Non-immune goat serum	S-1012-50	Vector
Paraformaldehyde	p6148	Sigma Aldrich
Penicillin/Streptomycin	P4333	Sigma Aldrich
Sirius Red (Picric Acid)	STPSRPT	StatLab
Tween 20	P7949	Sigma Aldrich
Vectashield mounting medium with DAPI	H1200	Vector
Xylene	X0250	Fisher scientific
Lipofectamine™ 3000	L3000001	ThermoFisher
Acidic HIER	CTS014	R&Dsystems
Basic HIER	CTS013	R&Dsystems
Neutral HIER	CTS023	R&Dsystems
Tunel Assay kit	ab206386	abcam
Proteinase K	EO0491	ThermoFisher
REDtaq ReadyMix PCR Reaction Mix	R2523-20RXN	Sigma Aldrich
DPX mountant	44581	Sigma Aldrich
Hydrogen peroxide	7722-84	Sigma Aldrich
collagenase Type 1	17100017	ThermoFisher
bovine serum albumin (BSA)	A9418-500G	Sigma Aldrich
Methyl green, 3,3'-diaminobenzidine	D5637	Vector Labs

DAB Substrate Kit	SK-4100	Vector Labs
Harrys Haematoxylin and Eosin	HHS16	Leica
Recombinant Human LRP-1 Cluster II Fc	2368-L2	R&Dsystems
4-12% Bis-Tris NuPage Gels	NP0321BOX	ThermoFisher
Silver staining kit	<u>24612</u>	ThermoFisher
Polymyxin B	1405-20-5	Sigma Aldrich
siRNA oligonucleotides for LRP1	AM51331	Thermo Scientific

2.2 List of antibodies

Antibody	Species	Catalogue number	Supplier
ImmPRESS Goat Anti-Rabbit	Horse, recombinant	MP-7541-15	Vector, USA
Anti-his 6x	Mouse, monoclonal	Ab18184	Abcam
Anti-Beta chain LRP1	Rabbit, monoclonal	EPR3724	Abcam
Anti-SMAD2/3	Rabbit, recombinant	Ab202445	Abcam
Anti-phospho SMAD2/3	Rabbit, monoclonal	S465/S467	R&Dsystems
Anti-FAK	Rabbit, monoclonal	Ab40794	Abcam
Anti-phospho FAK	Rabbit, polyclonal	Ab4792	Abcam
Anti-SMAD7	Mouse, monoclonal	MAB2029	R&Dsystems
Anti-actin antibody	Goat, polyclonal	(I-19) sc-1616	Santa Cruz Biotechnology
Anti-ADAMTS-5 catalytic domain			(Gendron C et al., 2007)
Anti-A2M	Rabbit, polyclonal	Ab58703	Abcam

2.3 Transgenic mouse models

2.3.1 Declaration of Ethics

All procedures compiled during this research project were carried out in accordance with the UK Home Office guidelines and regulations under the Animals (Scientific Procedures) Act 1986 (ASPA) and the EU Directive 2010/63/EU. This work was conducted under the project licences granted to Professor George Bou-Gharios PPL70/9060, and a personal licence (PIL. ICCCC3E55) granted to Maria Martina Meschis for the experiments after the approval of Liverpool University's Animal Welfare and Ethical Review Body (AWERB), Schedule 1 (Sch1) humane killing of mice and the collection of the resultant tissue for analysis. *In vivo* experiments were conducted to find the optimal number of animals to use, as requested by the 3R (replacement, reduction, and refinement).

2.3.2 Mouse colony establishment and Cre/*loxP*-based system for LRP1 deletion *in vivo*

All mice were housed and maintained within the University of Liverpool's Biomedical Service Unit (BSU) in accordance with Home Office UK guidelines. Mice were maintained in a specific pathogen free (SPF) environment, under a 12-hour light/dark cycle, and granted access to food and drinking water *ad libitum*. The Cre/*lox* system is one of the most versatile and sophisticated tools generated for gene editing and manipulation. This genetic method is characterised by the presence of the Cre protein, a site-specific DNA recombinase, which allows the DNA recombination between specific sites, also known as *loxP*-flanked "stop" sequences (Nagy, 2000). These sites include two directly repeated specific binding sites for Cre protein where it can excise the *loxP* flanked DNA inducing the inactivation of the gene by recombination. The Cre-*loxP* is a spatiotemporally controlled system of mutant mice because of the presence of a Cre-driver strain where the Cre recombinase expression is regulated by a promoter of cells or tissue of interest

(McLellan, et al., 2017). By breeding the Cre-driver strain with a floxed mouse strain it is possible to generate conditional knockout mice, where the time and specificity of recombination occurs by a promoter and/or enhancer (Figure 2.1). To induce the Cre/loxP system activation in a precise time and cell, the exogenous inducer such as tamoxifen (tx) has been created (Kühn, et al., 1995; Gossen & Bujard, 1992). Tamoxifen-inducible cre system was produced by adding an oestrogen receptor containing a mutated ligand binding domain (ER-LBD) to the cre protein. The tamoxifen-induced modified cre protein is also known as CreERT and it is localised in the cytoplasm of cells bound to heat shock protein 90 (HSP90) (Metzger & Chambon, 2001). In the presence of tamoxifen, the complex between CreRT and HSP90 is altered and CreRT can translocate to the nucleus where upon its binding to loxP sites the recombination occurs. In this system, a systemic administration of tamoxifen was performed by intraperitoneal injection (IP) and oral gavage (OG).

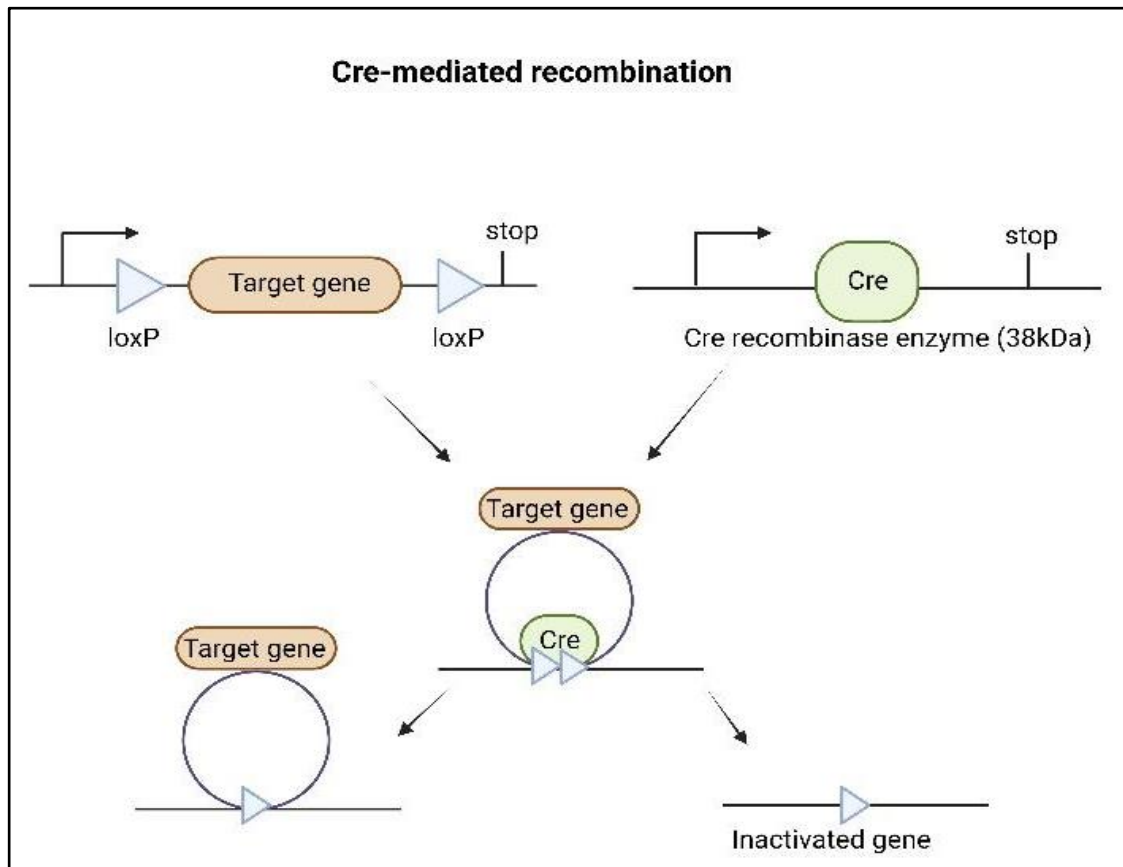


Figure 2.1 Tamoxifen-dependent gene deletion system. Mechanism of Cre-loxP system. Cre recombinase recognizes the loxP sites of specific 34 bp DNA sequences. General breeding strategy for conditional mutation using loxP and Cre driving mouse line. Figure realised using Biorender.com.

2.3.3 Inducible knockout of LRP1 in fibroblasts (COL1A2-LRP1fl) and pan tissue (ROSA-LRP1fl)

Mice containing the LRP1 floxed transgene were purchased from the Jackson Laboratory (Strain #:012604). The LRP1^{flx/flx} mice have a floxed Neo cassette upstream of the transcription start site (TSS) and a single loxP site downstream of exon 2 of the targeted *LRP1* gene were bred with mice carrying the transgene for a COL1A2 driven CreERT² B6CB-Tg (Col1a2-17=1.5kbenh-350mp-CreErt2) 3.18/Liv, generated by the Bou-Gharios Lab (Bou-Gharios et al., 1996; De Val et al., 2002; Li et al., 2017) and mice R26-CreERT2 (Strain #:008463). The resulting offspring were genotyped and

heterozygote LRP1 floxed +/-, Cre +/- animals were interbred to yield and maintain a colony of double transgenic mice (LRP1 floxed +/+, Cre +/-).

2.3.4 COL1A2-R26TmG fibroblast-specific Cre reporter mice

Female mice containing the reporter construct B6CB; 129-(Cg)-Gt (ROSA) 26Sortm4 (ACTB-tdTomato,-EGFP) Luo/Liv (purchased from Jackson Laboratories, 007676), were bred with male mice containing the COL1A2 driven CreERT2 B6CB-Tg (Col1a2-17=1.5kbenh-350mp-CreErt2) 3.18/Liv. The resulting offspring were genotyped for both mTmG and Cre transgenes as heterozygous, double transgenic (mTmG +/-, Cre +/-).

2.4 Mouse genotyping

2.4.1 Protein K based DNA extraction

Genomic DNA was extracted from ear notch biopsies to identify each genotype animal. Notches were obtained from mouse pups. Genomic DNA was extracted using the following protocol. Ear notches were digested in 100 μ L lysis buffer (50 mM Tris-HCl pH 8.0, 0.1 M NaCl, 1% SDS, 20 mM EDTA) (Table 2.1) and 10 μ L of proteinase K (Sigma Aldrich) to a final concentration of 2 mg/mL in 50 % glycerol incubated at 55 °C overnight in a water bath. The following day, samples were then vortexed at 13,000 rpm for 3 min, the supernatant transferred to clean, labelled 1.5 mL tubes (Eppendorf), and the remaining tissue was discarded. An equal volume of isopropanol (Sigma Aldrich) was added to the supernatant and samples were centrifuged at 14,000 x g for 3 minutes and the new supernatant was removed. A clear pellet of DNA was obtained in the bottom of the Eppendorf and was then washed with 500 μ L of 70% EtOH (Sigma Aldrich) and left to air dry at room temperature for 10 minutes. DNA was reconstituted and resuspended in 50 μ L ddH₂O for one hour at room temperature, or at 4 °C overnight. DNA concentration was then determined using a NanoDrop 200 (Thermo Scientific) prior to PCR analysis. A 260/230 value \geq 0.6 was acceptable for genotyping PCR. All the solutions

were stored at room temperature. Proteinase K was used from a stock concentration 20 mg/mL in 50 % Glycerol and stored at -20 °C.

Table 2.1 Lysis buffer reagents.

Reagents	Volume
50mM Tris-HCL (pH=8)	4.5 µL of 2M stock solution
0.1M NaCl	7 µL of 3M stock solution
1% SDS	8 µL of 10 % stock solution
20mM EDTA	7.2 µL of 500mM stock
ddH ₂ O	144.3 µL

2.4.2 Polymerase Chain Reaction (PCR)

For the gene PCR reaction 50 ng of genomic DNA was added to 12.5 µL of REDtaq ReadyMix PCR Reaction Mix (20 mM Tris-HCl pH 8.3, 100 mM KCl, 3 mM MgCl₂, 0.002% gelatin, 0.4 mM dNTP mix, 0.06 unit/mL of Taq DNA Polymerase, Sigma Aldrich) with the addition of 0.5 µM of each primer; ddH₂O was added to make a final reaction mixture volume of 25 µL. Primer pairs for genotyping were as follows (Table 2.2); LRP1 Flox forward 5'-CATACCCTCTTCAAACCCCTTCCTG - 3', LRP1 Flox Reverse 5'-GCAAGCTCTCCTGCTCAGACCTGGA - 3'. Cycle conditions were as follows: Genotyping - 1 cycle of 94°C for 3 min, 35 cycles of 94°C for 30 s; 65°C for 30 s; 72°C for 30 s, followed by a final cycle of 72°C for 2 min. PCR products were separated by gel electrophoresis and imaged using a BioRad Gel Doc XR+ System.

Table 2.2 Primer pairs for genotyping. Cycle conditions were followed by a final cycle of 72 °C for 5 min.

GENE		PRIMER SEQUENCE (5' > 3')	Cycle condition	AMPLICON
CRE	FOR	GCATTACCGGTTCGATGCAACGAGTGATGAG	68 °C for 5min	389bp

	REV	GAGTGAACGAACCTGGTCGAAATCAGTGCG		
INTERNAL	FOR	TGGACAGGACTGGACCTCTGCTTTCCTAGA	68°C for 15 sec	194bp
	REV	TAGAGCTTTGCCACATCACAGGTCATTGAG		
LacZ	FOR	GTTGCAGTGCACGGCAGATACACTTGCTGA	68°C for 40 sec	389bp
	REV	GCCACTGGTGTGGGCCATAATTCAATTCGC		
LRP1 flox	FOR	CATACCCTCTTCAAACCCCTTCCTG	72°C for 40 sec	291 bp (WT)
	REV	GCAAGCTCTCCTGCTCAGACCTGGA		350 bp (KO)

2.4.3 Agarose Gel Electrophoresis

Agarose gels of 1-2 % were prepared by melting agarose (Sigma Aldrich) in 1 % TAE in a microwave, 4 µL of SYBR Safe (Invitrogen) was added to 200 µL gel. Gels of 1 % were used for DNA fragments below 500 bp, 2 % was used for fragments larger than 500 bp. To estimate DNA fragment size, one well was loaded with 5 µL of 2-Log DNA Ladder (New England Biolabs). 15 µL of PCR reaction mix was added to each well. Samples were electrophoresed for ≥ 50 minutes at 120 V on a 2 % agarose gel.

2.5 Animal Research Sample Size Calculation

Treatments in loss of function experiments were performed in 5-6 months old animals. First Tx was administered followed by bleomycin injury. Sample size for the *in vivo* experiments were piloted to find the optimal number of animals to use, as requested by the 3R. Power calculation for sample size were performed using OpenEpi an free on-line platform for calculation as advised in “How to calculate sample size in animal studies?”, published by Journal of Pharmacology and Pharmacotherapeutics (Charan & Kantharia, 2013). The power calculation is related to the number of mice used for the bleomycin experiment. I used a level of bilateral confidence of 90%, as the method was efficient in reproducing the desired phenotype. The main purpose of the bleomycin administration was to reproduce a human fibrosis model in

terms of progressive increase of disease hallmarks, an exposure to non-expose ratio equal to 0.25 was used. A percentage of outcome in the control group was set at 2% as no treatment was administered in the control group, as distilled water could potentially induce a mild parenchymal damage. The confidence was set as 25%, as suggested in literature. Not exposed versus exposed ratio was set at 0.5. The percentage of adverse event in the control group was set at 20% as treatment was non-toxic at 0.005 ng/mL.

Table 2.3 Power calculation. OpenEpi and BioMath calculated a total sample size of 25 mice divided in 17 for the bleomycin-treated group and 8 for the control group.

BILATERAL CONFIDENCE	90%
POWER	80% (advised by OpenEpi)
EXPOSE/NOT EXPOSE (RATIO)	0.25
NOT EXPOSED WITH OUTCOME	2%

2.6 Tamoxifen preparation

A final concentration of 10 mg/mL was added to 4.5 mL corn oil (Sigma Aldrich) and 500 µL 100 % molecular biology grade Ethanol (Sigma Aldrich) from 50 mg Tamoxifen (Sigma Aldrich). This was sonicated using the Soniprep 150 ultrasonic disintegrator (Henderson Biomedical) for a total of 5 minutes until tamoxifen crystals fully dissolved in 4,500 µl of corn oil (Sigma Aldrich).

2.6.1 Tamoxifen - COL1A2-LRP1fl, ROSA-LRP1fl and COL1A2-R26tdTomato mice

Three doses of 2mg/mouse were administered intraperitoneally (IP) to each animal with at least one day interval. All animals were weighed prior to dosing and the volume adjusted accordingly based on whole grams of weight. Tx was also administered by oral gavage to a group of ROSA-LRP1fl mice at two different doses: 0.5 mg and 2 mg/mouse within a two days interval. All the tamoxifen-treated mice were then allowed to recover and maintained for 7 days.

2.7 Histological examination

2.7.1 Paraffin wax histology

Lungs previously fixed with PBS at 4% of PFA and dehydrated using ethanol at 70% were processed using Leica EMTP6 tissue processor set-up for the following protocol in Table 2.4:

Table 2.4 Paraffin-embedding protocol.

Reagent	Immersion time	Drain time
Ethanol 70%	30mins	Room temperature
Ethanol 90%	30mins	Room temperature
Ethanol 100%	10mins	Room temperature
Ethanol 100%	10mins	Room temperature
Ethanol 100%	10mins	Room temperature
Ethanol 100%	15mins	Room temperature
Xylene	10mins	Room temperature
Xylene	20mins	Room temperature
Xylene	30mins	40 °C
Wax	240mins	60 °C

After tissue processing, lungs were removed from the tissue processor machine and finally embedded in wax using a Leica EG1150 Tissue Embedder with a caudal orientation. Sections of 4.5 µm thickness were obtained using a RM2265 Leica microtome.

2.7.2 Tissue Sectioning

4,5 µm sections were cut using the Micron HM355S microtome with cool-cut and tissue transfer system (Thermo Scientific) and collected on Superfrost™ Plus microscope slides (Thermo Scientific). Slides were stored at room temperature prior to use for staining and analysis.

2.7.3 Preparation for slides staining: dewax

Slides were de-waxed using the following protocol in Table 2.5. Once dewaxed, slides were stored in water until staining.

Table 2.5 Dewaxing protocol.

Reagent	Immersion time
Xylene	2mins
Xylene	2mins
Ethanol 100%	2mins
Ethanol 100%	2mins
H ₂ O	until starting the exp.

2.7.4 Haematoxylin Eosin Stain (H&E)

Sections were stained with Harrys Haematoxylin (Leica) for 5 minutes, H₂O for 1 minute, acid alcohol for 5 seconds, H₂O for 5 minutes, aqueous Eosin (Leica) for 3 minutes, H₂O for 15 seconds, followed by dehydration through graded ethanol and xylene. Slides were cover-slipped with DPX mounting media (Sigma Aldrich). Stained slides were imaged using a Zeiss LSM 800 confocal microscope.

Table 2.6 Haematoxylin Eosin Staining protocol.

Reagent	Immersion time (minutes)
Haematoxylin	5
H ₂ O	1
Acid Alcohol	0.25
H ₂ O	5
Eosin	3
H ₂ O	0.25
Ethanol 70%	0.5
Ethanol 90%	0.5
Ethanol 100%	0.5
Xylene	2
Xylene	2

2.7.5 Immunohistochemistry (IHC)

This protocol was adapted from DAB (Vector Labs, SK-4100), Avidin/Biotin blocking kit (Vector Labs, SP-2001), and Vectastain (Vector Labs, PK-6100). Slides were dewaxed following the protocol described in Table 2.6.). A ring was drawn around each lung section using a Pap pen (Abcam). Slides

were incubated with citric acid (Catalog # CTS014) antigen unmasking solution (R&D Systems) by placing a polypropylene Coplin staining jar filled with the respective retrieval solution into a water bath at 92-95 °C for 3-8 minutes. Slides were then washed with distilled water then re-rinsed with PBS and blocked for endogenous peroxidase with 0.3% hydrogen peroxide for 15 min at 37 °C (Sigma-Aldrich). Further blocking for endogenous Avidin/Biotin binding was performed with an Avidin/Biotin Blocking Kit (Vector Labs) for 15 minutes each. Sections were incubated with Avidin solution for 15 minutes and then with the Biotin solution for 15 minutes at room temperature. After washing with PBS, a blocking solution for non-specific binding sites was added to the slides and incubated for 3 hours. Blocking solution was prepared with 10% v/v goat serum (Vector Labs S-1000-20) 0.1%, bovine serum albumin (BSA) (Sigma-Aldrich) in PBS1x at room temperature. Anti-LRP1 beta-chain rabbit monoclonal antibody (Abcam) to LRP1 (1 in1000) was incubated overnight at 4 °C. Rabbit IgG (1µg/mL) (Vector Labs) was used as isotype control. Slides were washed in PBS1x containing 0.1% Tween 20 (PBST) three times for 10 minutes each. Slides were then incubated with secondary antibody ImmPRESS peroxidase-micropolymer conjugated horse anti-rabbit IgG (Vector Labs) for 30 minutes at room temperature followed by incubation with Vectastain solution (Vector Labs) for 30 minutes at room temperature. The slides were washed in PBST three times for 10 minutes each. Slides were stained with 3,3'-diaminobenzidine (DAB) (Vector Labs).

2.7.6 Histology imaging acquisition

Slides were imaged using an Olympus BX60 microscope with or without a polarized filter (Nikon) as Brightfield microscopy and polarized light microscopy. Slides were imaged at 4X, 10X and 20X magnification with or without polarised filter. Polarised light was obtained positioning the polarising filter at 90° orientation. This technique relies on the birefringent properties of collagen molecules (Rittié, 2017). Quantitative measurement of the dichroism

was calculated through ImageJ Fiji using a macro, which measured the area of colour developed by dichroisms.

2.8 Cell culture

2.8.1 Isolation and maintenance of murine primary lung fibroblasts

Mice were euthanised by CO₂ and the lungs were immediately isolated and transferred in falcon tubes containing fresh media in an animal primary tissue culture hood. Lungs were placed in Petri dishes and dissected to remove hearts and trachea. Tissues were chopped into small slices (1-2 mm³) using a sterile scalpel. The tissue slices were then incubated for 2 hours in a DMEM/F12 supplemented with at 1% of Penicillin/Streptomycin (P/S) and 10% w/v of crude collagenase Type 1 (Sigma Aldrich) from clostridium histolyticum. Cells were resuspended and filtered through a 100 µm cell strainer (Starlab). Following this, the mixture was centrifuged at 300 g for 5 minutes, to obtain a cellular pellet. The pellet was resuspended in DMEM/F12 and centrifuged at 300 g for 5 minutes. After centrifugation, the supernatant was discarded, and the pellet resuspended in 5 mL of DMEM/F12. The cells were cultured in complete DMEM/F12 containing 10% FBS at 37°C and 5% CO₂ for 3-4 days, until cells reached confluence.

2.8.2 Maintenance of human primary lung cells

MRC5 immortalised lung fibroblast cell lines (human lung fibroblast cells), BEAS-2B (human epithelial bronchial lung cells) and A549 adenocarcinoma bronchial epithelial cells were purchased by ATCC and after amplification were stored in liquid nitrogen, maintained and grown in DMEM/F-12 Ham (Sigma-Aldrich) media supplemented with 10% FBS and 1% P/S (Thermo Fisher Scientific) and incubated at 37 °C with 5% CO₂.

2.9 Statistical Analysis

Statistical tests were used to discern between different experimental groups, using Student t-test for comparison between two groups, and 1 and 2-way-

Analysis of variance (1-way ANOVA and 2-way ANOVA) for more than 2 groups. 1-way-ANOVA was used for multiple comparison for analysis between experimental samples greater than 2, the analysis was also accompanied by Tukey's multiple comparisons test for further comparisons between groups. All statistical analyses were performed using Prism. Information regarding power calculation of sample sizes are referred to paragraph 2.5 in Table 2.3.

Chapter 3 Detrimental effect of global *Lrp1* deletion in adult mice

Summary

Global deletion of *Lrp1* was induced to investigate its role in lungs, since lung tissue consists of a variety of cell types. Although, embryonic lethality of total deletion of *LRP1* has been reported (Herz, et al., 1992), in this chapter I found that total *Lrp1* ablation in adulthood causes a rapid loss of weight (>20%). *Lrp1* deletion resulted in abnormalities in the gastro-intestinal tract of mice.

3.1 Introduction

Lungs are the essential component of the respiratory system. The complexity and difficulty of studying lung tissue is associated with the presence of a high number of different types of cell. In fact, it has been estimated that lung tissue consists of 58 different cell populations including 41 out of 45 previously known cell types and 14 previously unknown ones (Travaglini, et al., 2020). Due to the presence of a mixture of cells in lungs, a global deletion of *Lrp1* gene is advantageous to better explore its role in lung tissue.

Previous studies have demonstrated that total loss of *Lrp1* can lead to lethality during the embryonic development exercising a necessary function in the vascular wall formation and integrity (Nakajima, et al., 2014; Herz, et al., 1992). Moreover, LRP1 protein results ubiquitously expressed and are involved not only during the embryonic development but also for the maintenance of adult tissue homeostasis. Its expression is reported in many cell types including hepatocytes, adipocytes, neurons, vascular smooth muscle cells, fibroblasts and macrophage (Rohlmann, et al., 1996; Liu, et al., 2015; Boucher, et al., 2003; May, et al., 2004). To study the effects of *Lrp1* loss in adult, a transgenic mouse model phenotype was explored inducing a global LRP1-deficiency in the postnatal stage.

3.2 Aim and objectives

A global deletion of *Lrp1* was induced to explore its role in the lung .

The overarching aims for this study were:

- i. Establishment of global conditional deletion of LRP1 in mice. The objective was to determine *Lrp1* loss in different tissues for validation of this system.
- ii. To determine the impact of global *Lrp1* loss in lung fibrosis. This aim was re-formulated due to an expected rapid loss of weight (>20%) after deletion of *Lrp1* in the whole body. The new aim was to define a role of *Lrp1* in the maintenance of gastro-intestinal tract functions.

3.3 Chapter-specific methods

3.3.1 Transgenic mice and tamoxifen administration routes

LRP1^{flox/flox} mutant mice were crossed with tamoxifen-inducible Cre recombinase transgene R26CreERT2 mice to generate LRP1 conditional pan tissue KO mice as described in paragraph 2.3.4. (Figure 3.1). Tx injections were performed as described in 2.6.1 paragraph (Table 3.1). Additionally, transgenic homozygous and heterozygous mice were administered with Tx by OG administration at two different doses: 0.5 mg/mL and 2mg/ mL three times over a week with 2 and 4 days of interval (Table 3.2).

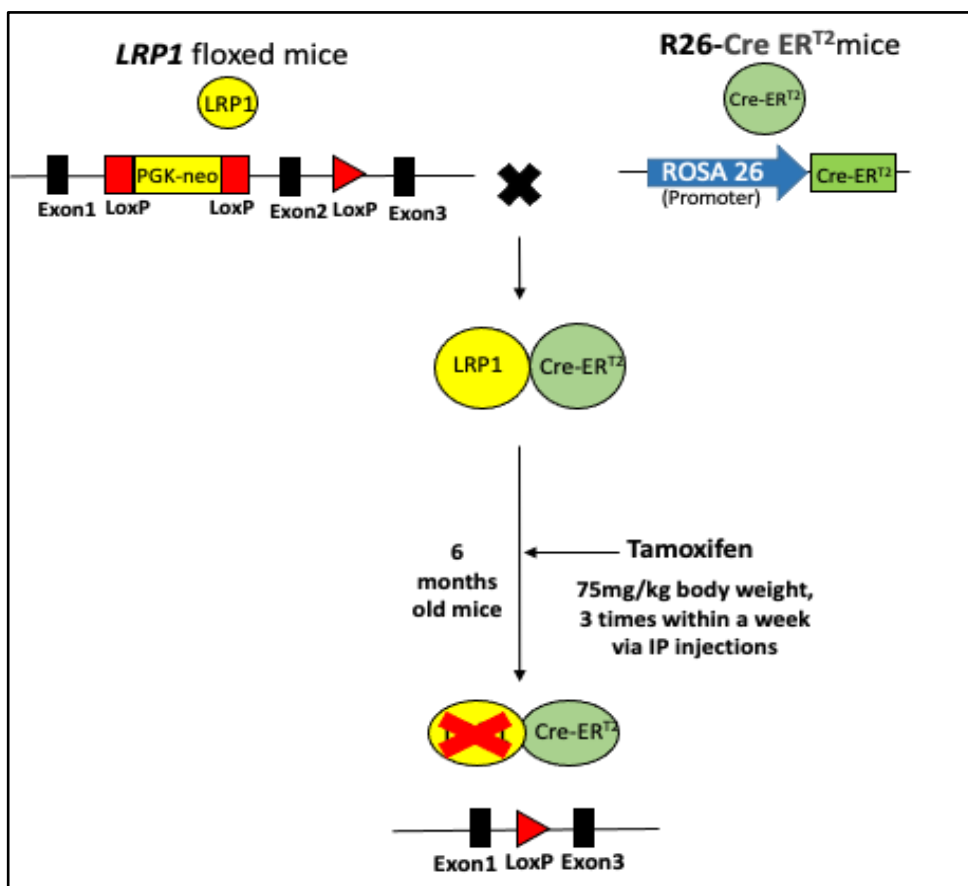


Figure 3.1 Flowchart of generating conditional knockout mice: LRP1 (flox/flox) /ROSA26 (cre/ERT2) (KO). Tamoxifen -inducible Cre/loxP enables LRP1 gene control both spatially and temporally. Tx-induced excision of the loxP-flanked STOP cassette upstream enables LRP1 transcription. These R26CreER mutant mice have a tamoxifen-inducible Cre-mediated recombination system driven by the endogenous mouse Gt(ROSA)26Sor promoter.

Table 3.1 Tamoxifen administration by intraperitoneal (IP) injection (2mg/mL).

IDs	Genotyping
LRP1 36.2	Lpr1fl: +/-
LRP1 36.4	Lpr1fl: +/+
LRP1 37.1	Lpr1fl: +/-
LRP1 37.3	Lpr1fl: +/-
Lrp1Col1a 54.1	Ert2Cre: +/ LPR1fl: +/+
LRP1Col1a2 56.1	Ert2Cre: +/+ LPR1fl: +/+
LRP1Col1a2 56.2	Ert2Cre: +/ LPR1fl: +/+
LRP1Col1a2 56.3	Ert2Cre: +/ LPR1fl: +/+
LRP1Col1a2 57.1	Ert2Cre: +/+ LPR1fl: +/+
LRP1Col1a2 59.1	Ert2Cre: +/+ LPR1fl: +/+
LRP1Col1a2 59.2	Ert2Cre: +/+ LPR1fl: +/+
LRP1Col1a2 59.3	Ert2Cre: +/+ LPR1fl: +/+
LRP1Col1a2 60.1	Ert2Cre: +/+ LPR1fl: +/+
LRP1Col1a2 61/1	Ert2Cre: +/+ LPR1fl: +/+
LRP1Col1a2 61/2	Ert2Cre: +/+ LPR1fl: +/+
LRP1Col1a2 61/3	Ert2Cre: +/+ LPR1fl: +/+
LRP1Rosa 47.1	LPR1fl: +/+ RosaCre: +/+
LRP1Rosa 51/1	LPR1fl: +/ RosaCre: +/+
LRP1Rosa 54.1	LPR1fl: +/+ RosaCre: +/+
LRP1Rosa 54.2	LPR1fl: +/+ RosaCre: +/+
LRP1Rosa 54.3	LPR1fl: +/+

	RosaCre: +/+
LRP1Rosa 57/1	LPR1fl: +/+ RosaCre: +/+
LRP1Rosa 59.1	LPR1fl: +/+ RosaCre: +/+
LRP1Rosa 59.2	LPR1fl: +/ RosaCre: +/+
LRP1Rosa 62.1	LPR1fl: +/+ RosaCre: +/+
LRP1Rosa 62.3	LPR1fl: +/+ RosaCre: +/+
LRP1Rosa 62.4	LPR1fl: +/+ RosaCre: +/+
LRP1Rosa 63.1	LPR1fl: +/+ RosaCre: +/+
LRP1Rosa 63.2	LPR1fl: +/+ RosaCre: +/+

Table 3.2 Tamoxifen administration by oral gavage (OG).

IDS	Genotyping	Dose
LRP1ROSA 72/1	LRP1 fl: WT RosaCre: +/-	2 mg/mouse
LRP1ROSA 72/2	LRP1 fl: +/+ RosaCre: +/-	2 mg/mouse
LRP1ROSA 73/1	LRP1 fl: WT RosaCre: +/-	2 mg/mouse
LRP1ROSA 73/2	LRP1 fl: +/+ RosaCre: +/+	2 mg/mouse
LRP1ROSA 73/3	LRP1 fl: +/+ RosaCre: +/-	0.5 mg/mouse
LRP1ROSA 73/4	LRP1 fl: WT RosaCre: wt	0.5 mg/mouse
LRP1ROSA 76.2	LRP1 fl: +/+ RosaCre: wt	0.5 mg/mouse
LRP1ROSA 76.3	LRP1 fl: +/+ RosaCre: +/-	0.5 mg/mouse
LRP1ROSA 77.1	LRP1 fl: +/+ RosaCre: +/+	2 mg/mouse
LRP1ROSA 77.2	LRP1 fl: +/- RosaCre: +/-	2 mg/mouse
LRP1ROSA 79.2	LRP1 fl: +/- RosaCre: wt	0.5 mg/mouse
LRP1ROSA 79.3	LRP1 fl: +/- RosaCre: +/-	0.5 mg/mouse
LRP1ROSA 80.1	LRP1 fl: +/- RosaCre: +/-	2 mg/mouse
LRP1ROSA 80.4	LRP1 fl: +/+ RosaCre: +/-	2 mg/mouse

3.3.2 Quantitative reverse transcriptase (qRT)-PCR

Approximately 30 mg of skin tissue was frozen in liquid nitrogen, then samples were reduced to fine powder, using a bioPulverizer. RNA was then extracted using the RNeasy Mini Kit (Qiagen) following the manufacturer's instructions. Briefly, 350 µl of RLT buffer was added directly to the powder

obtained from mouse tissue. Lysates were centrifuged for 3 minutes at full speed, and the supernatant was carefully transferred to RNase free Eppendorf tubes for further processing. A total of 66 ng of RNA was used from each sample to prepare cDNA using the High-Capacity cDNA Reverse Transcription Kit with RNase Inhibitor (Thermo Fisher Scientific) following the manufacturer's protocol. The 2.5 ul of the cDNA was used for each qRT-PCR reaction. Mouse TaqMan Primer/Probes sets with FAM-MGB dye from Thermo Fisher Scientific were as follows: LRP1(Mm00464608_m1), RPLP0 (Mm00725448_s1). FastStart Essential DNA Probes Master (Roche # 06402682001) was used for the detection of Real-Time PCR amplification on the LightCycler® 96 Instrument system (Roche).

3.4 Results

3.4.1 Global LRP1 loss leads to rapid weight loss of adult mice

To evaluate the effect of global loss of *Lrp1* in adult mice, pan-tissue conditional inducible LRP1 KO mice ($LRP1^{loxP/loxP}/ROSA-Cre-ER^{T2}$) were analysed. Cre-negative mice ($LRP1^{loxP/loxP}$) and fibroblast-specific conditional inducible LRP1 KO mice ($LRP1^{loxP/loxP}/COL1A2-Cre-ER^{T2}$) were tested as control groups. LRP1 KO animals ($LRP1^{loxP/loxP}/ROSA26-Cre-ER^{T2}$) started to exhibit an abrupt onset of distress including hunched posture, lack of movement with loss of muscle tone and grooming behaviour. Those mice showed a drastic weight loss (>20%) with average weight loss being 6.1, 9.4 and 20.1% at 3, 5 and 7 days from the first dose of tamoxifen, respectively (Figure 3.2 A). Due to the animal ethics compliance, seven mice were euthanized after the second dose of tamoxifen and the remaining three were terminated the day after the third dose. The control group did not show any significant weight loss over the course of the experiment (Figure 3.2 A-B).

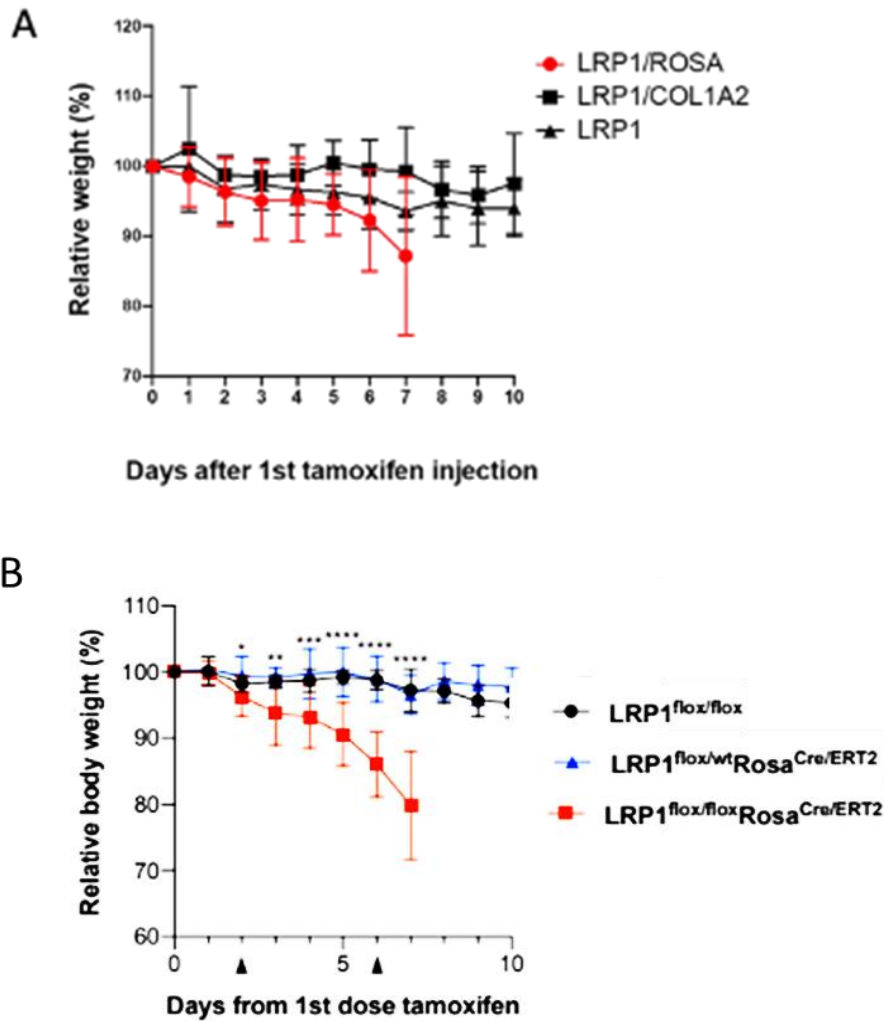


Figure 3.2 Global deletion of *Lrp1* induces rapid weight loss in adult mice. Tamoxifen-treated control (black line) and tamoxifen-treated mutant (red line for LRP1^{flox/flox} Rosa^{Cre/ERT2} and blue line for LRP1^{flox/wt} Rosa^{Cre/ERT2}) mice were administered with Tx on day 2 and 6 as indicated by arrows. Total number of controls=4 and mutant LRP1^{flox/flox} COL1A2^{CRE/ERT2} n=12, LRP1^{flox/flox} ROSA^{CRE/ERT2}=13 are shown for survival estimation. In figure B are shown the combined values within a simple linear regression. p value <*0.05 **0.01 ***0.001 ****0.0001, student t-test.

3.4.2 Assessment of LRP1 depletion in adult mice tissues

mRNA and protein levels were measured by qPCR and WB, respectively. qPCR analysis of total RNA extracted from the mouse skin tissue showed >87% reduction of LRP1 mRNA in the KO compared to wild-type mice

(Figure 3.3). LRP1 protein level in the KO skin tissue was also reduced by >86% compared to Cre-negative mice ($LRP1^{loxP/loxP}$) (WT) tissue (Figure 3.4). These results confirmed that the deletion of LRP1 after tamoxifen administration was accomplished.

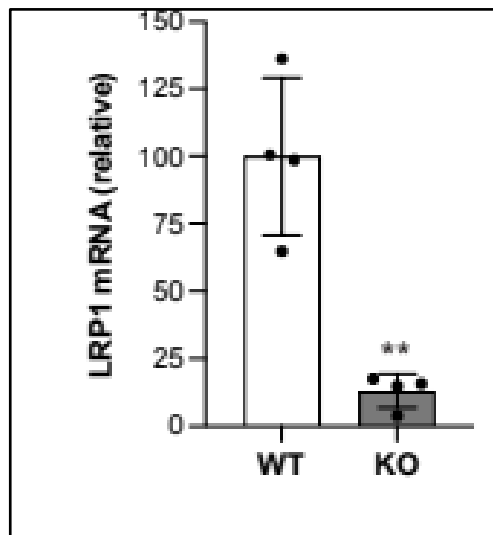


Figure 3.3 Reduced gene expression level of LRP1 in total KO mice. Comparison of LRP1 gene expression levels $LRP1^{loxP/loxP}$ (WT) and $LRP1^{loxP/loxP}/ROSA-Cre-ER^{T2}$ (KO) mice by quantitative real-time PCR (qPCR). qPCR analysis of LRP1 gene expression in the skin WT KO mice. $p < 0.01^{**}$, paired t-test.

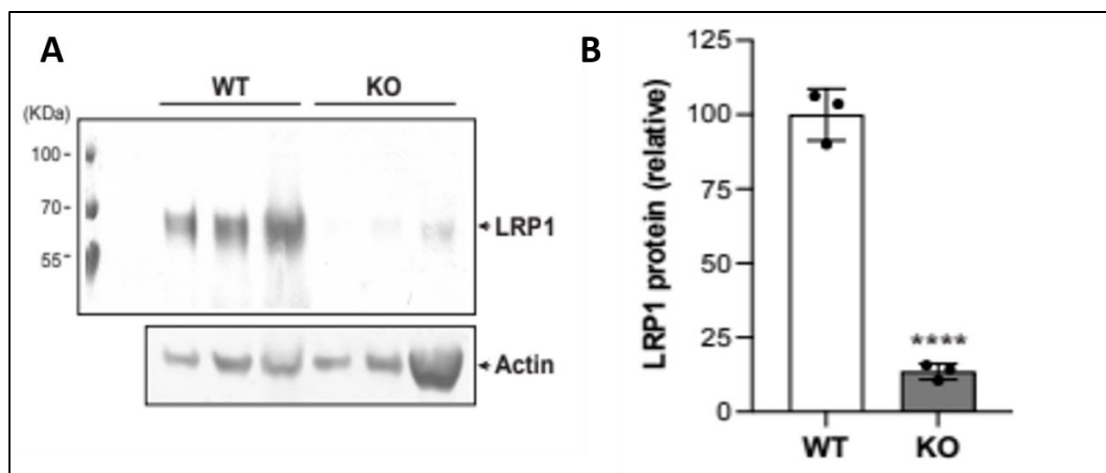


Figure 3.4 Reduced protein expression level of LRP1 in total KO mice. A) WB showing the expression of LRP1 in skin protein extracts of WT and LRP1 KO mice. B) Changes in protein expression were quantified using densitometric analysis ($n = 3$ mice per group) and normalised to actin. $****p < 0.0001$, paired t-test.

3.4.3 Evaluation of LRP1 deletion in tissue by IHC analysis

To further confirm the effective deletion of LRP1 in the whole body, investigation of expression and distribution of LRP1 protein was performed in lung and sartorius muscle tissues by IHC analysis. Results by IHC revealed that LRP1 protein is markedly diminished in KO mice on both muscle and lung tissues, while it is abundantly expressed in WT mice (Figure 3.5)

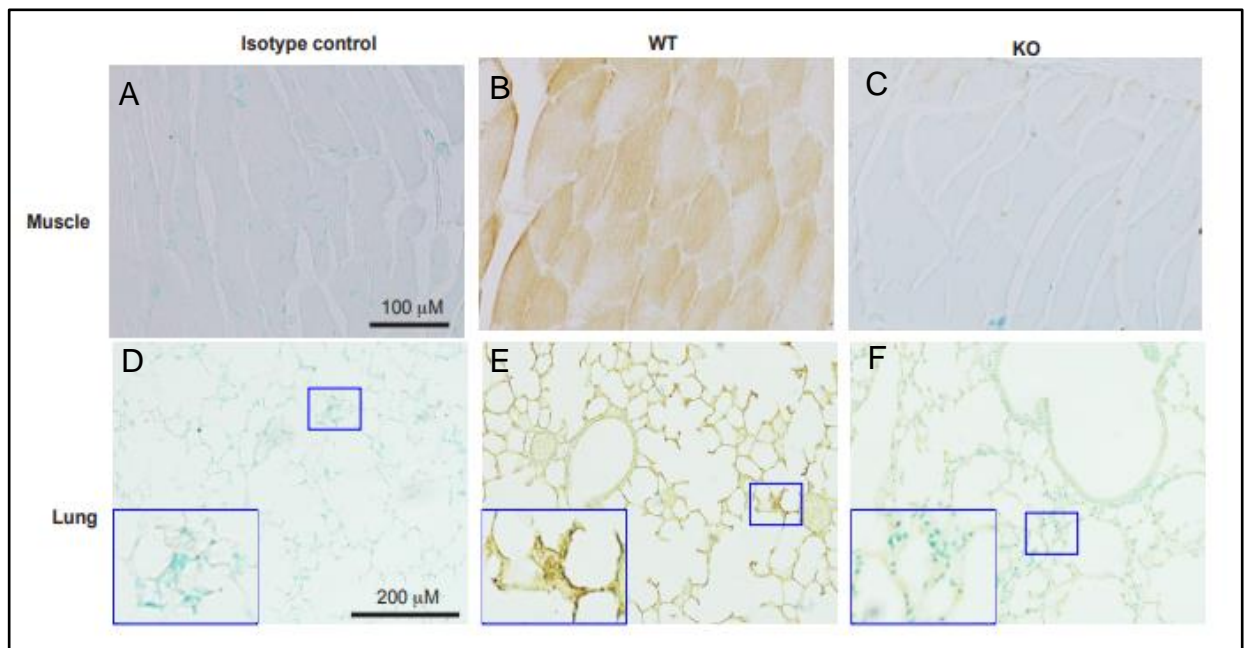


Figure 3.5 LRP1 deletion in lung and muscle tissues. LRP1 expression is shown in muscle and lung tissue in WT and KO mice. Isotype control is shown in A-D. LRP1 staining is compared between WT mice (sartorius muscle tissue in B and lung tissue in E), where it is absent in KO tissue C-F. LRP1 protein is indicated by brown staining in muscle (B) and lung (F) while fast green as counterstaining is shown in lung tissue (D-E-F). Scale bar=100μM; 200μM.

3.4.4 Global LRP1 loss results in gastrointestinal dysfunction and impairs digestive system

To determine the cause for the rapid weight loss in KO mice, a gross examination of the internal organs was performed after termination by CO₂. Dissection of intestines, stomach, liver and kidneys was made. An increased volume and altered aspect of intestine, stomach and liver tissues was observed (Figure 3.6). More specifically, the small intestine was yellowish pale

and fluid-distended in the LRP1 KO compared to WT mice. No phenotypic difference was observed in the kidneys between WT and LRP1 KO mice (Figure 3.7).

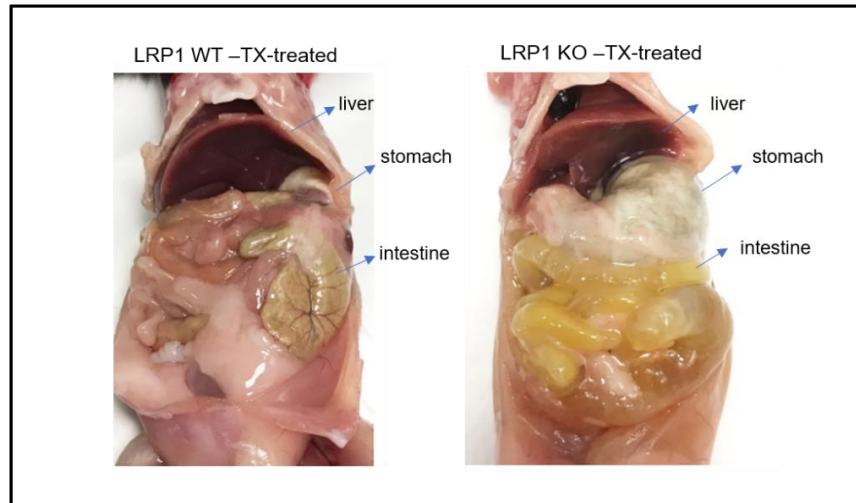


Figure 3.6 Abnormalities of gastro-intestinal tract observed during gross examination. Representative pictures of internal organs from tamoxifen-treated WT (n = 4) and homozygote LRP1 mutant (n=13) mice. Liver, stomach, and intestine are indicated by arrows.

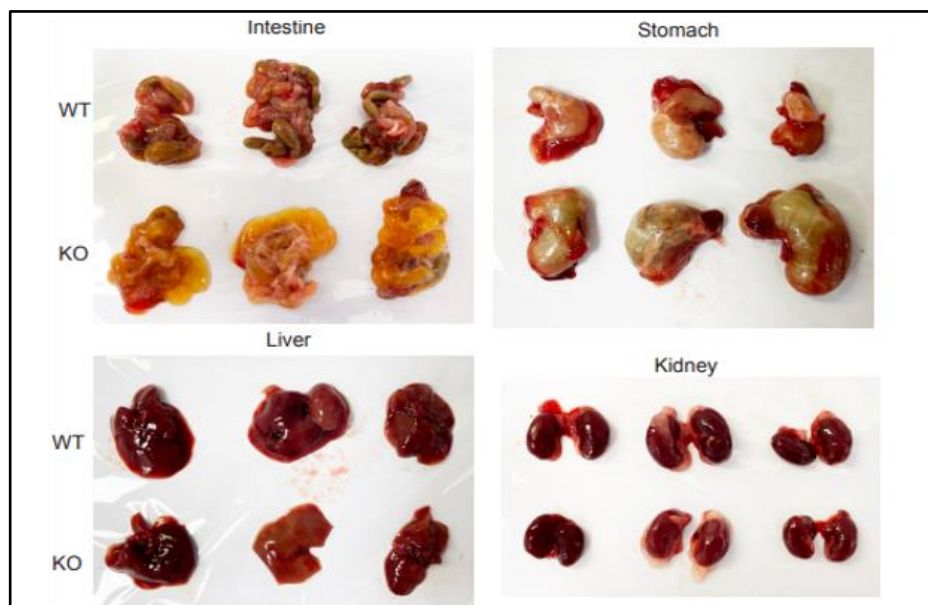


Figure 3.7 Enlarged intestine and stomach in LRP1 KO mice. Representative mice organs (intestine, stomach, liver, and kidneys) isolated from KO and WT tamoxifen-

treated mice showing the altered phenotype associated with LRP1 KO mouse in adult stage.

3.4.5 Histological abnormalities in the gastro-intestinal tract of tamoxifen-treated LRP1-KO mice

To investigate the cause of rapid weight loss of total LRP1 KO animals, intestine and stomach were analysed by histological examination. The immunohistochemical analysis of LRP1 in the digestive tracts showed the presence of LRP1 in the villi intestine whereas it was mostly negative in KO mice (Figure 3.8 A-B). LRP1 expression was not clearly localised in the stomachs of WT (Figure 3.8 C) and KO mice (Figure 3.8 D).

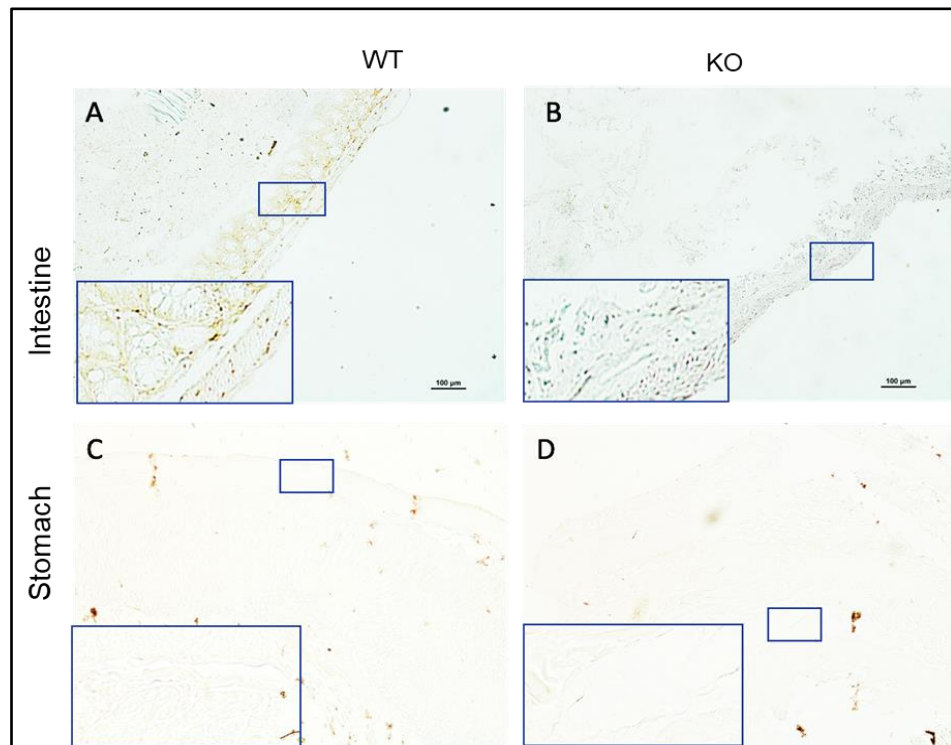


Figure 3.8 LRP1 is expressed in intestine and stomach. A-B LRP1 immunostaining in intestine of WT (A) and KO (B) mice. C-D LRP1 immunostaining in the stomach of WT (A) and KO (B) mice. Brown signal indicates LRP1 presence in tissues. Increased magnification for visualisation of villi and submucosa in intestine and stomach, respectively. Scale bar 100µm for both intestine and stomach figures.

H&E staining of stomach, intestine, liver and kidneys revealed anatomical and histological differences between WT and LRP1 KO mice (Figure 3.18).

Different parts of the intestine including duodenum and ileum showed a major difference in the villi structures and muscle cell layers between KO and WT mice (Figure 3.9). KO intestine exhibited disrupted and abnormal or sometimes absent villi compared to WT mice. An increased intestinal epithelial cell shedding was potentially detected in KO mice (Figure 3.10). Loss of the intestinal barrier integrity where smooth muscle cells appeared distorted was detected in KO when compared to WT mice (Figure 3.11). The similarly altered smooth muscle cells were observed in the stomach of KO mice. Dysregulated submucosa and muscularis layers structures were observed in KO compared to the stomach of WT mice (Figure 3.12).

Small anatomical differences were also observed in liver and kidneys between WT and KO mice (Figure 3.13). Adipose tissue was detected in the liver of KO tamoxifen-treated mice compared to WT mice where normal hepatocytes and central veins within the presence of sinusoids were found. Although no difference of both WT and KO kidneys was observed after gross examination, a high cellular infiltration was detected by H&E in kidneys of KO tamoxifen-treated mice compared to the WT (Figure 3.13).

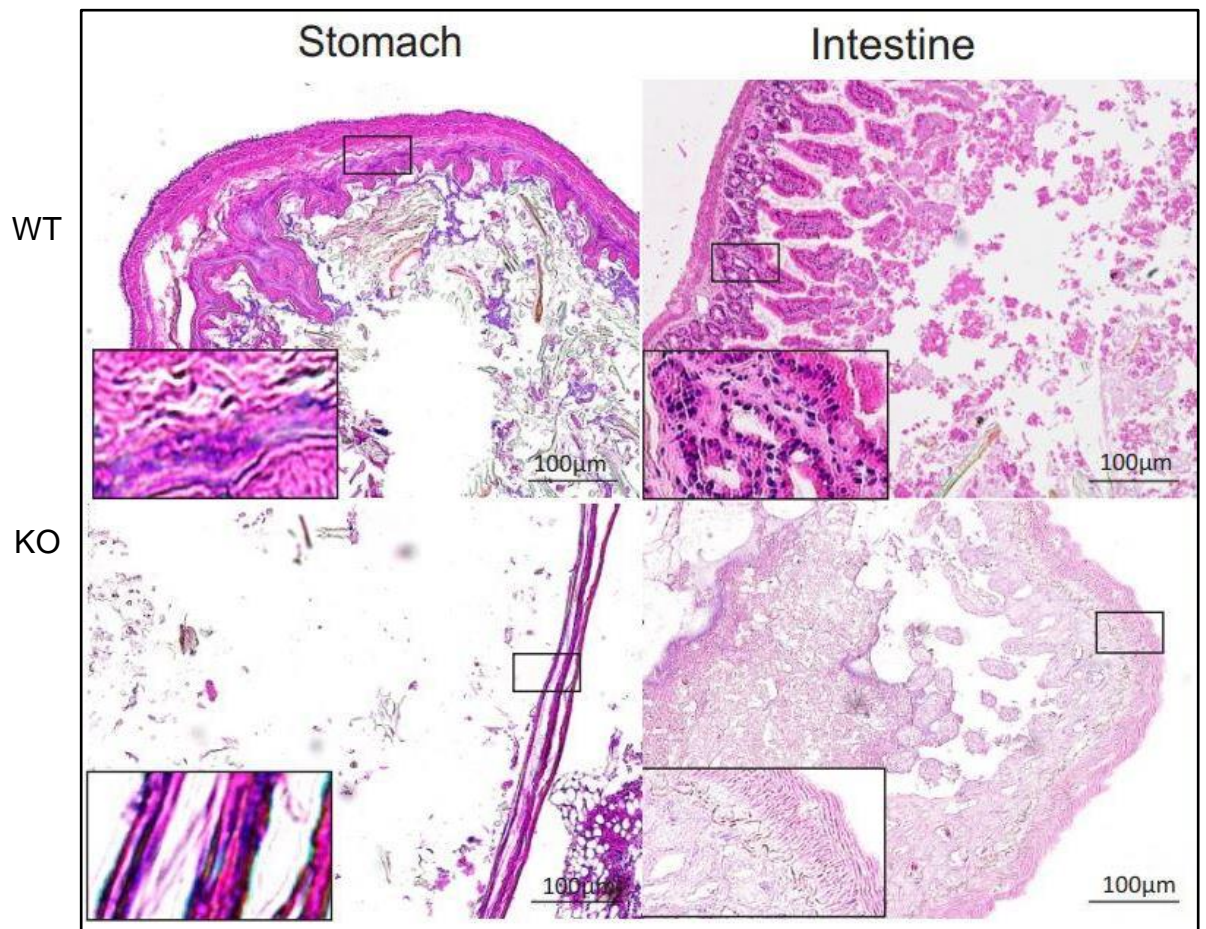


Figure 3.9 LRP1 loss causes abnormalities in stomach and intestine. Representative images of H&E-stained of WT and LRP1 KO mice are shown in a cross section. Increased magnification for the visualisation of villi and submucosa layer in intestine and stomach, respectively. Scale bar=100µm.

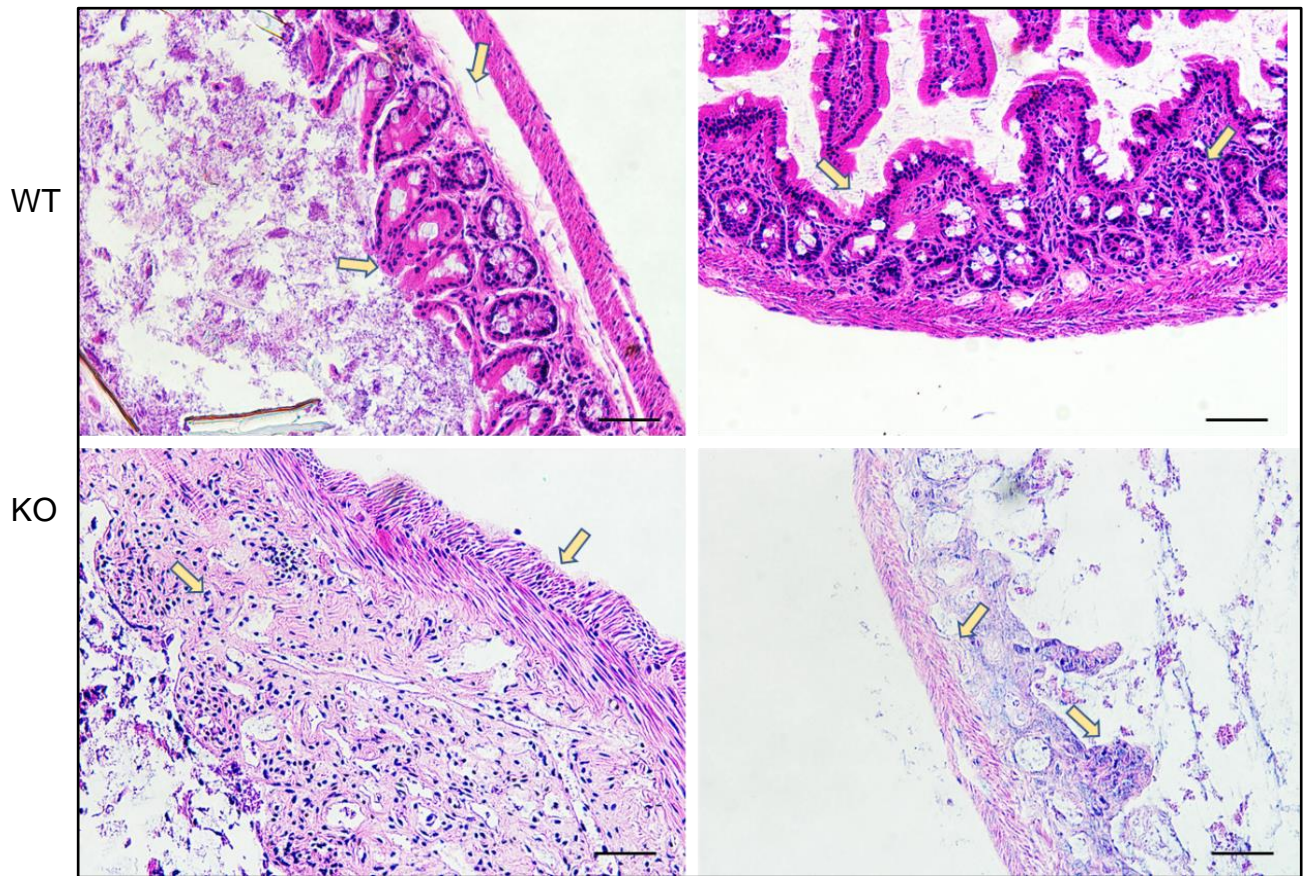


Figure 3.10 Representative H&E of intestine of WT and LRP1 KO treated mice by IP injection. Scale bar= 50 μ m. Yellow arrows indicate villi structures and muscle layer.

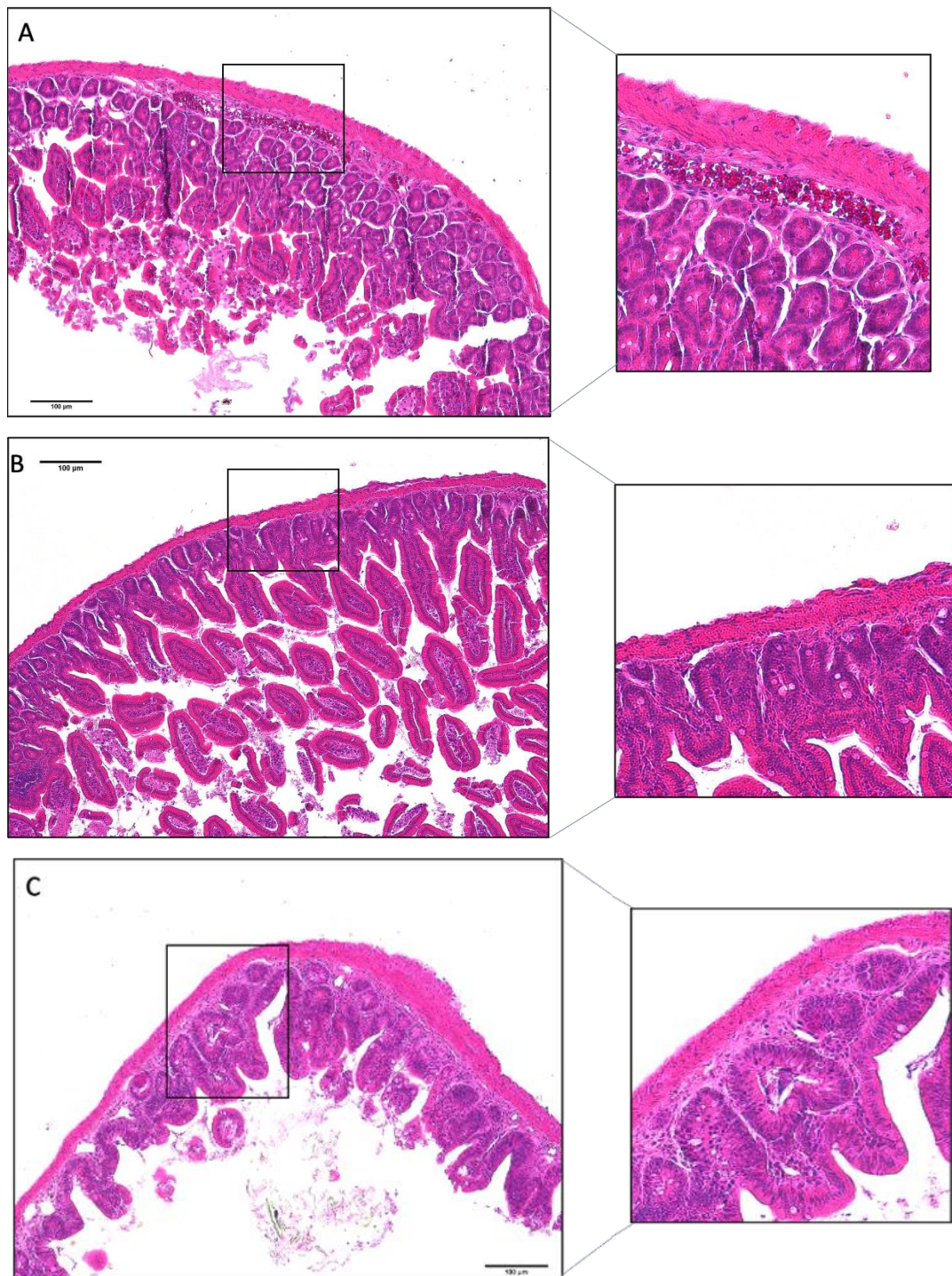


Figure 3.11 Representative images of intestine of mice by OG administration. A shows intestine of WT mouse. B and C show intestines of KO mice after Tx administration. Increased magnification for the visualisation of villi structures and submucosa. Scale bar=100µm.

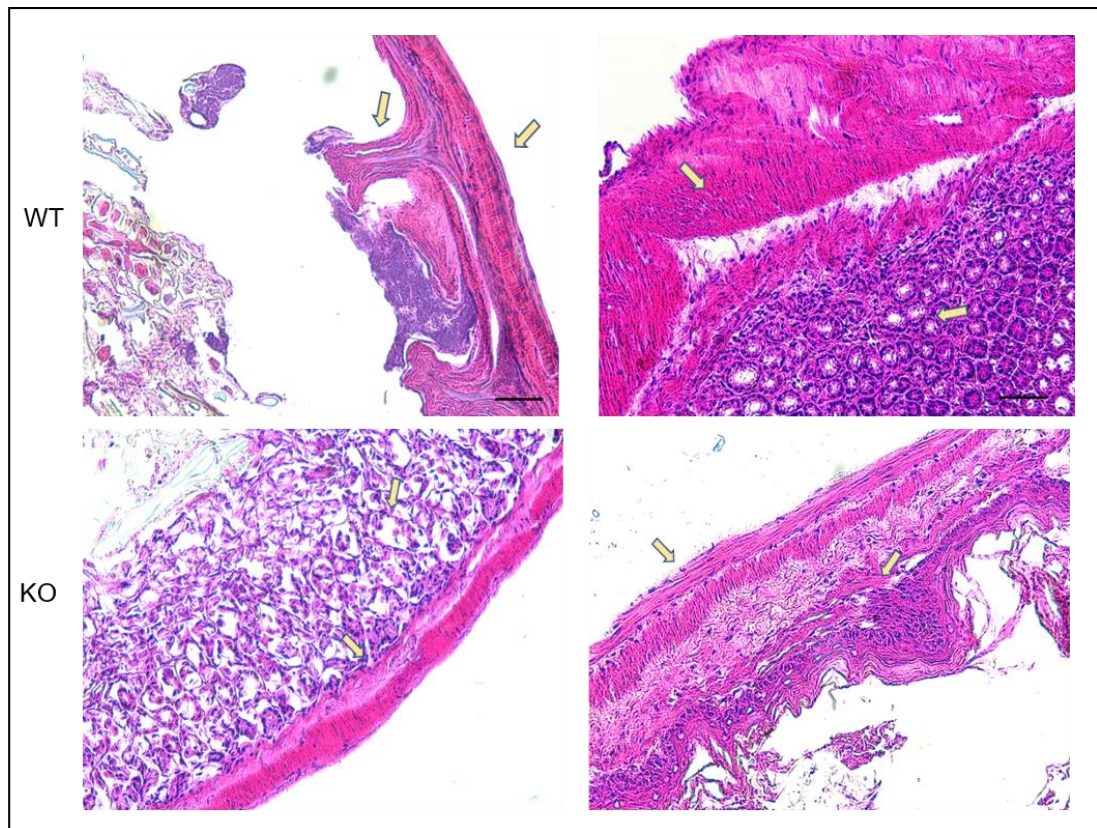


Figure 3.12 H&E of the stomach of WT and KO treated mice by IP injection. Scale bar=50 μ m. Yellow arrows indicate the distinctive structure of submucosa and muscularis layers.

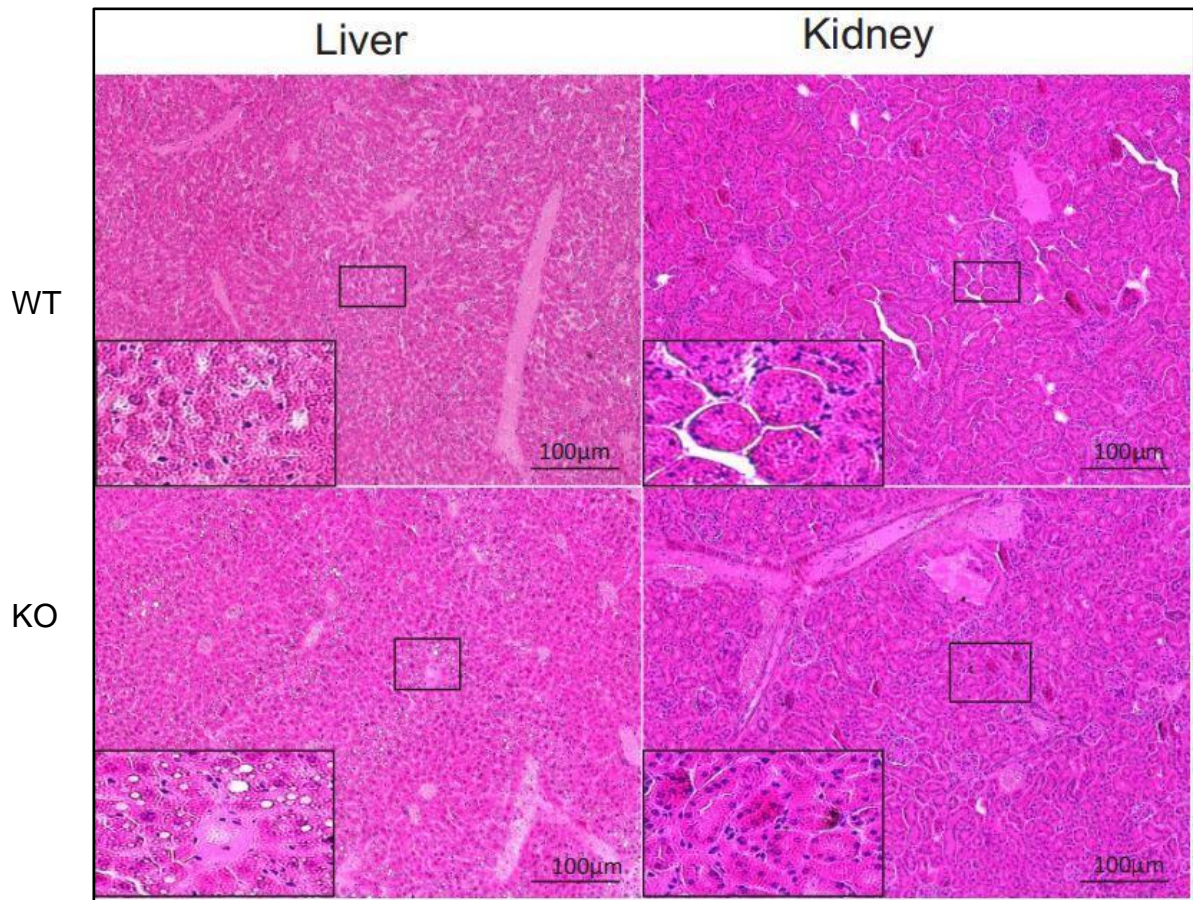


Figure 3.13 Adipocytes in liver and inflammatory cells infiltrate in kidneys of LRP1 KO mice. Representative images of H&E-stained of WT and LRP1 KO mice are shown in a cross section. Increased magnification for the visualisation of the presence of adipose cells in KO liver and inflammatory cell infiltration in KO kidney. WT liver and kidney show the presence of normal hepatocytes and glomerulus, respectively. Scale bar=100µm



Figure 3.14 Representative H&E stained auto scanned section of stomach of WT mice. Main stomach structures are indicated as m=muscularis; sm=submucosa.

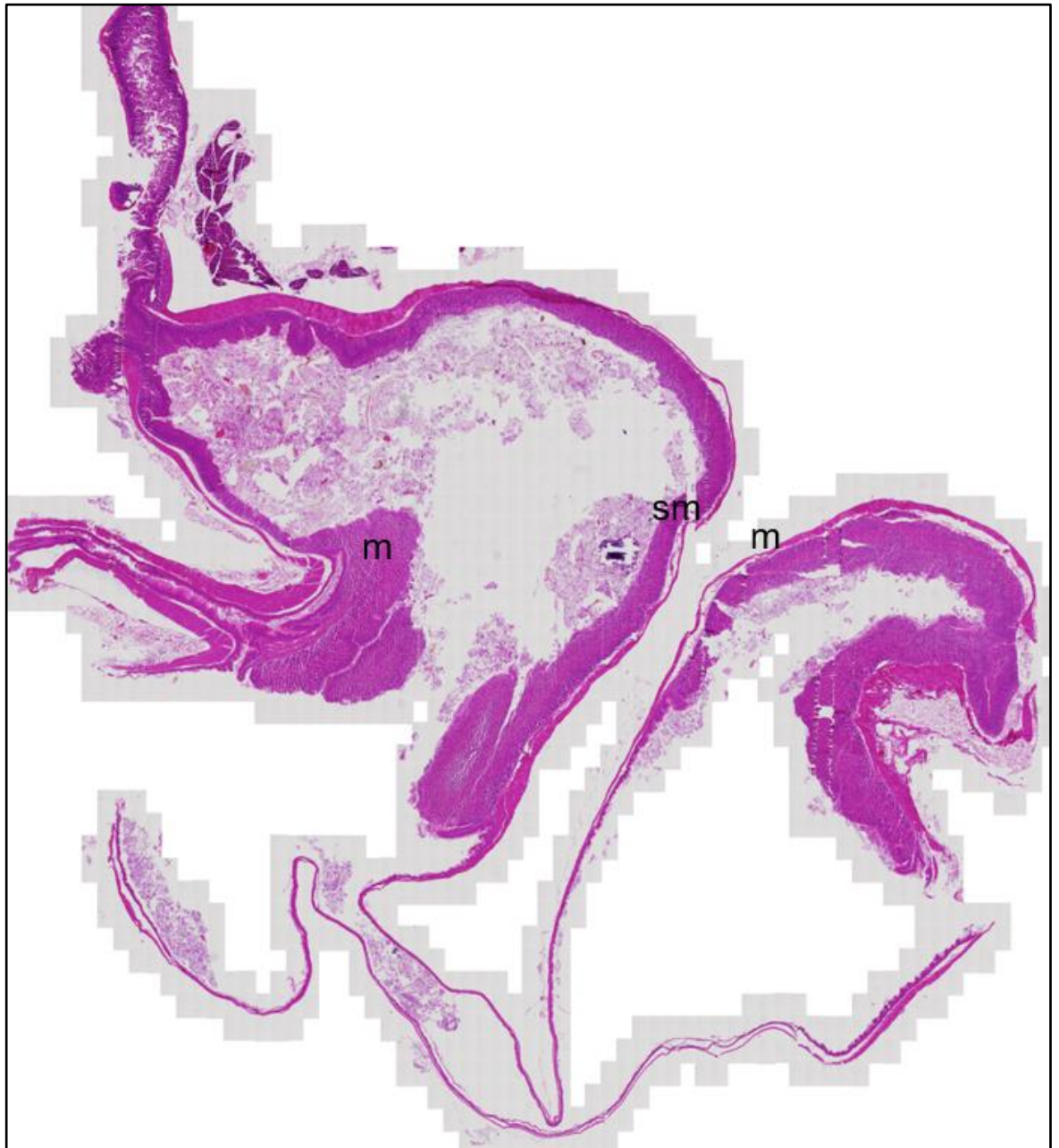


Figure 3.15 Representative H&E stained auto scanned section of stomach of LRP1 KO mice. Main stomach structures are indicated as m=muscularis; sm=submucosa.

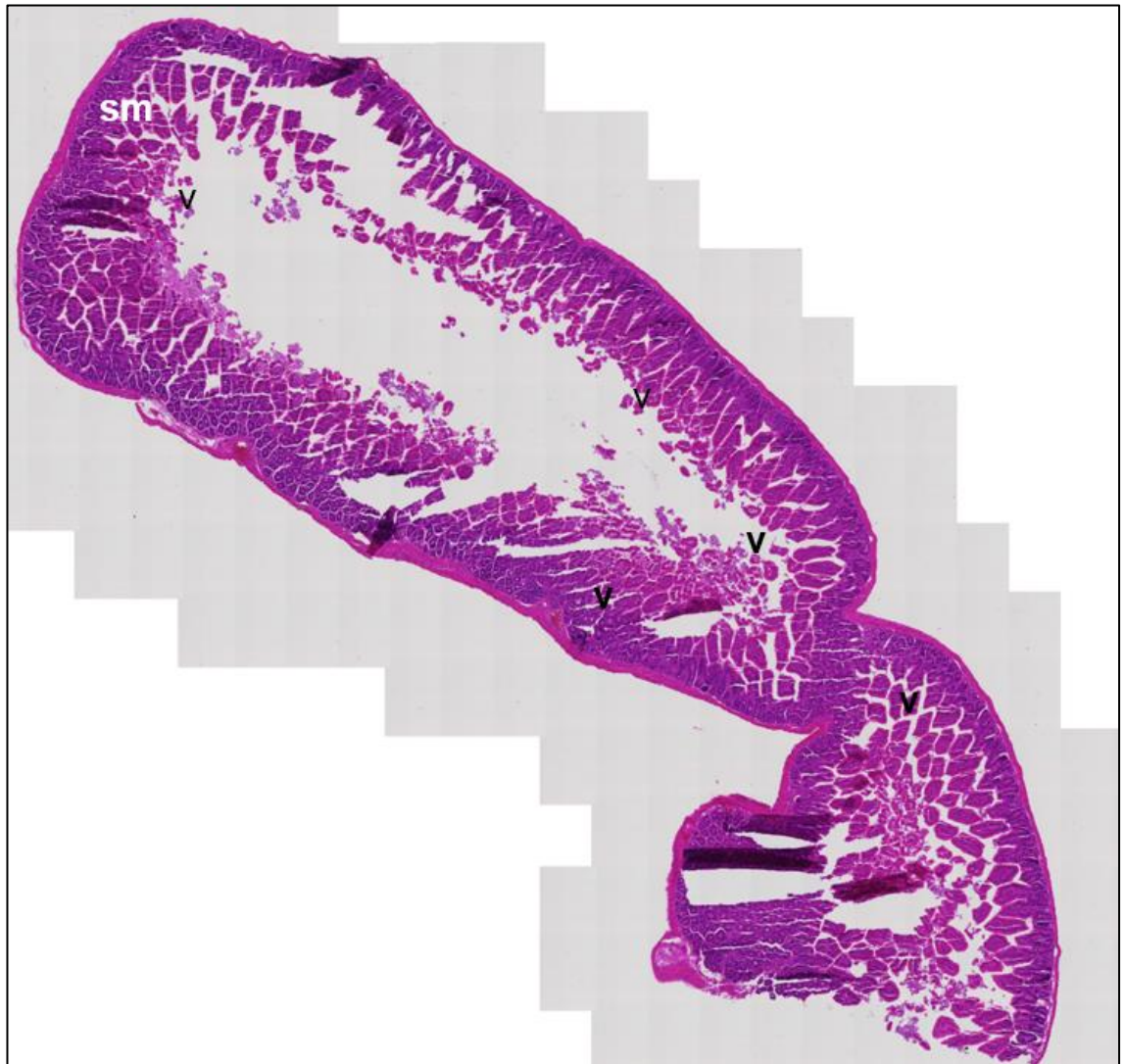


Figure 3.16 Representative H&E stained autoscanned sections of intestine of WT mice. Main intestine structures are indicated as v=villi; sm=submucosa.

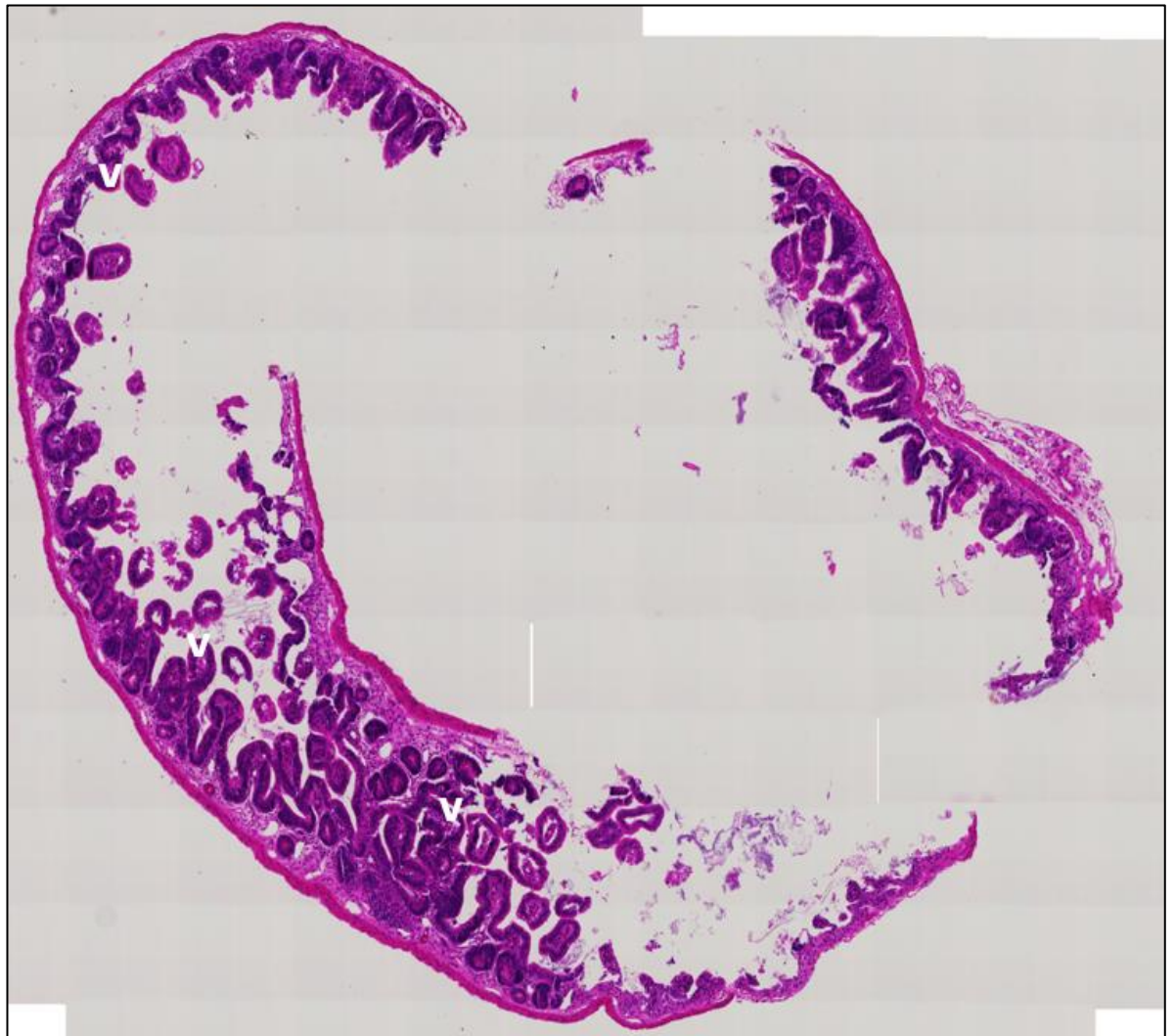


Figure 3.17 Representative H&E stained autoscanned sections of intestine of LRP1 KO mice. Main intestine structures are indicated as v=villi; sm=submucosa.

LRP1 TOTAL KO – Key findings

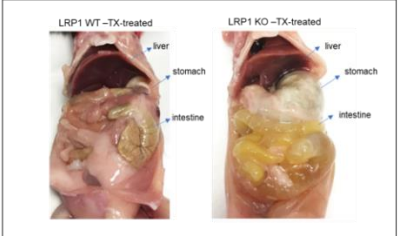
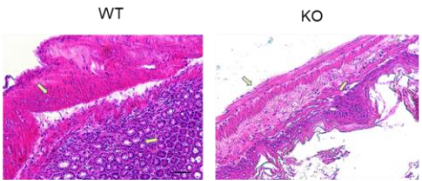
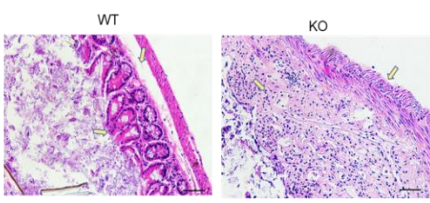
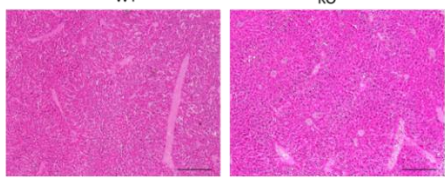
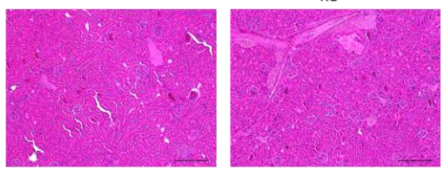
	<ul style="list-style-type: none"> • Rapid weight loss was found between LRP1 WT and KO mice (>20%). • Gross examination of the mice evidenced a difference between stomach, intestine and liver
<p style="text-align: center;">Stomach</p> 	<ul style="list-style-type: none"> • Enlarged stomach was found in LRP1 KO mice • Histological examination revealed normal muscle layers in WT compared to LRP1 KO mice where they are now well-defined.
<p style="text-align: center;">Intestine</p> 	<ul style="list-style-type: none"> • Intestine was yellowish pale and fluid-distended in the LRP1 KO compared to WT • WT mice showed normal villi structures compared to the LRP1 KO where there is a distortion of smooth muscle cells
<p style="text-align: center;">Liver</p> 	<ul style="list-style-type: none"> • Enlarged liver were observed in KO mice during the dissection • WT mice showed a normal liver tissue compared to the LRP1 KO where an accumulation of fat was detected.
<p style="text-align: center;">Kidneys</p> 	<ul style="list-style-type: none"> • No difference was observed between WT and LRP1 KO mice during the dissection • Inflammatory cells infiltration was detected by H&E in KO mice

Figure 3.18 Summary of the key findings in LRP1 total KO mice in adult stage. Comparison between WT and LRP1 KO mice is shown after gross and histological examination. Stomach, intestine, liver and kidneys were analysed by H&E staining. Scale bars of H&E pictures=100 µm and 50µm.

3.5 Discussion

The effect of global LRP1 deletion in adult mice was investigated. The major findings reported in this work were a rapid weight loss (>20%) and digestive dysfunction-observed in total LRP1 KO adult mice, which was primarily restricted to the gastro-intestinal tract.

3.5.1 Why does global deletion of LRP1 in adult mice cause rapid weight loss?

Based on our results, we hypothesise that rapid weight loss was potentially due to a lack of food absorption. To note, intestinal enlargement with yellowish fluid in KO mice can be due to a loss of villi's digestive functions leading to a decreased intestinal surface area. Shedding of intestinal epithelial cells was also observed in KO mice by H&E staining. Inefficient motility and absorption capacities of the gastro-intestinal tract can coincide with an abnormal phenotype in LRP1-KO mice. Initially, we aimed to identify any potential toxicity linked to tamoxifen administration that causes rapid loss of weight in mice. In literature, a potential toxic effect of ligand-dependent Cre recombinase for the generation of a conditional KO mouse has been previously tested by Hameyer et al., in 2007. They aimed to determine if there is any background activity for conducting conditional in vivo experiments with the ROSA26-CreERT2 in different organs including colon and lungs. No pathological effect was found in their work, suggesting that any background activity associated with the ROSA26-CreERT2 deleter system will not interfere (Hameyer et al., in 2007). Based on this, we attempted to assess whether tamoxifen administration via IP injection caused any misinjection. For this reason, the same experiment was repeated using OG injection, which confirmed our previous results. Therefore, we concluded that the IP injection was an adequate means of drug delivery. It is important to note that LRP1 WT mice did not lose weight after either IP or OG tamoxifen administration. In fact, during the dissection, no evidence of altered phenotype and abnormalities in

the gastro-intestinal tract were observed in the WT compared to non-treated mice.

Although it has not been previously reported that LRP1 plays an important role in the digestive system function, during the work of this thesis a study by Fields et al., in 2019 showed a similar result after global deletion of Laminin- γ 1 (Fields et al., 2019). They demonstrated the deletion of laminin- γ 1 leads to rapid weight loss in mice in adulthood due to gastro-intestinal defects similar to our results. Recently, another work by Li et al., 2018, found that the *Cldn7*-deficient mice had severe intestinal defects that included mucosal ulcerations, epithelial cell sloughing and inflammation. The *Cldn7*-deficient mice survived for only seven days, making it difficult to further investigate the function of *Cldn7* in the intestine. Next, they decided to generate *Cldn7* intestinal conditional knockout mice using the Cre/LoxP system upon induction with tamoxifen. They demonstrated that by deleting *Cldn7* in the intestine of mice, a severe intestinal inflammatory reaction and disruption of the intestine occurs, including the mucous membrane epithelium cells which were necrotic and detached (Li, et al., 2018). A recent paper published by Won et al. (Won, et al., 2022), evidenced that deletion of one of the LRP1 ligands known as Cellular Communication Network Factor 1 (CCN1) affects intestinal stem cells (ISCs) leading to a loss of intestinal absorption function.

Total LRP1 KO mice did not allow us to explore its role in lung and we unexpectedly found that total loss of *Lrp1* in adults can be deleterious for the maintenance of the digestive functions.

3.5.2 Does *LRP1* loss affect liver and kidneys?

The essential contribution for tissue homeostasis maintenance of LRP1 was previously assessed in vascular remodelling (Boucher, et al., 2003), lipid metabolism (Basford, et al., 2011), cell survival in the central nervous system, and in the molecular mechanisms of diseases such as atherosclerosis and Alzheimer's disease (Loukinova, et al., 2002; Huang & Huang, 2005). It has

been reported that deletion of *Lrp1* in the liver of LDL receptor-deficient mice results in the accumulation of cholesterol-rich remnant lipoproteins in the circulation, suggesting its involvement in the clearance of cholesterol-rich remnant lipoproteins (Rohlmann, et al., 1996). Moreover, in our total LRP1 KO mice an abnormal formation and distribution of fat content in the liver was observed and this could be the result of a loss of an efficient hepatic metabolism. Therefore, one hypothesis is that the enlarged liver observed in KO mice can be linked to a clinical condition called “fatty liver disease”, which rather than a disease is a disorder caused by the accumulation of fat. In our findings, we also detected the presence of inflammatory cell infiltration in kidneys of KO mice potentially due to the activation of inflammatory signalling pathways. Previous studies showed that tPA binds to LRP1 on kidney fibroblasts inducing its phosphorylation and activation of Erk1/2 MAPK pathway for fibroblast proliferation in fibrosis response (Lin et al., 2010). Although those previous tissue-specific knockout studies have provided information of LRP1 and linked it to cellular mechanisms such as lipid metabolism, glucose homeostasis and obesity, the core function of this receptor remains elusive.

3.5.3 Limitations

Our research showed that global deletion of LRP1 caused a rapid weight loss and gastrointestinal defects. However, this study presented different limitations. Firstly, due to a lack of time I was limited to only assessing a gross pathology examination of the gastro-intestinal tract by H&E and LRP1-immunostaining. Practical problems have come up during the paraffin-embedding orientation due to the deterioration of the tissue followed by thawing from -80 C. Moreover, the inadequate thickness of the LRP1-KO mice intestine did not allow to consistently have the right orientation for the visualisation of the villi and other digestive structures.

3.5.4 Conclusions and future plans

Improvements of paraffin-embedding orientation is essential for future analysis of the digestive system. It would be useful to analyse other areas of intestine, such as ileum and colon improving the visualisation of projections of microvilli, lamina propria, and intestinal crypts. For example, a “swiss-roll” technique is reported in literature to differentiate intestinal structural features with intestinal inflammation and abnormalities along the entire length (Bialkowska et al., 2016). Global deletion of LRP1 could be also monitored in intestine and stomach by performing a time-course experiment upon Tx administration. For example, termination of mice at different time points after Tx administration could reveal how total loss of LRP1 could affect the dysfunction of gastro-intestinal system. This experiment can potentially discover any detectable morphological changing over the duration of the experiment. For a better understanding of the gastro-intestinal function a further analysis of mucosa layers and lymphoid tissue in the intestine of total LRP1 KO mice might provide important information about the metabolism, mechanical digestion and absorption. In fact, previous studies have shown that the normal microflora of the large intestine can be affected by loss of genes such as riboflavin transporter-3 (RFVT-3) (Subramanian et al., 2016). It has been shown that mice deficient for ATP-gated P2X receptor cation channel family (P2X) receptors lost distention and peristalsis capacity in the small intestine (Bian et al., 2003). Combining the advanced *ex vivo* 3-dimensional models culturing would be useful to test any possible mechanobiological involvement of LRP1 in the intestinal peristalsis of total LRP1 KO mice.

Since a rapid weight loss was shown, a different transgenic mouse model was used in Chapter 4 to investigate LRP1 function in lung tissue *in vivo*.

Chapter 4 Major contribution of fibroblast LRP1 to excessive accumulation of collagen in lung fibrosis

Summary

Lung fibrosis is classified as the end stage of lung diseases and characterised by an excessive collagen deposition in the pulmonary interstitium. Transdifferentiation of fibroblasts to myofibroblasts plays a key role in the pathological mechanism of lung fibrosis for the excessive collagen deposition and inefficient wound healing repair process.

In this chapter, a bleomycin-induced pulmonary fibrosis model was assessed in a COL1A2-selective LRP1 knockout mice model. A series of experiments were performed for this chapter to address the initial hypothesis: LRP1 reduces bleomycin-induced lung fibrosis by mediating the lysosome degradation of pro-fibrotic molecules (Figure 4.1). Finally, the localisation and distribution of COL1A2-expressing cells upon bleomycin injury was tracked and visualised using COL1A2-R26TmG reporter mice model. Our results were contrary to the initial hypothesis. In fact, we found that loss of LRP1 in COL1A2-expressing cells results in a reduced collagen deposition upon bleomycin injury.

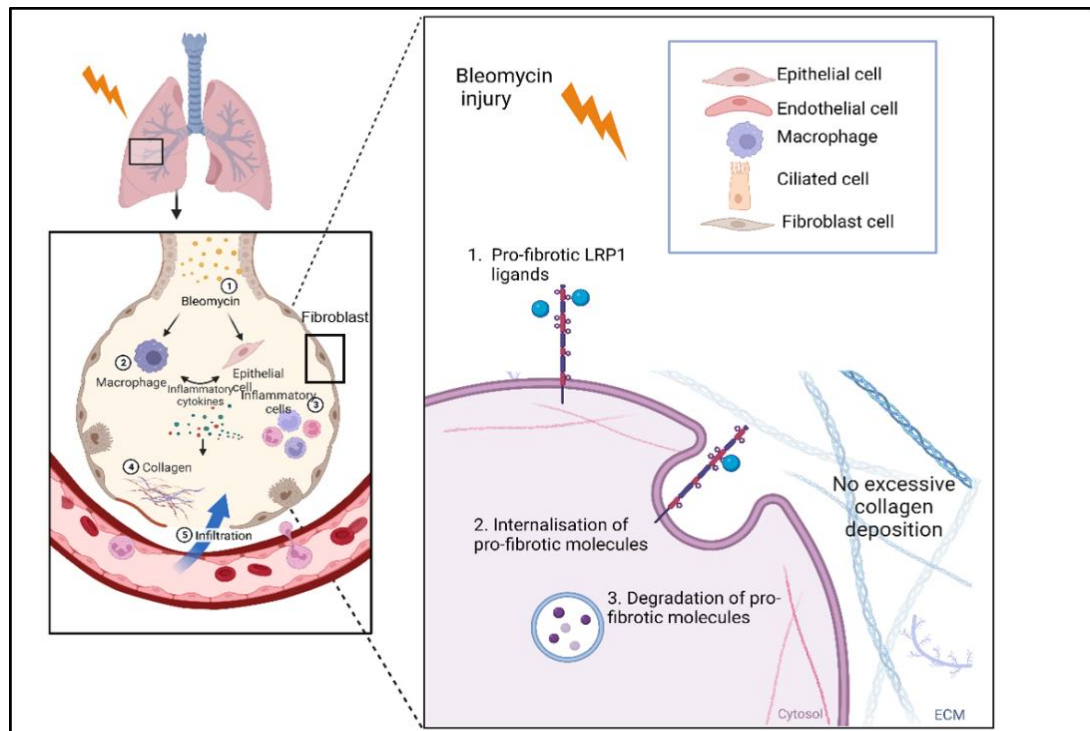


Figure 4.1 Initial hypothesis: LRP1 prevents collagen deposition and is protective in lung fibrosis. (1) Pro-fibrotic LRP1 ligands are internalised by LRP1 (2) and it mediates their degradation in lysosome (3). LRP1-mediated endocytosis prevents the excessive collagen deposition upon bleomycin injury. Figure released with Biorender.

4.1 Introduction

Lung fibrosis is characterized by a fatal loss of lung function and a survival rate lower than most human cancers. Three important hallmarks have been identified in lung fibrosis pathogenesis: excessive collagen deposition, fibroblast to myofibroblast differentiation and inflammatory cell infiltration. The progress of new therapies relies on the use of robust *in vivo* models, although its pathogenesis remains elusive and not completely understood. Various animal models have been developed to mimic features of human lung fibrosis including recurrent exposure to radiations (Paun & Haston, 2012), instillation of asbestos (Cyphert, et al., 2014; Rasmussen & Pfau, 2011), silica and bleomycin (Lakatos, et al., 2006; Nakayama, et al., 2009; Moore, et al., 2013). The most common agent for inducing lung fibrosis is bleomycin (Adamson,

1976; Umezawa, et al., 1967; Ponticos, et al., 2009; Egger, et al., 2013; Scotton, et al., 2013; Gilhodes, et al., 2017) which is also used for treating different types of cancer. However, it has been shown that it upregulates collagen synthesis by modulating fibroblast proliferation through TGF- β response and alters the fibrinolytic system leading to fibrin deposition (Reinert, et al., 2013). The most common adverse effect of bleomycin is interstitial pneumonitis, followed by pulmonary fibrosis. Bleomycin-induced pulmonary disease occurs in more than 46% of patients treated with bleomycin and lung toxicity has been reported during treatment. Molecular mechanisms beyond the development of pulmonary fibrosis after bleomycin treatment remain unknown (Izumikawa, et al., 2008). It has been hypothesised that bleomycin causes an overactivation of fibroblasts and subsequent fibrosis due to a lack of the enzyme bleomycin hydrolase in the lung tissue (Chaudhary, et al., 2006).

In this chapter, I investigated LRP1 role in lung fibrosis development using *in vivo* μ CT scan and histological examination. Finally, I have used an optimised open-source software for collagen quantification in lung tissue after Masson's trichrome staining.

4.2 Aims and objectives

The aims of this chapter were as follows:

- I. Establishment of COL1A2-selective LRP1 knockout mice for bleomycin-induced lung fibrosis model. The first objective for this aim was to detect changes in body weight and signs of sickness behaviour in this tissue-specific KO mouse model.
- II. Determine the effect of LRP1 loss in COL1A2-expressing cells upon bleomycin administration. The objective for this aim was to investigate the contribution of LRP1 in lung fibrosis development by *in vivo* μ CT and histological examination.
- III. Identify COL1A2-expressing cells in normal and fibrotic lung tissue. The objective for this aim was to characterize collagen-producing cell

populations in murine lungs by using tdTomato-expressing mice under the control of the inducible enhancer COL1A2-CreER.

4.3 Chapter-specific methods

4.3.1 Bleomycin Administration: oropharyngeal route (OA)

Different routes of bleomycin administration to the lungs have been developed such as: subcutaneous (SC), intravenous (IV), intratracheal (IT), intranasal (IN) and oropharyngeal (OA) (Lindenschmidt, et al., 1986; Braun, et al., 1996; Egger, et al., 2013; Williamson, et al., 2015). Lakatos and collaborators in 2006, made an important comparison between the IN and OA routes to induce lung fibrosis by silica administration (Lakatos, et al., 2006). They found a difference of fibrosis development in terms of localization: the IN route was causing fibrosis in the proximal area of the lungs, while the OA route causes fibrosis in the distal lungs (Lakatos, et al., 2006). Since this group also showed a certain level of complexity during the IN administration, we decided to adopt the OA route to induce lung fibrosis in this experimental procedure (Figure 4.2). Animals were anaesthetised using 2.0 % isoflurane during the bleomycin administration. An elastic band wrapped around a gloves box was used as a suspension system to open the mouth and expose the back of the throat. Animals were suspended via their incisors and a pair of forceps was used to hold the tongue outside and administer 25 μ L of solution with a micropipette. Since the bleomycin is also registered for the level of pain, I checked and monitored the animals over the 4 weeks. More specifically, I supervised any change in body weight and any sign of distress together with the level of lung fibrosis every week by *in vivo* μ CT.

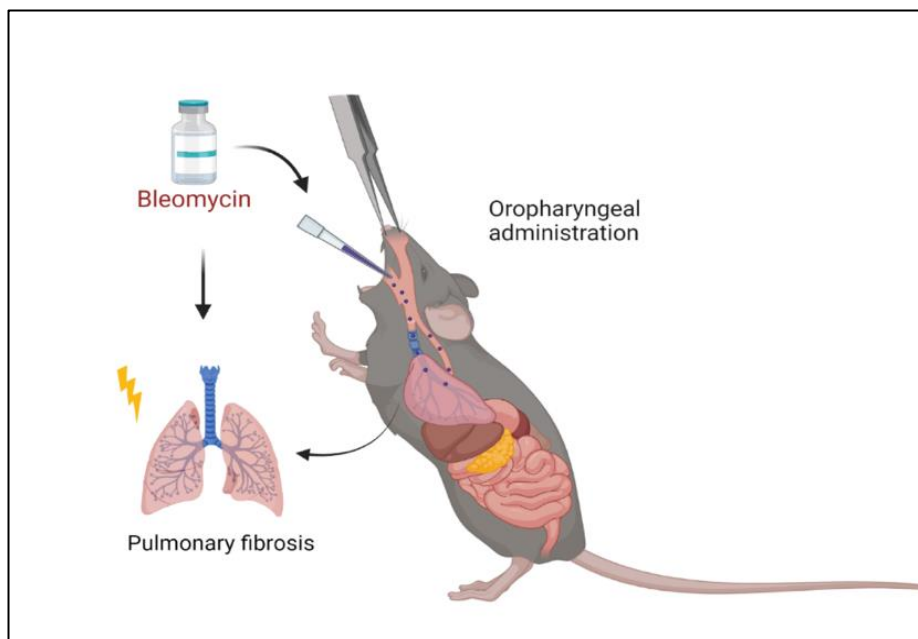


Figure 4.2 Illustration of OA administration route in mice. Mice were previously anaesthetised and suspended on a thin rubber band, exposing the tongue in order to open the mouth and gently administer bleomycin in the posterior pharynx through the base of the tongue. Image was realised using Biorender.com.

4.3.2 Bleomycin dose

A stock solution of bleomycin (15000 IU Powder for solution for injection/ infusion per mouse) was kindly provided by Dr Sonya Craig and prepared in sterile PBS before the first administration and then stored, in aliquots, at -80°C . The initial optimization was delivered via oropharyngeal aspiration (OA) at different doses: 5 ng/g, 0.5 ng/g and 0.05 ng/g per mouse (Table 4.1). Following the optimisation experiment, a single dose of 0.1ng/g was chosen and administered to all the rest of the mice for this research project.

Table 4.1 Initial optimisation Bleomycin dose.

Mouse IDs	Genotyping	Bleomycin dose (I.U.)	CT-scan	Termination
LRP1AggTmr (2.3)	Lpr1fl (het)/AggCre (het)	ctrl	Time 0,1,2,3,4, weeks	4 weeks
LRP1AggTmr (1.1)	Lpr1fl (het)/AggCre (het)	0.05ng/g	Time 0,1,2,3,4, weeks	4 weeks after Bleomycin
LRP1AggTmr (2.1)	Lpr1fl (het)/AggCre (het)	0.5ng/g	Time 0,1,2,3 weeks	3 weeks after bleomycin
LRP1AggTmr (2.4)	Lpr1fl (het)/AggCre (het)	5ng/g	Time 0, 1 weeks	1 week after bleomycin

4.3.3 Bleomycin administration in transgenic mice

TX-dependent CreER^{T2} inducible knockout of LRP1 in fibroblasts (COL1A2 LRP1 KO) transgenic mice, as described in paragraph 2.3.3, were used for this chapter. Tx was administered before bleomycin to obtain knockout mice of interest. Therefore, after tamoxifen injection, bleomycin was administered to induce lung fibrosis. Different time points were established for the lung fibrosis evaluation during the 4 weeks. Lungs treated with different concentrations of bleomycin were collected and analysed by *in vivo* μ Ct and histological examination. We did not observe any sign of rapid weight loss at the concentration of 0.1ng/g of bleomycin.

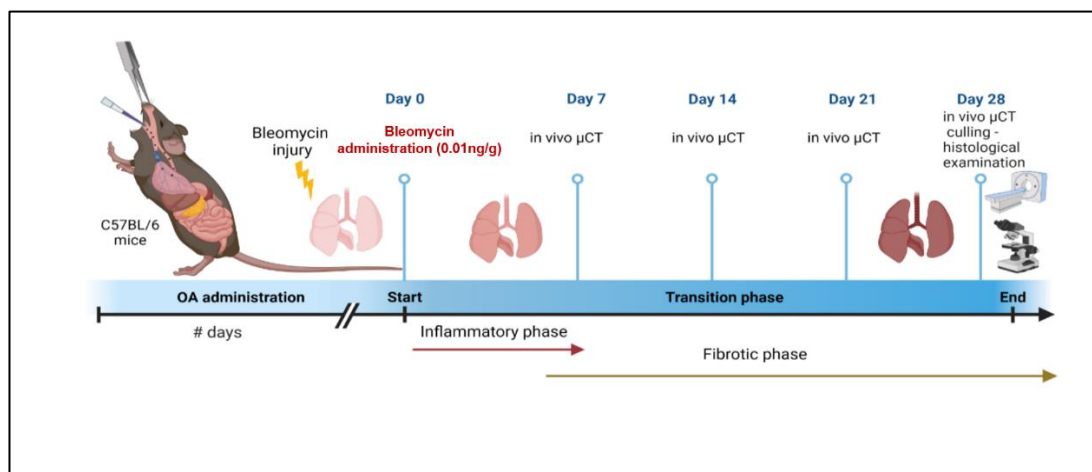


Figure 4.3 Lung fibrosis development upon bleomycin injury. The transgenic mice were previously tamoxifen injected. Pulmonary fibrosis has been monitored at day 0, 7, 14, 28 by *in vivo* μ Ct scan. Mice were culled at day 28 from the first treatment

and the lungs were isolated and analysed by histological examination. Image was realised using biorender.com

4.3.4 *In vivo* micro computed tomography (μ Ct) live imaging of the lungs

For the *in vivo* experiment conducted in this chapter, lungs from transgenic mice were imaged by *in vivo* μ CT using a Quantum GX-2 system Version: 3.0.39.5100 Copyright © Rigaku Corporation 2010-2018 (PerkinElmer) (Figure 4.4). *In vivo* μ CT provided evidence in real time on the effects of bleomycin treatment. Mice were imaged at day 0, 7, 14, 21, 28 for the late stage of fibrotic disease. Images were acquired with a respiratory gated technique with the following parameters: X-ray tube voltage 90 KV, X-ray tube current 88 μ A, total scan time of 4 min. The retrospectively gated acquisition protocol in “high speed” mode, resulted in two 3D datasets with 50 μ m isotropic reconstructed voxel size, corresponding to the two different phases of the breathing cycle: inspiration and expiration. An X-ray filter of copper (Cu) 0.06mm and aluminium (Al) 0.5mm was used for lung scans. Live CT view allowed the camera to be positioned in the region of interest before starting the CT scanning session. At the end of the lung scanning, mice were gently transferred and acclimated to a dedicated box at 37°C for recovery and observed for 15 minutes.



Figure 4.4 Quantum GX µ-CT machine (PerkinElmer, Inc. Waltham, MA) located at the Centre for Pre-Clinical Imaging (CPI) facility at the University of Liverpool.

4.3.5 Inflation and isolation of lungs

Mice were euthanized with CO₂ inhalation in a chamber for 7 minutes and positioned in dorsal recumbence with full extension of pelvic and pectoral limbs. The abdominal cavity was then opened using sterile scissors and forceps and the entire skin was manually removed bilaterally. A ventral midline incision was made into the abdomen to expose the peritoneal cavity and the xiphoid process. Neck muscles were removed leaving the trachea opened. Liver portal vein was cut, and a small incision was performed on the bottom part of the diaphragm. Extreme care was taken during this incision to not cause any damage to the lungs while cutting the whole circumference. The xiphoid process was exposed with the forceps and the scissors were used to cut the ribs on each side of the sternum. The thymus, which is located above the heart in the anterior superior thorax, was carefully removed after cutting and lifting the ribs. A sterile string was then passed underneath, and then up tracheal space using blunt forceps and wrapped around tracheal rings, leaving an opened knot. A transverse incision in the cartilaginous rings in the superior region of the trachea without cutting through the posterior portion was made.

Gently, the needle was inserted into the trachea while the knot between the needle and the trachea was holding in place. The lungs were gently inflated with air until they were fully expanded to fill the chest thorax (1.5mL). After removal of the needle, a tight knot was closed around the trachea to avoid any air leak. Lung was dissected out from the dorsal cavity as an inflated lung. Lungs for the histological examination were placed in a falcon tube containing 4% of PFA and placed at 4°C, while some lobes were stored at -80°C for RNA extraction. After 24 hours, PBS at 4% PFA was discarded under a fume hood and replaced with cold 70% Ethanol ready for the tissue processing process.

4.3.6 Histological examination

Inflated lungs were immersed in a solution of PFA 4%. The lung tissue was fixed in EtOH 70% and processed as described in 2.9.1 and 2.9.4 paragraphs.

4.3.7 Masson-Goldner's Trichrome Stain

Masson-Goldner's Trichrome Stain was performed to evaluate the collagen content in paraffin-embedded lung tissue samples (Table 4.2). The collagen was stained in blue/light green by analine blue/fast green, the nuclei in black and the background and muscle fibres were stained in red. Following the dehydration step, stained slides were mounted in DPX mountant solution and imaged using a Zeiss LSM 800 microscope. All the reagents were previously prepared freshly to use. Weigert's Haematoxylin solution was prepared by mixing equal parts of solution A and solution B, respectively made of 10 g Haematoxylin crist. (C.I.75290) added to 1L of 95 % EtOH and 12 g of ferric chloride added to 40 mL water and 10 mL hydrochloric acid. ddH₂O was added to make a total volume of 1 L. Next acid fuchsin-ponceau solution was made by adding 6 mL of a solution prepared with 1 g Ponceau 2R in 100 mL ddH₂O and 2 mL of a solution made of 1g acid Fuchsin in 100 mL ddH₂O. This was added to 9 mL of 2 % Acetic acid and 73 mL ddH₂O. Finally, 3g of phosphotungstic-acid- orange G and 2g of phosphotungstic acid Orange G

was added to 100 mL distilled water. Counterstaining solution was prepared by adding 1g of light green powder to 1 mL of acetic acid and 500 mL ddH₂O.

Table 4.2 Masson's trichrome staining steps and reagents details.

Reagent/step	Immersion time (minutes)
Weigert's Haematoxylin	10
H ₂ O	10
Acid Fuschin	15
1% Acetic Acid	2
PTA Orange	5
1% Acetic Acid	0.5
Fast Green/Aniline blue	10
1% Acetic Acid	3
70% Ethanol	2
90% Ethanol	2
100% Ethanol	3
Xylene	5
Xylene	5

4.3.8 Picrosirius red staining

PFA fixed sections were dewaxed through Xylene for 5 minutes and hydrated through decreasing ethanol concentrations, while cryosections were incubated for 1 minute in PBS. PFA sections were incubated with Weigert's haematoxylin for 8 minutes allowing nuclear staining. Slides were then washed in running tap water. This step was not used for cryosections as the procedure destroyed tissue architecture. Slides were then incubated for 1 hour in Picrosirius red, which colours collagen fibres. Sections were washed through two dips in water with 1% of acetic acid. Slides were dehydrated in ethanol, cleared in xylene and mounted in a resinous medium with a coverslip. Slides were then incubated for 1 hour in a fume hood at room temperature to evaporate traces of xylene.

4.3.9 Collagen quantification on lung tissue

A quantitative analysis of collagen was performed on lungs treated with bleomycin at 28th day after termination of the mice. Sections were stained by Masson's trichrome staining as described in 4.3.7 and auto scanned and then loaded in a software entirely assessed by Professor Rob Vant' Hoff (van 't Hof, et al., 2017). More specifically, he developed an open source software for semi-automated histomorphometry of bone sections and he adapted that on the lung tissue.

The analysis was performed as following:

- Selection of the lobes

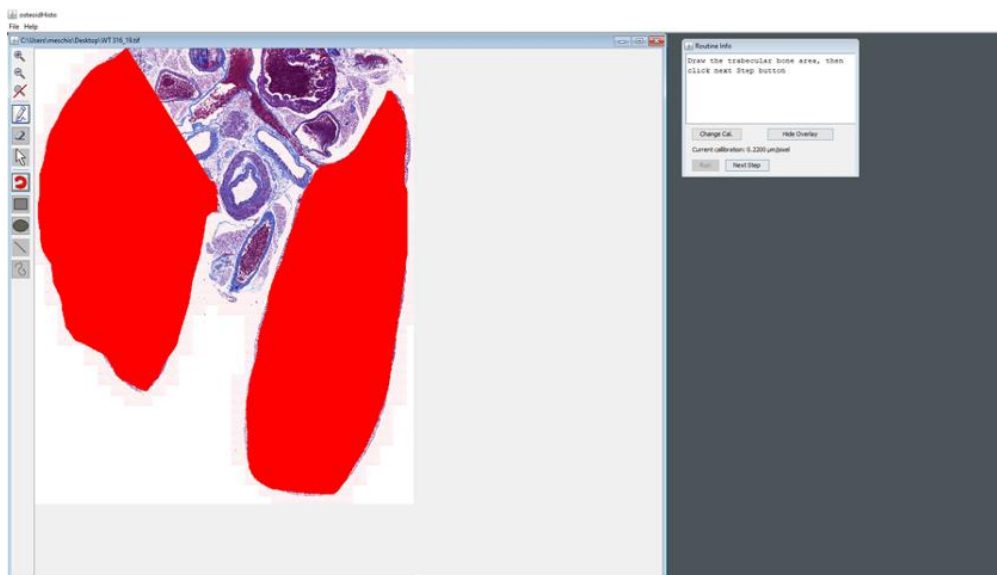


Figure 4.5 First step of the collagen quantification analysis showing the selection of the area of interest.

- Identification of the air spaces. This step was adapted to the identification of the bone threshold. The air space was identified by the adjustment of the threshold parameters.

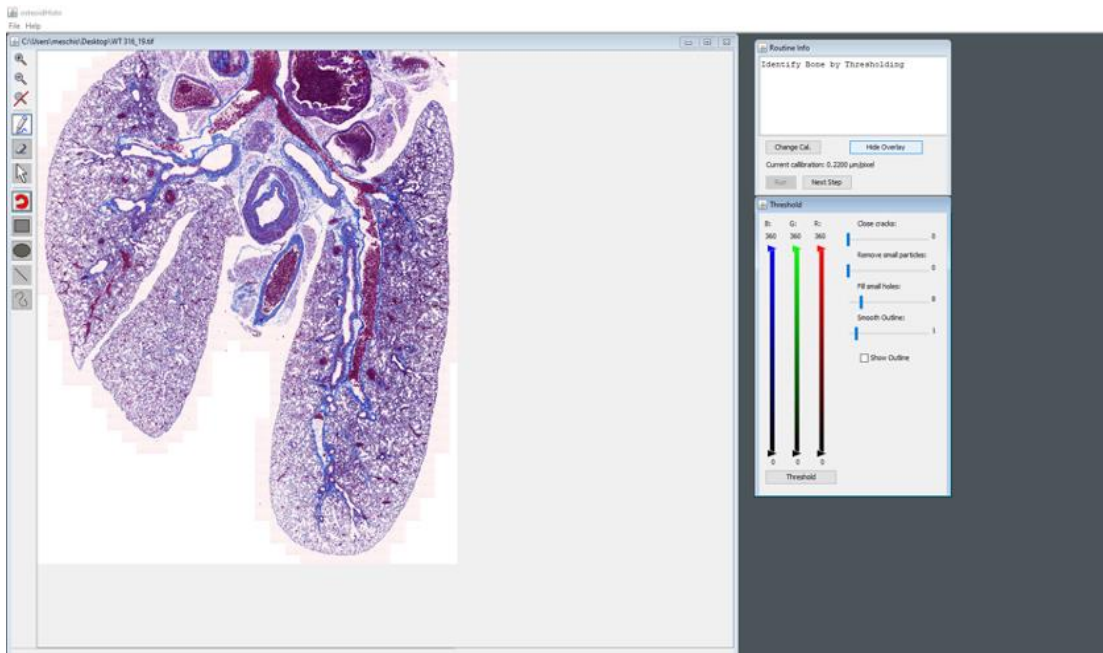


Figure 4.6 Adjustment of the parameters threshold for the identification of the air spaces in the lung tissue.

- Removal of the unspecific air space by regulating the colour parameters. The aim of this step is to select all the air spaces in “yellow” as shown in the figure.

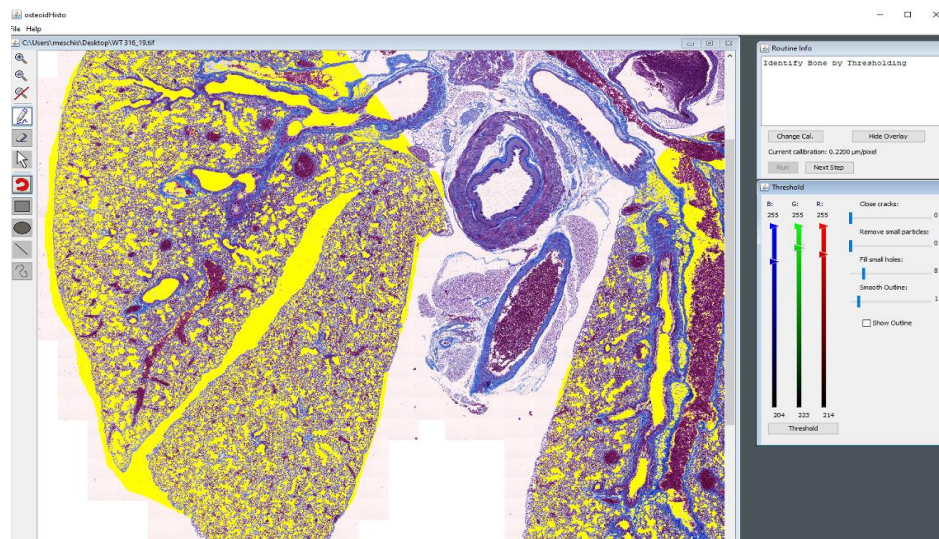


Figure 4.7 Highlighting selection of air space in the lung

- Final selection of the air space in yellow avoiding the vessels overlapping. This is a crucial step for the final step of the quantification.

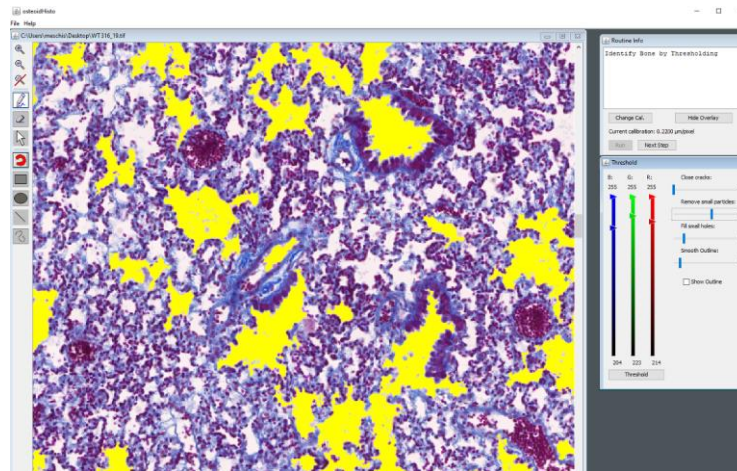


Figure 4.8 Air space selection removing the blood vessels.

Identification of collagen. This step was adapted to the “identification osteoid by threshold”. Collagen was identified as “pink” by adjusting the other threshold parameters.

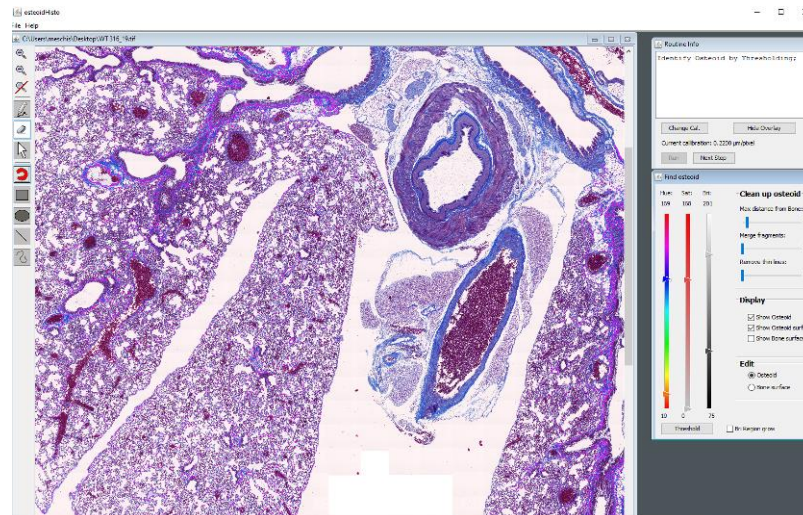


Figure 4.9 Final tracking of the collagen in “pink” to be quantified.

- Quantification obtained. Running this image analysis, I obtained these values to plot as OV/BV which is the air/space expressed in percentage.

Filename	Calibration	T.Ar	B.Ar	B.Pm	O.Pm	O.Ar	BV/TV	BS/BV	Tb.Th	OS/BS	OV/BV	O.Th
	um	um2	um2	um	um	um2	%	mm-1	um	%	%	um
WT 316_...	0.2200	1292626.59	339574.88	266033.01	1.50	44125.31	29.68	940.12	2.40	0.00	11.50	2.10

Figure 4.10 Results obtained by quantification analysis. Different parameters were obtained by the lung analysis. The OV/BV value was considered as air/space in percentage (%).

4.3.10 Immunohistochemistry

IHC was performed as described in paragraph 2.7.5. A panel of fibroblast markers was assessed for the localization of fibroblast cells in lung tissue. Vimentin, alpha muscle actin, HSP47 and S100A4 antibodies were tested on sections of isolated lung tissue at two different concentrations: 1:500 and 1: 1000 (Table 4.3).

Table 4.3 Panel of fibroblast marker tested in lung tissue.

Fibroblast marker	work concentration	Catalogue number- supplier
Vimentin	1 in 1000	EPR3776-ab92547
Alpha smooth muscle Actin	1 in 500	E184-ab32575
Hsp47	1 in 500	EPR4217 - ab109117
S100A4	1 in 500	EPR14639 - ab197896

4.3.11 Cryosectioning

Lungs filled with O.C.T. at 30% v/v of Sucrose/PBS were placed in -20°C 20 minutes before cryostat and then cut with a Leica CM1850 cryostat producing slides of 5µm.

4.3.12 Inducible COL1A2-Cre/tdTomato mice

To generate mice expressing tdTomato in COL1A2-expressing cells (COL1A2-Cre/tdTomato), was used a reporter mouse which express the red fluorescent protein, tdTomato with flanking LoxP sites (Rosa26 TdTomato

mice). Mice containing the reporter construct B6CB; 129-(Cg)-Gt (ROSA) 26Sortm4 (ACTB- tdTomato) Luo/Liv, were purchased from Jackson Laboratories (007676). These were bred with male mice containing the COL1A2 driven CreERT2 B6CB-Tg (Col1a2-17=1.5kbenh-350mp-CreErt2) 3.18/Liv (Figure 4.10). These animals were used for lineage tracing experiments to determine the distribution pattern in COL1A2-CreERT2 in response to bleomycin injury. Cre-recombinase expression of the resulting offspring was induced by tamoxifen injection. Mice were treated with bleomycin (0.05ng/ml) and sacrificed at time points of 1 and 3 weeks (Table 4.4). Lungs were isolated and inflated and prepared for cryosectioning procedure. The lungs slides were stained using 4',6-diamidino-2-phenylindole (DAPI) and mounted before imaging. Lung histology was carried out using the Zeiss apotome microscope under TdTomato and DAPI fluorescent imaging.

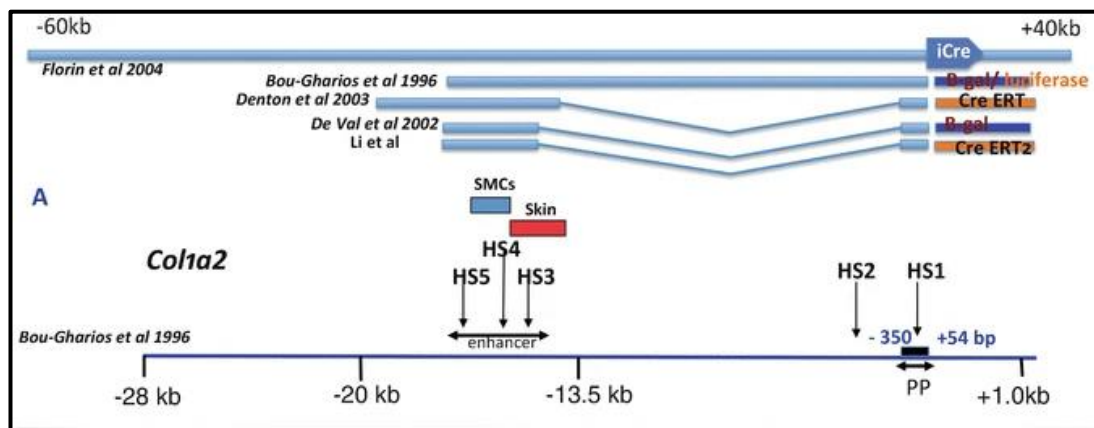


Figure 4.11 Characterization of Mesenchymal-Fibroblast Cells Using the Col1a2 Promoter/Enhancer. Schematic diagram of COL1A2 gene localised on the hypersensitive sites (HSs) and proximal promoter (pp). (Figure revised from Li et al., 2017).

Table 4.4 The table displays the experiment's plan at different time points.

Mouse	Mouse Genotyping	Tamoxifen	Bleomycin	Termination
1	COL1A2-Cre +/+ Tmr +/+	None	+	3 weeks
2	COL1A2-Cre +/+ Tmr +/+	3 doses	+	1 week

3	COL1A2-Cre +/+ Tmr +/+	3 doses	+	3 weeks
4	COL1A2-Cre +/+ Tmr +/+	3 doses	-	3 weeks
5	COL1A2-Cre +/+ Tmr +/+	3 doses	-	3 weeks

4.3.13 TGF- β 1 treatments on WT and LRP1^{-/-} MEF cells and western blotting

WT mouse embryonic fibroblasts (MEFs) and LRP1-deficient MEFs were generated as previously described by E. Willnow and J. Herz in 1994 were cultured in 48-multiwell plates until confluency and the media was replaced with serum-free media. After 24 hours, cells were treated with TGF- β 1 at 0.01, 1, 10 ng/mL for 20 minutes and 1 hour. Next, the media was removed, and the cells were lysed with 50 μ L of 2x SDS-sampling buffer containing 5% 2-mercaptoethanol. Samples were analysed by SDS-PAGE under reducing conditions and immunoblotting using anti-SMAD2/3, anti-FAK, anti-P-FAK and anti-actin antibodies. Immune signals were quantified using ImageJ and the amount of the protein was normalised by the actin.

4.4 Results

4.4.1 Establishing the dose-response effects of bleomycin-induced lung fibrosis *in vivo*

An initial experiment of optimisation was performed testing different bleomycin doses. A mortality rate of 50% was observed among 4 mice during the bleomycin optimisation dose experiment. The respiratory function was measured and monitored by *in vivo* micro-CT scan before and after BLM instillation. Mice that experienced weight loss exceeding 20% of their start weight and/or exhibited signs of illness (hunching, piloerection) were culled via CO₂ to negate a breach of Home Office licence conditions. The sections stained with Masson Trichrome staining, H&E and Picrosirius red under polarised light microscopy, enabled the visualisation of the extent of fibrosis that had formed at each time point and dose. 7 days after OA BLM administration at a dose of 5ng/g caused the worst lung tissue alterations among the treated mice with a high level of inflammation. In this mouse (Figure 4.12 D) scarred areas and obliterated alveolar architecture were observed. Moreover, the presence of early fibrotic foci surrounding the bronchiole spaces were also detected. 21 days after OA BLM administration at the dose of 0.5mg/mL a lower grade of lung tissue obliteration compared to the first one was shown. Fibroblastic foci were interfacing with the normal lung and the background architecture was still distorted within the presence of honeycomb, enlarged spaces lined by the bronchiolar epithelium (Figure 4.12 C). 28 days after bleomycin administration at 0.05ng/g (Figure 4.12 B), any body weight changes were observed post-bleomycin installation over the entire duration of the experiment similar to the untreated mouse. An accumulation of fibers of collagen was detected in the alveolar and bronchial spaces by picrosirius red reflecting the development of lung fibrosis (Figure 4.13). By contrast, the control lungs did not show any alteration in the lung architecture (Figure 4.13 A). This was confirmed under polarized light where the control lung (Figure

4.13 A) did not show any event of dichroism usually indicated by the presence of different types of collagen (I and II-III) seen in other bleomycin-treated mice (Figure 4.13 B-C-D). These results were confirmed by H&E staining, in which bleomycin-treated mice at the doses of 0.5-0.05 and 5ng/g showed the same grade of fibrosis as observed in Masson's trichrome and Picrosirius red stainings (Figure 4.14). In addition, an increase in cell density around the alveolar walls was observed among those treated mice at higher doses indicating immune cells infiltration (Figure 4.14 C-D).

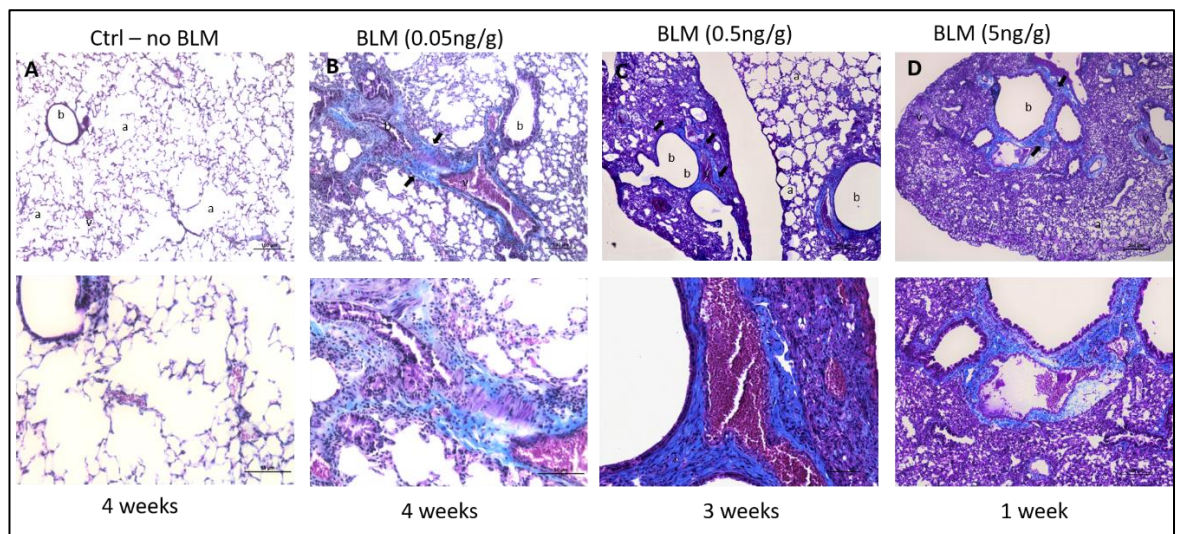


Figure 4.12 Lung fibrosis development observed by Masson's trichrome staining. C57Bl/6 mice treated at different bleomycin doses: control – no bleomycin administration (A); bleomycin-treated at 0.05ng/g (B); bleomycin-treated at 0.5ng/g (C) and bleomycin-treated at 5ng/g (D). The anatomical features in the lung tissue are indicated as follows: “a” (alveolar space), “b” (bronchiole space), “v” (vessel). The black arrows indicate the excessive collagen deposition (blue) upon bleomycin administration with the fibrosis development. Scale bars= 100 μ m and 50 μ m.

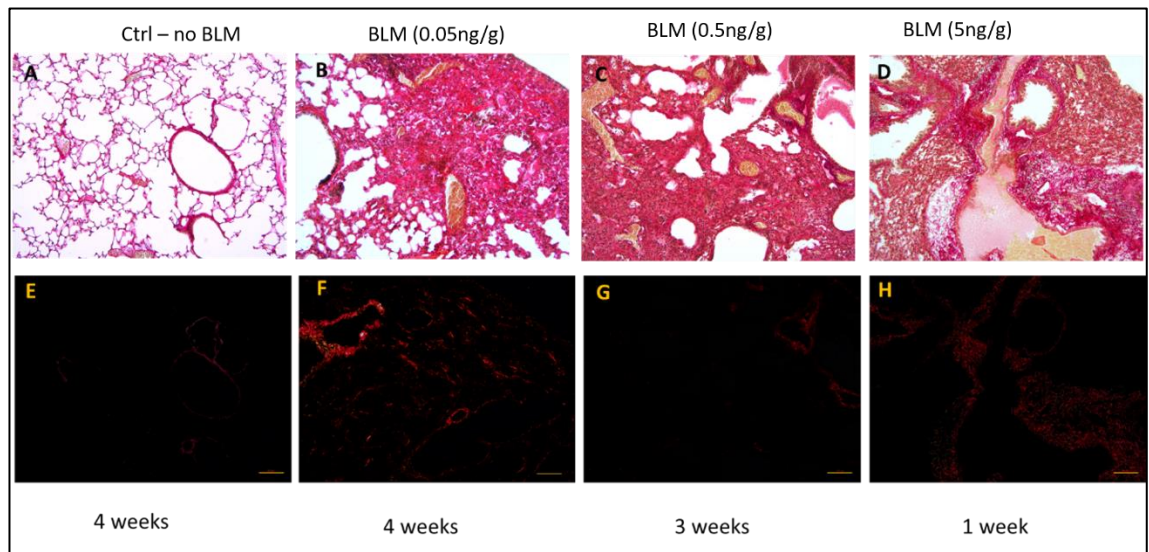


Figure 4.13 Collagen fibers detected under polarized light by Picrosirius red staining. C57Bl/6 mice untreated and treated at different bleomycin doses: control – no bleomycin administration (A); bleomycin-treated at 0.05ng/g (B); bleomycin-treated at 0.5ng/g (C) and bleomycin-treated at 5ng/g (D). The images were obtained by polarised light microscopy where it provides complementary information about collagen fiber types, and spatial distribution. Scale bars= 100 μ m and 50 μ m.

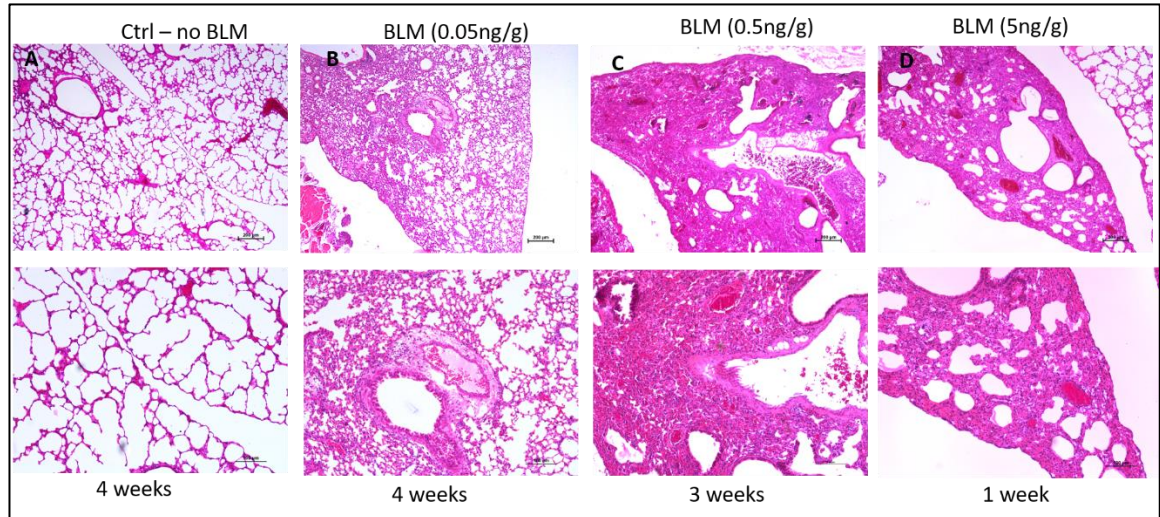


Figure 4.14 Cell infiltration observed in pulmonary fibrosis by H&E staining. C57Bl/6 mice untreated and treated at different bleomycin doses: control – no bleomycin administration (A); bleomycin-treated at 0.05ng/g (B); bleomycin-treated at 0.5ng/g (C) and bleomycin-treated at 5ng/g (D). Haematoxylin and eosin staining shows the extent of lung fibrosis in the BLM-treated mice (B,C,D) compared with the control mouse (A). Scale bars= 100 μ m and 50 μ m.

4.4.2 *In vivo* μ CT: a preliminary densitometric analysis of the lungs

In this study a comparison of lung inspiration volume between wild type mice and LRP1-COL1A2 KO mice was performed by *in vivo* μ CT scan. More scar tissue distribution in WT mice was observed compared to the LRP1 COL1A2 KO mice (Figure 4.15). These evaluations were made by simple observation under Professor Rob Vant'off's supervision who suggested all the setting parameters for the acquisition protocol. During the elaboration of the scanned lung, anatomical features were localised and identified such as heart, ribs, vertebra and spinal cord and sternum. To note a background's variability was observed among the analysed lungs. Therefore, the presence of background was more consistent 28 days after bleomycin administration. For this reason, a direct quantification by histology of the focal fibrotic lesions and collagen deposition was required in parallel to the *in vivo* μ CT scan.

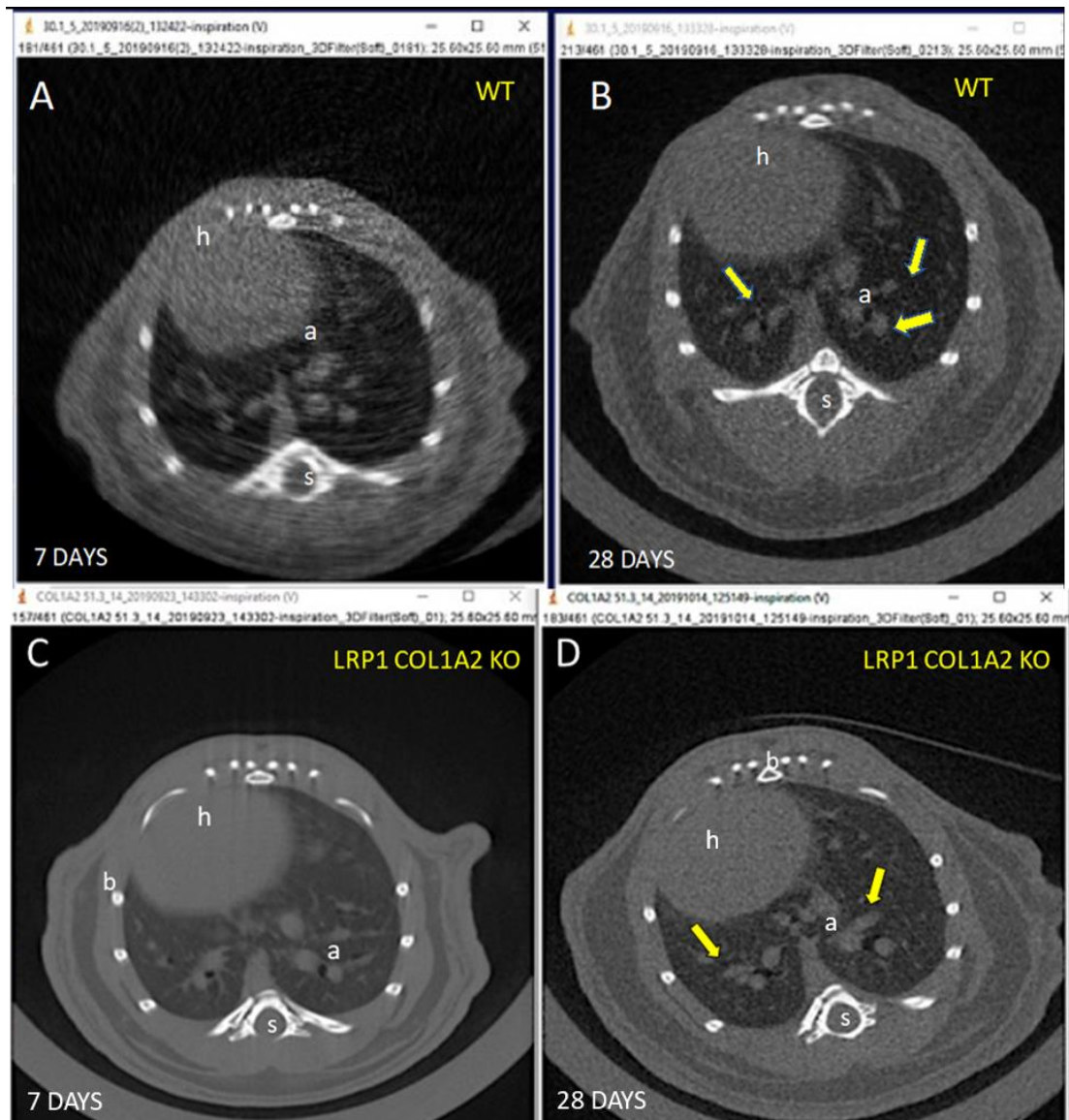


Figure 4.15 Lung fibrosis observed by *in vivo* μ CT. These are the most representative pictures taken during the *in vivo* CT scan at 7 and 28 days after the OA bleomycin administration. WT mice (A) image show the development of lung fibrosis at 28 days in comparison with the LRP1 COL1A2 KO (C-D) where the deposition of collagen and scar tissue formation result to be less consistent. All the anatomical features are indicated as: heart (h), air (a); bones (b); sternum (s). The arrows point to the presence of pulmonary fibrosis.

4.4.3 Bleomycin-induced lung fibrosis is markedly reduced in COL1A2-selective LRP1 KO mice

The aim of this experiment was to determine the effects of loss of LRP1 from COL1A2-expressing cells in lung fibrosis upon bleomycin administration. Masson's trichrome staining for collagen deposition and inflammatory cells infiltration in representative inflated lung sections was obtained at day 28 post-bleomycin (0.01ng/g) where WT mice (Figure 4.16 B) showed an excessive collagen deposition compared to the LRP1-COL1A2 KO (Figure 4.16 D). LRP1 COL1A2 KO mice showed less fibrosis and inflammatory cell infiltration similarly to no treated mice (Figure 4.16 A). However, examination of sections at 28 days revealed some regions of fibrosis remained. In WT mice we could clearly see almost absent alveoli spaces (Figure 4.17) where in LRP1 COL1A2 KO mice resulted to be well maintained (Figure 4.18). In WT bleomycin-treated mice a thickening of alveolar spaces was observed in regions adjacent to tissue deposits (Figure 4.19). Regions of fibrosis were closely associated with the bronchioles, with tissue deposition observed and fibrotic foci formation occurring most frequently in the immediate vicinity of the bronchioles. It was also observed around the bronchiole's spaces the presence of collagen indicating a preferer deposition localisation during the fibrosis development (Figure 4.19 C-D). A high grade of nuclear staining was detected in the fibrotic lungs compared to the LRP1 COL1A2 KO mice (Figure 4.20) where it was possible to distinguish a normal structure of alveolar and bronchial space with less cellular infiltration. Increase of collagen content upon bleomycin treatment was also assessed by imaging quantification analysis using Professor Rob Vant' off software. The analysis included the relative amount of air and fibrosis content (Figure 4.22). The air surface detected by imaging analysis determined a >45% amount of air in control (no bleomycin) mice compared to LRP1 WT bleomycin-treated mice (p value ** <0.0011) and >30% compared to the LRP1 COL1A2 KO bleomycin-treated mice (p value ** <0.0079). Not statistically significant difference was found between LRP1 WT bleomycin-treated mice

and LRP1 COL1A2 KO bleomycin-treated mice (Figure 4.22 A). Moreover, the relative amount of fibrosis was higher in the LRP1 WT bleomycin-treated mice compared to LRP1 COL1A2 KO bleomycin-treated mice and control no-bleomycin mice (p value ***<0.0009 and p value **<0.0006, respectively). Not statistically significant difference was found between control mice and LRP1 COL1A2 KO bleomycin-treated mice (Figure 4.22 B).

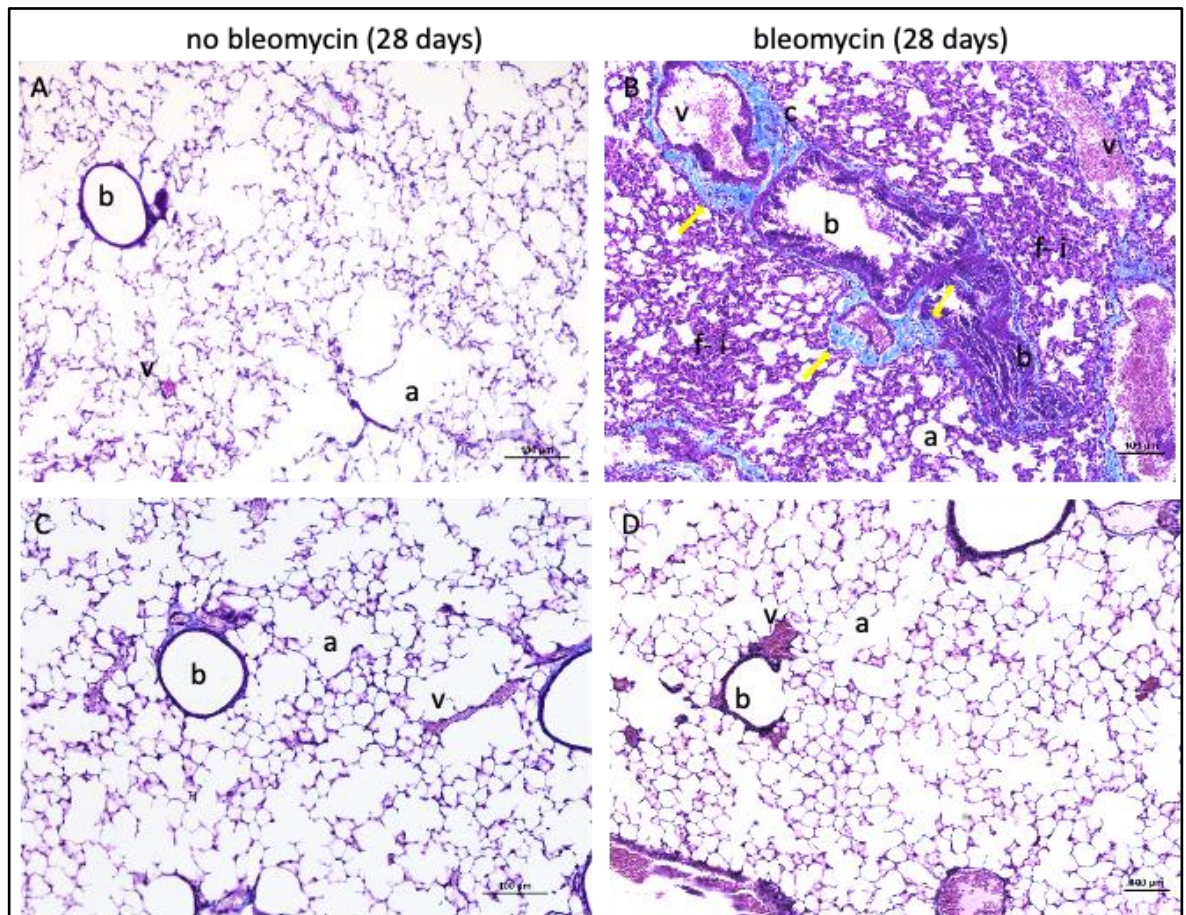


Figure 4.16 Reduced collagen deposition is observed in LRP1 COL1A2 KO mice compared to WT. These pictures are respectively showing the no treated WT (A) and LRP1 COL1A2 KO (C) mice. 28 days after the bleomycin administration lungs were isolated and stained for the collagen visualisation. Fibrotic foci were observed (indicated by arrows) in WT lungs. Anatomical features are indicated as follows: b (bronchiole), a (alveolar space), v (vessel), f-i (fibrosis and inflammatory cells infiltration). Collagen depositions is indicated in figure B with yellow arrows, and it mostly surrounds the bronchiole spaces. Pictures taken at the 10x magnification. Scale bar=100μm.



Figure 4.17 Lung fibrosis in a WT mouse 4 weeks after bleomycin administration. Histological evaluation of whole lung samples isolated from bleomycin-treated mice up to 28 Days using Masson's trichrome staining. Lungs were isolated immediately after termination by CO₂ and manually inflated. Main features of the lungs are indicated as a=alveolar space; b=bronchiole; v=vessel; c=collagen; h=heart. All images were by the autoscanner machine.

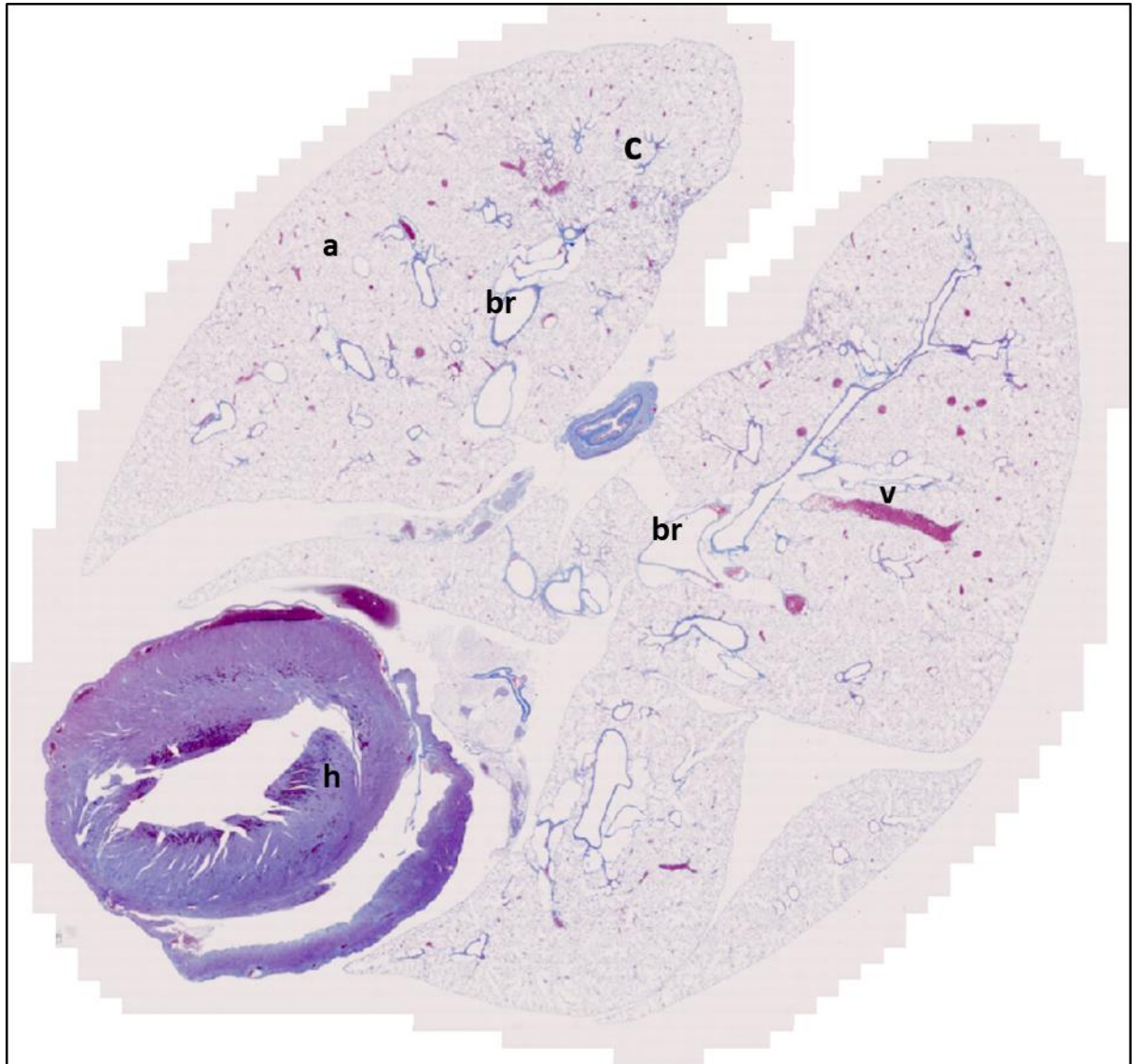


Figure 4.18 Lung fibrosis in LRP1 COL1A2 KO 4 weeks after bleomycin administration. Histological evaluation of whole lung samples isolated from bleomycin-treated mice up to 28 Days using Masson's trichrome staining. Lungs were isolated immediately after termination by CO₂ and manually inflated. Main features of the lungs are indicated as a=alveolar space; br=bronchiole; v=vessel; c=collagen; h=heart. All images were by the autoscanner machine.

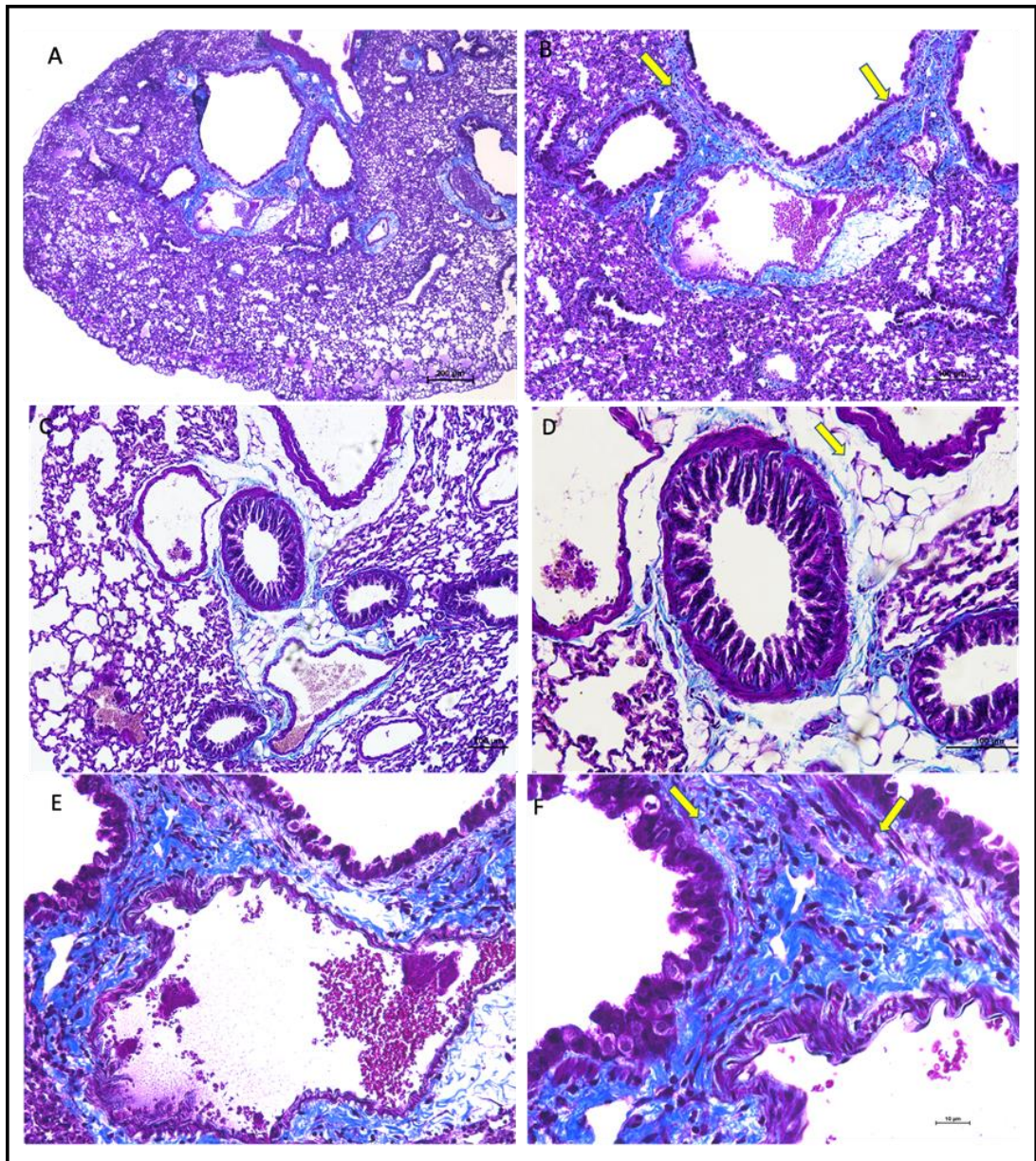


Figure 4.19 Histological examination by Masson's trichrome staining of WT mice after bleomycin administration. In these pictures is possible to distinguish the anatomical features of the lungs: A-B are showing the lung fibrosis upon bleomycin injury; C-D is showing the bronchiole structure in the lungs where the arrow (yellow) is indicating the suspected presence of adipose tissue; E-F purely show the collagen distribution upon bleomycin administration which is mainly localised around the bronchiole space. Scale bar= 100 and 50μm.

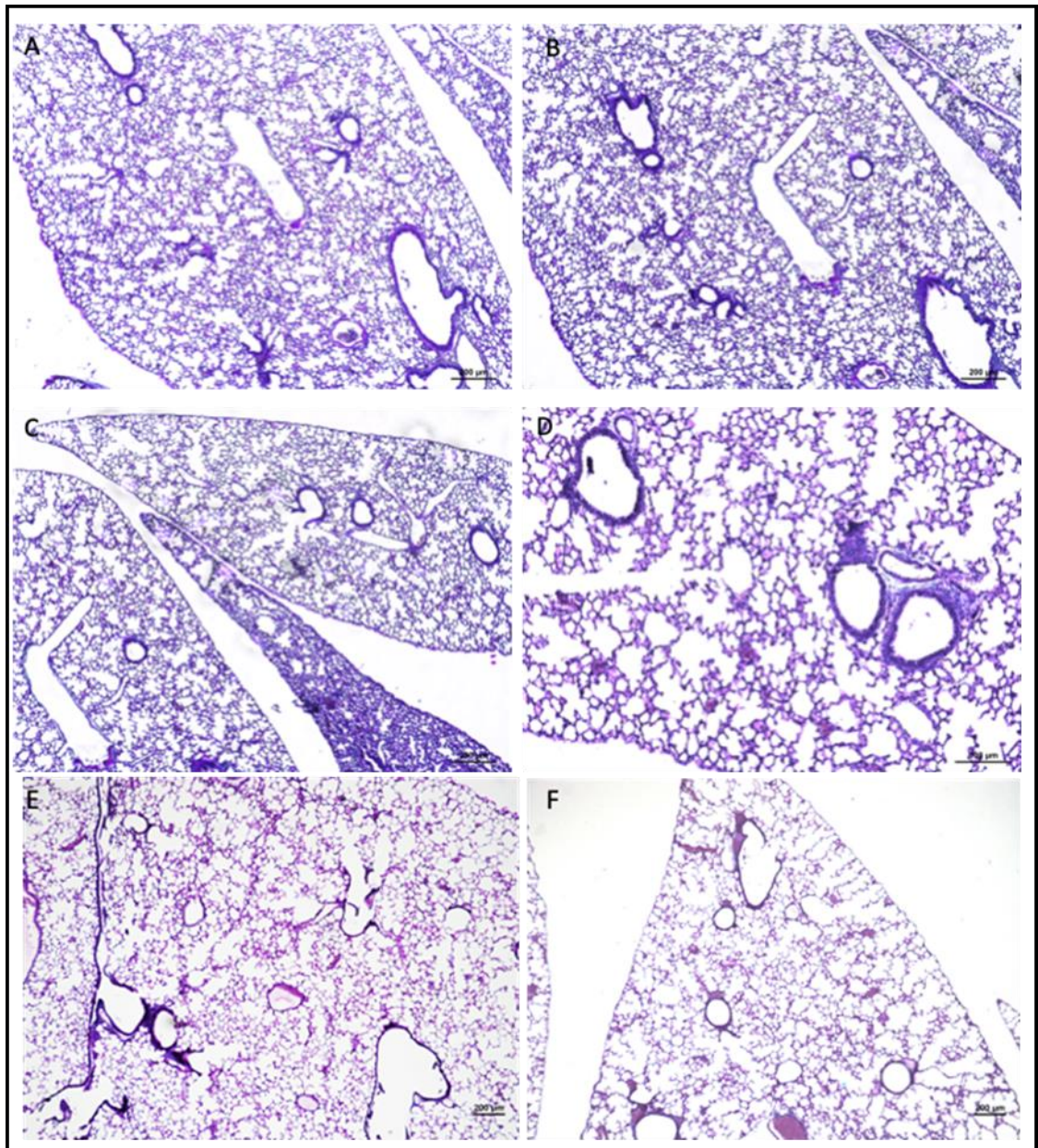


Figure 4.20 Reduced collagen deposition and less cell infiltration in COL1A2 LRP1 KO mice after bleomycin administration by Masson's trichrome staining.

As shown the most representative lung tissue from mice. In these mice the lung tissue structure and architecture are well maintained compared to the WT. A-F shows different areas of the lungs. However, a low level of fibrosis (A-B) with a small cellular infiltration is shown. In the figure C is shown the presence of fibrotic tissue with some inflammatory cell infiltration in the minor lobe of the left lung. Scale bars at 100 and 50μm.

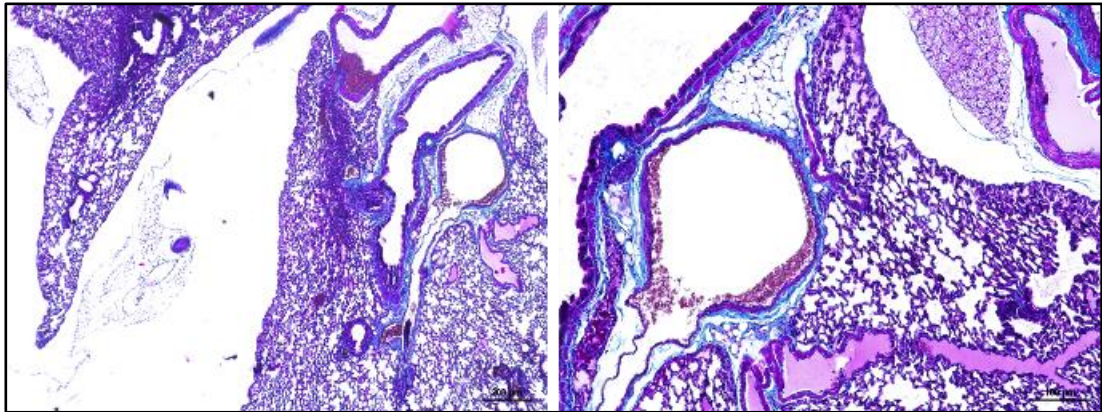


Figure 4.21 Representative lung fibrosis in COL1A2 LRP1 KO. It is shown pulmonary fibrosis due to the genetic variability among the mice after tamoxifen and bleomycin administration. Collagen deposition is indicated in blue. Scale bars at 100 and 50 μ m.

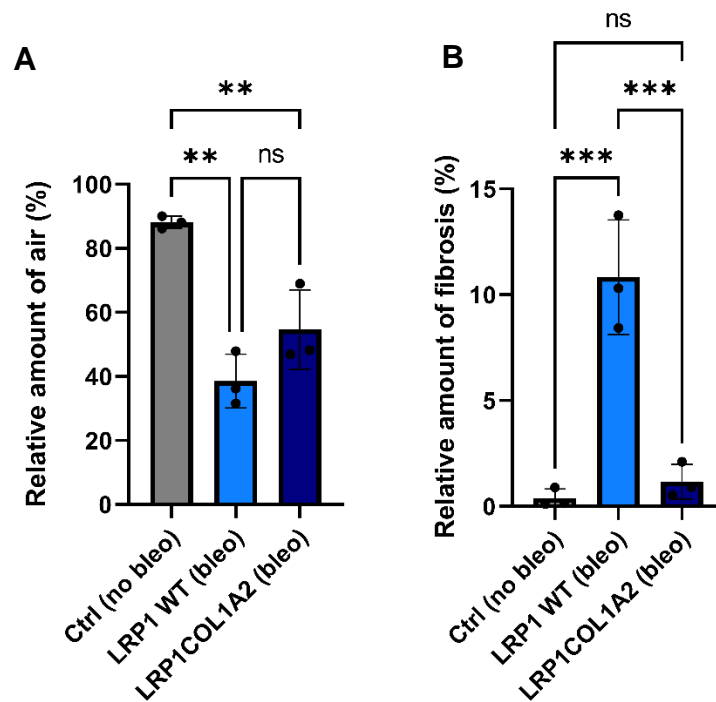


Figure 4.22 Quantification analysis of ctrl lung tissue (no bleomycin), WT mice-treated and COL1A2 LRP1 KO mice. Graph **A** shows the amount of air spaces where it results normal no bleomycin-treated mice compared to WT and LRP1 KO-treated mice. Data were analysed using one-way ANOVA with Tukey's multiple comparisons test: Ctrl (no bleo) vs. LRP1 WT (bleo) ** $p < 0.0011$; Ctrl (no bleo) vs. LRP1COL1A2 (bleo) ** $p < 0.0079$; LRP1 WT (bleo) vs. LRP1COL1A2 (bleo) ns (not statistically significant). The graph **B** represents the amount of fibrotic tissue, which is related to air space (alveoli)/ tissue values expressed in %. The majority of WT mice-

treated with bleomycin showed a high level of fibrosis reflecting the presence of an increased stiffness and reduced alveolar spaces compared to the COL1A2 LRP1 KO mice where the specific deletion of LRP1 most likely prevents the pulmonary fibrosis. Data were analysed using one-way ANOVA with Tukey's multiple comparisons test: Ctrl (no bleo) vs. LRP1 WT (bleo) *** $p < 0.0006$; Ctrl (no bleo) vs. LRP1COL1A2 (bleo) ns (not statistically significant); LRP1 WT (bleo) vs. LRP1COL1A2 (bleo) *** $p < 0.0009$.

4.4.4 Reduced deposition of collagen type I and III in COL1A2 LRP1 KO mice upon bleomycin injury

Picosirius Red staining allowed a direct comparison between the lung structure, fibrosis and collagen deposition among the bleomycin-treated samples. The WT samples (Figure 4.23) clearly show much higher levels of lung fibrosis and damage compared to both the COL1A2 LRP1 KO (Figure 4.24). By looking at the polarised light samples, two main colours of collagen fibres are distinguished: the red indicates type I collagen and the green indicates type III collagen. LRP1 WT lungs- bleomycin treated show tissue aggregates with parenchymal disruption and collagen deposition surrounding within the bronchioles. Polarised light microscopy highlighted the event of dichroism around alveoli with bright colour intensification (Figure 4.23). By contrast, COL1A2 LRP1 KO-bleomycin treated group shows slight collagen deposition within the alveoli. To note the bronchial walls are much thicker in the WT samples compared to COL1A2 KO lung tissue. Furthermore, in the WT samples, there appears to be some inflammatory cells infiltration. Quantification of the polarised light images using image J software, showed that LRP1 WT bleomycin-treated resulted in a significant 3.2-fold compared to COL1A2 LRP1 KO mice bleomycin-treated (p -value** < 0.0001). Moreover, LRP1 COL1A2 KO mice bleomycin-treated did not show statistically significant difference compared to the control (no-bleomycin) (Figure 4.25).

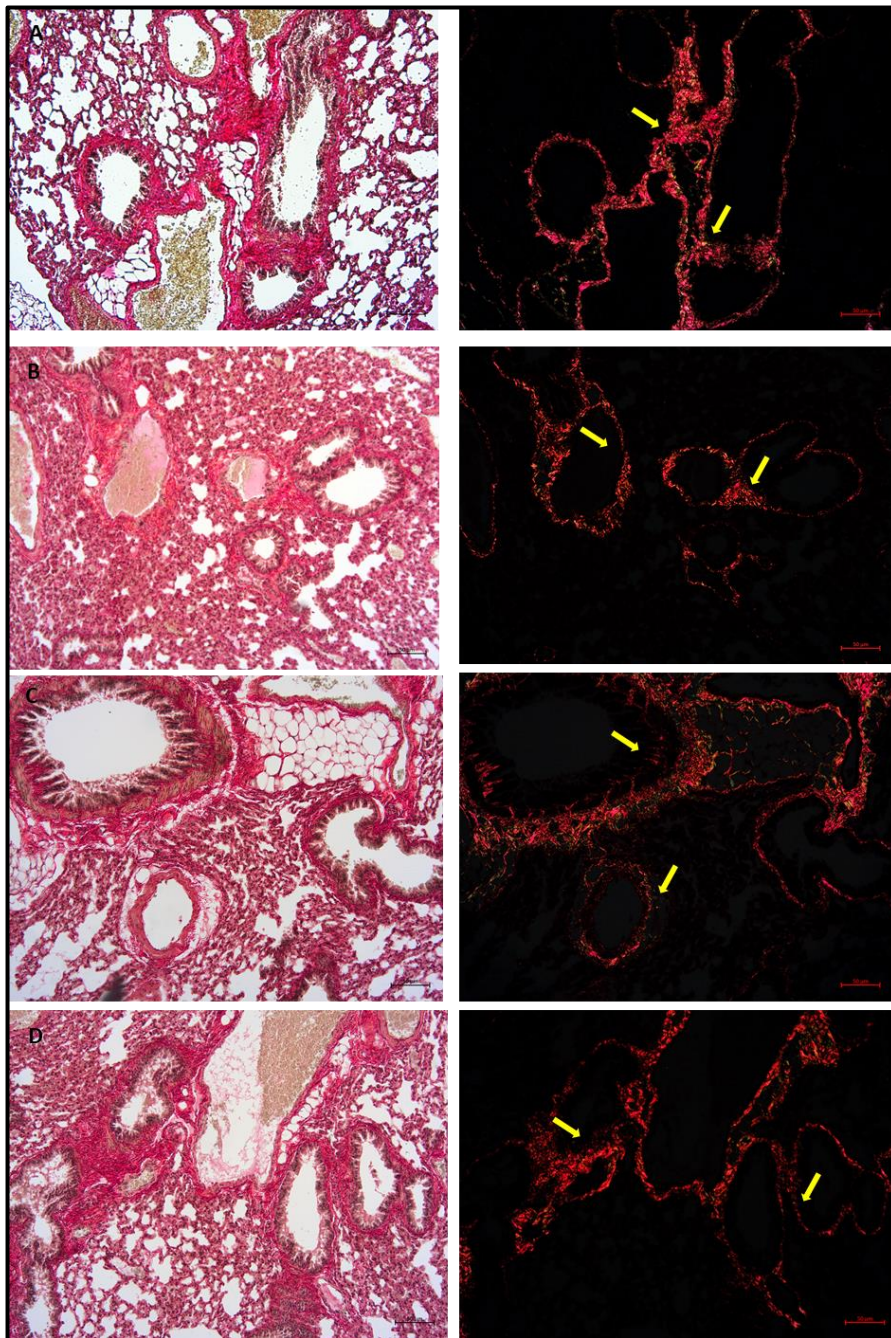


Figure 4.23 Representative collagen fibres deposition by Picosirius Red staining of WT fibrotic lung samples. Picosirius Red staining to detect the levels of fibrosis and collagen deposition. These images provide the best representation of all the samples stained through a 10x magnification through both normal and polarised light, allowing the detection of type I and type III collagen indicated by the arrows. Scale bar= 50 μ m.

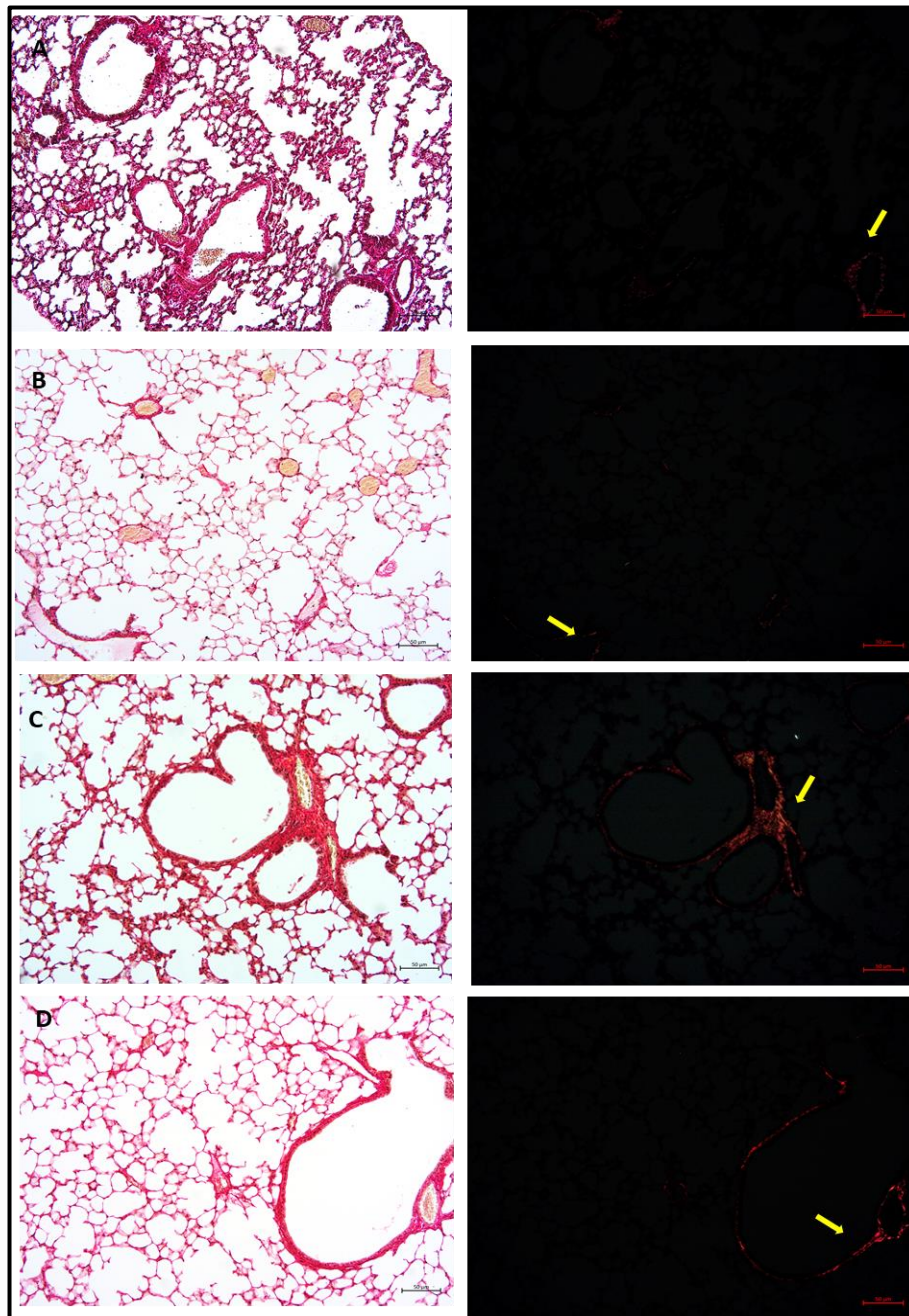


Figure 4.24 Reduced collagen deposition was detected by Picrosirius Red staining in COL1A2 fibrotic lung samples. Picrosirius Red staining to detect the levels of fibrosis and collagen deposition. These images provide the best representation of all the samples stained through a 10x magnification through both normal and polarised light, allowing the detection of type I and type III collagen. Arrow heads highlight areas of very mild collagen deposition. Scale bar= 50µm.

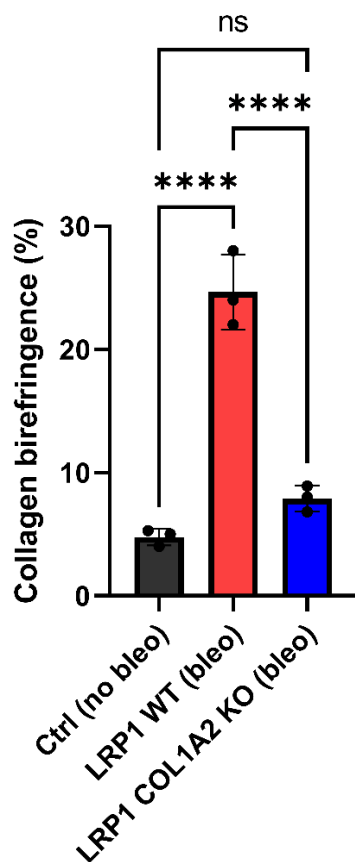


Figure 4.25 Lower collagen birefringence is detected in COL1A2 LRP1 KO mice upon bleomycin injury. Data were analysed using 1-way ANOVA with Tukey's multiple comparisons test: Ctrl (no bleo) vs. LRP1 WT (bleo) ****p < 0.0001; Ctrl (no bleo) vs. LRP1COL1A2 (bleo) ns (not statistically significant); LRP1 WT (bleo) vs. LRP1COL1A2 (bleo) ****p value < 0.0001.

4.4.5 Detection of COL1A2-expressing cells in the bleomycin-induced lung fibrosis model using a COL1A2-R26tdTomato reporter mice

To investigate collagen transcription and therefore fibrosis in the presence of COL1A2-expressing, cells were visualised by red fluorescence at different time points after bleomycin administration. The inducible COL1A2-CreER^{T2} activity was examined using tdTomato red fluorescent signal in lung tissue samples from tamoxifen-treated mice. More specifically, transgenic adult COL1A2-R26TmG reporter mice containing the mT/mG reporter construct (Muzumdar et al., 2007) and COL1A2-CreERT2 gene (Li et al., 2017) were used for the experiment. The positive control slides displayed normal lung tissue with thin lined alveolar septa and normal alveolar architecture (Figure 4.26 B). The negative control (Figure 4.26 A), which only received

bleomycin treatment did not show red fluorescence under the microscope. The transcription of COL1A2 gene in adult mice at 1 and 3 weeks after bleomycin administration was tracked reflecting the highest amount of fluorescence in mice which had been treated with bleomycin and for the longest period which was up to 21 days. Red fluorescence was also detected under the microscope in the lung slides which had an incubation time of 1 week after exposure to bleomycin and tamoxifen. However, lung sections with a 3-weeks bleomycin treatment time showed higher levels of fluorescence when compared to the 1-week treated mice (Figure 4.27). Disrupted alveolar architecture and infiltration of inflammatory cells was visualised in the bleomycin-treated mice lung tissue, with higher levels of disruption seen in the 3-week bleomycin- tamoxifen treated mice when compared with the 1-week bleomycin- tamoxifen treated mice (Figure 4.27). Apotome fluorescent microscopy detected the presence of COL1A2- expressing cells by red fluorescence (Figure 4.28).

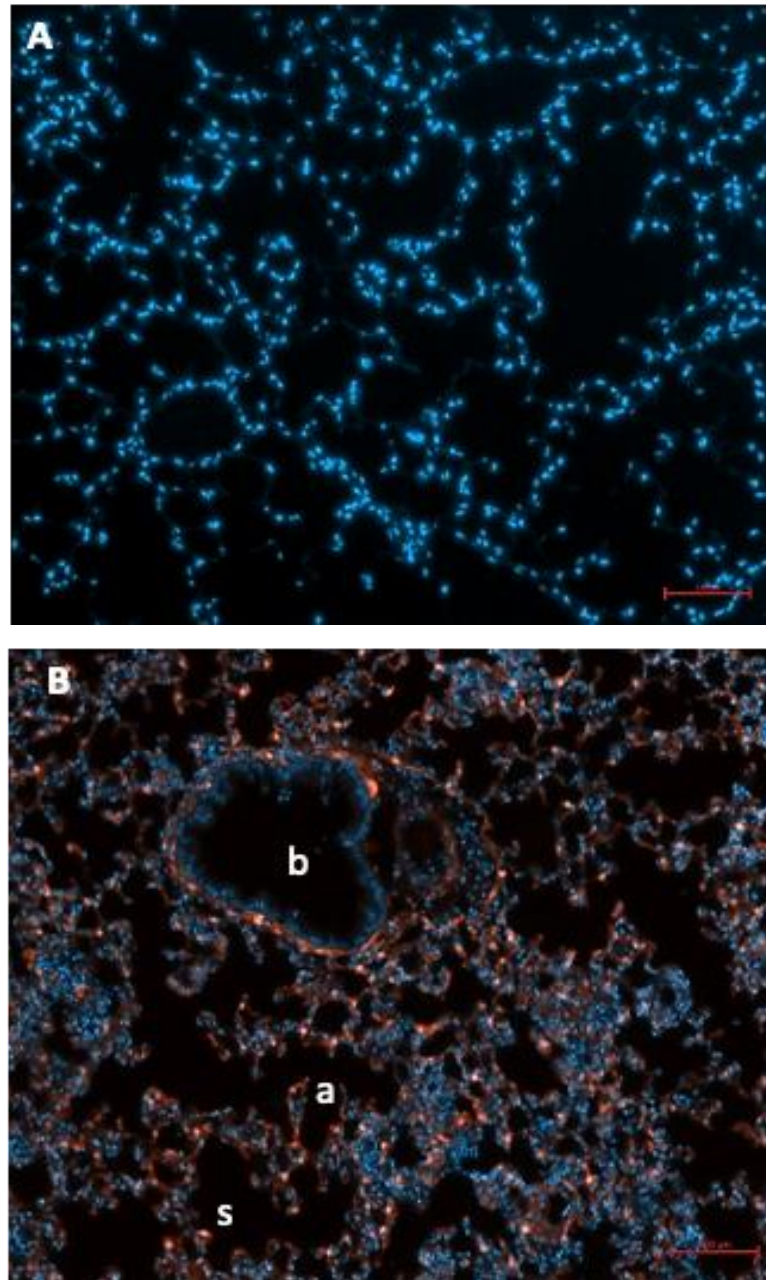


Figure 4.26 COL1A2-expressing cells and nuclei visualisation. Comparing the negative control showing only DAPI (A) and the positive control (B) shows the COL1A2-CreERT2 activity indicated by the tdTomato signal (red; mCherry 610 nm fluorescence channel) which provides a profile of general cell morphology and structure in the normal lung tissue without bleomycin administration. However, the positive control (B) displays innate red. Normal alveolar architecture is seen in the positive control as no fibrosis is present. b = bronchiole, a = alveoli, s= interalveolar septa. Tissues were imaged using a Zeiss Axio Observer apotome microscope and Axio Cam MR R3 camera. Inserts show enlarged areas of image. Scale bars represent 100 μm .

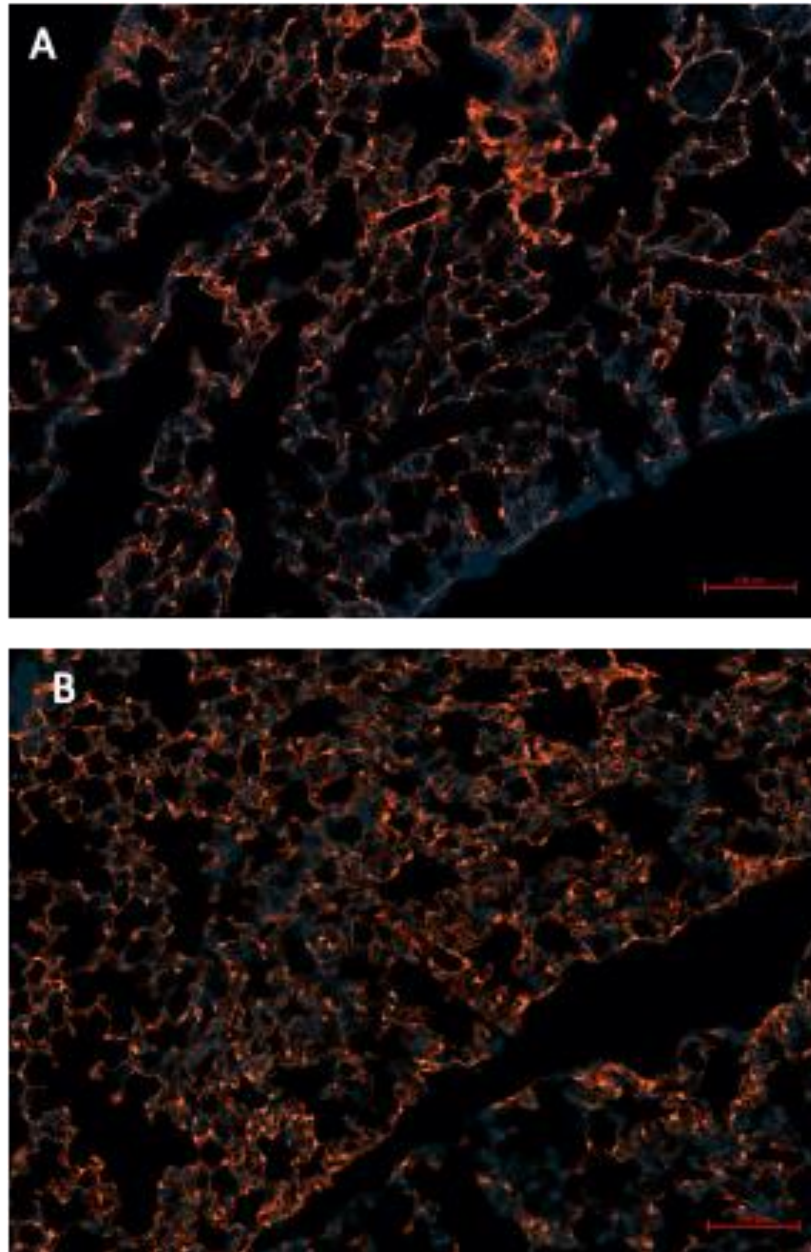


Figure 4.27 Lung tissue treated with bleomycin show collagen-producing cells. for 1 week (A) and 3 weeks (B) shown after staining with DAPI for nuclei visualisation. A greater number of cells shows red fluorescence, which indicates presence of Col1a2 expressing cells. They result more visible in the 3-week bleomycin treated sample(B). Red fluorescence is also seen more widely spread in the 3 week treated mouse slides when compared to the 1- week bleomycin treated slides. Disrupted alveolar architecture shown. Tissues were imaged using a Zeiss Axio Observer apotome microscope and Axio Cam MR R3 camera. Inserts show enlarged areas of image. Scale bars represent 100 μm .

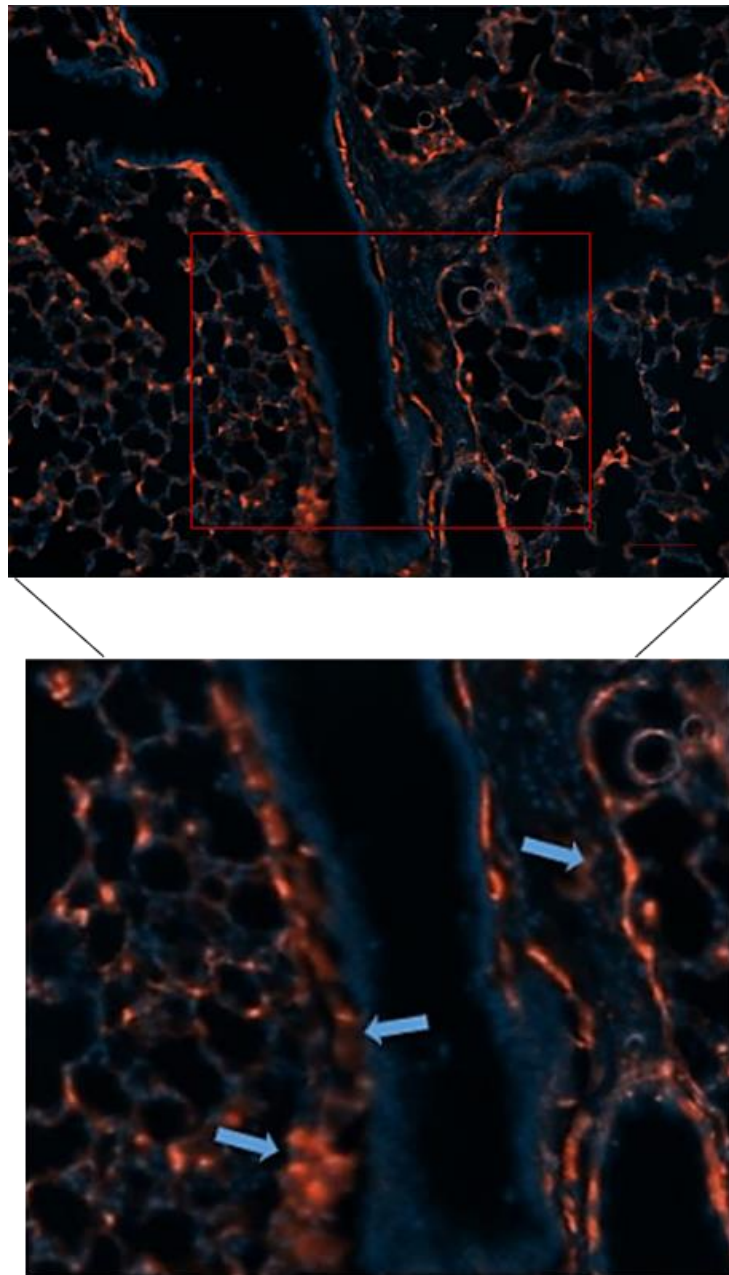


Figure 4.28 Visualisation of COL1A2-expressing cells. Red fluorescence indicates the presence of COL1A2-expressing cells. Disrupted alveolar architecture is also shown and the COL1A2 gene transcription looks more localised around the bronchiole space where the collagen is preferentially deposited during the lung fibrosis development. Blue arrows indicate the presence of elongated shaped cells which are thought to be fibroblast cells. Tissues were imaged using a Zeiss Axio Observer apotome microscope and Axio Cam MR R3 camera. Inserts show enlarged areas of image. Scale bars represent 100 μm .

4.4.6 Spatial distribution of fibroblast cells in lung tissue by Immunohistochemistry

To discriminate the spatial distribution of fibroblast cells an IHC analysis was performed in lungs with or without fibrosis from WT and COL1A2-LRP1 KO mice. LRP1 antibody was tested on WT fibrotic lungs and a positive staining was observed. Specifically, LRP1 expression was highly detected in alveolar cells surrounding the hyperplastic alveolar epithelium and in the thickened bronchioles (Figure 4.29). Lower LRP1 expression was observed in COL1A2 LRP1 KO fibrotic lungs, where LRP1 protein localised around the small alveolar spaces (Figure 4.30).

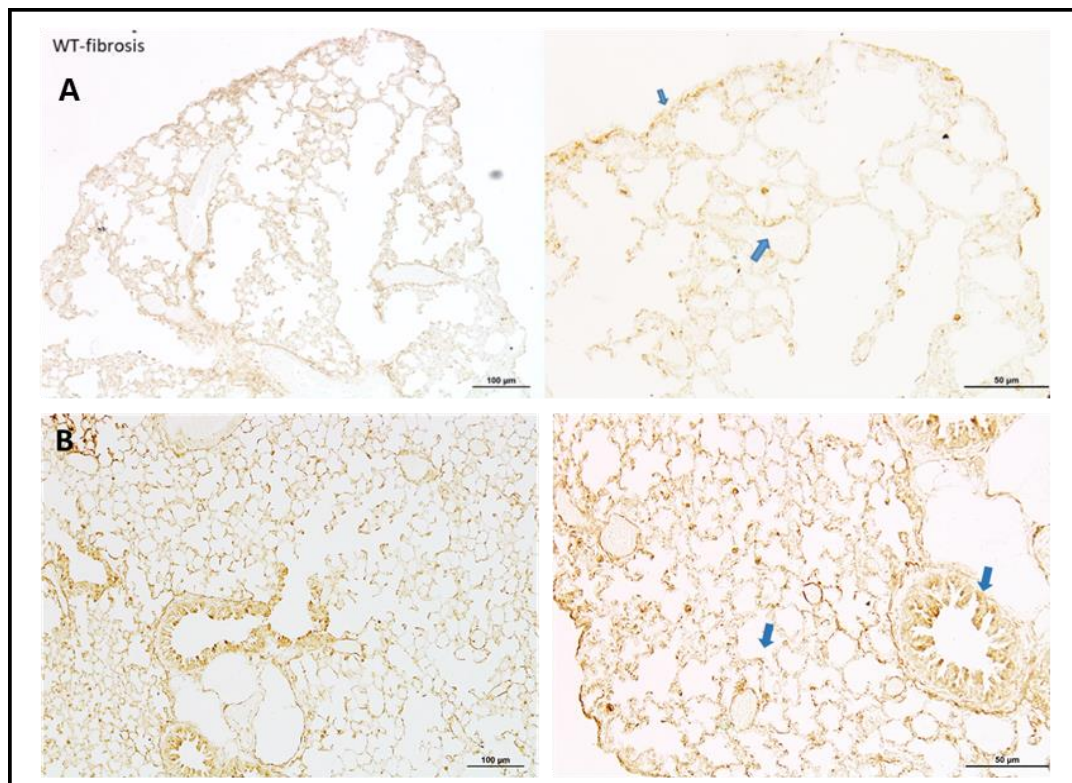


Figure 4.29 Representative LRP1 staining of WT fibrotic lung samples. These images provide the best representation of all the WT samples LRP1 immunostained through a 10x and 20X magnification. A show the presence of LRP1 in alveolar spaces while B show its presence in bronchioles both indicated by arrows, Scale bar= 100µm and 50 µm.

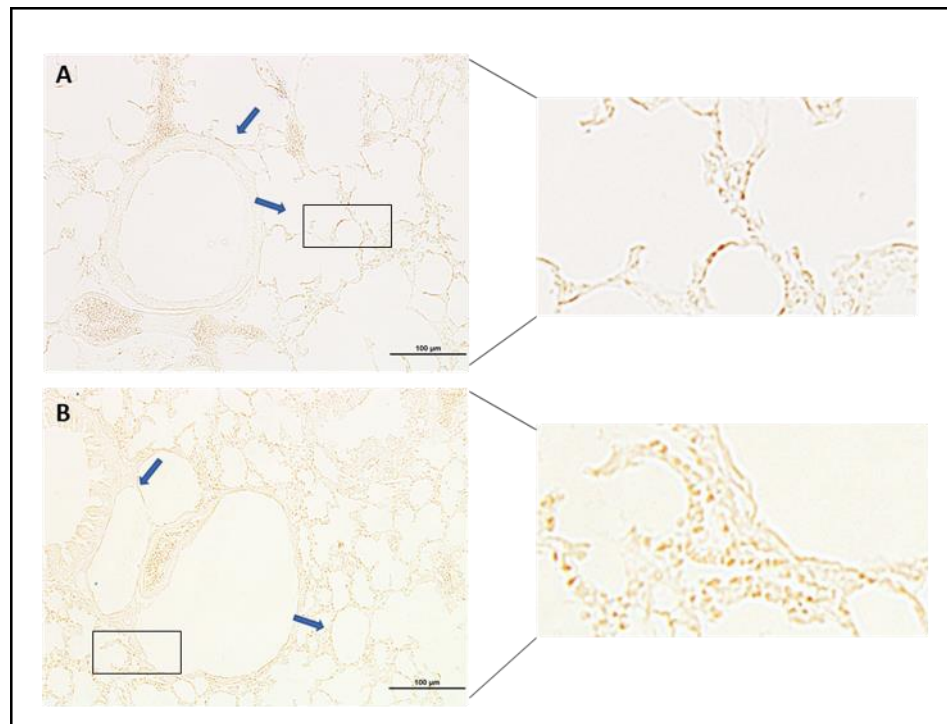


Figure 4.30 Representative LRP1 staining of COL1A2 KO fibrotic lung sample. Each of these samples were treated with bleomycin to induce fibrosis in lungs and then stained using LRP1 antibody. These images provide the best representation of all the samples stained through a 10x magnification, allowing the detection of LRP1. LRP1 is seen surrounding the alveoli and bronchioles indicated by the arrows. (A) and (B) LIV201COL1A2 KO. Scale bar= 100µm.

A panel of different fibroblast markers was performed on lung tissue by IHC. 4 recombinant rabbit monoclonal antibodies against human and mouse Vimentin, alpha smooth muscle Actin, Hsp47, S100A4 were tested on lung tissue to track the presence of fibroblast cells in the lung tissue before and after lung fibrosis development. A positive staining was found for this panel of fibroblast markers (Figure 4.31). Initially, different concentrations of the cited antibodies were tested to distinguish which provided the clearest staining. It was determined that the most consistent and strongest stain was Vimentin at a 1:1000 concentration. Whilst Hsp47 shows a strong stain at a 1:1000 concentration, it was more inconsistent as the 1:500 concentration showed weaker staining despite the higher concentration of primary antibody (Figure 4.31). Vimentin was the strongest marker for fibroblasts and so it was used

alongside the primary anti-LRP1 monoclonal antibody to stain the fibroblasts and determine LRP1 localisation in comparison with fibroblast cells (Figure 4.32). The fibroblast specific and LRP1 expression analysis suggests co-localisation between fibroblasts and LRP1 in fibrotic tissue (Figure 4.33).

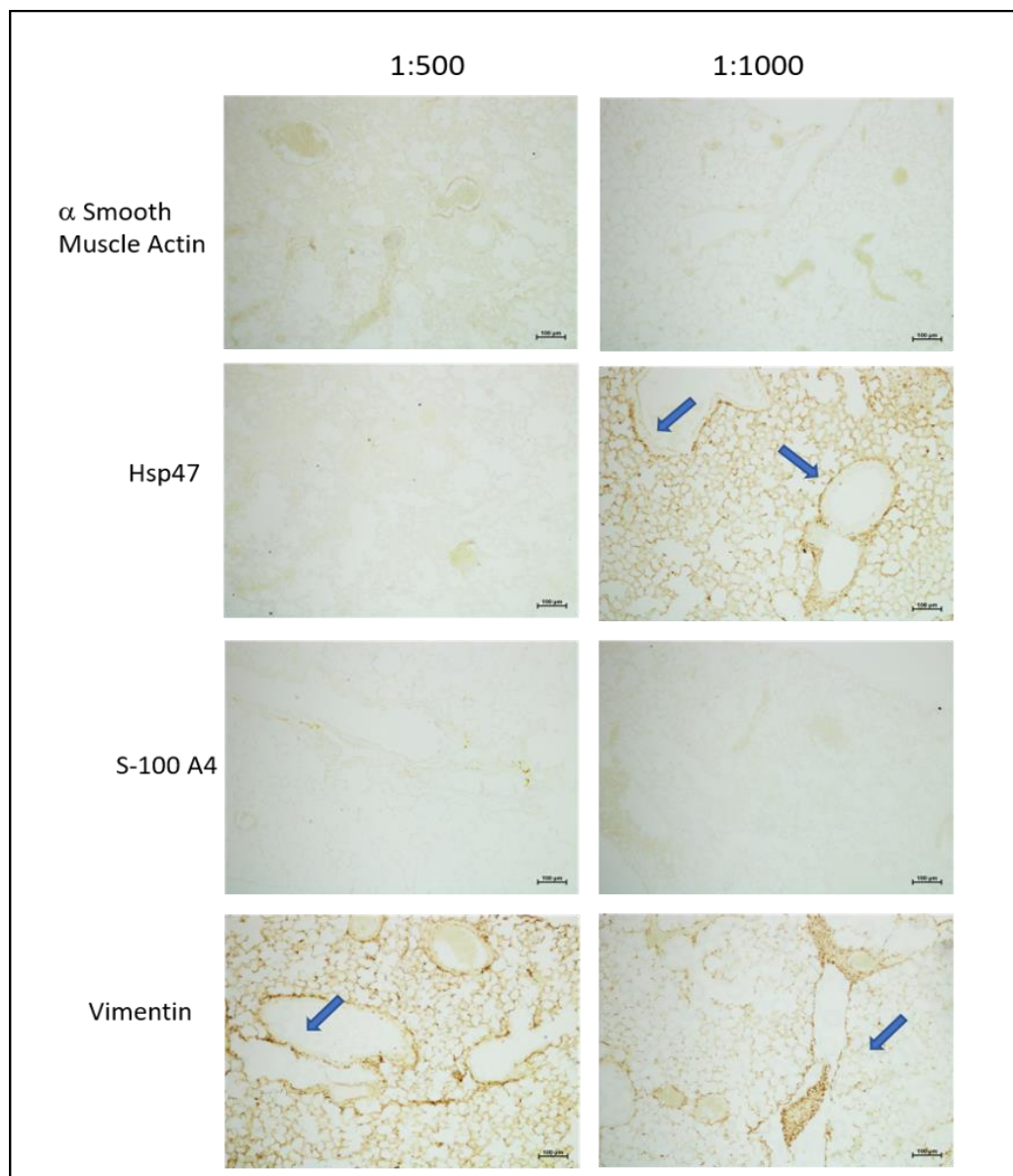


Figure 4.31 Representative optimisation of fibroblast staining on lung samples. Each of these samples were treated with bleomycin to induce fibrosis in lungs and then stained using fibroblast staining using a variety of primary antibodies staining. These images provide the best representation of all the samples stained through a

10X magnification, allowing the detection of fibroblasts. Fibroblasts surrounding the bronchioles and blood vessels are indicated by the arrows. Scale bar= 100µm.

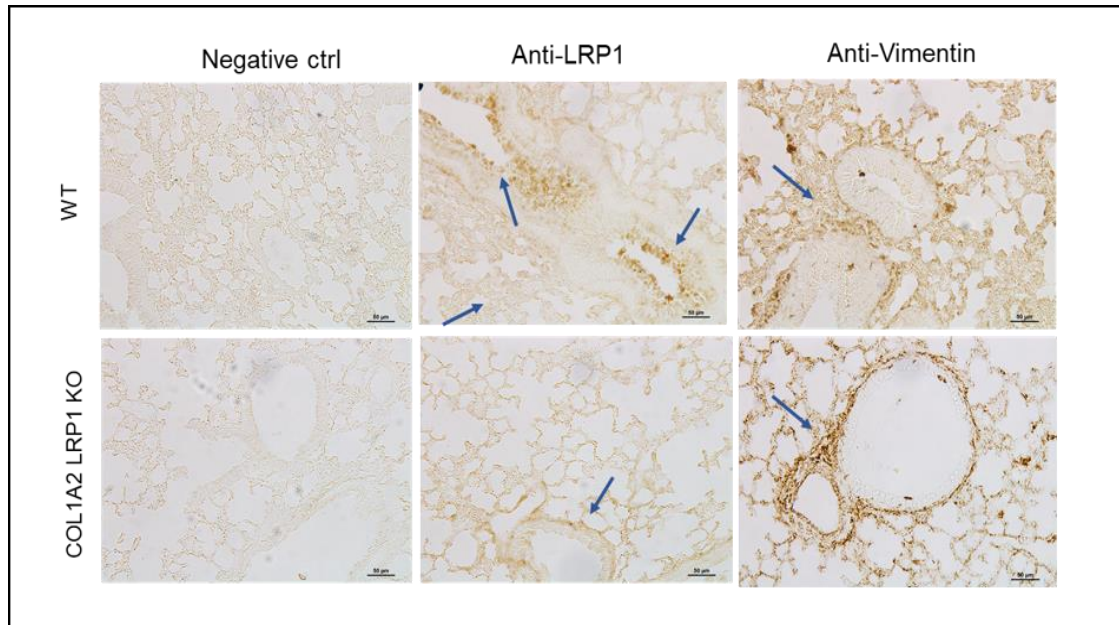


Figure 4.32 Representative LRP1 and fibroblast staining comparison on fibrotic lung tissue. Each of these samples were treated with bleomycin to induce fibrosis in lungs and then stained using either LRP1 antibody staining or the previously optimised Vimentin. These images provide the best representation of all the samples

stained through a 10X magnification, allowing the detection of LRP1 and fibroblasts. LRP1 and Vimentin localisation are indicated by the arrows. Scale bar= 100µm.

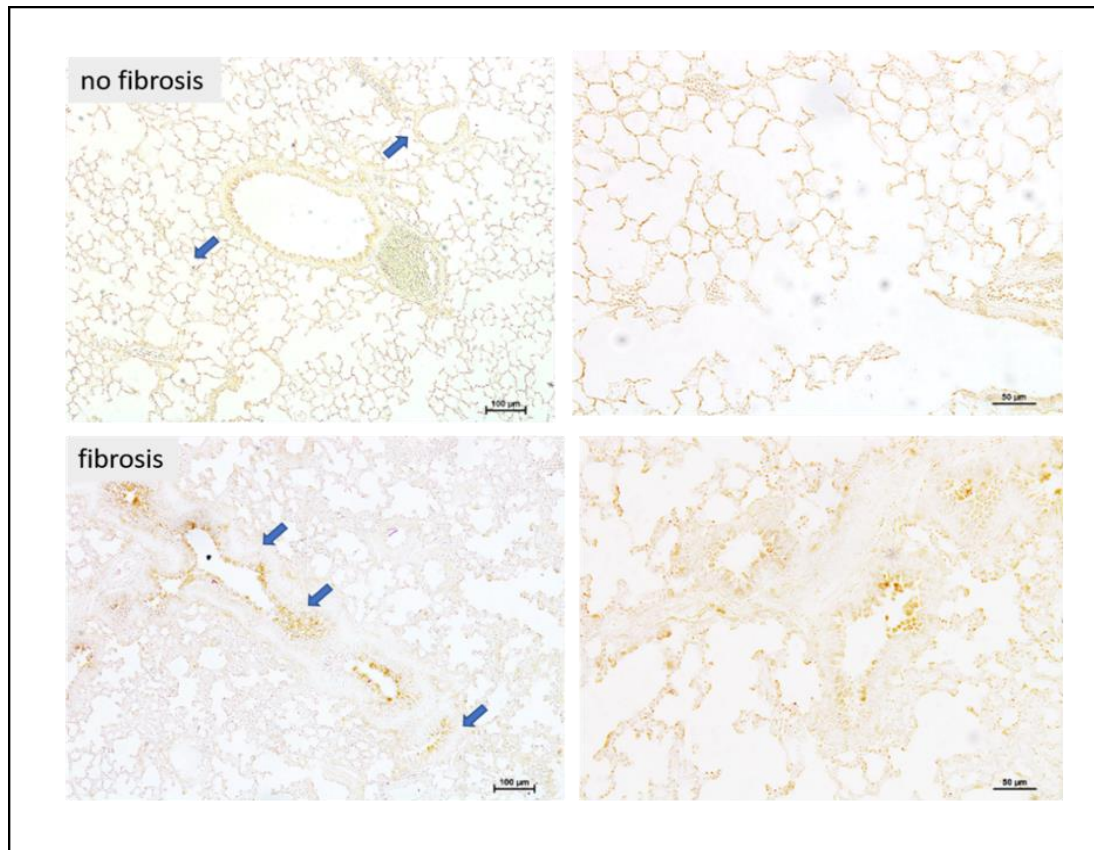
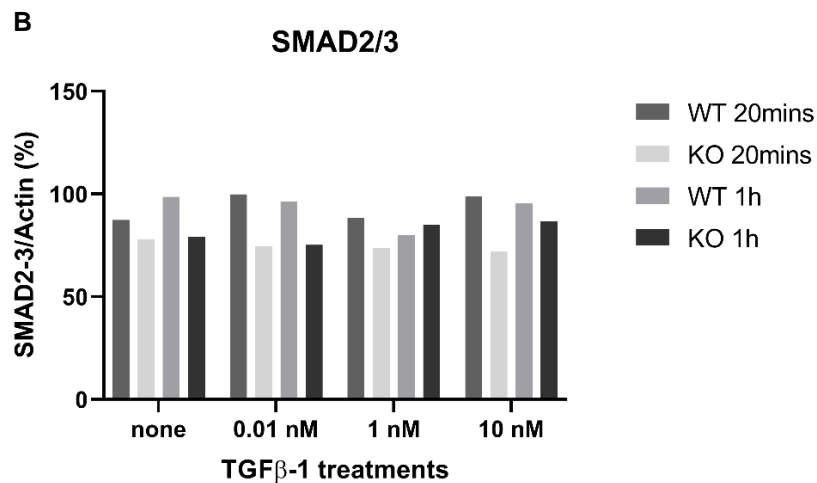
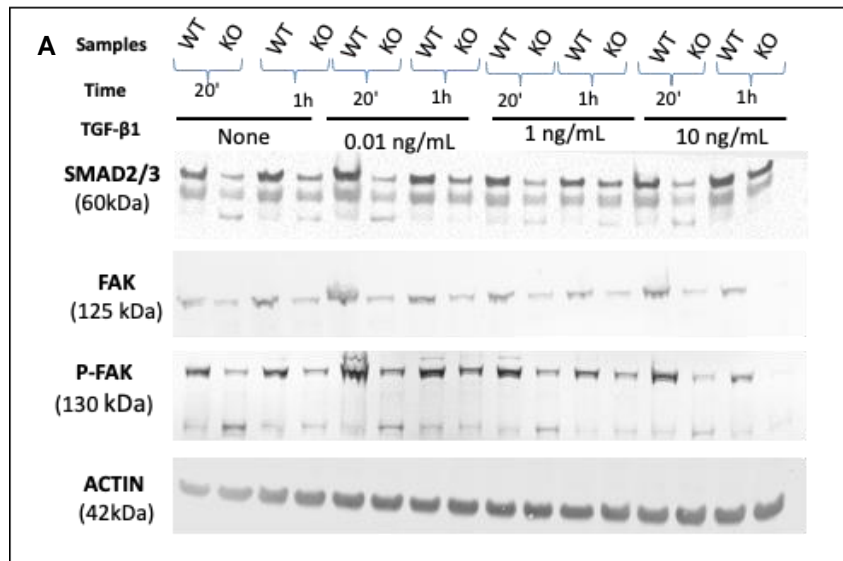


Figure 4.33 Immunostaining for vimentin protein in normal and fibrotic lung tissue. The staining is showing the spatial distribution of vimentin in lung around the bronchioles and in the alveolar cells indicated by the arrows. Scale bar= 100µm and 50µm.

4.4.7 LRP1 involvement upon TGF- β 1 presence

LRP1 involvement in pro-fibrotic response upon TGF- β 1 presence was investigated using WT and LRP1 KO MEF cells. Among the regulators identified upon TGF- β 1 activation, SMAD2/3 expression was analysed by WB. Time-course experiment showed a sustained difference between WT and LRP1 KO MEF cells, where the protein level of SMAD2/3 protein was higher in the WT upon TGF- β 1 treatments (Figure 4.34). However, a slight increase of SMAD2/3 expression level appeared using a concentration of 0.01 ng/mL for 20 minutes compared to the lower protein expression in KO. Next, we

examined the consequential expression upon phosphorylation of focal adhesion kinase (FAK), essential factor to the TGF- β 1-mediated myofibroblasts differentiation (Greensberg et al., 2006). WB results from FAK and p-FAK proteins evidenced the increased levels for both proteins in WT compared to LRP1 KO cells.



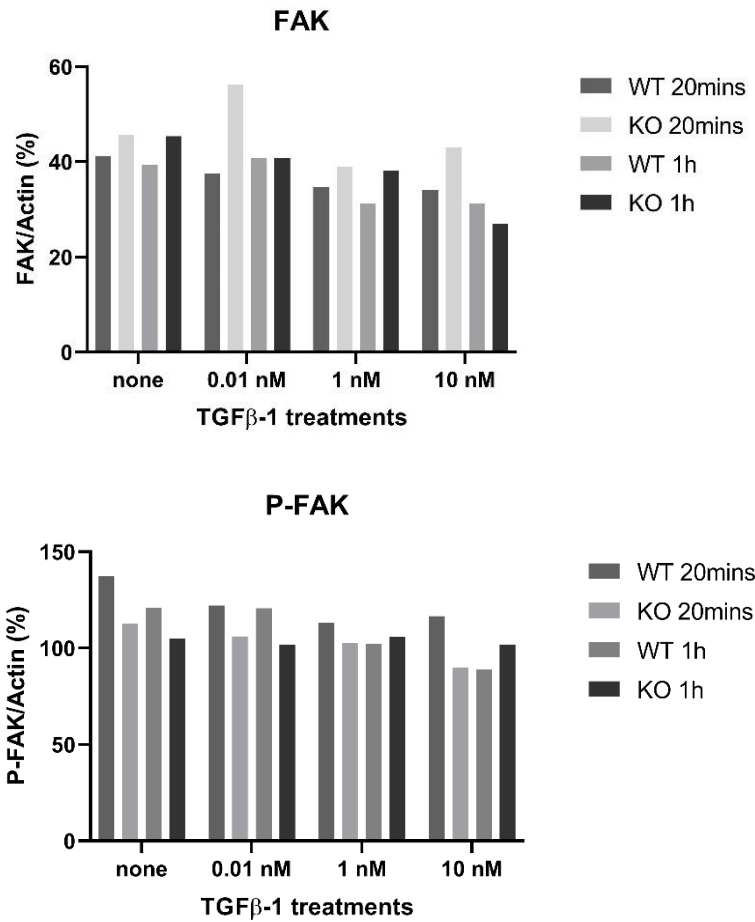


Figure 4.34 TGFβ1 treatments of MEFs cells is accompanied by expression and activation of SMAD2/3, FAK and p-FAK proteins. MEF cells were grown and then serum-starved overnight, and stimulated with 0.01, 1, and 10 ng/mL TGF-b1 for 20' and 1h. The cell extracts were analyzed by Western blotting with antibodies against SMAD2/3, FAK, P-FAK, AKT, P-AKT and actin as shown. (B) Relative protein amounts were normalised by actin as shown in the graphs below the western blotting figures (n=1).

4.5 Discussion

Bleomycin optimisation allowed us to obtain the fibrotic features such as excessive collagen deposition and inflammation. In contrast with the initial hypothesis LRP1 presence was unexpectedly found to facilitate the

development of lung fibrosis. Deletion of LRP1 in COL1A2-expressing cells resulted in a reduced collagen deposition upon bleomycin injury.

4.5.1 Why is LRP1 important for collagen deposition upon bleomycin injury?

Collagen deposition is a key characteristic of bleomycin-induced lung fibrosis (Limjunyawong, et al., 2014). Elevated grade of fibrosis was seen within the WT samples compared to COL1A2 LRP1 KO lung samples indicating that LRP1 could be a contributing factor for the development of lung fibrosis. For instance, LRP1 COL1A2 KO mice did not show lung damage and excessive collagen deposition as observed in WT mice. Whilst collagen does appear in normal lungs, specifically around blood vessels, an excessive quantity around the bronchioles was present upon bleomycin injury in WT mice.

A recent work from Tam and colleagues in 2021 showed that removal of CTGF, one of the LRP1 ligands, could attenuate the development of a fibrotic lung phenotype in vivo (Tam, et al., 2021). In this case, it is possible to speculate that in the absence of CTGF, LRP1 may internalise other pro-fibrotic molecules from the ECM, preventing the development of lung fibrosis. In lung fibrosis, the balance between MMPs and TIMPs is lost (Giannandrea & Parks, 2014). Therefore, we could assume that loss of LRP1 in COL1A2-expressing cells facilitates the accumulation of MMPs, including MMP-2 and MMP-9, which are responsible for collagen degradation during fibrosis (Liu, et al., 2011; Wilson & Wynn, 2009). Of our interest is the recent work of Chang et al., in 2020 where it has been demonstrated that collagen fibrils need to be internalised by cells to produce and release the mature molecule (Chang, et al., 2020). If LRP1 mediates collagen endocytosis and its release to the ECM to facilitate the formation of new collagen fibrils, this evidence could strongly support our findings, which showed that COL1A2 LRP1 KO mice had less collagen deposition after bleomycin injury (Fig. 4.35).

Certainly, further research is required to fully understand the relationship between the LRP1 function in COL1A2-expressing cells and more specifically which type of cells are involved in the collagen deposition.

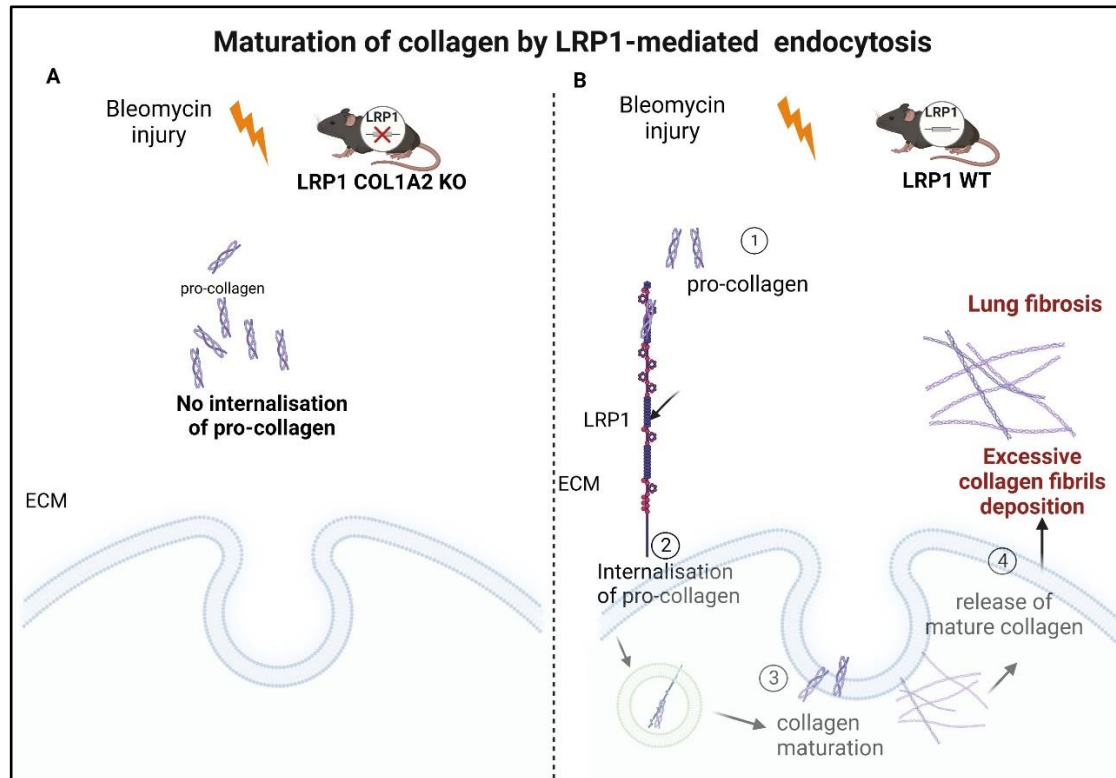


Figure 4.35 Possible involvement of LRP1 in collagen internalisation for its maturation and release to the ECM. Diagram showing a putative role of LRP1 in pro-collagen molecules internalisation for their maturation and release in the ECM. In LRP1 COL1A2 KO (A) pro-collagen is not internalised for the maturation preventing excessive collagen fibrils deposition in the ECM upon bleomycin injury. In LRP1 WT mice (B) pro-collagen is internalised by LRP1 and released in the ECM after maturation process. Excessive collagen deposition in the ECM upon bleomycin injury causes the development of lung fibrosis. Figure created in Biorender.com.

4.5.2 Is LRP1 involved in the vascular integrity?

Of interest was the presence of an unusual aneurism-phenotype in WT fibrotic lungs maybe due to a lack of oxygen in which LRP1 could contribute to the formation of blood clots. The molecular mechanism of LRP1 in the vascular system has been abundantly explored. LRP1 plays an essential role in maintaining vessel structure and homeostasis by modulating specific cellular

signalling pathways. The regulation of LRP1 on vascular homeostasis-related cells has been previously noticed and is well researched. For example, it has been reported that LRP1 function in smooth muscle cells (SMCs) can be involved in pulmonary arterial hypertension (IPAH) in a hypoxic tissue (Lugano et al. 2013). SM LRP1 KO mice showed an aneurism-phenotype suggesting an important role in the protection of the vascular tension to various pathological stimuli. Similar results were seen in the absence of LRP1 in endothelial cells (Guo. et al., 2019). However, this feature was not observed in COL1A2 LRP1 KO bleomycin-treated mice, confirming that LRP1 plays a unique tissue-specific function. It can be hypothesised that the tissue-specific deletion of the LRP1 gene in COL1A2-expressing cells prevents not only the excessive collagen deposition but also the integrity of vascular structures.

4.5.3 Are we sure that only fibroblast express COL1A2?

In parallel, we explored the presence of COL1A2-expressing cells in lung tissue by COL1A2 tdT mice. Our results suggested it is most likely that other cell types, apart from fibroblast cells, such as epithelial and macrophages cells are responsible for collagen production and deposition upon bleomycin injury. As lung fibrosis progresses, an increased differentiation of fibroblasts into myofibroblast, activated by TGF- β and other pro-fibrotic stimuli causes exaggerated secretion of ECM and thus compromises the primary pathological fibroblast phenotype in IPF (Hinz, 2015; Scotton & Chambers, 2007; Wolters, et al., 2014). A recent paper published during this work from Simoes et al., 2020, showed that macrophages directly contribute to collagen deposition contrasting with previous scientific finding where collagen production and release was exclusively attributed to myofibroblast cells. A consistent transcription of *Col1a2* was observed in the whole lung surface suggesting an expanded cellular network as response to the bleomycin injury. Therefore, the origin of fibroblasts, which differentiate into myofibroblasts in lung fibrosis, is

still an issue of dispute. In a recent work from Tzukui et al., 2020, a single-cell RNA-sequencing was performed to provide an atlas of all collagen-producing cells in normal and fibrotic lungs. In particular, they showed that smooth muscle cells and pericytes express low levels of collagen in both mice and humans (Tzukui, et al., 2020).

Reyfman and colleagues' data set represents the largest data set in lung fibrosis reported to date. Their analysis revealed an unexpected heterogeneity within macrophages and epithelial cells and distinct profibrotic macrophage populations in IPF (Reyfman, et al., 2019). In fact, Aran et al., identified a profibrotic macrophage subtype, between alveolar and monocyte-derived macrophages, upon bleomycin injury (Aran, et al., 2019).

Of interest, it is also the work of Adams et al., in 2020, that recognised the existence of previously unidentified epithelial cell population, that co-express epithelial and mesenchymal markers of IPF which are located in myofibroblast foci of fibrotic lung. Moreover, they detected two independent fibrotic archetypes in the normal lung: invasive fibroblasts likely related to resident lung fibroblasts and IPF myofibroblasts related to resident normal lung myofibroblasts (Adams, et al., 2020).

In our study we were able to track COL1A2-expressing cells in murine lungs upon bleomycin stimulation. By comparing the collagen-producing cells map from the study of Tzukui et al., in 2020 to our COL1A2 tdT bleomycin-treated mice, we may attempt to identify the subpopulations of COL1A2-expressing cells in lung upon bleomycin injury (Fig 4.36). In addition, in our study a migration of local fibroblasts around the bronchioles as a preferential area where collagen is produced and deposited was observed after bleomycin injury. Certainly, we strongly support the idea that many other cells apart from fibroblasts are able to express *Col1a2* gene in response to lung injury including smooth muscle cells, epithelial and immune cells. These findings confirmed the heterogeneity of lung fibroblast cells in both normal and fibrotic lungs.

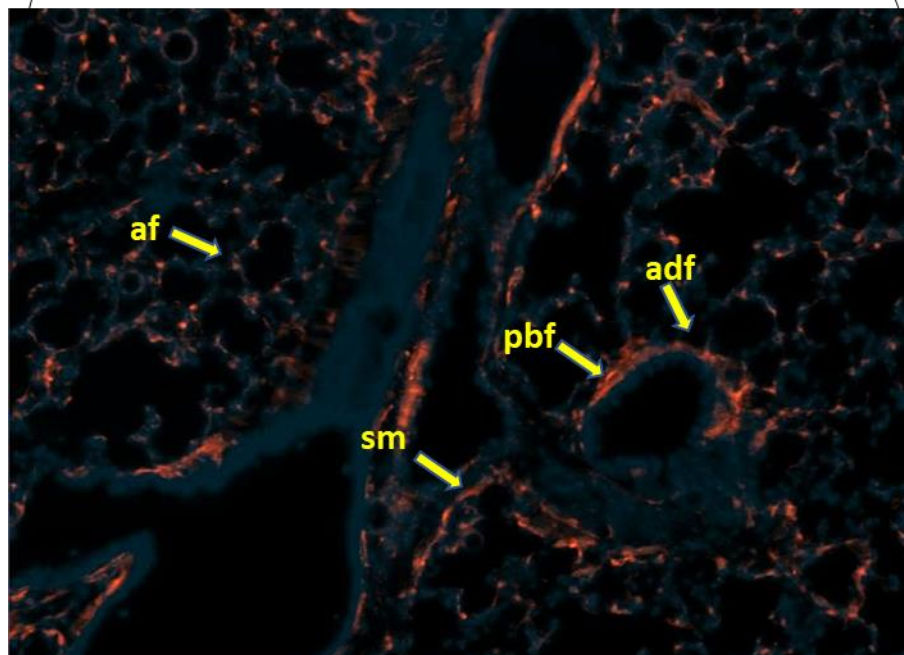
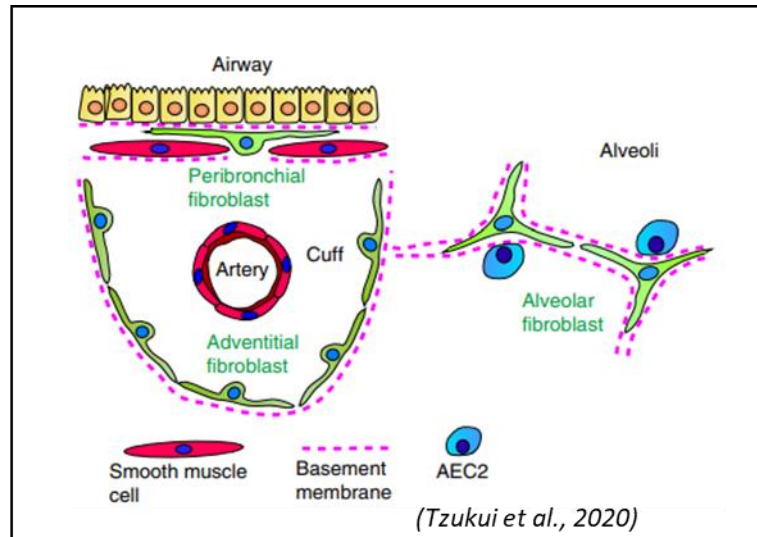


Figure 4.36 Distinct localisation of fibroblast subpopulations in respiratory tissue. Figure revised from Tzukui et al., 2020. Nomenclature indicated as af=alveolar fibroblast; pbf=peribronchial fibroblast; sm=smooth muscle cells; adf=adventitial fibroblast. Scale bar=50µm.

4.5.4 Molecular mechanisms of LRP1 in lung fibrosis development

A novel regulatory role has been shown for LRP1 as a receptor of TGF- β 1 through the activation of Smad-2/3 signalling pathway in fibrosis development (Lin, et al., 2010; Zakrzewicz, et al., 2007). TGF- β 1 is the best characterised isoform with a pivotal role in controlling fibrosis development (Letterio & Roberts, 1998; Walton, et al., 2017) in rodents by inducing the transdifferentiation of fibroblasts to myofibroblasts (Sime et al., 1997). Based on these findings, in this chapter was shown that absence of LRP1 reduces the TGF- β -mediated Smad-2/3 signalling and consequentially a myofibroblasts migration through the activation of FAK and p-FAK proteins. Certainly, further investigations are required to better explore molecular mechanisms behind LRP1 involvement in the response to fibrotic stimuli.

4.5.5 Molecules with anti-fibrotic effects on bleomycin-induced lung fibrosis model

The majority of current research has shown that the suppression of pro-fibrotic molecules including TGF- β , CTGF, uPA, collagen I, PDGF, IFN- γ , and IL-4. can prevent the development of lung fibrosis (Chambers, et al., 2008) (Willis, et al., 2005; KOTTMANN, et al., 2009). There is also a clear evidence that MMPs play an anti-fibrotic effect by their collagenolytic functions. Recent studies showed that MMP-8 and MMP-7 deficient mice developed less lung fibrosis than their wildtype counterparts after bleomycin administration (Zuo, et al., 2002; García-Prieto, et al., 2010). By contrast, overexpression of MMP-9 prevents the development of lung fibrosis (Cabrera et al., 2009).

To the best of our knowledge, very limited information has been reported in literature about other cell-surface receptors with pro-fibrotic and anti-fibrotic effects. In a work from Li et al., in 2015, it was found that suppression of N-methyl-D-aspartate receptor (NMDAR) could prevent the development of lung fibrosis after bleomycin injury (Li, et al., 2015). A recent

study showed that treatment with selective antagonist of A2B adenosine receptor (A2BAR) determines a significant reduction of lung fibrosis mediators in mice (Liu, et al., 2019). Based on this limited information, it would be essential to better explore molecular mechanisms behind the involvement of LRP1 in the modulation on fibroblast proliferation and collagen deposition.

4.5.6 Limitations

Within the clinical field, tomography-based analysis is considered the golden standard as a diagnostic tool. However, genetic variability in mice and the difficulty of working with fibrotic lung tissue, represented one of the limitations on performing specific procedures shown in this chapter. For instance, the in vivo μ -CT analysis approach was useful to visualise lung injury due to bleomycin administration resulting in ECM deposition and increased lung stiffness. Whilst the abnormalities seen within the scans could be a result of lung injury, these observations required further analysis to draw any definitive conclusions and to identify if the levels of fibrosis have changed throughout the development of the samples post-bleomycin administration. The retrospectively gated acquisition protocol in “high speed” mode with 50 mm reconstructed voxel size did not allow us to obtain clear and suitable images for the image post-processing. In fact, images noise acquired during the analysis caused artefacts. For this reason, histological examination in parallel was required due to the background problem post-acquisition image analysis algorithms.

4.5.7 Conclusions and future plans

LRP1 does not appear to have a protective function as seen in previous evidences (Wygrecka, et al., 2011; Yamamoto, et al., 2017). Based on our results it can be hypothesised that LRP1 loss results in the accumulation of anti-fibrotic molecules, impaired pro-fibrotic signalling pathways and inefficient collagen maturation and release in the ECM (Figure 4.35). Further

characterisation of COL1A2-expressing cells and their co-localisation with LRP1 is required to determine the internalisation process of newly synthesised collagen for its consequential excessive release in lung fibrosis pathogenesis.

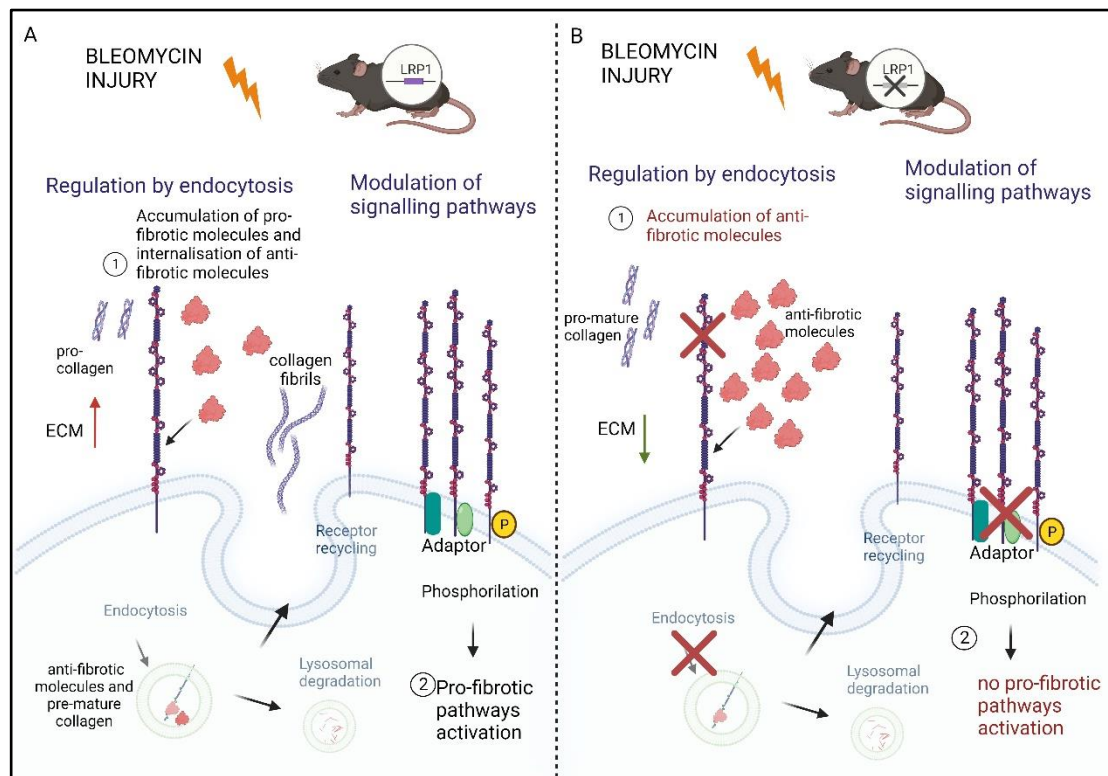


Figure 4.37 LRP1 loss in COL1A2-expressing cells is preventing fibrosis development. A shows the development of fibrosis after bleomycin injury in the presence of LRP1 gene. Accumulation of pro-fibrotic molecules and internalisation of anti-fibrotic molecules and pro-collagen molecules could lead to the collagen deposition after bleomycin injury. LRP1 can also activate pro-fibrotic signalling pathway. B Loss of LRP1 in COL1A2-expressing cells facilitate the accumulation of anti-fibrotic molecules in the ECM and prevents the internalisation of pro-collagen molecules. Figure released using Biorender.com.

Chapter 5 Identification of LRP1 ligands in lung tissue

Summary

Investigation of LRP1 ligands in lung cells was performed during the *in vivo* experiments. LRP1 ligandome in lung is necessary to discover novel LRP1 interactions and possibly to pioneer new scientific prospects in the respiratory field.

The work presented in this chapter aimed to identify and characterise LRP1 ligands in healthy lung cells. To identify LRP1 ligands in lung, LRP1-conjugated magnetic beads were used to isolate LRP1 ligands in the medium of human and murine primary lung fibroblasts. Those molecules were identified by mass-spectrometry analysis. This study was in part carried out by a collaboration which took place in Enghild's lab with Professor Jan J. Enghild and Dr Carsten in Denmark (Department of Molecular Biology and Genetics (MBG), University of Aarhus, Denmark).

5.1 Introduction

LRP1 is a large ubiquitous endocytic receptor mediating the uptake of various molecules from the extracellular matrix to the cells. Through its endocytic function and effective LRP1 recycling facilitates the transport of its ligands to lysosomes mediating their degradation, therefore maintaining a homeostatic balance in the extracellular matrix microenvironment (Gonias & Campana, 2014). More than 100 ligands have been found to bind and interact with LRP1 (Lillis, et al., 2008; Yamamoto, et al., 2022). However, LRP1 ligands in lung tissue have not been explored so far. Lung fibroblasts constitute less than 20% of the total lung cell populations and are responsible for the collagen production and deposition in lung fibrosis. Our previous results showed that LRP1 protein is highly expressed in lung fibroblast cells and is required for excess collagen deposition. The main aim of this chapter was to identify the presence of LRP1 ligands in human lung fibroblast cells and murine lung cells in healthy condition to provide a better understanding of its pulmonary function.

5.2 General aims and objectives

LRP1 has been identified as relevant gene for the lung function. It results to cover a tissue-specific function and for this reason could bind a variety of ligands depending on its localisation. In our lab, Yamamoto et al., 2022 have identified a number of new LRP1 ligands in cartilage.

For this reason, the aims of this chapter were as following:

- I. Identify the presence of new LRP1 ligands in lung tissue: the first objective for this aim was to determine a number of proteins bound to LRP1 by mass spectrometry analysis. Human lung fibroblast cells (MRC5) and murine lung cells, isolated from mice, were used for this aim.
- II. Evaluate the effects of LRP1 blockade *in vitro*: the objective for this aim was to test the effect of molecules accumulated in the presence of sLRP1-2 fraction and RAP, which physically binds to LRP1 receptor. Cell survival assay were performed by cell counting and MTS assay.

5.3 Chapter-specific methods

5.3.1 Endocytosis Assays

Cells were grown to confluence in 24-well plates. Cells were with serum-free DMEM/F12 media 24 hours before the experiment treatments at 37 °C. The day after cells were incubated with serum-free DMEM/F12 media containing 0.1 % BSA with or without GM6001 (10 µM), RAP (500 nM) (Figure 5.1). Following this, ADAMTS-5 (100 nM) was added and incubated for different time points up to 24 h. After incubation, the conditioned medium was collected at: 5mins, 3, 8 and 24h. Samples (15 µL) was resuspended in 30 µL of 2x reducing sample buffer and analysed by SDS-PAGE (10 % acrylamide) and WB with the anti- catalytic domain ADAMTS-5 antibody.

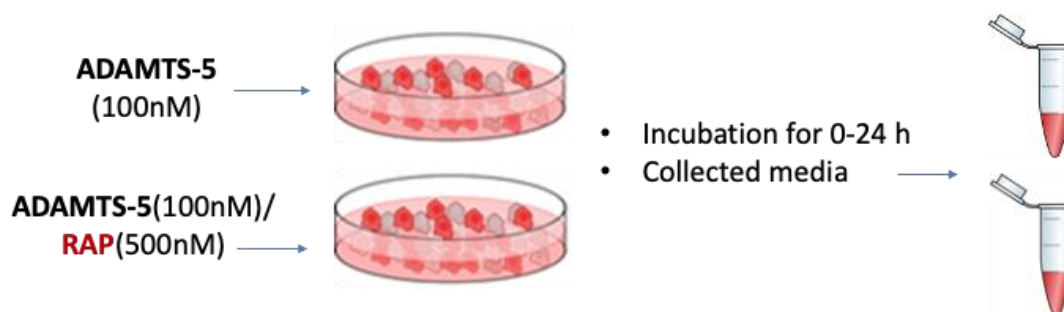


Figure 5.1 Schematic experiment's design for the endocytosis assay. ADAMTS-5 was added to the media of human primary lung fibroblast cells (MRC5) and murine lung cells isolated from mice. Cells were plated and incubated with ADAMTS-5 (100nM) with or without the presence of RAP (500nM) and media was collected at: time 0, 5 mins, 3 hours, 8 hours and 28 hours incubation time.

5.3.2 Protein purification of sLRP1-2 and RAP

Isolation of sLRP1 has been reported from fresh-frozen human plasma by a modification of previously published methods (Quinn, et al., 1997). The expression vector for the selected portions (ligand binding domain clusters I-IV) of LRP1 has been prepared previously from Mikhailenko I. et al. in 2001. Secreted fragments of LRP1 containing individual ligand binding domain clusters were transiently expressed in HEK293 cells using TransIT-2020 transfection reagent (Mirus) according to the manufacture's protocol. Cells growing in 150-mm dishes (~70% confluence) were transfected in serum-containing DMEM with 30 µg of pSecTagB (Invitrogen) carrying cDNA for various LRP1 fragments. After 6 h of transfection, the medium was replaced with serum-free DMEM, and cells were further incubated for 72h. The resultant conditioned medium was directly applied to a nickel-nitrilotriacetic acid affinity column (Qiagen) that had previously been equilibrated with 50 mM HEPES (pH 7.5) buffer containing 150 mM NaCl and 5 mM CaCl₂. The column was washed with 10 column volumes of 50 mM HEPES (pH 7.5) buffer containing 1 mM NaCl, 5 mM CaCl₂, and 20 mM imidazole. It was then eluted by 500 mM imidazole in HEPES (pH 7.5) buffer containing 150 mM NaCl and 5 mM CaCl₂. For analysis of N-linked glycosylation of soluble LRP1 fragments, the preparations were treated with peptide N-glycosidase F (New England Biolabs,

Ipswich, MA) according to the manufacturer's protocol. Recombinant human C-terminally His-tagged RAP was purified as described previously (Figure 5.2) (Yamamoto, et al., 2014).

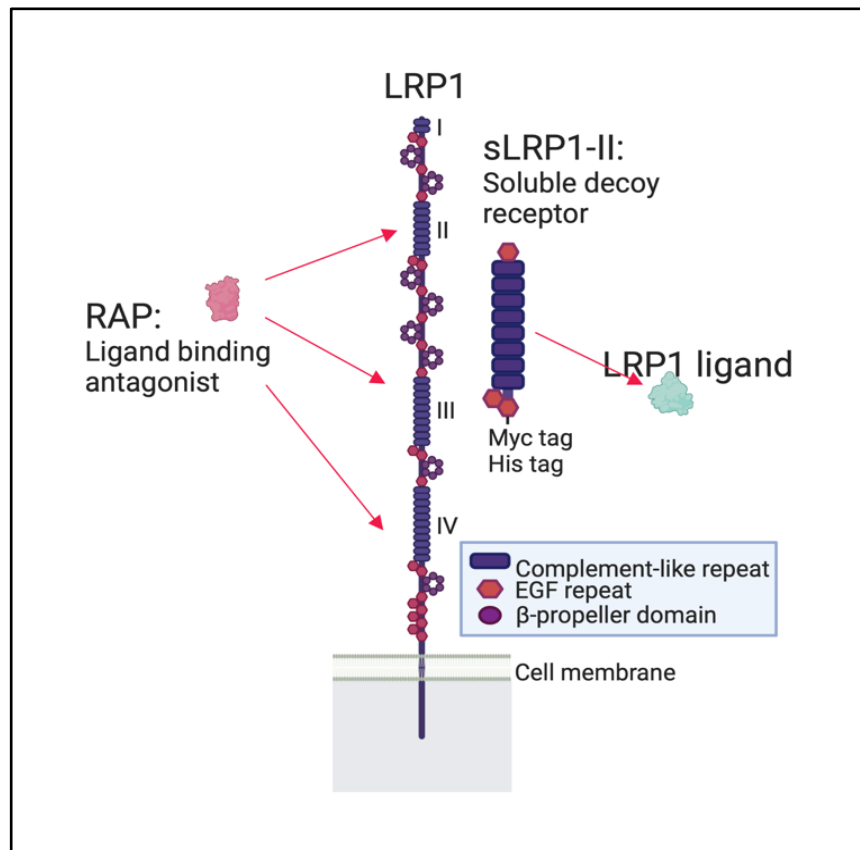


Figure 5.2 LRP1 and its soluble receptor domains. The four clusters binding domains are shown as I-IV together with RAP, also known as LRP1-antagonist (Yamamoto et al., 2022).

5.3.3 Silver staining

Purified proteins were separated under reducing conditions on a 4-12% Bis-Tris NuPage Gels (Thermo Fisher) and stained with a commercially available silver staining kit (Thermo Fisher). The gel was washed in ultra-pure water and fixed in 30% ethanol:10% acetic acid solution twice for 15 minutes. The gel was washed in 10% ethanol solution and then sensitized in a Sensitizer Working Solution containing 50 μ L Sensitizer and 25mL of ultrapure water for 1 minute. Next, the gel was incubated with a previously prepared

Stain Working Solution, containing 0.5mL of Enhancer and 25mL Stain solution for 30 minutes. Then a Developer Working Solution was prepared adding 0.5mL Enhancer to 25mL Developer solution. Finally, the gel was developed for 3-5 minutes until bands appeared and the reaction was stopped adding a 5% acetic acid solution for 10 minutes.

5.3.4 Mass-spectrometry analysis

The conditioned medium was collected and further incubated with anti-c-Myc paramagnetic Dynabeads at 4°C for 1 h. sLRP1-2 and the magnetic beads complexes were then isolated using the magnetic stand, washed with the buffer consisting of 50 mM Tris-HCl (pH 7.5), 150 mM NaCl, 5 mM CaCl₂ (TNC), and 0.02% Brij35 (TNCB) for three times, and eluted with 200 ml of 0.1 M glycine buffer (pH 3.0) for 10 min at 4°C. The eluents were neutralised with 10 ml of 1 M Tris-HCl (pH 8.0). Next, samples were denatured and reduced in 8 M Urea containing 5 mM Dithiothreitol for 1 h, alkylated with 15 mM Iodoacetamide for 1 h and diluted 10-fold with 50 mM NH₄HCO₃. Sequencing grade trypsin was added (1:50 w/w) and the sample was digested overnight 37 °C. The sample was desalted using self-packed reverse phase micro-columns containing C18 column material (Empore™). LC-MS/MS was performed using an EASY-nLC 1000 (Thermo Scientific) connected to an Q Exactive Plus mass spectrometer (Thermo Scientific) (Figure 5.3). The peptides were separated on a 15-cm analytical column (75 µm inner diameter). The column was packed in-house with ReproSil-Pur C18-AQ 3 µm resin (Dr. Maisch GmbH, Ammerbuch-Entringen, Germany). The flow rate were 250 nl/min and a 50 min gradient from 5% to 35% phase B (0.1% formic acid, 90% acetonitrile). The acquired MS data were processed in Proteome Discoverer 2.4 (Thermo Scientific). The collected MS files were converted to generic Mascot format (MGF) using the Sciex MS Data Converter beta 1.1 or RawConverter (He, at al., 2015). The data was searched against the human proteome (UniProt).

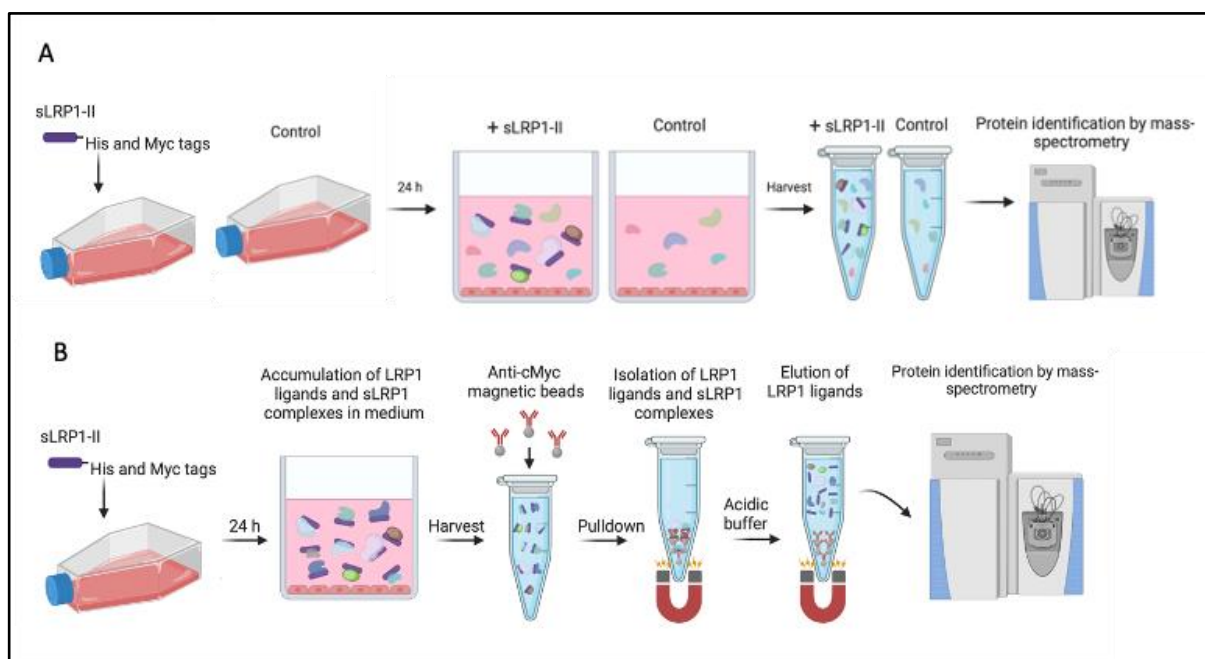


Figure 5.3 Schematic diagram of the experiment's plan for the mass spectrometry analysis. A shows the experiment's design for the ligandome assay and B shows the methodology for the pulldown assay. Following this methodology, LRP1 ligands are accumulated in the media of the cells. New LRP1 ligands candidates were then identified by mass spec analysis.

5.3.5 Cell survival assay human primary lung cells

MRC-5 lung cells were grown on 48 well plate with DMEM/F12 containing 10% FBS. Once the cells reached 70-80% confluency, the medium was removed and the cells were rested in 0.2 mL of serum-free (SF) DMEM/F12 for 24 hours. The cells were then incubated with 0.2 mL of fresh SF DMEM/F12 and with 0.2 mL of DMEM/F12 containing 1% of FBS in the absence or presence of 10 nM sLRP1-2 or 500 nM RAP for 0-72 hours. Cell images after incubation were acquired by Nikon Eclipse Ti-E and Diaphot with ToupCam camera (Nikon, Tokyo, Japan). Cell viability at 72-h incubation was measured by MTS cell proliferation colorimetric assay (CellTiter 96® AQueous One Solution Cell Proliferation Assay system, Promega, G3582). Cell numbers at 0, 24, 48 and 72-n incubation were counted by the hemocytometer (Hausser Scientific).

5.3.6 Cell survival assay of murine lung cells after isolation

LRP1-expressing and -deficient murine primary lung cells were seeded at a density of $0.03 \times 10^6 / \text{cm}^2$ in 48-well plates in serum-containing media and serum-free media. Cell survival was monitored by a combination of microscope visualisation and manual cell counting for 5 days. Cells were trypsinised and resuspended in a final volume of 200 μ L DMEM. 15 μ L of cell suspension was added into each chamber of the hemocytometer (Hausser Scientific). Images were acquired by Nikon Eclipse Ti-E and Diaphot with ToupCam camera (Nikon).

5.3.7 siRNA-mediated gene silencing of LRP1

siRNA oligonucleotides for LRP1 (On-TargetPlus SMARTpool siRNA), and non-targeting oligonucleotide were purchased from Thermo Scientific Dharmacon (Lafayette). Cells were seeded in 24-well plate with DMEM containing 10% FBS and incubated until 40-50% confluency. Transfection of siRNA into MRC-5 was carried out using Invitrogen™ Lipofectamine™ 3000 Transfection Reagent (Invitrogen) according to the manufacturer's instructions. Cells were transfected with siRNA at a final concentration of 20 and 40 nM in Gibco™ Opti-MEM™ Reduced Serum Medium (Thermo Fisher Scientific). The siRNA-lipofectamine complex was added to the wells and the Opti-MEM was replaced with fresh DMEM/F-12 media after 6 hours.

5.4 Results

5.4.1 LRP1 is highly expressed in human and murine primary lung cells

Initially, a LRP1 protein expression check was performed in MRC-5 (human primary lung fibroblasts), BEAS-2B (Human epithelial bronchial cell), murine primary lung cells, and A549 (Human cancer epithelial cells) in comparison with human chondrocytes cells since LRP1 protein has been previously found abundantly expressed in our lab (Yamamoto, et al., 2014). LRP1 protein level was compared to purified sLRP1 full length, 5ng and 25ng respectively, as positive control (Figure 5.4 A-B). WB results showed a high expression of LRP1 protein in a variety of lung cells. However, LRP1 expression was 41.1% higher in MRC5 compared to BEAS-2B and Murine primary lung cells and A549.

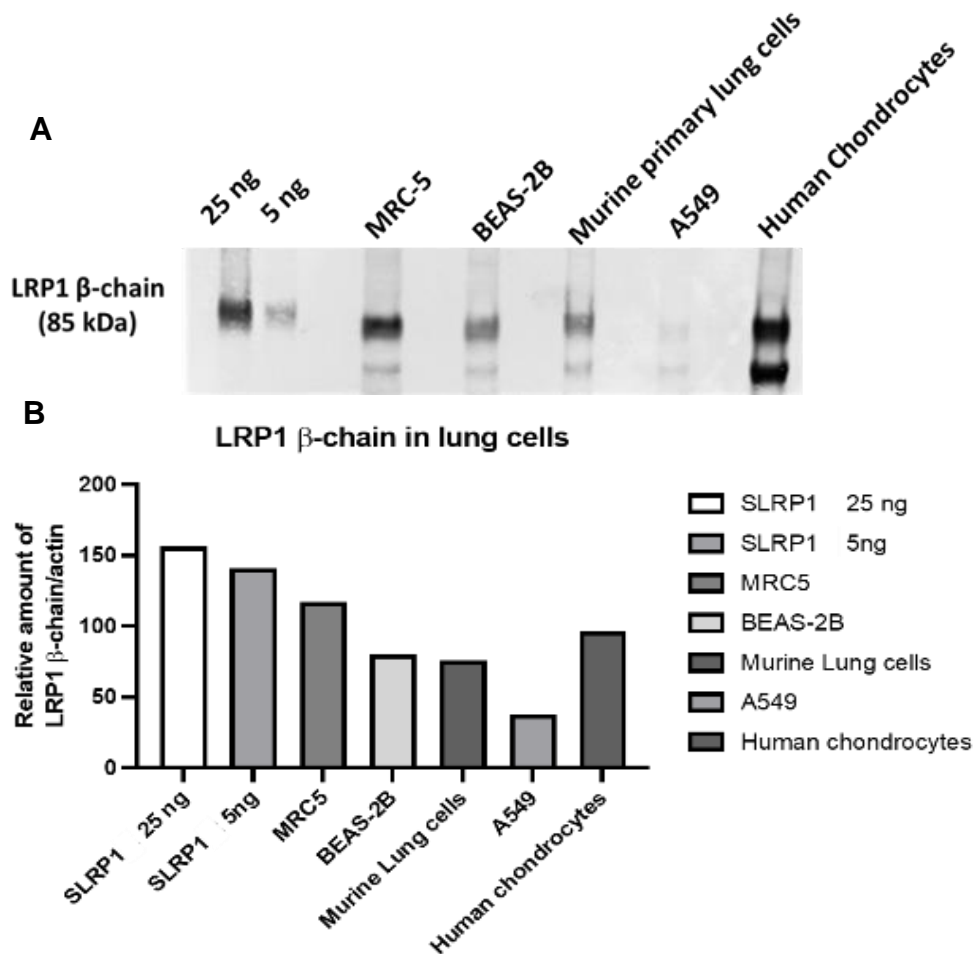


Figure 5.4 LRP1 is highly expressed in lung cells. Purified sLRP1 (25-5ng) and protein extracted of 50000 cells from human primary lung fibroblasts (MRC-5), human epithelial lung cells (BEAS-2B), murine primary lung cells, adenocarcinomic human alveolar basal epithelial cells (A549) and human primary chondrocytes were separated on a 4-12% gel under reducing conditions and analyzed by Western blotting using an anti-LRP-1 β -chain antibody (A). (B) Graph shows the relative amount expressed in percentage (%) and normalised by actin.

5.4.2 Rapid clearance of ADAMTS-5 by human and murine lung cells

To investigate the ability of LRP1 to endocytose molecules in lung cells, an endocytosis assay was performed for the detection of exogenously added ADAMTS-5 protein which is considered not detectable in lung since nobody reported it in the Human Protein database. The amount of ADAMTS-5 in the medium of cells reduced over a 24h time (Figure 5.5). Protein level results

suggested that exogenously added ADAMTS-5, was internalised by the cells with half-life of <8-hours (Figure 5.5 B). Importantly, the presence of the antagonist RAP, which blocks directly to LRP1 on the cell surface, allowed us to unquestionably confirm that the ADAMTS-5 endocytosis was mediated by LRP1 in lung cells (Figure 5.5 B).

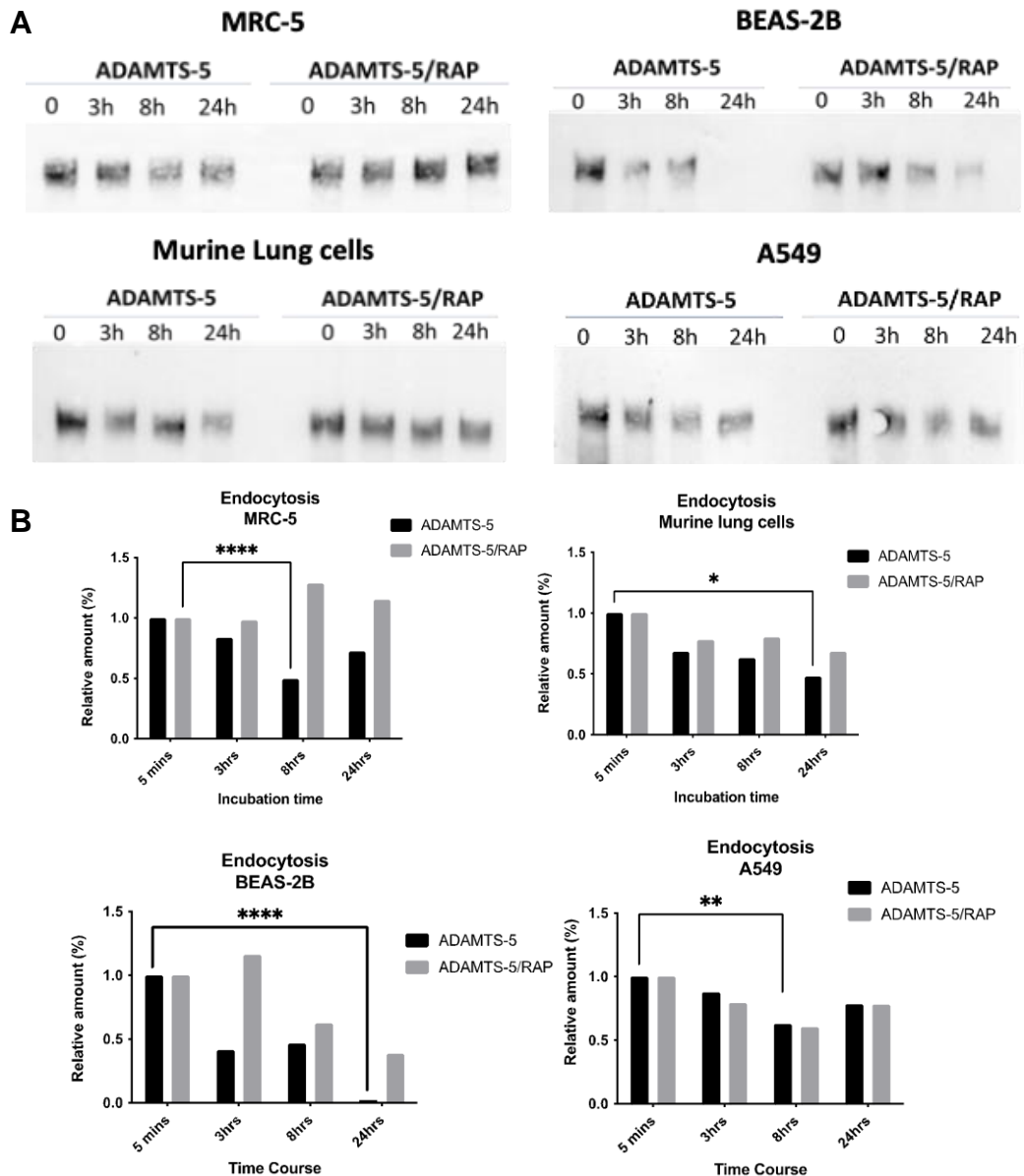


Figure 5.5 ADAMTS-5 is rapidly internalised by LRP1 in lung cells. Cells were incubated with 100 nM ADAMTS-5 and with RAP (500nM) up to 24h. ADAMTS-5 in the media was detected by Western blotting analysis using an anti-ADAMTS-5

catalytic domain antibody. Amount of ADAMTS-5 is expressed as a percentage of the amount of ADAMTS-5 at 0 h in the graphs (B). Statistical analysis was performed using one-way Anova with Tukey's multiple comparisons: p-value * <0.0127 ** <0.0013 *** <0.0003 .

5.4.3 Novel LRP1 ligands candidates in human and murine lung cells

To identify molecules that potentially could directly interact with LRP1, cells were incubated with sLRP1-2 (10nM). The list of molecules in the control samples was used to estimate a fold-difference with the ligands in the presence of sLRP1-2. A total number of 490 molecules were detected including 374 intracellular 49 cell-membrane and 74 secreted molecules according to the Uniprot annotation (Figure 5.6). Among these molecules, previously reported LRP1 ligands were identified such as TIMP-3, CTGF and Fibrinogen gamma chain (FGG), Fibronectin, Decorin, TIMP-2, while 10 were novel LRP1 ligands candidates in both human and murine lung cells such as A disintegrin and metalloproteinase with thrombospondin motifs 1 (ADAMTS-1), Complement C4-B, Nephronectin, Galectin-1, Cathepsin B, Biglycan, Fibrillin-1, Insulin-like growth factor-binding protein 7, Gremlin-1 and Lumican (Table 5.3).

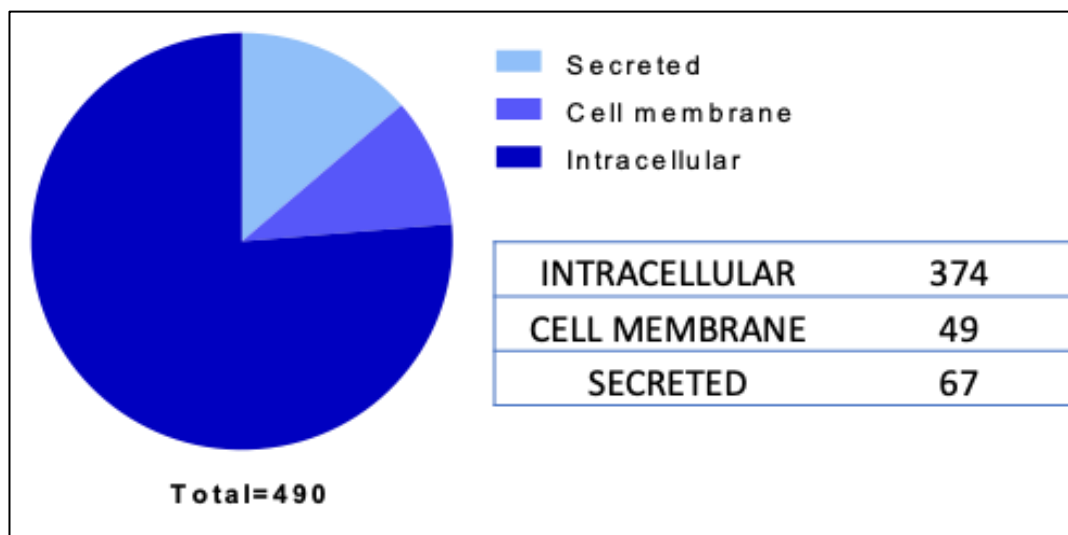


Figure 5.6 Pie chart showing number of secreted, transmembrane, and intracellular proteins found by mass-spectrometry analysis in human and murine lung cells.

Table 5.1 Novel LRP1 ligands candidates identified in Human primary lung fibroblast cells (MRC-5).

Novel LRP1 ligand candidates	
P29279	Connective tissue growth factor
P14174	Macrophage migration inhibitory factor
Q99584	Protein S100-A13
P07339	Cathepsin D
O94813	Slit homolog 2 protein
Q92820	Gamma-glutamyl hydrolase
Q9HCB6	Spondin-1
P02765	Alpha-2-HS-glycoprotein
P55001	Microfibrillar-associated protein 2
P15018	Leukemia inhibitory factor
Q15063	Periostin
P98160	Basement membrane-specific heparan sulfate proteoglycan core protein
P61769	Beta-2-microglobulin
P02461	Collagen alpha-1(III) chain
P07942	Laminin subunit beta-1
Q12805	EGF-containing fibulin-like extracellular matrix protein 1
Q12841	Follistatin-related protein 1
P00736	Complement C1r subcomponent
O00300	Tumor necrosis factor receptor superfamily member 11B
Q9UBP4	Dickkopf-related protein 3
Molecules already known as LRP1 ligands	
O00622	Protein CYR61
Q8IUL8	Cartilage intermediate layer protein 2
P35625	Metalloproteinase inhibitor 3
O14558	Heat shock protein beta-6
P07996	Thrombospondin-1
P01024	Complement C3
P00749	Urokinase-type plasminogen activator
P02751	Fibronectin
P07585	Decorin
Q14624	Inter-alpha-trypsin inhibitor heavy chain H4
P16035	Metalloproteinase inhibitor 2
P53680	AP-2 complex subunit sigma
F>10	(Molecules detected in treated cells with SLRP1-2)
Novel LRP1 ligand candidates in both Human and Murine lung cells	
P09382	Galectin-1
P07858	Cathepsin B
Novel LRP1 ligand candidates	
Q99715	Collagen alpha-1(XII) chain
P09429	High mobility group protein B1
P62937	Peptidyl-prolyl cis-trans isomerase A
P04083	Annexin A1

Table 5.2 Novel LRP1 ligands candidates identified in primary murine lung cells.

Novel LRP1 ligand candidates
Protein Wnt-11
High mobility group protein B1
Slit homolog 3 protein
Stromelysin-1
C-X-C motif chemokine 14
Fibulin-1
Carboxypeptidase Q
Cartilage intermediate layer protein 2
Peptidyl-prolyl cis-trans isomerase A
Aminopeptidase B
SPARC-related modular calcium-binding protein 1
Microfibrillar-associated protein 2
Afamin
NAD(P)H-hydrate epimerase
Procollagen C-endopeptidase enhancer 1
C-C motif chemokine 6
Pentraxin-related protein PTX3
Insulin-degrading enzyme
Beta-2-glycoprotein 1
Collagen alpha-1(XV) chain
Fibulin-2
Collagen alpha-2(V) chain
Nidogen-1
Slit homolog 2 protein
Cell migration-inducing and hyaluronan-binding protein
Progranulin
Follistatin-related protein 1
Protein-lysine 6-oxidase
Bone morphogenetic protein 1
72 kDa type IV collagenase
Macrophage colony-stimulating factor 1
Laminin subunit gamma-1
Stromal cell-derived factor 1
Macrophage migration inhibitory factor
Collagen alpha-1(V) chain
Cartilage-associated protein
Molecules already known as LRP1-ligands
Metalloproteinase inhibitor 2
Midkine
Pigment epithelium-derived factor
Tissue-type plasminogen activator
Complement C3 OS=Mus musculus
Connective tissue growth factor
Antithrombin-III OS=Mus musculus
Apolipoprotein E
Alpha-2-macroglobulin-P
Metalloproteinase inhibitor 1
Platelet factor 4
Complement C1q subcomponent subunit C

Table 5.3 List of LRP1 ligands in both human and murine lung cells.

Novel LRP1 Ligands candidates in both Human and Murine lung cells	
P97857	A disintegrin and metalloproteinase with thrombospondin motifs 1
P01029	Complement C4-B
Q91V88	Nephronectin
P28653	Biglycan
Q61554	Fibrillin-1
Q61581	Insulin-like growth factor-binding protein 7
O70326	Gremlin-1
P51885	Lumican
P10605	Cathepsin B
P16045	Galectin-1

5.4.4 Blockade of LRP1 effects on lung cells

Floating cells upon treatment of SLPR1-2 (10nM) in human and murine lung cells has been surprisingly found by microscopy observation (Figure 5.7). A cell survival assay was assessed by cell counting and colorimetric MTS assay in lung cells in the presence of LRP1 blockers such as RAP and sLRP1-2. 24h incubation with either the inhibitor or soluble receptor resulted in a significant number of the cell death (>60%) (Figure 5.8). Cell counting showed that compared to 0 h, approximately 40% and 60% of the cells respectively MRC5 and murine lung cells were dead after 24 and 48h incubation with both sLRP1-2 and RAP (Figure 5.9). The MTS cell metabolic assay further confirmed the cell counting results with the exception of A549 cells where a small decreased was observed compared to time 0 (Figure 5.10).

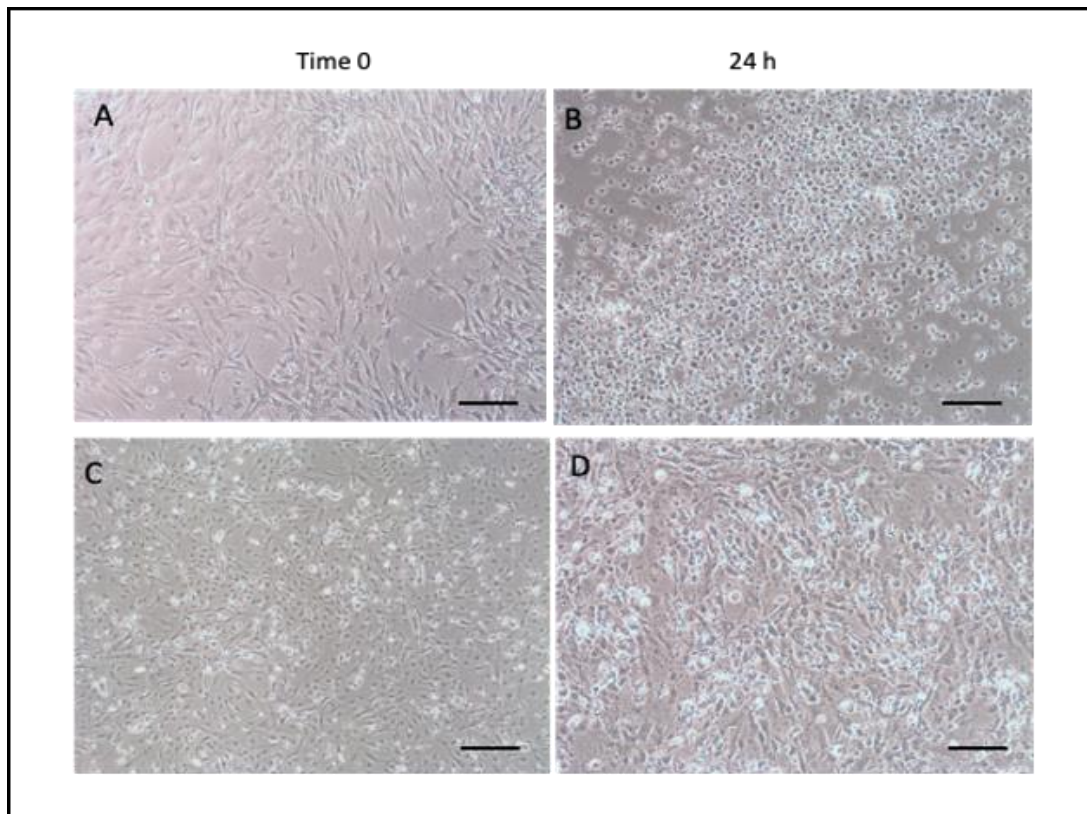


Figure 5.7 Human primary lung fibroblast cells (MRC-5) (A-B) and Murine lung cells. Cells were isolated from mice (C-D) are shown with and without the presence of sLRP1-2. Cells were incubated for 24 hours with sLRP1-2 (10nM) to allow the accumulation of the ligands in the media for the mass spec analysis. Floating cells were observed after 24h (B-D) compared to the control cells without treatment (A-C). Scale bar=100 μ m.

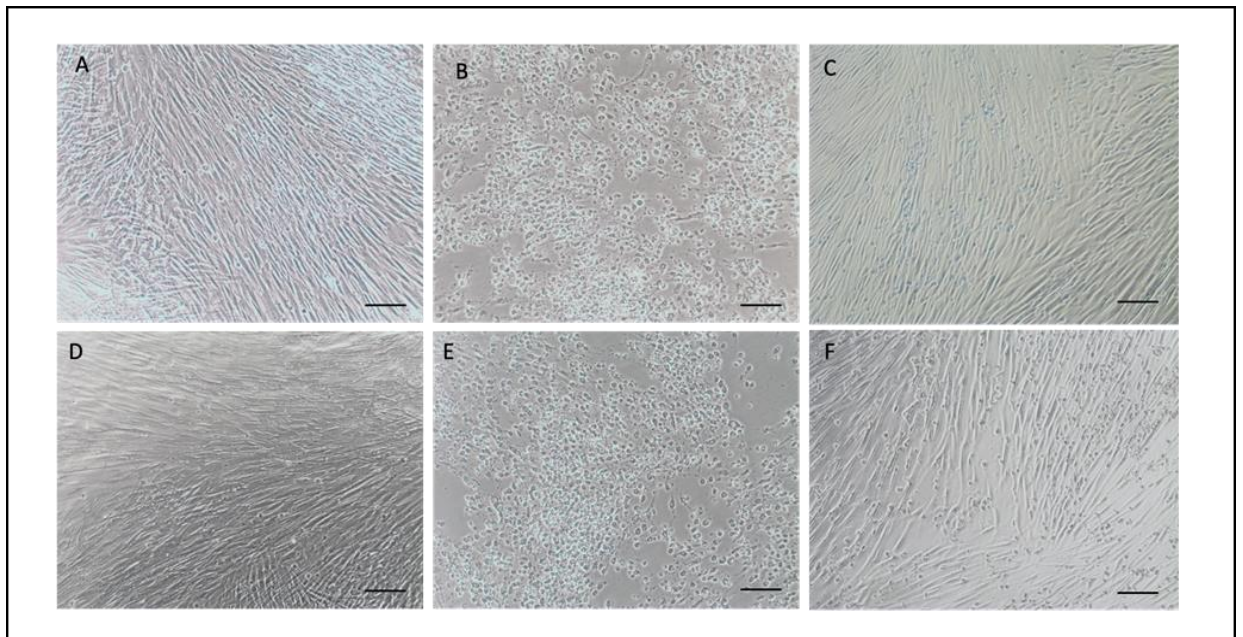


Figure 5.8 Representative with or without treatment at 24 and 48 hours. MRC5 are shown as control respectively at 24 h (A) and 48 h (D). Cells were treated with sLRP1-2 (10nM) and photos were taken after 24 and 48h treatment (B-E). Cells were also incubated with RAP (500nM) and photos were taken at 24 and 48 hours (C-F). Scale bar=100um.

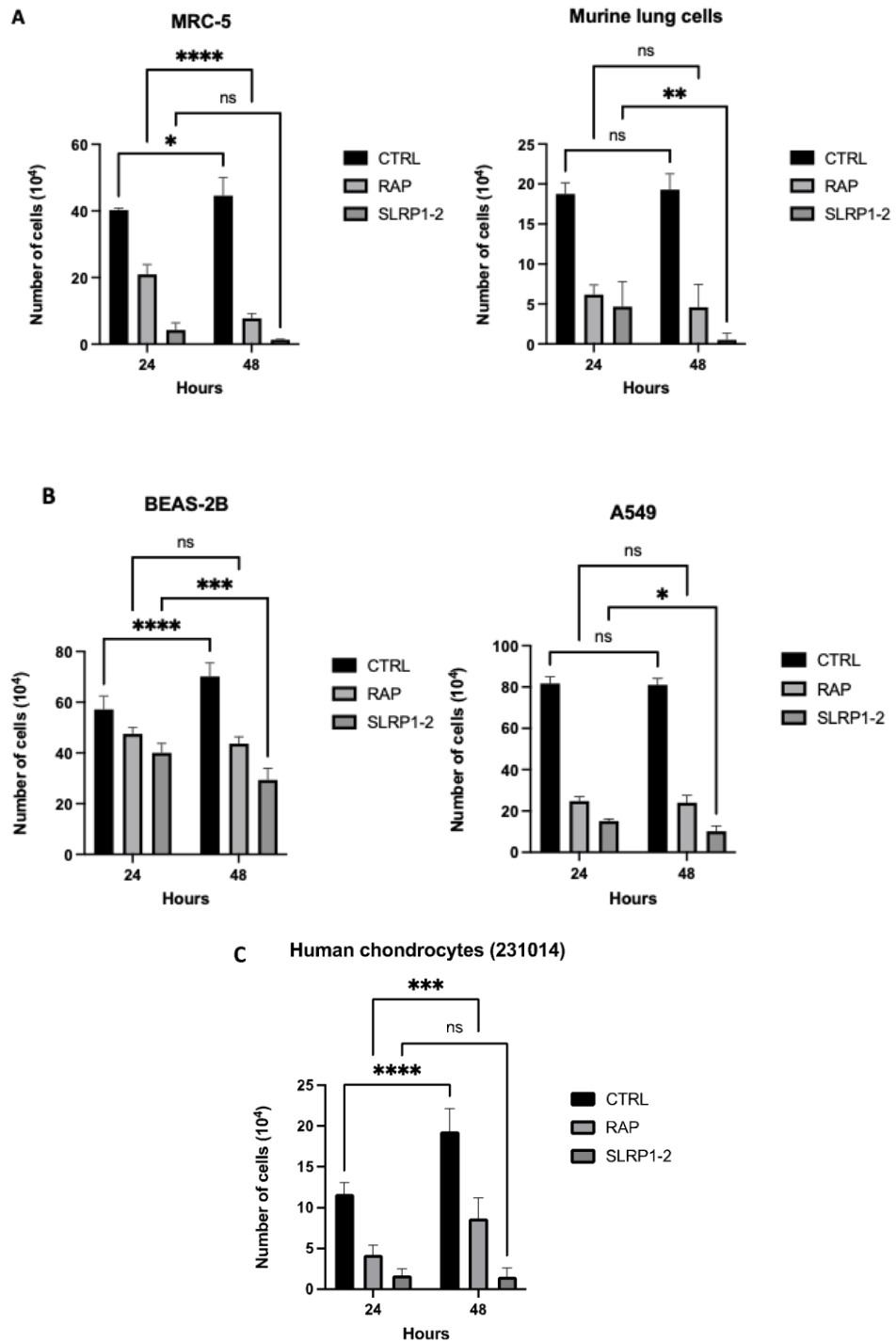


Figure 5.9 Cell death in the presence of sLRP12 and RAP in the media of lung cells. Values are shown as mean \pm SEM. 2-way Anova test was performed and statistically different values of * $P < 0.05$ and ** $P < 0.01$ and *** $P < 0.0004$ **** $P < 0.0001$ were determined.

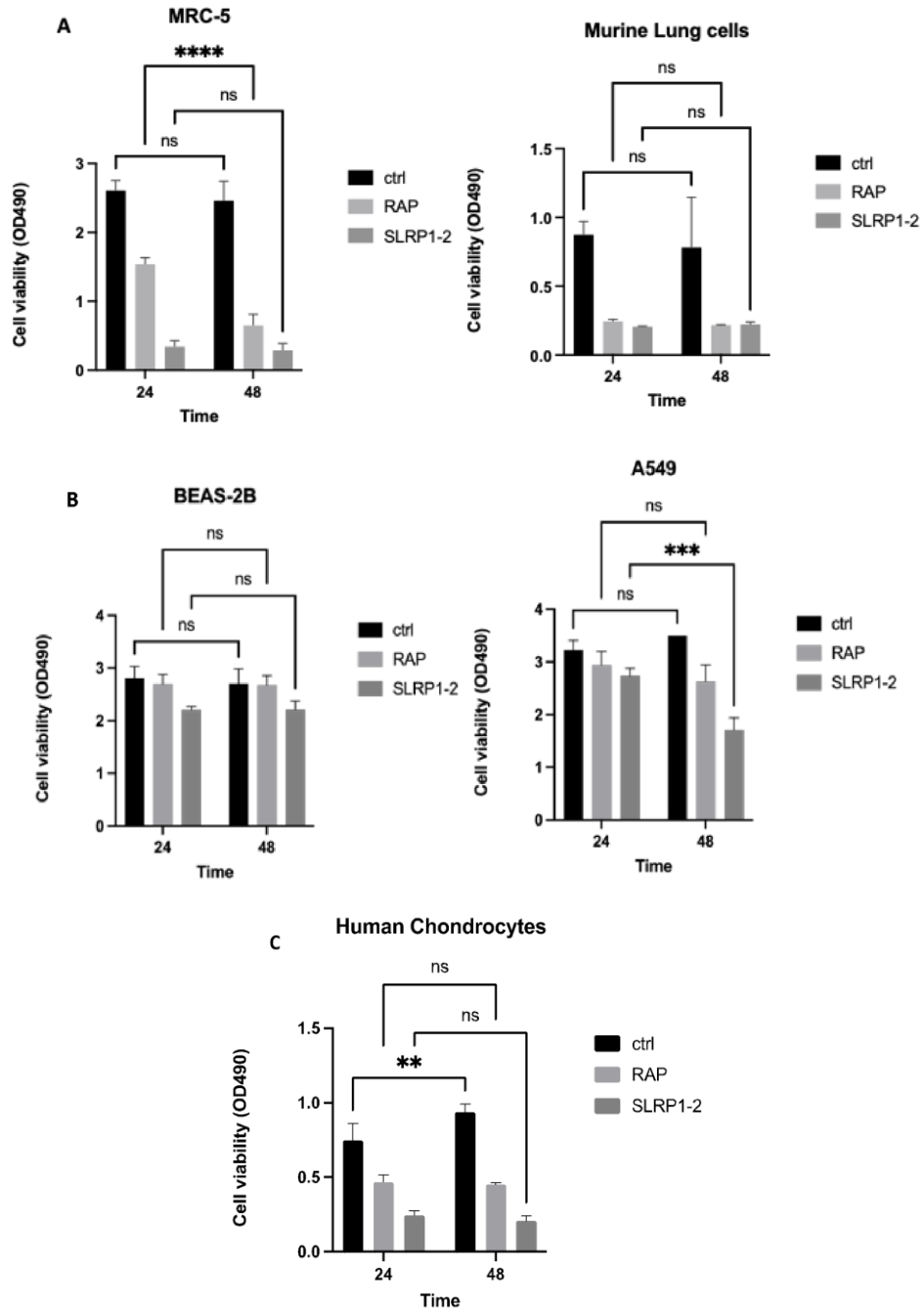


Figure 5.10 Reduction of cell survival upon treatment with sLRP1-2 and RAP. Cell availability by MTT assay is expressed in percentage (%). Graph of MRC-5, BEAS2B, Murine Lung cell and A549 after 24h and 48h incubation with sLRP1-2 and RAP. 2-way Anova test was performed and statistically different values of *p value <0.05, **p value <0.02, ***p value <0.003 and ****p value < 0.0002 were determined.

5.4.5 siRNA-mediated knockdown of LRP1 in human lung cells

LRP1 was silenced in normal lung fibroblasts cells using a gene-specific siRNA to investigate the consequential effects *in vitro*. Cell counting was performed at different concentrations of LRP1 targeting siRNA, respectively 20 and 40 nM, for six days (Figure 5.11). A reduction in terms of cell number was observed over the time, with a significant difference after 3 days at 40nM concentration compared to the scramble. Cells transfected with 20nM of LRP1 targeting siRNA demonstrated a higher capability of proliferation compared to the 40nM-treated cells. In parallel, a measurement of LRP1 protein level was proved by WB to confirm the efficiency of the siRNA transfection. A decrease of LRP1 protein level in 40nM siRNA transfected cells, compared to the scramble samples (Figure 5.12 A-B).

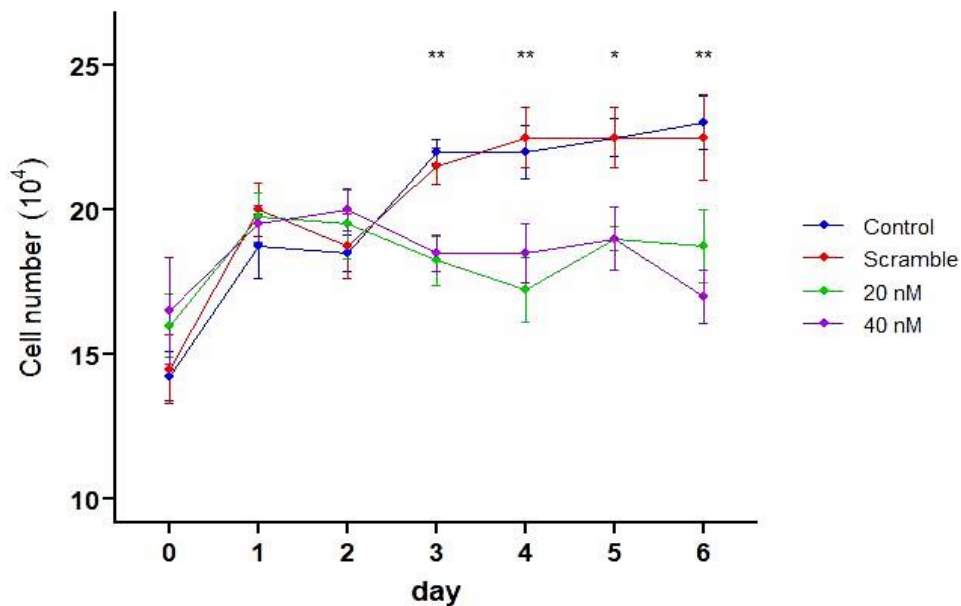


Figure 5.11 Reduced cell number in siRNA-mediated knockdown of LRP1 in human primary lung fibroblast cells (MRC-5). MRC-5 transfected with nontargeting siRNA (scramble) or LRP1 targeting siRNA (siLRP1) at 20 and 40 nM concentrations, were cultured for 6 days in DMEM containing 10% FCS. Values are shown as mean \pm SEM. 2-way Anova was performed comparing groups within each day. Statistically different values of *p value < 0.05 and **p value < 0.01 are determined compared with the control.

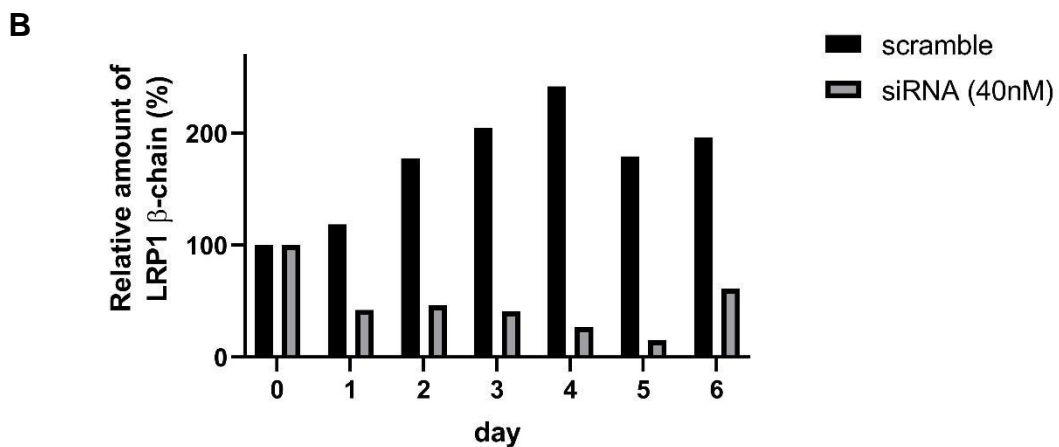
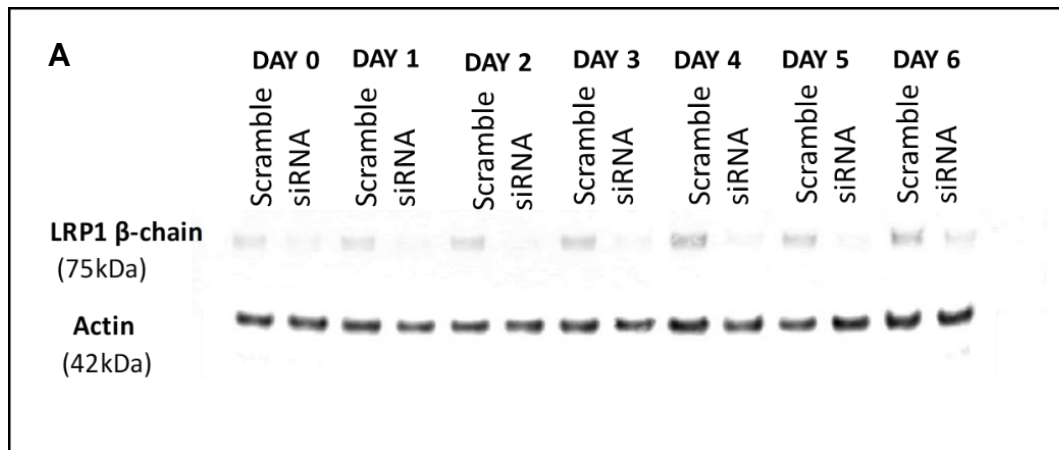


Figure 5.12 Reduced protein level of LRP1 in siRNA-mediated knockdown human lung fibroblasts cells. Human chondrocytes transfected with nontargeting siRNA (scramble) or LRP-1 targeting siRNA (siLRP-1) were cultured for 6 days in DMEM containing 10% FCS. **A:** b chain (85 kDa) in cell lysates were assessed by Western blot analysis using anti-LRP-1 light-chain antibody. **B:** densitometric analysis of immunoreactive LRP1 bands detected in the cell lysate normalised by the actin.

5.4.6 Cell survival assay of LRP1-expressing and LRP1 KO murine lung cells

To investigate the impact of LRP1 loss on cellular level, we isolated lung cells from lung of wild type and LRP1-KO mice. After primary fibroblast cells' isolation, cultured cells were observed under the optical microscope and a variety of cell morphology was found, due to the presence of not only fibroblast cells, but also macrophages, epithelial bronchial cells, cuboidal cells and

alveolar type I and II cells. Both WT and LRP1 KO cells followed a similar proliferation pattern over the time with no significant difference in terms of cell number. However, in the absence of serum in the media (Figure 5.13). LRP1 KO cells showed a lower number of cells compared to the WT. These results confirm the involvement of LRP1 in the cell proliferation function in the lung tissue.

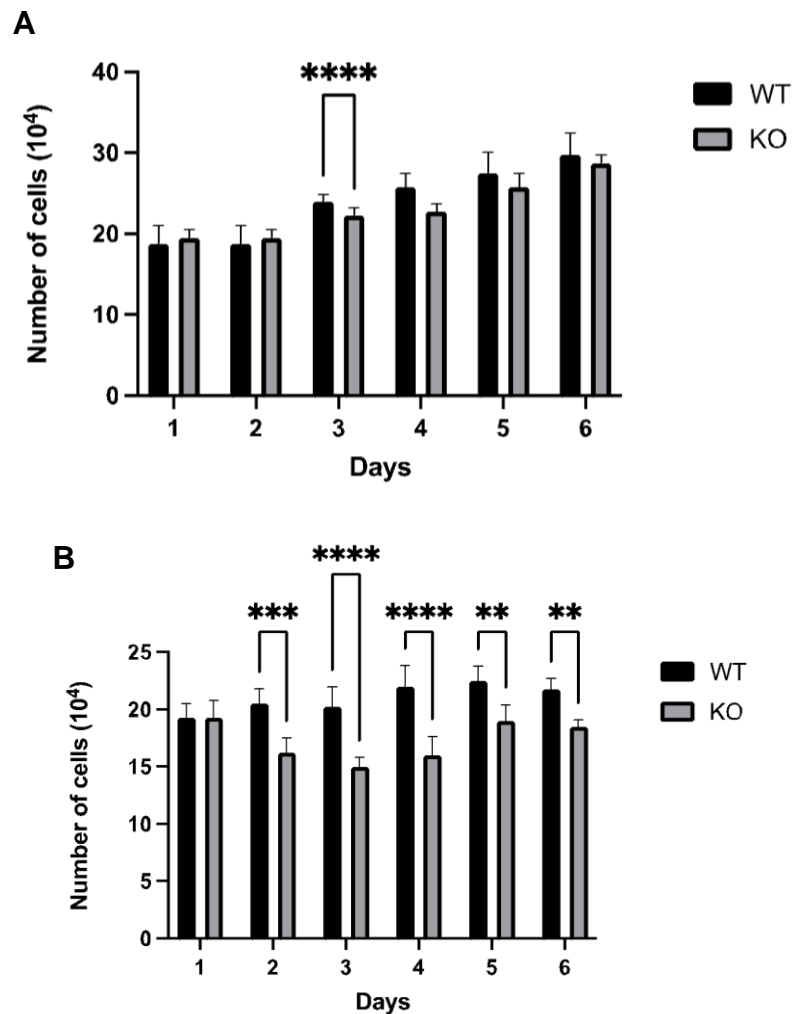
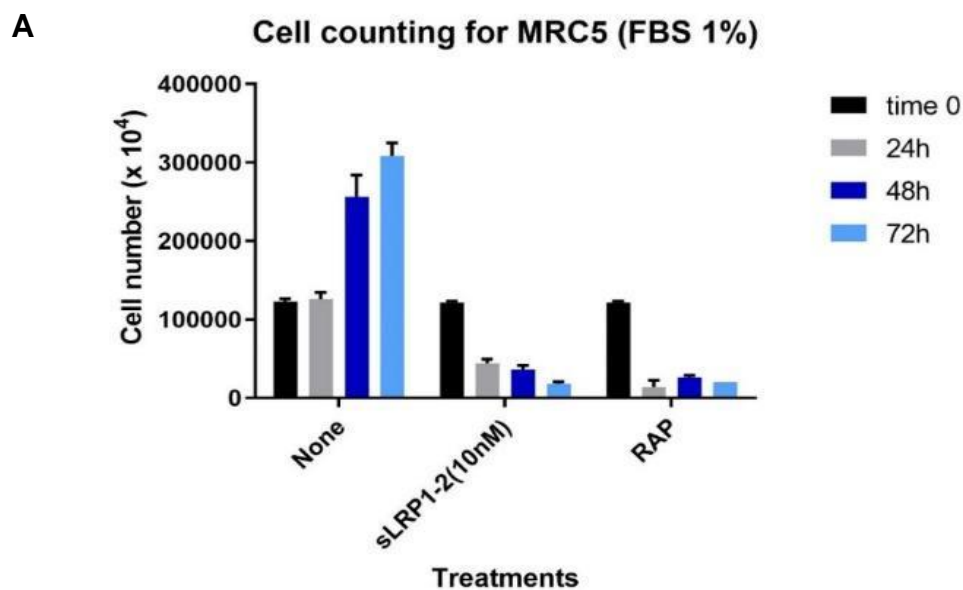


Figure 5.13 Reduction in cell number in LRP1 KO cells compared to WT. Graphs show the number of cells in the presence or not of serum in the media. Fig A: 10% serum was added to the media of cells. Fig B: the media of cells was serum free. 2way Anova test performed and statistically different values **p value <0.0044; ***p value<0.0004; ****p value <0.0001 were determined.

5.4.7 Investigation of the dose-dependent response of sLRP1-2 on lung cells

To exclude the possibility of a cell death or detachment response due to the FBS depletion, cells were incubated with 1% of serum. Cell viability was still affected in the presence of serum after treatments with sLRP1-2 by cell counting and MTS assay (Figure 5.14). A decrease in cell attachment and cell number viability was observed after 24 hours in the presence of 1% FBS. A dose-dependent response experiment was performed on MRC-5 in a comparison between the homemade purified sLRP1-2 and the Human LRP1-2 Fc Chimera Protein recombinant, purchased from R&D, at different concentrations (1nM, 2.5nM, 5nM and 10nM) and time points (0, 6, 24, 48, 72 hours). By cell counting and MTS assay it was identified 5nM as the optimal concentration of sLRP1-2 that does not induce cell death up to 24-h incubation (Figure 5.15).



B

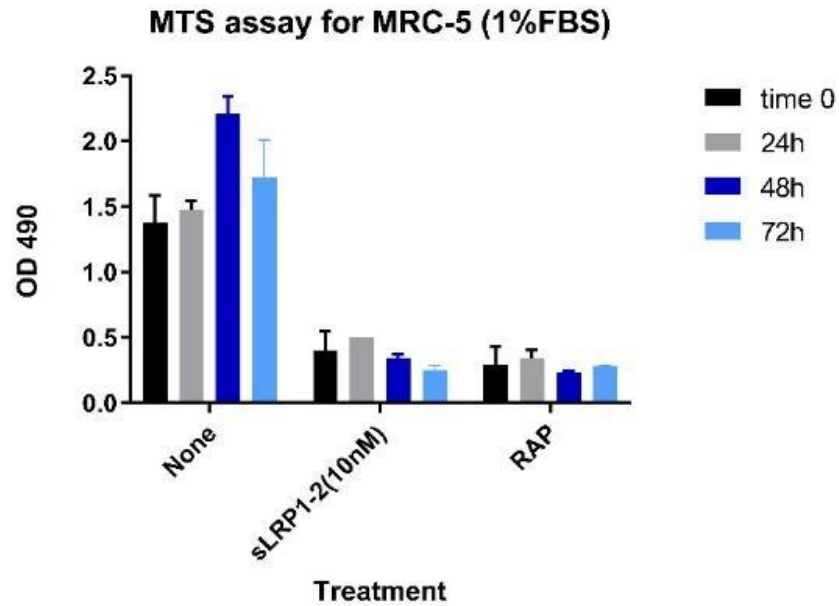
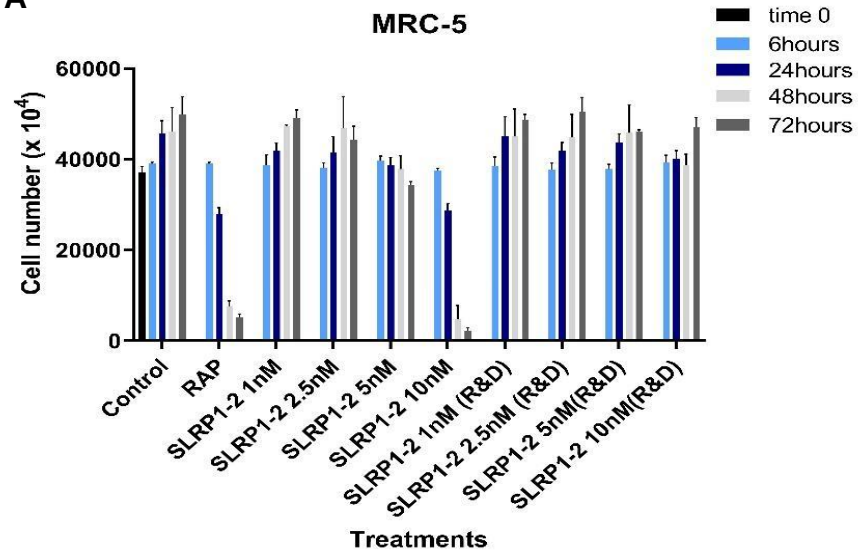


Figure 5.14 Reduction of cell number and survival in LRP1-mediated endocytosis blockade. A reduction is observed in both cells counting (A) and MTS assay (B) after 24,48 and 72h of treatment with sLRP1-2 and RAP. Error bars represent standard error (n=2).

A



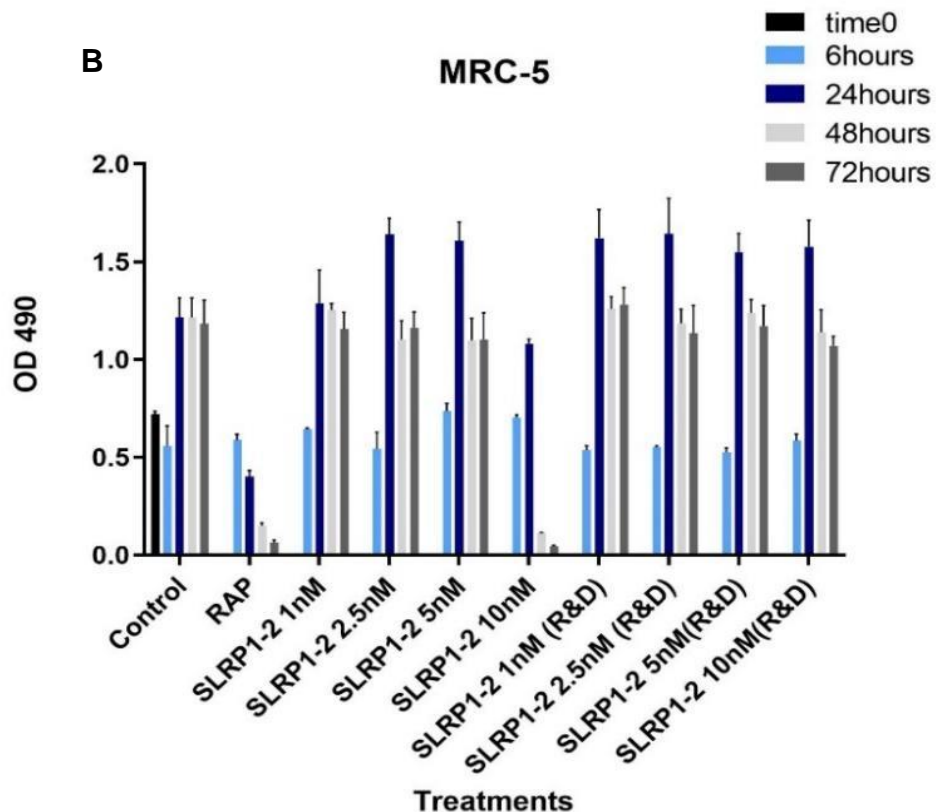


Figure 5.15 Inhibition of LRP1-mediated endocytosis by sLRP12 induces a cell death at 10nM concentration. Graphs show cell counting (A) and MTS assay results (B). Error bars represent standard error (n=2).

5.4.8 Co-purified molecules can induce cell death and detachment

Mass-spectrometry analysis of sLRP1-2 purified, revealed the presence of co-purified proteins (Table 5.4 and 5.5). By silver staining detection, a big amount of co-purified protein was found in the commercially purified sLRP1-2 with high molecular weight such as A2M, one of the well-established LRP1-ligands. Its presence was also confirmed by WB analysis (Figure 5.16 A-B). Our final western blotting results confirmed that the commercial sLRP1-2 R&D contains a much higher level of co-purified A2M compared to the home purified sLRP1-2 which was able to induce cell death and detachment at 10nM after 24hours (Figure 5.16 A-B).

Table 5.4 co-purified molecules with sLRP1-2 from conditioned medium of HEK293 cells.

Accession	Description
P00750	Tissue-type plasminogen activator
P28799	Progranulin
O94813	Slit homolog 2 protein
P13645	Keratin, type I cytoskeletal 10
O96014	Protein Wnt-11
P02768	Serum albumin
Q8IUL8	Cartilage intermediate layer protein 2
Q6UXI9	Nephronectin
P49908	Selenoprotein P
P02765	Alpha-2-HS-glycoprotein
P55001	Microfibrillar-associated protein 2
Q9UHI8	A disintegrin and metalloproteinase with thrombospondin motifs 1
Q9H4F8	SPARC-related modular calcium-binding protein 1
P10909	Clusterin
P98160	Basement membrane-specific heparan sulfate proteoglycan core protein
P09429	High mobility group protein B1
Q9NS15	Latent-transforming growth factor beta-binding protein 3
P35625	Metalloproteinase inhibitor 3
O76061	Stanniocalcin-2
Q99435	Protein kinase C-binding protein NELL2
P01023	Alpha-2-macroglobulin

**In yellow are indicated the known LRP1 ligands*

Table 5.5 List of molecules identified by mass-spectrometry analysis in R&D sample.

Accession	Description
Q91ZX7	Prolow-density lipoprotein receptor-related protein 1
P97430	Antileukoproteinase
Q61543	Golgi apparatus protein 1
P10126	Elongation factor 1-alpha 1
P97351	40S ribosomal protein S3a
Q01149	Collagen alpha-2(I) chain
P55302	Alpha-2-macroglobulin receptor-associated protein
P47915	60S ribosomal protein L29
P02798	Metallothionein-2
P11680	Properdin
Q9D1R9	60S ribosomal protein L34
P62908	40S ribosomal protein S3
P82198	Transforming growth factor-beta-induced protein ig-h3
P83882	60S ribosomal protein L36a
P63017	Heat shock cognate 71 kDa protein
P62702	40S ribosomal protein S4, X isoform
P25444	40S ribosomal protein S2
P62852	40S ribosomal protein S25

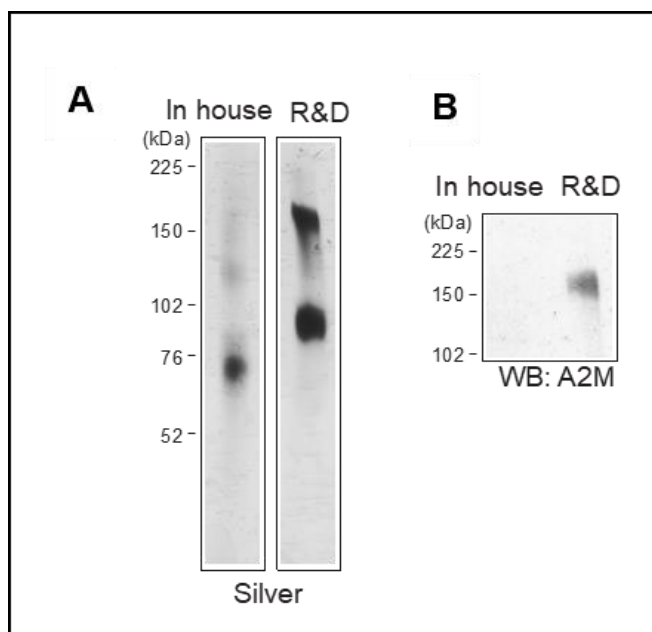


Figure 5.16 A2M co-purified in sLRP1-2 from commercial R&D is higher than sLRP1-2 home purified. Silver staining (A) and Western blotting analysis (B) performed on home purified sLRP1-2 and commercial R&D sLRP1-2. Silver staining shows the presence of co-purified protein in the commercial fraction sLRP1-2 with high molecular weight. Western blotting result shows the presence of A2M in the R&D fraction where it is absent in the home purified sLRP1-2.

5.5 Discussion

The proteomic approach used for this study, allowed to detect the presence of ligands by directly and indirectly blocking LRP1-mediated endocytosis. The data presented in this study, revealed new LRP1 ligands in human and murine lung cells including ADAMTS-1, C4-B, Nephronectin, Biglycan, Fibrillin-1, Insuline-like growth factor binding protein 7, Gremlin-1, Lumican, Cathepsin B and Galectin-1. In this study, it was also shown that inhibition of LRP1-mediated endocytosis induced cell death and detachment in both human and murine lung cells.

5.5.1 Biological functions of LRP1 ligands detected in lung cells

A total number of 490 molecules have been identified by mass-spectrometry analysis in human and primary murine lung cells. Among those

molecules, 374 were distinguished as intracellular, 49 as cell membrane and 67 as secreted molecules. Both human and murine lung cells revealed 10 new secreted molecules and LRP1 ligand candidates. A high number of intracellular molecules were detected by mass-spectrometry analysis, suggesting a potential activation of a stress-induced cell death by the presence of sLRP1-2. LRP1 interacts with more than 100 ligands mediating the endocytosis and degradation in the intracellular lysosomes (Lillis, et al., 2008); (Yamamoto, et al., 2022). It can also bind the A2M and antithrombin III (ATIII), involved in the thrombotic cascades (Strickland, et al., 2002). The difficulty of outlining a specific LRP1's role in the cell, advances from its capacity to interact with a large variety of ligands, each of which covers distinctive biological functions. However, it is possible to hypothesise that the accumulation of anti-fibrotic molecules due to the inhibition of LRP1-mediated endocytosis can block the development of lung fibrosis upon bleomycin injury.

5.5.2 Why the suppression of LRP1-mediated endocytosis induces cell death?

The data shown in this chapter demonstrated that the blockade of LRP1-mediated endocytosis induces pro-death and detachment response in vitro. For instance, floating cells were observed after 24 hours of sLRP1-2 treatment compared to the untreated cells. The time-dependent effect of sLRP1-2 on cell death and detachment found in lung cells and in the work conducted by Yamamoto in chondrocytes cells, indicates that the accumulation of LRP1 ligands in the media is detrimental to the cells and leads to cell death. Moreover, a lower dose of sLRP1-2 (5nM) was then employed for LRP1 screening in the pulmonary and cartilage studies (Yamamoto, et al., 2022) as able to not induce cell death and efficiently blocking LRP1-mediated endocytosis (Figure 5.13). Previous studies established that LRP1 suppression can trigger cells to stress-induced cell death (Fuentealba, et al., 2009; Campana, et al., 2006; Leslie, et al., 2018). Thus, it is challenging to

delineate the specific connection of inhibition of LRP1-mediated endocytosis and its detrimental effect in the lung cells from these preliminary results.

It can be hypothesised that a transcriptional modulation caused by the LRP1 blockade in the ligand's interactions might affect the cell survival and a reduced activity of LRP1. The consequential accumulation of LRP1 ligands could alter the cellular balance. However, the methodology shown in this study represents a starting point for elucidating novel LRP1 physiological functions in the lung tissue and the deleterious results of its inhibition.

5.5.3 Limitations

This work presents new important findings on LRP1 ligandome in lung tissue. However, few limitations were met in this study. Firstly, mass-spectrometry analysis was challenging for the analysis of LRP1 ligands in primary murine lung cells previously isolated due to cell viability and number of biological replicates. In fact, more mice were required to be tested for lung cell isolation. Also, several LRP1 ligands were discovered as intracellular molecules due to a cell death response upon treatment with sLRP1-2 at 10nM. Secondly, I was not able to determine if blockade of LRP1-mediated endocytosis caused either cell death or cell detachment in lung cells due to a lack of time. Certainly, a more detailed analysis was required for the identification of specific activated cellular pathways. We also hypothesise that the presence of co-purified molecules in the preparation of the commercial sLRP1-2 (R&D) could potentially affect the LRP1-mediated endocytosis while performing the experiments.

5.5.4 Conclusions and future plans

Certainly, it is difficult to speculate about the reason behind a cell death response upon blockade of LRP1-mediated endocytosis. However, the identification of new LRP1 ligands in lung tissue through the methodology established in this work, can open new important information about possible roles of LRP1. Therefore, the same approach used for the detection of new

ligands candidates in healthy lung cells, could be adopted upon treatment with bleomycin to mimic a fibrotic response in the presence and absence of LRP1 *in vitro*.

Chapter 6 General discussion

IPF is the most serious and lethal lung condition amongst all pulmonary fibrotic diseases. Different mechanisms have been proposed on IPF pathogenesis, however the identification of specific molecular pathways remains elusive. Artigas et al., in 2011 identified *LRP1* gene as being essential in lung function by a large genome-wide study (Artigas, et al., 2011).

My initial hypothesis is therefore “*LRP1 plays a key physiological role in healthy lung and its dysregulation leads to pathological lung conditions*”.

Initially, since lung tissue consists of a variety of cell types, I first induced a global deletion *Lrp1* in the whole body in adulthood. Total deletion of *Lrp1* gene caused a rapid weight loss (>20%) and abnormalities in gastro-intestinal tract, suggesting a crucial role of LRP1 in the digestive system. This system revealed the difficulty of using this mouse model to investigate LRP1 role in the respiratory system. As described in this thesis, fibroblast plays a key role in the production and deposition of collagen upon lung injury. Therefore, I specifically deleted *Lrp1* in COL1A2-expressing cells and challenged them with bleomycin. Unexpectedly, this study showed that deletion of *Lrp1* in COL1A2-expressing cells attenuates collagen deposition in lung tissue upon bleomycin-induced injury. In contrast to my original hypothesis, I discovered a crucial pathological role of LRP1 in the development of lung fibrosis.

Based on these assumptions, our initial hypothesis was amended as following: “*Deletion of Lrp1 in COL1A2-expressing cells attenuates collagen deposition in the development of lung fibrosis*”.

In parallel, a study *in vitro* was conducted in this thesis to further investigate the molecular mechanisms behind LRP1 function in lung tissue. Little information is available about LRP1 ligands in the lung. For this specific aim, mass-spectrometry analysis was performed at Enghild’s lab in Denmark.

During the work of this thesis, Yamamoto et al., 2022 identified the presence of new LRP1 ligands in cartilage such as HGFAC, HMGB1, HMGB2, CEMIP, SLIT2, ADAMTS1, TSG6, IGFBP7, SPARC and LIF. Total number of 10 new LRP1 ligands candidates were found in lung tissue by mass-spectrometry analysis including ADAMTS-1, C4-B, Nephronectin, Biglycan, Fibrillin-1, Insuline-like growth factor binding protein 7, Gremlin-1, Lumican, Cathepsin B and Galectin-1. Notably, a large number of intracellular molecules were identified by mass-spectrometry in lung cells compared to the work conducted in cartilage by Yamamoto et al., in 2022 (Yamamoto, et al., 2022). Differences found between lung and cartilage ligandome confirmed that LRP1 functions in a tissue-specific manner. Among LRP1 ligands in lung of interest is nephronectin which has been previously found to be involved in the maintenance and development of lung tissue (Wilson C.L. et al., 2021) and in lung metastasis (Magnussen et al., 2020), and biglycan which has been shown to differentially modulate TGF- β -mediated fibrotic responses in the lung (Kolb et al., 2001).

Therefore, the identification of LRP1 ligands with different biological functions reflects the difficulty of defining a specific role of LRP1 in lung tissue. Certainly, identifying tissue-specific LRP1 ligandomes is essential for a better understanding of LRP1's physiological functions and the detrimental effects of its dysregulation.

I also found that inhibition of LRP1-mediated endocytosis of lung cells *in vitro* showed consistent cell death in a variety of lung cells, revealing a certain cytotoxicity upon accumulation of LRP1 ligands. This finding was confirmed from Yamamoto et al., 2022 in human chondrocytes cells where a combined alteration of secretome and transcriptional modulation was found.

6.1 Final thoughts

Future studies targeting other lung cell populations are needed to further delineate LRP1 cell-specific contribution to the development of

pulmonary fibrosis in vivo. In addition, it will be important to further identify collagen-producing cell types in lung tissue. Moreover, our proteomic findings need to be further explored in the context of pulmonary fibrosis to define whether deletion of LRP1 in COL1A2-expressing cells is associated with the accumulation of anti-fibrotic molecules in the ECM or the inhibition of pro-fibrotic signalling pathways.

In conclusion, controversial aspects of LRP1 have been discussed in this thesis such as its importance for tissue homeostasis and its deleterious effect after its total deletion. Why the loss of LRP1 in COL1A2-expressing cells exhibit antifibrotic effects in bleomycin-induced lung fibrosis and its total deletion appears to be detrimental in the gastro-intestinal tract is an intriguing question.

This project sought out to reveal the role of LRP1 in lung tissue, but more questions will have to be answered about its multifunctional involvement in respiratory diseases and other diseases alike. Deletion of LRP1 in a cell-specific manner in the lung might eventually be used to target molecular pathways behind the activation of fibroblast proliferation, with the aim of developing novel anti-fibrotic therapeutics.

Chapter 7 Bibliography

Adams, T. S., Schupp, J. C., Poli, S., Ayaub, E. A., Neumark, N., Ahangari, F., Chu, S. G., Raby, B. A., Deluliis, G., Januszyk, M., Duan, Q., Arnett, H. A., Siddiqui, A., Washko, G. R., Homer, R., Yan, X., Rosas, I. O. and Kaminski, N. (2020) 'Single-cell RNA-seq reveals ectopic and aberrant lung-resident cell populations in idiopathic pulmonary fibrosis', *Science Advances*, 6(28).

Adamson, I. Y. R. (1976) 'Pulmonary toxicity of bleomycin', *Environmental Health Perspectives*, 16, p. 119.

Afratis, N. A., Bouris, P., Skandalis, S. S., Multhaupt, H. A., Couchman, J. R., Theocharis, A. D. and Karamanos, N. K. (2017) 'IGF-1R cooperates with ERKs to inhibit breast cancer cell aggressiveness by regulating the expression and localisation of ECM molecules', *Scientific Reports* 2017 7:1, 7(1), pp. 1-12.

Aran, D., Looney, A. P., Liu, L., Wu, E., Fong, V., Hsu, A., Chak, S., Naikawadi, R. P., Wolters, P. J., Abate, A. R., Butte, A. J. and Bhattacharya, M. (2019) 'Reference-based analysis of lung single-cell sequencing reveals a transitional profibrotic macrophage', *Nature Immunology*, 20(2), pp. 163-172.

Armanios, M. Y., Chen, J. J.-L., Cogan, J. D., Alder, J. K., Ingersoll, R. G., Markin, C., Lawson, W. E., Xie, M., Vulto, I., Phillips, J. A., Lansdorp, P. M., Greider, C. W. and Loyd, J. E. (2007) 'Telomerase mutations in families with idiopathic pulmonary fibrosis', *The New England journal of medicine*, 356(13), pp. 1317-1326.

Aronson, J. F. (1983) 'Human Retinal Pigment Cell Culture on JSTOR'. Available at: <https://www.jstor.org/stable/4292721>.

Artigas, M. S., Loth, D. W., Wain, L. V., Gharib, S. A., Obeidat, M. E., Tang, W., Zhai, G., Zhao, J. H., Smith, A. V., Huffman, J. E., Albrecht, E., Jackson, C. M., Evans, D. M., Cadby, G., Fornage, M., Manichaikul, A., Lopez, L. M., Johnson, T., Aldrich, M. C., Aspelund, T., Barroso, I., Campbell, H., Cassano, P. A., Couper, D. J., Eiriksdottir, G., Franceschini, N., Garcia, M., Gieger, C., Gislason, G. K., Grkovic, I., Hammond, C. J., Hancock, D. B., Harris, T. B., Ramasamy, A., Heckbert, S. R., Helivaara, M., Homuth, G., Hysi, P. G., James, A. L., Jankovic, S., Joubert, B. R., Karrasch, S., Klopp, N., Koch, B., Kritchevsky, S. B., Launer, L. J., Liu, Y.,

Loehr, L. R., Lohman, K., Loos, R. J. F., Lumley, T., Al Balushi, K. A., Ang, W. Q., Barr, R. G., Beilby, J., Blakey, J. D., Boban, M., Boraska, V., Brisman, J., Britton, J. R., Brusselle, G. G., Cooper, C., Curjuric, I., Dahgam, S., Deary, I. J., Ebrahim, S., Eijgelsheim, M., Francks, C., Gaysina, D., Granell, R., Gu, X., Hankinson, J. L., Hardy, R., Harris, S. E., Henderson, J., Henry, A., Hingorani, A. D., Hofman, A., Holt, P. G., Hui, J., Hunter, M. L., Imboden, M., Jameson, K. A., Kerr, S. M., Kolcic, I., Kronenberg, F., Liu, J. Z., Marchini, J., McKeever, T., Morris, A. D., Olin, A. C., Porteous, D. J., Postma, D. S., Rich, S. S., Ring, S. M., Rivadeneira, F., Rochat, T., Sayer, A. A., Sayers, I., Sly, P. D., et al. (2011) 'Genome-wide association and large-scale follow up identifies 16 new loci influencing lung function', *Nature Genetics*, 43(11), pp. 1082-1090.

Auderset, L., Cullen, C. L. and Young, K. M. (2016) 'Low density lipoprotein-receptor related protein 1 is differentially expressed by neuronal and glial populations in the developing and mature mouse central nervous system', *PLoS ONE*, 11(6).

Baecher-Allan, C., Kaskow, B. J. and Weiner, H. L. (2018) 'Multiple Sclerosis: Mechanisms and Immunotherapy', *Neuron*, 97(4), pp. 742-768.

Barkauskas, C. E., Crouce, M. J., Rackley, C. R., Bowie, E. J., Keene, D. R., Stripp, B. R., Randell, S. H., Noble, P. W. and Hogan, B. L. M. (2013) 'Type 2 alveolar cells are stem cells in adult lung', *Journal of Clinical Investigation*, 123(7), pp. 3025-3036.

Barnes, P. J. (2000) 'Chronic Obstructive Pulmonary Disease', *New England Journal of Medicine*, 343(4), pp. 269-280.

Barresi, R. and Campbell, K. P. (2006) 'Dystroglycan: from biosynthesis to pathogenesis of human disease', *Journal of cell science*, 119(Pt 2), pp. 199-207.

Barron, L., Gharib, S. A. and Duffield, J. S. (2016) 'Lung Pericytes and Resident Fibroblasts: Busy Multitaskers', *The American journal of pathology*, 186(10), pp. 2519-2531.

Barry, F. P. and Murphy, J. M. (2004) 'Mesenchymal stem cells: Clinical applications and biological characterization', *International Journal of Biochemistry and Cell Biology*, 36(4), pp. 568-584.

Basford, J. E., Wancata, L., Hofmann, S. M., Gangani, R. A., Silva, D., Davidson, W. S., Howles, P. N. and Hui, D. Y. (2011) 'Hepatic Deficiency of Low Density Lipoprotein Receptor-related Protein-1 Reduces High Density Lipoprotein Secretion and Plasma Levels in Mice *'.

Basil, M. C., Katzen, J., Engler, A. E., Guo, M., Herriges, M. J., Kathiriya, J. J., Windmueller, R., Ysasi, A. B., Zacharias, W. J., Chapman, H. A., Kotton, D. N., Rock, J. R., Snoeck, H. W., Vunjak-Novakovic, G., Whitsett, J. A. and Morrissey, E. E. (2020) 'The Cellular and Physiological Basis for Lung Repair and Regeneration: Past, Present, and Future', *Cell Stem Cell*, 26(4), pp. 482-502.

Bates, J. H. T. and Suki, B. (2008) 'Assessment of peripheral lung mechanics', *Respiratory physiology & neurobiology*, 163(1-3), pp. 54-63.

Baumgartner, C. F., Kolbitsch, C., McClelland, J. R., Rueckert, D. and King, A. P. (2017) 'Autoadaptive motion modelling for MR-based respiratory motion estimation', *Medical Image Analysis*, 35, pp. 83-100.

Baumgartner, K. B., Samet, J. M., Stidley, C. A., Colby, T. V. and Waldron, J. A. (1997) 'Cigarette smoking: a risk factor for idiopathic pulmonary fibrosis', *American Journal of Respiratory and Critical Care Medicine*, 155(1), pp. 242-248.

Beers, M. F. and Moodley, Y. (2017) 'PERSPECTIVE When Is an Alveolar Type 2 Cell an Alveolar Type 2 Cell? A Conundrum for Lung Stem Cell Biology and Regenerative Medicine'.

Bellani, G., Laffey, J. G., Pham, T., Fan, E., Brochard, L., Esteban, A., Gattinoni, L., Van Haren, F. M. P., Larsson, A., McAuley, D. F., Ranieri, M., Rubinfeld, G., Thompson, B. T., Wrigge, H., Slutsky, A. S. and Pesenti, A. (2016) 'Epidemiology, Patterns of Care, and Mortality for Patients With Acute Respiratory Distress Syndrome in Intensive Care Units in 50 Countries', *JAMA*, 315(8), pp. 788-800.

Bernfield, M., Gtte, M., Park, P. W., Reizes, O., Fitzgerald, M. L., Lincecum, J. and Zako, M. (1999) 'Functions of cell surface heparan sulfate proteoglycans', *Annual review of biochemistry*, 68, pp. 729-777.

Berrier, A. L., Yamada and Kenneth, M. (2007) 'Cell–Matrix Adhesion', *Journal Cellular Physiology*, 211(3)(May), pp. 736-747.

Betts, G. N., Van Der Geer, P. and Komives, E. A. (2008) 'Structural and Functional Consequences of Tyrosine Phosphorylation in the LRP1 Cytoplasmic Domain *'.

Bitsikas, V., Corra, I. R. and Nichols, B. J. (2014) 'Clathrin-independent pathways do not contribute significantly to endocytic flux', *eLife*, 2014(3), pp. 1-26.

Bonnans, C., Chou, J. and Werb, Z. (2014) 'Remodelling the extracellular matrix in development and disease', *Nature reviews. Molecular cell biology*, 15(12), pp. 786-801.

Borgia, A., Borgia, M. B., Bugge, K., Kissling, V. M., Heidarsson, P. O., Fernandes, C. B., Sottini, A., Soranno, A., Buholzer, K. J., Nettels, D., Kragelund, B. B., Best, R. B. and Schuler, B. (2018) 'Extreme disorder in an ultrahigh-affinity protein complex', *Nature*, 555(7694), pp. 61-66.

Boucher, P., Gotthardt, M., Li, W. P., Anderson, R. G. W. and Herz, J. (2003) 'LRP: role in vascular wall integrity and protection from atherosclerosis', *Science (New York, N.Y.)*, 300(5617), pp. 329-332.

Braun, V., Hundsberger, T., Leukel, P., Sauerborn, M. and Von Eichel-Streiber, C. (1996) 'Definition of the single integration site of the pathogenicity locus in *Clostridium difficile*', *Gene*, 181(1-2), pp. 29-38.

Breitkreutz, D., Mirancea, N. and Nischt, R. (2009) 'Basement membranes in skin: unique matrix structures with diverse functions?', *Histochemistry and cell biology*, 132(1), pp. 1-10.

Brode, S. K., Ling, S. C. and Chapman, K. R. (2012) 'Alpha-1 antitrypsin deficiency: a commonly overlooked cause of lung disease', *CMAJ : Canadian Medical Association journal = journal de l'Association medicale canadienne*, 184(12), pp. 1365-1371.

Broekelmann, T. J., Limper, A. H., Colby, T. V. and McDonald, J. A. (1991) 'Transforming growth factor beta 1 is present at sites of extracellular matrix gene expression in human pulmonary fibrosis', *Proceedings of the National Academy of Sciences of the United States of America*, 88(15), p. 6642.

Brown, M. S. and Goldstein, J. L. (1976) 'Analysis of a mutant strain of human fibroblasts with a defect in the internalization of receptor-bound low density lipoprotein', *Cell*, 9(4), pp. 663-674.

- Brown, N. H. (2011) 'Extracellular Matrix in Development: Insights from Mechanisms Conserved between Invertebrates and Vertebrates', *Cold Spring Harbor Perspectives in Biology*, 3(12).
- Burgess, J. K., Mauad, T., Tjin, G., Karlsson, J. C. and Westergren-Thorsson, G. (2016) 'The extracellular matrix – the under-recognized element in lung disease?', *The Journal of Pathology*, 240(4), pp. 397-409.
- Burgstaller, G., Oehrle, B., Gerckens, M., White, E. S., Schiller, H. B. and Eickelberg, O. (2017) 'The instructive extracellular matrix of the lung: basic composition and alterations in chronic lung disease', *European Respiratory Journal*, 50(1), p. 1601805.
- Burri, P. H. (2006) 'Structural Aspects of Postnatal Lung Development – Alveolar Formation and Growth', *Neonatology*, 89(4), pp. 313-322.
- Busse, W. W. and Lemanske, R. F. (2001) 'Asthma', *New England Journal of Medicine*, 344(5), pp. 350-362.
- Byron, A., Humphries, J. D. and Humphries, M. J. (2013) 'Defining the extracellular matrix using proteomics INTERNATIONAL JOURNAL OF EXPERIMENTAL PATHOLOGY', *Int. J. Exp. Path*, 94, pp. 75-92.
- Campana, W. M., Li, X., Dragojlovic, N., Janes, J., Gaultier, A. and Gonias, S. L. (2006) 'The Low-Density Lipoprotein Receptor-Related Protein Is a Pro-Survival Receptor in Schwann Cells: Possible Implications in Peripheral Nerve Injury', *Journal of Neuroscience*, 26(43), pp. 11197-11207.
- Cao, J., Packer, J. S., Ramani, V., Cusanovich, D. A., Huynh, C., Daza, R., Qiu, X., Lee, C., Furlan, S. N., Steemers, F. J., Adey, A., Waterston, R. H., Trapnell, C. and Shendure, J. (2017) 'Comprehensive single-cell transcriptional profiling of a multicellular organism', *Science*, 357(6352), pp. 661-667.
- Chambers, R., Lo, B. C. Y. and Allen, N. B. (2008) 'The impact of intensive mindfulness training on attentional control, cognitive style, and affect', *Cognitive Therapy and Research*, 32(3), pp. 303-322.
- Chang, J., Garva, R., Pickard, A., Yeung, C.-Y. C., Mallikarjun, V., Swift, J., Holmes, D. F., Calverley, B., Lu, Y., Adamson, A., Raymond-Hayling, H., Jensen, O., Shearer, T., Meng, Q. J. and Kadler, K. E. (2020) 'Circadian

control of the secretory pathway maintains collagen homeostasis', *Nature Cell Biology*, 22(1), pp. 74-86.

Charan, J. and Kantharia, N. (2013) 'How to calculate sample size in animal studies?', *Journal of pharmacology & pharmacotherapeutics*, 4(4), pp. 303-306.

Chasman, D. I., Schürks, M., Anttila, V., de Vries, B., Schminke, U., Launer, L. J., Terwindt, G. M., van den Maagdenberg, A. M. J. M., Fendrich, K., Völzke, H., Ernst, F., Griffiths, L. R., Buring, J. E., Kallela, M., Freilinger, T., Kubisch, C., Ridker, P. M., Palotie, A., Ferrari, M. D., Hoffmann, W., Zee, R. Y. L. and Kurth, T. (2011) 'Genome-wide association study reveals three susceptibility loci for common migraine in the general population', *Nature Genetics*, 43(7), pp. 695-698.

Chaudhary, N. I., Schnapp, A. and Park, J. E. (2006) 'Pharmacologic Differentiation of Inflammation and Fibrosis in the Rat Bleomycin Model', *American Journal of Respiratory and Critical Care Medicine*, 173(7), pp. 769-776.

Chilosi, M., Poletti, V. and Rossi, A. (2012) 'The pathogenesis of COPD and IPF: Distinct horns of the same devil?', *Respiratory Research*, 13(1), p. 3.

Chiquet, M., Renedo, A. S., Huber, F. and Flück, M. (2003) 'How do fibroblasts translate mechanical signals into changes in extracellular matrix production?', *Matrix Biology*, 22(1), pp. 73-80.

Coraux, C., Hilmi, C., Rouleau, M., Spadafora, A., Hinnrasky, J., Ortonne, J. P., Dani, C. and Aberdam, D. (2003) 'Reconstituted Skin from Murine Embryonic Stem Cells', *Current Biology*, 13(10), pp. 849-853.

Cox, T. R. and Eler, J. T. (2011) 'Remodeling and homeostasis of the extracellular matrix: implications for fibrotic diseases and cancer', *Disease models & mechanisms*, 4(2), pp. 165-178.

Crapo, J. D., Barry, B. E., Gehr, P., Bachofen, M. and Weibel, E. R. (1982) 'Cell number and cell characteristics of the normal human lung', *American Review of Respiratory Disease*, 126(2), pp. 332-337.

Cyphert, J. M., Carlin, D. J., Nyska, A., Schladweiler, M. C., Ledbetter, A. D., Shannahan, J. H., Kodavanti, U. P. and Gavett, S. H. (2014) 'Comparative Long-Term Toxicity of Libby Amphibole and Amosite

Asbestos in Rats After Single or Multiple Intratracheal Exposures', *Journal of Toxicology and Environmental Health, Part A*, 78(3), pp. 151-165.

Datta, A., Scotton, C. J. and Chambers, R. C. (2011) 'Novel therapeutic approaches for pulmonary fibrosis', *British Journal of Pharmacology*, 163(1), pp. 141-172.

Davidson, J. M., Zoia, O. and Liu, J. M. M. (1993) 'Modulation of transforming growth factor-beta 1 stimulated elastin and collagen production and proliferation in porcine vascular smooth muscle cells and skin fibroblasts by basic fibroblast growth factor, transforming growth factor- β , and insulin-like growth factor', *Journal of Cellular Physiology*, 155(1), pp. 149-156.

Desai, T. J., Brownfield, D. G. and Krasnow, M. A. (2014) 'Alveolar progenitor and stem cells in lung development, renewal and cancer', *Nature*, 507(7491), pp. 190-194.

Devine, J. F. (2008) 'Chronic Obstructive Pulmonary Disease: An Overview', *American Health & Drug Benefits*, 1(7), p. 34.

Doherty, G. J. and McMahon, H. T. (2009) 'Mechanisms of Endocytosis'.

Eaton, D. C., Chen, J., Ramosevac, S., Matalon, S. and Jain, L. (2004) 'Regulation of Na⁺ channels in lung alveolar type II epithelial cells', *Proceedings of the American Thoracic Society*, 1(1), pp. 10-16.

Ebrahimi, H., Aryan, Z., Saeedi Moghaddam, S., Bisignano, C., Rezaei, S., Pishgar, F., Force, L. M., Abolhassani, H., Abu-Gharbieh, E., Advani, S. M., Ahmad, S., Alahdab, F., Alipour, V., Aljunid, S. M., Amini, S., Ancuceanu, R., Andrei, C. L., Andrei, T., Arabloo, J., Arab-Zozani, M., Asaad, M., Ausloos, M., Awedew, A. F., Baig, A. A., Bijani, A., Biondi, A., Bjrge, T., Braithwaite, D., Brauer, M., Brenner, H., Bustamante-Teixeira, M. T., Butt, Z. A., Carreras, G., Castaeda-Orjuela, C. A., Chimed-Ochir, O., Chu, D. T., Chung, M. T., Cohen, A. J., Compton, K., Dagnew, B., Dai, X., Dandona, L., Dandona, R., Dean, F. E., Derbew Molla, M., Desta, A. A., Driscoll, T. R., Faraon, E. J. A., Faris, P. S., Filip, I., Fischer, F., Fu, W., Gallus, S., Gebregiorgis, B. G., Ghashghaee, A., Golechha, M., Gonfa, K. B., Gorini, G., Goulart, B. N. G., Guerra, M. R., Hafezi-Nejad, N., Hamidi, S., Hay, S. I., Herteliu, C., Hoang, C. L., Horita, N., Hostiuc, M., Househ, M., Iavicoli, I., Ilic, I. M., Ilic, M. D., Irvani, S. S. N., Islami, F., Kamath, A., Kaur, S., Khalilov, R., Khan, E. A., Kocarnik, J. M., Kucuk Bicer, B., Kumar,

G. A., La Vecchia, C., Lan, Q., Landires, I., Lasrado, S., Lauriola, P., Leong, E., Li, B., Lim, S. S., Lopez, A. D., Majeed, A., Malekzadeh, R., Manafi, N., Menezes, R. G., Miazgowski, T., Misra, S., Mohammadian-Hafshejani, A., Mohammed, S., Mokdad, A. H., Molassiotis, A., Monasta, L., et al. (2021) 'Global, regional, and national burden of respiratory tract cancers and associated risk factors from 1990 to 2019: a systematic analysis for the Global Burden of Disease Study 2019', *The Lancet Respiratory Medicine*, 9, pp. 1030-1049.

Effros, R. M. (2006) 'Anatomy, development, and physiology of the lungs', *GI Motility online*, Published online: 16 May 2006; | doi:10.1038/gimo73.

Egger, C., Cannet, C., Grard, C., Jarman, E., Jarai, G., Feige, A., Suply, T., Micard, A., Dunbar, A., Tigani, B. and Beckmann, N. (2013) 'Administration of Bleomycin via the Oropharyngeal Aspiration Route Leads to Sustained Lung Fibrosis in Mice and Rats as Quantified by UTE-MRI and Histology', *PLOS ONE*, 8(5), p. e63432.

El Asmar, Z., Terrand, J., Jenty, M., Host, L., Mlih, M., Zerr, A., Justiniano, H., Matz, R. L., Boudier, C., Scholler, E., Garnier, J.-M., Bertaccini, D., Thiers, D., Schaeffer, C., Van Dorsselaer, A., Herz, J., Bruban, V. and Boucher, P. (2016) 'Convergent Signaling Pathways Controlled by LRP1 (Receptor-related Protein 1) Cytoplasmic and Extracellular Domains Limit Cellular Cholesterol Accumulation', *The Journal of biological chemistry*, 291(10), pp. 5116-27.

Etique, N., Verzeaux, L., Dedieu, S. and Emonard, H. (2013) 'Lrp-1: A checkpoint for the extracellular matrix proteolysis', *BioMed Research International*, 2013.

Exposito, J.-Y., Valcourt, U., Cluzel, C. and Lethias, C. (2010) 'The Fibrillar Collagen Family', *International Journal of Molecular Sciences*, 11(2), pp. 407-426.

Fan, L., Li, D., Xue, H., Zhang, L., Liu, Z., Zhang, B., Zhang, L., Yang, W., Xie, B., Duan, X., Hu, X., Cheng, K., Peng, L., Yu, N., Song, L., Chen, H., Sui, X., Zheng, N., Liu, S. and Jin, Z. (2020) 'Progress and prospect on imaging diagnosis of COVID-19', *Chinese Journal of Academic Radiology*, 3(1), p. 4.

Fehrenbach, H. (2001) 'Alveolar epithelial type II cell: defender of the alveolus revisited', *Respiratory research*, 2(1), pp. 33-46.

Flaherty, K. R., Wells, A. U., Cottin, V., Devaraj, A., Walsh, S. L. F., Inoue, Y., Richeldi, L., Kolb, M., Tetzlaff, K., Stowasser, S., Coeck, C., Clerisme-Beaty, E., Rosenstock, B., Quresma, M., Haeufel, T., Goeldner, R.-G., Schlenker-Herceg, R. and Brown, K. K. (2019) 'Nintedanib in Progressive Fibrosing Interstitial Lung Diseases', *New England Journal of Medicine*, 381(18), pp. 1718-1727.

Fraga, M. V. and Guttentag, S. (2012) 'Lung Development: Embryology, Growth, Maturation, and Developmental Biology', *Avery's Diseases of the Newborn*, pp. 571-583.

Francis, C. M., Futschik, M. E., Huang, J., Bai, W., Sargurupremraj, M., Teumer, A., Breteler, M. M. B., Petretto, E., Ho, A. S. R., Amouyel, P., Engelter, S. T., Bülow, R., Völker, U., Völzke, H., Dörr, M., Imtiaz, M.-A., Aziz, N. A., Lohner, V., Ware, J. S., Debette, S., Elliott, P., Dehghan, A. and Matthews, P. M. (2022) 'Genome-wide associations of aortic distensibility suggest causality for aortic aneurysms and brain white matter hyperintensities', *Nature Communications*, 13(1).

Frantz, C., Stewart, K. M. and Weaver, V. M. (2010) 'The extracellular matrix at a glance', *Journal of cell science*, 123(Pt 24), pp. 4195-4200.

Fredberg, J. J., Inouye, D., Miller, B., Nathan, M., Jafari, S., Raboudi, S. H., Butler, J. P. and Shore, S. A. (1997) 'Airway smooth muscle, tidal stretches, and dynamically determined contractile states', *American journal of respiratory and critical care medicine*, 156(6), pp. 1752-1759.

Fuentealba, R. A., Liu, Q., Kanekiyo, T., Zhang, J. and Bu, G. (2009) 'Low density lipoprotein receptor-related protein 1 promotes anti-apoptotic signaling in neurons by activating Akt survival pathway', *The Journal of biological chemistry*, 284(49), pp. 34045-34053.

García-Prieto, E., González-Lpez, A., Cabrera, S., Astudillo, A., Gutiérrez-Fernández, A., Fanjul-Fernández, M., Batalla-Sols, E., Puente, X. S., Fueyo, A., López-Otin, C. and Alcaiceta, G. M. (2010) 'Resistance to Bleomycin-Induced Lung Fibrosis in MMP-8 Deficient Mice Is Mediated by Interleukin-10', *{PLoS} {ONE}*, 5(10), p. e13242.

Garcia, E. L. and Mills, A. A. (2002) 'Getting around lethality with inducible Cre-mediated excision', *Seminars in cell {&} developmental biology*, 13(2), pp. 151-158.

- Gaultier, A., Wu, X., Moan, N. L., Takimoto, S., Mukandala, G., Akassoglou, K., Campana, W. M. and Gonias, S. L. (2009) 'Low-density lipoprotein receptor-related protein 1 is an essential receptor for myelin phagocytosis', *Journal of Cell Science*, 122(8), pp. 1155-1162.
- George, B. M., Nayak, S. B. and Marpalli, S. (2014) 'Morphological variations of the lungs: a study conducted on Indian cadavers', *Anatomy & Cell Biology*, 47(4), p. 253.
- Giannandrea, M. and Parks, W. C. (2014) 'Diverse functions of matrix metalloproteinases during fibrosis', *Disease Models & Mechanisms*, 7(2), pp. 193-203.
- Gilhodes, J.-C., Jul, Y., Kreuz, S., Stierstorfer, B., Stiller, D. and Wollin, L. (2017) 'Quantification of Pulmonary Fibrosis in a Bleomycin Mouse Model Using Automated Histological Image Analysis', *{PLOS} {ONE}*, 12(1), p. e0170561.
- Gonias, S. L. and Campana, W. M. (2014) 'LDL receptor-related protein-1: A regulator of inflammation in atherosclerosis, cancer, and injury to the nervous system', *American Journal of Pathology*, 184(1), pp. 18-27.
- Gool, B. V., Dedieu, S., Emonard, H. and Roebroek, A. J. M. (2015) 'The Matricellular Receptor LRP1 Forms an Interface for Signaling and Endocytosis in Modulation of the Extracellular Tumor Environment', *Frontiers in Pharmacology*, 6.
- Gordon, M. K. and Hahn, R. A. (2010) 'Collagens', *Cell and tissue research*, 339(1), pp. 247-257.
- Gordon, S. B. and Read, R. C. (2002) 'Macrophage defences against respiratory tract infections', *British Medical Bulletin*, 61(1), pp. 45-61.
- Gossen, M. and Bujard, H. (1992) 'Tight control of gene expression in mammalian cells by tetracycline-responsive promoters', *Proceedings of the National Academy of Sciences of the United States of America*, 89(12), pp. 5547-5551.
- Grant, B. D. and Donaldson, J. G. (2009) 'Pathways and mechanisms of endocytic recycling'.

Greenlee, K. J., Werb, Z. and Kheradmand, F. (2007) 'Matrix Metalloproteinases in Lung: Multiple, Multifarious, and Multifaceted', *Physiological reviews*, 87(1), p. 69.

Hanover, J. A., Rudick, J. E., Willingham, M. C. and Pastan, I. (1983) '\$\$2-macroglobulin binding to cultured fibroblasts: Identification by affinity chromatography of high-affinity binding sites', *Archives of Biochemistry and Biophysics*, 227(2), pp. 570-579.

Harburger, D. S. and Calderwood, D. A. (2009) 'Integrin signalling at a glance', *Journal of Cell Science*, 122(2), pp. 159-163.

He, L., Diedrich, J., Chu, Y. Y., and Yates, J. R., 3rd. (2015) Extracting accurate precursor information for tandem mass spectra by RawConverter. *Anal. Chem.* 87, 11361–11367.

Henson, P. M., Vandivier, R. W. and Douglas, I. S. (2006) 'Cell Death, Remodeling, and Repair in Chronic Obstructive Pulmonary Disease?', *Proceedings of the American Thoracic Society*, 3(8), pp. 713-717.

Herz, J., Clouthier, D. E. and Hammer, R. E. (1992) 'LDL receptor-related protein internalizes and degrades uPA-PAI-1 complexes and is essential for embryo implantation', *Cell*, 71(3), pp. 411-421.

Herz, J., Kowal, R. C., Goldstein, J. L. and Brown, M. S. (1990) Proteolytic processing of the 600 kd low density lipoprotein receptor-related protein (LRP) occurs in a trans-Golgi compartment (6). [Online]. Available at: <https://www.ncbi.nlm.nih.gov/pmc/articles/PMC551881/pdf/emboj00233-0094.pdf>.

Hinz, B. (2015) 'The extracellular matrix and transforming growth factor-\$\$1: Tale of a strained relationship', *Matrix Biology*, 47, pp. 54-65.

Hsia, C. C. W., Hyde, D. M. and Weibel, E. R. (2016) 'Lung Structure and the Intrinsic Challenges of Gas Exchange', *Comprehensive Physiology*, 6(2), pp. 827-895.

Huang, S. S. and Huang, J. S. (2005) 'TGF-\$\$ control of cell proliferation', *Journal of Cellular Biochemistry*, 96(3), pp. 447-462.

Hubbard, R., Venn, A., Lewis, S. and Britton, J. (2000) 'Lung cancer and cryptogenic fibrosing alveolitis. A population-based cohort study', *American journal of respiratory and critical care medicine*, 161(1), pp. 5-8.

- Hussell, T. and Bell, T. J. (2014) 'Alveolar macrophages: plasticity in a tissue-specific context', *Nature reviews. Immunology*, 14(2), pp. 81-93.
- Hynes, R. O. (2009) 'The extracellular matrix: not just pretty fibrils', *Science (New York, N.Y.)*, 326(5957), pp. 1216-1219.
- Hynes, R. O. and Naba, A. (2012) 'Overview of the matrisome--an inventory of extracellular matrix constituents and functions', *Cold Spring Harbor perspectives in biology*, 4(1).
- Ito, Y., Iwashita, J. and Murata, J. (2019) 'Type IV collagen reduces mucin 5AC secretion in three-dimensional cultured human primary airway epithelial cells', *Biochemistry and Biophysics Reports*, 20, p. 100707.
- Izumikawa, K., Tashiro, M., Yoshioka, D., Nakamura, S., Kurihara, S., Sakamoto, N., Seki, M., Kakeya, H., Yamamoto, Y., Yanagihara, K., Mukae, H., Hayashi, T., Fukushima, K., Tashiro, T. and Kohno, S. (2008) 'Lung Fibrosis 10 Years after Cessation of Bleomycin Therapy', *Tohoku J. Exp. Med*, 216(1), pp. 77-80.
- Javazon, E. H., Beggs, K. J. and Flake, A. W. (2004) 'Mesenchymal stem cells: Paradoxes of passaging', *Experimental Hematology*, 32(5), pp. 414-425.
- Jayadev, R. and Sherwood, D. R. (2017) 'Basement membranes', *Current Biology*, 27(6), pp. R207-R211.
- Jelaska, A. and Korn, J. H. (2000) 'Role of apoptosis and transforming growth factor 1 in fibroblast selection and activation in systemic sclerosis', *arthritis & rheumatism*, 43(10), pp. 2230-2239.
- Jones, G. T., Phillips, L. V., Williams, M. J. A., van Rij, A. M. and Kabir, T. D. (2016) 'Two C-C Family Chemokines, Eotaxin and RANTES, Are Novel Independent Plasma Biomarkers for Abdominal Aortic Aneurysm', *Journal of the American Heart Association*, 5(5).
- Jrvelinen, H., Sainio, A., Koulu, M., Wight, T. N. and Penttinen, R. (2009) 'Extracellular matrix molecules: Potential targets in pharmacotherapy', *Pharmacological Reviews*, 61(2), pp. 198-223.
- Jun, J. I. and Lau, L. F. (2018) 'Resolution of organ fibrosis', *The Journal of clinical investigation*, 128(1), pp. 97-107.

- Kalchier-Dekel, O., Galvin, J. R., Burke, A. P., Atamas, S. P. and Todd, N. W. (2018) 'Interstitial Lung Disease and Pulmonary Fibrosis: A Practical Approach for General Medicine Physicians with Focus on the Medical History', *Journal of clinical medicine*, 7(12).
- Kalluri, R. (2016) 'The biology and function of fibroblasts in cancer', *Nature reviews. Cancer*, 16(9), pp. 582-598.
- Kavian, N., Marut, W., Servettaz, A., Nicco, C., Chreau, C., Lemarchal, H., Borderie, D., Dupin, N., Weill, B. and Batteux, F. (2012) 'Reactive oxygen species-mediated killing of activated fibroblasts by arsenic trioxide ameliorates fibrosis in a murine model of systemic sclerosis', *Arthritis and rheumatism*, 64(10), pp. 3430-3440.
- Kawata, K., Kubota, S., Eguchi, T., Aoyama, E., Moritani, N. H., Kondo, S., Nishida, T. and Takigawa, M. (2012) 'Role of LRP1 in transport of CCN2 protein in chondrocytes', *Journal of Cell Science*, 125(12), pp. 2965-2972.
- Keating, A. (2012) 'Mesenchymal Stromal Cells: New Directions', *Cell Stem Cell*, 10(6), pp. 709-716.
- Kendall, R. T. and Feghali-Bostwick, C. A. (2014) 'Fibroblasts in fibrosis: novel roles and mediators', *Frontiers in pharmacology*, 5.
- Khalil, N., O'Connor, R. N., Unruh, H. W., Warren, P. W., Flanders, K. C., Kemp, A., Berezney, O. H. and Greenberg, A. H. (1991) 'Increased production and immunohistochemical localization of transforming growth factor-beta in idiopathic pulmonary fibrosis', *American journal of respiratory cell and molecular biology*, 5(2), pp. 155-162.
- Khñ, R., Schwenk, F., Aguet, M. and Rajewsky, K. (1995) 'Inducible Gene Targeting in Mice', *Science*, 269(5229), pp. 1427-1429.
- Kia'i, N. and Bajaj, T. (2022) 'Histology, Respiratory Epithelium', *StatPearls*.
- Kim, H., Kim, M., Im, S.-K. and Fang, S. (2018) 'Mouse Cre-LoxP system: general principles to determine tissue-specific roles of target genes', *Laboratory animal research*, 34(4), p. 147.
- Kim, S. H., Turnbull, J. and Guimond, S. (2011) 'Extracellular matrix and cell signalling: the dynamic cooperation of integrin, proteoglycan and growth factor receptor', *Journal of Endocrinology*, 209(2), pp. 139-151.

- Kim, S. H., Turnbull, J. and Guimond, S. (2011) 'Extracellular matrix and cell signalling: the dynamic cooperation of integrin, proteoglycan and growth factor receptor', *Journal of Endocrinology*, 209(2), pp. 139-151.
- Kitani, A., Fuss, I., Nakamura, K., Kumaki, F., Usui, T. and Strober, W. (2003) 'Transforming Growth Factor (TGF)- β 1-producing Regulatory T Cells Induce Smad-mediated Interleukin 10 Secretion That Facilitates Coordinated Immunoregulatory Activity and Amelioration of TGF- β 1-mediated Fibrosis', *The Journal of Experimental Medicine*, 198(8), p. 1179.
- Kleinman, H. K., Philp, D. and Hoffman, M. P. (2003) 'Role of the extracellular matrix in morphogenesis', *Current Opinion in Biotechnology*, 14(5), pp. 526-532.
- Kottmann, R. M., Hogan, C. M., Phipps, R. P. and Sime, P. J. (2009) 'Determinants of initiation and progression of idiopathic pulmonary fibrosis', *Respirology*, 14(7), pp. 917-933.
- Kowal, R. C., Herz, J., Goldstein, J. L., Esser, V. and Brown, M. S. (1989) Low density lipoprotein receptor-related protein mediates uptake of cholesteryl esters derived from apoprotein E-enriched lipoproteins (fl-very low density lipoproteins/chylomicrons/familial hypercholesterolemia/cell-surface receptors/lysosomal hydrolysis).
- Kuure, S., Vuolteenaho, R. and Vainio, S. (2000) 'Kidney morphogenesis: cellular and molecular regulation', *Mechanisms of Development*, 92(1), pp. 31-45.
- Lakatos, H. F., Burgess, H. A., Thatcher, T. H., Redonnet, M. R., Hernady, E., Williams, J. P. and Sime, P. J. (2006) 'Oropharyngeal aspiration of a silica suspension produces a superior model of silicosis in the mouse when compared to intratracheal instillation', *Experimental lung research*, 32(5), pp. 181-199.
- Lambrecht, B. N. (2006) 'Alveolar macrophage in the driver's seat', *Immunity*, 24(4), pp. 366-368.
- Lechner, A. J., Driver, I. H., Lee, J., Conroy, C. M., Nagle, A., Locksley, R. M. and Rock, J. R. (2017) 'Recruited Monocytes and Type 2 Immunity Promote Lung Regeneration following Pneumonectomy', *Cell Stem Cell*, 21(1), pp. 120-134.e7.

Lee, J. K., Lee, J., Kim, S., Kim, S., Youk, J., Park, S., An, Y., Keam, B., Kim, D. W., Heo, D. S., Kim, Y. T., Kim, J. S., Kim, S. H., Lee, J. S., Lee, S. H., Park, K., Ku, J. L., Jeon, Y. K., Chung, D. H., Park, P. J., Kim, J., Kim, T. M. and Ju, Y. S. (2017) 'Clonal History & genetic predictors of transformation into small-cell carcinomas from lung adenocarcinomas', *Journal of Clinical Oncology*, 35(26), pp. 3065-3074.

Leslie, P. L., Franklin, D. A., Liu, Y. and Zhang, Y. (2018) 'p53 Regulates the Expression of LRP1 and Apoptosis through a Stress Intensity-Dependent MicroRNA Feedback Loop', *Cell Reports*, 24(6), pp. 1484-1495.

Letterio, J. J. and Roberts, A. B. (1998) 'REGULATION OF IMMUNE RESPONSES BY TGF- β ', *Annual Review of Immunology*, 16(1), pp. 137-161.

Li, W.-J., Xu, C., Wang, K., Li, T.-Y., Wang, X.-N., Yang, H., Xing, T., Li, W.-X., Chen, Y.-H., Gao, H. and Ding, L. (2018) 'Severe Intestinal Inflammation in the Small Intestine of Mice Induced by Controllable Deletion of Claudin-7', *Digestive Diseases and Sciences*, 63(5), pp. 1200-1209.

Li, Y., Liu, Y., Peng, X., Liu, W., Zhao, F., Feng, D., Han, J., Huang, Y., Luo, S., Li, L., Yue, S. J., Cheng, Q., Huang, X. and Luo, Z. (2015) 'NMDA Receptor Antagonist Attenuates Bleomycin-Induced Acute Lung Injury', *{PLOS} {ONE}*, 10(5), p. e0125873.

Lillis, A. P., Duyn, L. B. V., Murphy-Ullrich, J. E. and Strickland, D. K. (2008) 'LDL Receptor-Related Protein 1: Unique Tissue-Specific Functions Revealed by Selective Gene Knockout Studies', *Physiological Reviews*, 88(3), pp. 887-918.

Lillis, A. P., Mikhailenko, I. and Strickland D., K. (2005) 'Beyond endocytosis: LRP function in cell migration, proliferation and vascular permeability', *Journal of Thrombosis and Haemostasis*, 3(8), pp. 1884-1893.

Lillis, A. P., Muratoglu, S. C., Au, D. T., Migliorini, M., Lee, M.-J., Fried, S. K., Mikhailenko, I. and Strickland, D. K. (2015) 'LDL Receptor-Related Protein-1 (LRP1) Regulates Cholesterol Accumulation in Macrophages', *{PLOS} {ONE}*, 10(6), p. e0128903.

Lillis, A. P. and van Duyn, L. B. (2008) 'LRP tissue-specific knockout studies', *Physiol Rev*, 88, pp. 887-918.

Limjunyawong, N., Mitzner, W. and Horton, M. R. (2014) 'A mouse model of chronic idiopathic pulmonary fibrosis', *Physiological Reports*, 2(2), p. e00249.

Lin, L., Bu, G., Mars, W. M., Reeves, W. B., Tanaka, S. and Hu, K. (2010) 'TPA activates LDL receptor-related protein 1-mediated mitogenic signaling involving the p90RSK and GSK3 pathway', *American Journal of Pathology*, 177(4), pp. 1687-1696.

Lin, L. and Hu, K. (2014) 'LRP-1: Functions, Signaling and Implications in Kidney and Other Diseases', *International Journal of Molecular Sciences*, 15(12), pp. 22887-22901.

Lindenschmidt, R. C., Tryka, A. F., Goad, M. E. and Witschi, H. P. (1986) 'The effects of dietary butylated hydroxytoluene on liver and colon tumor development in mice', *Toxicology*, 38(2), pp. 151-160.

Liu, A.-r., Liu, L., Chen, S., Yang, Y., Zhao, H.-j., Liu, L., Guo, F.-m., Lu, X.-m. and Qiu, H.-b. (2013) 'Activation of canonical wnt pathway promotes differentiation of mouse bone marrow-derived MSCs into type II alveolar epithelial cells, confers resistance to oxidative stress, and promotes their migration to injured lung tissue in vitro', *Journal of Cellular Physiology*, 228(6), pp. 1270-1283.

Liu, B., Bing, Q., Li, S., Han, B., Lu, J., Baiyun, R., Zhang, X., Lv, Y., Wu, H. and Zhang, Z. (2019) 'Role of A2B adenosine receptor-dependent adenosine signaling in multi-walled carbon nanotube-triggered lung fibrosis in mice', *Journal of Nanobiotechnology*, 17(1).

Liu, C.-C., Hu, J., Tsai, C.-W., Yue, M., Melrose, H. L., Kanekiyo, T. and Bu, G. (2015) 'Neuronal LRP1 Regulates Glucose Metabolism and Insulin Signaling in the Brain', *Journal of Neuroscience*, 35(14), pp. 5851-5859.

Liu, M., Shan, M., Zhang, Y. and Guo, Z. (2021) 'Progranulin Protects Against Airway Remodeling Through the Modulation of Autophagy via HMGB1 Suppression in House Dust Mite-Induced Chronic Asthma', *Journal of Inflammation Research*, Volume 14, pp. 3891-3904.

- Liu, Q., Zhang, J., Tran, H., Verbeek, M. M., Reiss, K., Estus, S. and Bu, G. (2009) 'LRP1 shedding in human brain: roles of ADAM10 and ADAM17', *Molecular Neurodegeneration*, 4(1).
- Liu, Q., Zhang, J., Zerbinatti, C., Zhan, Y., Kolber, B. J., Herz, J., Muglia, L. J. and Bu, G. (2011) 'Lipoprotein Receptor LRP1 Regulates Leptin Signaling and Energy Homeostasis in the Adult Central Nervous System', *PLoS Biology*, 9(1), p. 1000575.
- Loukinova, E., Ranganathan, S., Kuznetsov, S., Gorlatova, N., Migliorini, M. M., Loukinov, D., Ulery, P. G., Mikhailenko, I., Lawrence, D. A. and Strickland, D. K. (2002) 'Platelet-derived growth factor (PDGF)-induced tyrosine phosphorylation of the low density lipoprotein receptor-related protein (LRP). Evidence for integrated co-receptor function between LRP and the PDGF', *Journal of Biological Chemistry*, 277(18), pp. 15499-15506.
- Maher, T. M., Bendstrup, E., Dron, L., Langley, J., Smith, G., Khalid, J. M., Patel, H. and Kreuter, M. (2020) 'Global incidence and prevalence of idiopathic pulmonary fibrosis', *Respir Res*, 22, p. 197.
- Maher, T. M., Bendstrup, E., Dron, L., Langley, J., Smith, G., Khalid, J. M., Patel, H. and Kreuter, M. (2021) 'Global incidence and prevalence of idiopathic pulmonary fibrosis', *Respiratory Research*, 22(1), pp. 1-10.
- Maher, T. M., Gat, M., Allen, D., Devaraj, A., Wells, A. U. and Geddes, D. M. (2008) 'Reproducibility of dynamically represented acoustic lung images from healthy individuals', *Thorax*, 63(6), pp. 542-548.
- Mantuano, E., Azmoon, P., Banki, M. A., Lam, M. S., Sigurdson, C. J. and Gonias, S. L. (2020) 'A soluble derivative of PrPC activates cell-signaling and regulates cell physiology through LRP1 and the NMDA receptor', *The Journal of biological chemistry*, 295(41), pp. 14178-14188.
- Mantuano, E., Lam, M. S. and Gonias, S. L. (2013) 'LRP1 assembles unique co-receptor systems to initiate cell signaling in response to tissue-type plasminogen activator and Myelin-associated glycoprotein', *Journal of Biological Chemistry*, 288(47), pp. 34009-34018.
- Marakasova, E., Olivares, P., Karnaukhova, E., Chun, H., Hernandez, N. E., Kurasawa, J. H., Hassink, G. U., Shestopal, S. A., Strickland, D. K. and Sarafanov, A. G. (2021) 'Molecular chaperone RAP interacts with LRP1 in a dynamic bivalent mode and enhances folding of ligand-binding regions of

other LDLR family receptors', *Journal of Biological Chemistry*, 297(1), p. 100842.

Marriott, S., Baskir, R. S., Gaskill, C., Menon, S., Carrier, E. J., Williams, J., Talati, M., Helm, K., Alford, C. E., Kropski, J. A., Loyd, J., Wheeler, L., Johnson, J., Austin, E., Nozik-Grayck, E., Meyrick, B., West, J. D., Klemm, D. J. and Majka, S. M. (2014) 'Cellular Mechanisms of Tissue Fibrosis: ABCG2pos lung mesenchymal stem cells are a novel pericyte subpopulation that contributes to fibrotic remodeling', *American Journal of Physiology - Cell Physiology*, 307(8), p. C684.

Marsh, M. and McMahon, H. T. (1999) 'The structural era of endocytosis', *Science*, 285(5425), pp. 215-220.

May, P., Rohlmann, A., Bock, H. H., Zurhove, K., Marth, J. D., Schomburg, E. D., Noebels, J. L., Beffert, U., Sweatt, J. D., Weeber, E. J. and Herz, J. (2004) 'Neuronal LRP1 Functionally Associates with Postsynaptic Proteins and Is Required for Normal Motor Function in Mice', *Molecular and Cellular Biology*, 24(20), p. 8872.

Mayor, S. and Pagano, R. E. (2007) 'Pathways of clathrin-independent endocytosis', *Nature Reviews Molecular Cell Biology*, 8(8), pp. 603-612.

McLellan, M. A., Rosenthal, N. A. and Pinto, A. R. (2017) 'Cre-loxP-Mediated Recombination: General Principles and Experimental Considerations', *Current Protocols in Mouse Biology*, 7(1), pp. 1-12.

Metzger, D. and Chambon, P. (2001) 'Site- and Time-Specific Gene Targeting in the Mouse', *Methods*, 24(1), pp. 71-80.

Moore, B. B., Lawson, W. E., Oury, T. D., Sisson, T. H., Raghavendran, K. and Hogaboam, C. M. (2013) 'Animal Models of Fibrotic Lung Disease', *American Journal of Respiratory Cell and Molecular Biology*, 49(2), pp. 167-179.

Mouratis, M. A. and Aidinis, V. (2011) 'Modeling pulmonary fibrosis with bleomycin', *Current opinion in pulmonary medicine*, 17(5), pp. 355-361.

Mueller, M. M. and Fusenig, N. E. (2004) 'Friends or foes — bipolar effects of the tumour stroma in cancer', *Nature Reviews Cancer* 2004 4:11, 4(11), pp. 839-849.

Mueller, P. A., Zhu, L., Tavori, H., Huynh, K., Stafford, J. M., Linton, M. F., Fazio, S. and Health, O. (2019) 'Deletion of Macrophage Low-Density Lipoprotein Receptor- Related Protein 1 (LRP1) Accelerates Atherosclerosis Regression and Increases CCR7 Expression in Plaque Macrophages', 138(17), pp. 1850-1863.

Myklebost, O., Arheden, K., Rogne, S., van Kessel, A. G., Mandahl, N., Herz, J., Stanley, K., Heim, S. and Mitelman, F. (1989) 'The gene for the human putative apoE receptor is on chromosome 12 in the segment q13-14', *Genomics*, 5(1), pp. 65-69.

Nagy, A. (2000) 'Cre Recombinase: The Universal Reagent for Genome Tailoring'.

Nakajima, C., Haffner, P., Goerke, S. M., Zurhove, K., Adelmann, G., Frotscher, M., Herz, J., Bock, H. H. and May, P. (2014) 'The lipoprotein receptor LRP1 modulates sphingosine-1-phosphate signaling and is essential for vascular development', *Development (Cambridge)*, 141(23), pp. 4513-4525.

Nakayama, Y., Igarashi, A., Kikuchi, I., Obata, Y., Fukumoto, Y. and Yamaguchi, N. (2009) 'Bleomycin-induced over-replication involves sustained inhibition of mitotic entry through the ATM/ATR pathway', *Experimental Cell Research*, 315(15), pp. 2515-2528.

Nalysnyk, L., Cid-Ruzafa, J., Rotella, P. and Esser, D. (2012) 'Incidence and prevalence of idiopathic pulmonary fibrosis: review of the literature', *European Respiratory Review*, 21(126), pp. 355-361.

Nomellini, V. and Chen, H. (2012) 'Murray and Nadel's Textbook of Respiratory Medicine | Murray and Nadel's Textbook of Respiratory Medicine, 5th Edition, Publisher: Saunders Elsevier. ISBN-13: 978-1416047100. 2400 pp, hardcover', *Journal of Surgical Research*, 173(1), p. 45.

Onursal, C., Dick, E., Angelidis, I., Schiller, H. B. and Staab-Weijnitz, C. A. (2021) 'Collagen Biosynthesis, Processing, and Maturation in Lung Ageing', *Frontiers in Medicine*, 8.

O'Toole, T. E., Katagiri, Y., Faull, R. J., Peter, K., Tamura, R., Quaranta, V., Loftus, J. C., Shattil, S. J. and Ginsberg, M. H. (1994) 'Integrin

cytoplasmic domains mediate inside-out signal transduction', *Journal of Cell Biology*, 124(6), pp. 1047-1059.

Ottani, V., Martini, D., Franchi, M., Ruggeri, A. and Raspanti, M. (2002) 'Hierarchical structures in fibrillar collagens', *Micron*, 33(7-8), pp. 587-596.

Paun, A. and Haston, C. K. (2012) 'Genomic and genome-wide association of susceptibility to radiation-induced fibrotic lung disease in mice', *Radiotherapy and Oncology*, 105(3), pp. 350-357.

Pechkovsky, D. V., Prasse, A., Kollert, F., Engel, K. M. Y., Dentler, J., Luttmann, W., Friedrich, K., Mller-Quernheim, J. and Zissel, G. (2010) 'Alternatively activated alveolar macrophages in pulmonary fibrosis-mediator production and intracellular signal transduction', *Clinical immunology (Orlando, Fla.)*, 137(1), pp. 89-101.

Petrova, R. and Joyner, A. L. (2014) 'Roles for Hedgehog signaling in adult organ homeostasis and repair', *Development*, 141(18), pp. 3445-3457.

Pflanzner, T., Janko, M. C., Andr-Dohmen, B., Reuss, S., Weggen, S., Roebroek, A. J. M., Kuhlmann, C. R. W. and Pietrzik, C. U. (2011) 'LRP1 mediates bidirectional transcytosis of amyloid- β across the blood-brain barrier', *Neurobiology of Aging*, 32(12), pp. 2323.e1-2323.e11.

Pieper, J. S., Van Der Kraan, P. M., Hafmans, T., Kamp, J., Buma, P., Van Susante, J. L. C., Van Den Berg, W. B., Veerkamp, J. H. and Van Kuppevelt, T. H. (2002) 'Crosslinked type II collagen matrices: preparation, characterization, and potential for cartilage engineering', *Biomaterials*, 23(15), pp. 3183-3192.

Piera-Velazquez, S., Li, Z. and Jimenez, S. A. (2011) 'Role of endothelial-mesenchymal transition (EndoMT) in the pathogenesis of fibrotic disorders', *The American journal of pathology*, 179(3), pp. 1074-1080.

Pirruccello, J. P., Chaffin, M. D., Chou, E. L., Fleming, S. J., Lin, H., Nekoui, M., Khurshid, S., Friedman, S. F., Bick, A. G., Arduini, A., Weng, L.-C., Choi, S. H., Akkad, A.-D., Batra, P., Tucker, N. R., Hall, A. W., Roselli, C., Benjamin, E. J., Vellarikkal, S. K., Gupta, R. M., Stegmann, C. M., Juric, D., Stone, J. R., Vasan, R. S., Ho, J. E., Hoffmann, U., Lubitz, S. A., Philippakis, A. A., Lindsay, M. E. and Ellinor, P. T. (2021) 'Deep learning enables genetic analysis of the human thoracic aorta', *Nature Genetics*, 54(1), pp. 40-51.

Ponticos, M., Holmes, A. M., Shi-Wen, X., Leoni, P., Khan, K., Rajkumar, V. S., Hoyles, R. K., Bou-Gharios, G., Black, C. M., Denton, C. P., Abraham, D. J., Leask, A. and Lindahl, G. E. (2009) 'Pivotal role of connective tissue growth factor in lung fibrosis: MAPK-dependent transcriptional activation of type I collagen', *Arthritis & Rheumatism*, 60(7), pp. 2142-2155.

Poole, J. J. A. and Mostao-guidolin, L. B. (2021) 'Optical Microscopy and the Extracellular Matrix Structure: A Review', *Cells* 2021, Vol. 10, Page 1760, 10(7), p. 1760.

Quaderi, S. A. and Hurst, J. R. (2018) 'The unmet global burden of COPD', *Global health, epidemiology and genomics*, 3.

Quinn, K. A., Grimsley, P. G., Dai, Y. P., Tapner, M., Chesterman, C. N. and Owensby, D. A. (1997) 'Soluble low density lipoprotein receptor-related protein (LRP) circulates in human plasma', *The Journal of biological chemistry*, 272(38), pp. 23946-51.

Quinn, K. A., Pye, V. J., Dai, Y.-P., Chesterman, C. N. and Owensby, D. A. (1999) Characterization of the Soluble Form of the Low Density Lipoprotein Receptor-Related Protein (LRP). [Online]. Available at: <http://www.idealibrary.com>.

Radotra, B., McCormick, D. and Crockard, A. (1994) 'CD44 plays a role in adhesive interactions between glioma cells and extracellular matrix components', *Neuropathology and Applied Neurobiology*, 20(4), pp. 399-405.

Rafii, S., Cao, Z., Lis, R., Siempos, I. I., Chavez, D., Shido, K., Rabbany, S. Y. and Ding, B.-S. (2015) 'Platelet-derived SDF-1 primes the pulmonary capillary vascular niche to drive lung alveolar regeneration'.

Raghu, G., Collard, H. R., Egan, J. J., Martinez, F. J., Behr, J., Brown, K. K., Colby, T. V., Cordier, J. F., Flaherty, K. R., Lasky, J. A., Lynch, D. A., Ryu, J. H., Swigris, J. J., Wells, A. U., Ancochea, J., Bouros, D., Carvalho, C., Costabel, U., Ebina, M., Hansell, D. M., Johkoh, T., Kim, D. S., King, T. E., Kondoh, Y., Myers, J., Miller, N. L., Nicholson, A. G., Richeldi, L., Selman, M., Dudden, R. F., Griss, B. S., Protzko, S. L. and Schnemann, H. J. (2011) 'An official ATS/ERS/JRS/ALAT statement: idiopathic pulmonary fibrosis: evidence-based guidelines for diagnosis and management',

American journal of respiratory and critical care medicine, 183(6), pp. 788-824.

Rasmussen, D. L. and Pfau, J. C. (2011) 'Asbestos activates CH12.LX B-lymphocytes via macrophage signaling', *Journal of Immunotoxicology*, 9(2), pp. 129-140.

Reinert, T., Serodio Da, C., Baldotto, R., Arthur, F., Nunes, P., Alves, A. and Scheliga, S. (2013) 'Bleomycin-Induced Lung Injury', *Journal of Cancer Research*, 2013.

Rennard, S. I. and Vestbo, J. (2006) 'COPD: the dangerous underestimate of 15%', *Lancet*, 367(9518), pp. 1216-1219.

Reyfman, P. A., Walter, J. M., Joshi, N., Anekalla, K. R., McQuattie-Pimentel, A. C., Chiu, S., Fernandez, R., Akbarpour, M., Chen, C.-I., Ren, Z., Verma, R., Abdala-Valencia, H., Nam, K., Chi, M., Han, S., Gonzalez-Gonzalez, F. J., Soberanes, S., Watanabe, S., Williams, K. J. N., Flozak, A. S., Nicholson, T. T., Morgan, V. K., Winter, D. R., Hinchcliff, M., Hrusch, C. L., Guzy, R. D., Bonham, C. A., Sperling, A. I., Bag, R., Hamanaka, R. B., Mutlu, G. M., Yeldandi, A. V., Marshall, S. A., Shilatifard, A., Amaral, L. A. N., Perlman, H., Sznajder, J. I., Argento, A. C., Gillespie, C. T., Dematte, J., Jain, M., Singer, B. D., Ridge, K. M., Lam, A. P., Bharat, A., Bhorade, S. M., Gottardi, C. J., Budinger, G. R. S. and Misharin, A. V. (2019) 'Single-Cell Transcriptomic Analysis of Human Lung Provides Insights into the Pathobiology of Pulmonary Fibrosis', *American Journal of Respiratory and Critical Care Medicine*, 199(12), pp. 1517-1536.

Ricard-Blum, S. (2011) 'The Collagen Family', *Cold Spring Harbor Perspectives in Biology*, 3(1), pp. 1-19.

Richeldi, L., Collard, H. R. and Jones, M. G. (2017) 'Idiopathic pulmonary fibrosis', *Lancet (London, England)*, 389(10082), pp. 1941-1952.

Ritti, L. (2017) 'Method for Picrosirius Red-Polarization Detection of Collagen Fibers in Tissue Sections', *Methods in Molecular Biology*, 1627, pp. 395-407.

Rnnov-Jessen, L. and Petersen, O. W. (1996) 'A function for filamentous alpha-smooth muscle actin: retardation of motility in fibroblasts', *Journal of Cell Biology*, 134(1), pp. 67-80.

Rock, J. R. and Hogan, B. L. M. (2011) 'Epithelial progenitor cells in lung development, maintenance, repair, and disease', *Annual review of cell and developmental biology*, 27, pp. 493-512.

Rohlfmann, A., Gotthardt, M., Willnow, T. E., Hammer, R. E. and Herz, J. (1996) 'Sustained somatic gene inactivation by viral transfer of Cre recombinase', *Nature biotechnology*, 14(11), pp. 1562-1565.

Royce, S. G., Cheng, V., Samuel, C. S. and Tang, M. L. K. (2012) 'The regulation of fibrosis in airway remodeling in asthma', *Molecular and Cellular Endocrinology*, 351(2), pp. 167-175.

Sakaue, S., Kanai, M., Tanigawa, Y., Karjalainen, J., Kurki, M., Koshiba, S., Narita, A., Konuma, T., Yamamoto, K., Akiyama, M., Ishigaki, K., Suzuki, A., Suzuki, K., Obara, W., Yamaji, K., Takahashi, K., Asai, S., Takahashi, Y., Suzuki, T., Shinozaki, N., Yamaguchi, H., Minami, S., Murayama, S., Yoshimori, K., Nagayama, S., Obata, D., Higashiyama, M., Masumoto, A., Koretsune, Y., Ito, K., Terao, C., Yamauchi, T., Komuro, I., Kadowaki, T., Tamiya, G., Yamamoto, M., Nakamura, Y., Kubo, M., Murakami, Y., Yamamoto, K., Kamatani, Y., Palotie, A., Rivas, M. A., Daly, M. J., Matsuda, K. and Okada, Y. (2021) 'A cross-population atlas of genetic associations for 220 human phenotypes', *Nature Genetics*, 53(10), pp. 1415-1424.

Schaefer, L. (2010) 'Extracellular matrix molecules: endogenous danger signals as new drug targets in kidney diseases', *Current opinion in pharmacology*, 10(2), pp. 185-190.

Schfer, I., Kaisler, J., Scheller, A., Kirchhoff, F., Haghikia, A. and Faissner, A. (2019) 'Conditional Deletion of LRP1 Leads to Progressive Loss of Recombined NG2-Expressing Oligodendrocyte Precursor Cells in a Novel Mouse Model', *Cells* 2019, Vol. 8, Page 1550, 8(12), p. 1550.

Schwartz, M. A. (2010) 'Integrins and Extracellular Matrix in Mechanotransduction', *Cold Spring Harbor Perspectives in Biology*, 2(12), pp. a005066-a005066.

Scotton, C. J. and Chambers, R. C. (2007) 'Molecular Targets in Pulmonary Fibrosis', *Chest*, 132(4), pp. 1311-1321.

Scotton, C. J., Hayes, B., Alexander, R., Datta, A., Forty, E. J., Mercer, P. F., Blanchard, A. and Chambers, R. C. (2013) '\$\$\$Ex vivo\$\$/\$\$micro-

computed tomography analysis of bleomycin-induced lung fibrosis for preclinical drug evaluation', *European Respiratory Journal*, 42(6), pp. 1633-1645.

Selman, M. and Pardo, A. (2006) 'Role of epithelial cells in idiopathic pulmonary fibrosis: from innocent targets to serial killers', *Proceedings of the American Thoracic Society*, 3(4), pp. 364-372.

Selvais, C., D'Auria, L., Tyteca, D., Perrot, G., Lemoine, P., Troeberg, L., Dedieu, S., Nol, A. s., Nagase, H., Henriot, P., Courtoy, P. J., Marbaix, E. and Emonard, H. (2011) 'Cell cholesterol modulates metalloproteinase-dependent shedding of low-density lipoprotein receptor-related protein-1 (LRP-1) and clearance function', *The FASEB Journal*, 25(8), p. 2770.

Shackleton, B., Crawford, F. and Bachmeier, C. (2016) 'Inhibition of ADAM10 promotes the clearance of A β across the BBB by reducing LRP1 ectodomain shedding', *Fluids Barriers CNS*, 13, p. 14.

Shannon, J. M. and Hyatt, B. A. (2004) 'Epithelial-mesenchymal interactions in the developing lung', *Annual review of physiology*, 66, pp. 625-645.

Shifren, A., Witt, C., Christie, C. and Castro, M. (2012) 'Mechanisms of Remodeling in Asthmatic Airways', *Journal of Allergy*, 2012, p. 12.

Sobin, S. S., Fung, Y. C. and Tremmer, H. M. (1988) 'Collagen and elastin fibers in human pulmonary alveolar walls', *Journal of Applied Physiology*, 64(4), pp. 1659-1675.

Soriano, J. B., Kendrick, P. J., Paulson, K. R., Gupta, V., Abrams, E. M., Adedoyin, R. A., Adhikari, T. B., Advani, S. M., Agrawal, A., Ahmadian, E., Alahdab, F., Aljunid, S. M., Altirkawi, K. A., Alvis-Guzman, N., Anber, N. H., Andrei, C. L., Anjomshoa, M., Ansari, F., Ant, J. M., Arabloo, J., Athari, S. M., Athari, S. S., Awoke, N., Badawi, A., Banoub, J. A. M., Bennett, D. A., Bensenor, I. M., Berfield, K. S. S., Bernstein, R. S., Bhattacharyya, K., Bijani, A., Brauer, M., Bukhman, G., Butt, Z. A., Cmera, L. A., Car, J., Carrero, J. J., Carvalho, F., Castaeda-Orjuela, C. A., Choi, J.-Y. J., Christopher, D. J., Cohen, A. J., Dandona, L., Dandona, R., Dang, A. K., Daryani, A., de Courten, B., Demeke, F. M., Demoz, G. T., Neve, J.-W. D., Desai, R., Dharmaratne, S. D., Diaz, D., Douiri, A., Driscoll, T. R., Duken, E. E., Eftekhari, A., Elkout, H., Endries, A. Y., Fadhil, I., Faro, A., Farzadfar, F., Fernandes, E., Filip, I., Fischer, F., Foroutan, M., Garcia-Gordillo, M. A.,

Gebre, A. K., Gebremedhin, K. B., Gebremeskel, G. G., Gezae, K. E., Ghoshal, A. G., Gill, P. S., Gillum, R. F., Goudarzi, H., Guo, Y., Gupta, R., Hailu, G. B., Hasanzadeh, A., Hassen, H. Y., Hay, S. I., Hoang, C. L., Hole, M. K., Horita, N., Hosgood, H. D., Hostiuc, M., Househ, M., Ilesanmi, O. S., Ilic, M. D., Irvani, S. S. N., Islam, S. M. S., Jakovljevic, M., Jamal, A. A., Jha, R. P., Jonas, J. B., Kabir, Z., Kasaeian, A., Kasahun, G. G., Kassa, G. M., Kefale, A. T., et al. (2020) 'Prevalence and attributable health burden of chronic respiratory diseases, 1990-2017: a systematic analysis for the Global Burden of Disease Study 2017', *The Lancet Respiratory Medicine*, 8(6), pp. 585-596.

Stewart, G. A., Hoyne, G. F., Ahmad, S. A., Jarman, E., Wallace, W. A. H., Harrison, D. J., Haslett, C., Lamb, J. R. and Howie, S. E. M. (2003) 'Expression of the developmental Sonic hedgehog (Shh) signalling pathway is up-regulated in chronic lung fibrosis and the Shh receptor patched 1 is present in circulating T lymphocytes', *The Journal of Pathology*, 199(4), pp. 488-495.

Stockley, R. A. (1999) 'Neutrophils and protease/antiprotease imbalance', *American journal of respiratory and critical care medicine*, 160(5 Pt 2).

Stone, J. R. and Marietta, M. A. (1994) 'Soluble Guanylate Cyclase from Bovine Lung: Activation with Nitric Oxide and Carbon Monoxide and Spectral Characterization of the Ferrous and Ferric States', *Biochemistry*, 33, pp. 5636-5640.

Strickland, D. K., Gonias, S. L. and Argraves, W. S. (2002) 'Diverse roles for the LDL receptor family', *Trends in Endocrinology and Metabolism*, 13(2), pp. 66-74.

Strickland, J. H. and Dudley, K. (2001) 'LRP: a multifunctional scavenger and signaling receptor', *The Journal of Clinical Investigation*, 108(6).

Sugiyama, T., Kumagai, H., Morikawa, Y., Wada, Y., Sugiyama, A., Yasuda, K., Yokoi, N., Tamura, S., Kojima, T., Nosaka, T., Senba, E., Kimura, S., Kadowaki, T., Kodama, T. and Kitamura, T. (2000) 'A Novel Low-Density Lipoprotein Receptor-Related Protein Mediating Cellular Uptake of Apolipoprotein E-Enriched VLDL in Vitro', *Biochemistry*, 39(51), pp. 15817-15825.

Tam, A. Y. Y., Horwell, A. L., Trinder, S. L., Khan, K., Xu, S., Ong, V., Denton, C. P., Norman, J. T., Holmes, A. M., Bou-Gharios, G. and

- Abraham, D. J. (2021) 'Selective deletion of connective tissue growth factor attenuates experimentally-induced pulmonary fibrosis and pulmonary arterial hypertension', *The International Journal of Biochemistry & Cell Biology*, 134, p. 105961.
- Taskar, V. S. and Coultas, D. B. (2006) 'Is idiopathic pulmonary fibrosis an environmental disease?', *Proceedings of the American Thoracic Society*, 3(4), pp. 293-298.
- Thai, A. A., Solomon, B. J., Sequist, L. V., Gainor, J. F. and Heist, R. S. (2021) 'Lung cancer', *The Lancet*, 398(10299), pp. 535-554.
- Theocharis, A. D., Skandalis, S. S., Gialeli, C. and Karamanos, N. K. (2016) 'Extracellular matrix structure', *Advanced drug delivery reviews*, 97, pp. 4-27.
- Todd, N. W., Luzina, I. G. and Atamas, S. P. (2012) 'Molecular and cellular mechanisms of pulmonary fibrosis', *Fibrogenesis & tissue repair*, 5(1).
- Travaglini, K. J., Nabhan, A. N., Penland, L., Sinha, R., Gillich, A., Sit, R. V., Chang, S., Conley, S. D., Mori, Y., Seita, J., Berry, G. J., Shrager, J. B., Metzger, R. J., Kuo, C. S., Neff, N., Weissman, I. L., Quake, S. R. and Krasnow, M. A. (2020) 'A molecular cell atlas of the human lung from single-cell RNA sequencing', *Nature*, 587(7835), pp. 619-625.
- Travis, W. D., Brambilla, E., Nicholson, A. G., Yatabe, Y., Austin, J. H. M., Beasley, M. B., Chirieac, L. R., Dacic, S., Duhig, E., Flieder, D. B., Geisinger, K., Hirsch, F. R., Ishikawa, Y., Kerr, K. M., Noguchi, M., Pelosi, G., Powell, C. A., Tsao, M. S. and Wistuba, I. (2015) 'The 2015 World Health Organization Classification of Lung Tumors: Impact of Genetic, Clinical and Radiologic Advances Since the 2004 Classification', *Journal of thoracic oncology : official publication of the International Association for the Study of Lung Cancer*, 10(9), pp. 1243-1260.
- Tsukui, T., Sun, K.-H., Wetter, J. B., Wilson-Kanamori, J. R., Hazelwood, L. A., Henderson, N. C., Adams, T. S., Schupp, J. C., Poli, S. D., Rosas, I. O., Kaminski, N., Matthay, M. A., Wolters, P. J. and Sheppard, D. (2020) 'Collagen-producing lung cell atlas identifies multiple subsets with distinct localization and relevance to fibrosis', *Nature Communications*, 11(1).
- Umezawa, H., Ishizuka, M., Maeda, K. and Takeuchi, T. (1967) 'Studies on bleomycin', *Cancer*, 20(5), pp. 891-895.

- Van Der Geer, P. (2002) 'Phosphorylation of LRP1: Regulation of transport and signal transduction'. *may*. pp. 160-165.
- Van Der Weijden, G. A., Timmerman, M. F., Danser, M. M. and Van Der Velden, U. (1998) 'Relationship between the plaque removal efficacy of a manual toothbrush and brushing force', *J Clin Periodontol*, 25, pp. 413-416.
- van Huizen, N. A., van den Braak, R. R. J. C., Doukas, M., Dekker, L. J. M., IJzermans, J. N. M. and Luidert, T. M. (2019) 'Up-regulation of collagen proteins in colorectal liver metastasis compared with normal liver tissue', *Journal of Biological Chemistry*, 294(1), pp. 281-289.
- Van 't Hof, R. J., Rose, L., Bassonga, E. and Daroszewska, A. (2017) 'Open source software for semi-automated histomorphometry of bone resorption and formation parameters', *Bone*, 99, pp. 69-79.
- Viola, A., Munari, F., Sanchez-Rodriguez, R., Scolaro, T. and Castegna, A. (2019) 'The metabolic signature of macrophage responses', *Frontiers in Immunology*, 10(JULY), p. 1462.
- Walker, C., Mojares, E. and Del Ro Hernandez, A. (2018) 'Role of Extracellular Matrix in Development and Cancer Progression', *International journal of molecular sciences*, 19(10).
- Walters, D. M. and Kleeberger, S. R. (2008) 'Mouse Models of Bleomycin-Induced Pulmonary Fibrosis', *Current Protocols in Pharmacology*, 40(1).
- Walton, K. L., Johnson, K. E. and Harrison, C. A. (2017) 'Targeting TGF- β Mediated SMAD Signaling for the Prevention of Fibrosis', *Frontiers in Pharmacology*, 8.
- Wang, C., Wang, X., Chi, C., Guo, L., Guo, L., Zhao, N., Wang, W., Pi, X., Sun, B., Lian, A., Shi, J. and Li, E. (2016) 'Lung ventilation strategies for acute respiratory distress syndrome: a systematic review and network meta-analysis', *Scientific reports*, 6.
- Wang, Z., Gerstein, M. and Snyder, M. (2009) 'RNA-Seq: a revolutionary tool for transcriptomics', *Nature Reviews Genetics*, 10(1), pp. 57-63.
- Weibel, E. R. (2015) 'On the tricks alveolar epithelial cells play to make a good lung', *American Journal of Respiratory and Critical Care Medicine*, 191(5), pp. 504-513.

Whitsett, J. A. and Alenghat, T. (2015) 'Respiratory epithelial cells orchestrate pulmonary innate immunity', *NATURE IMMUNOLOGY* VOLUME, 16.

Wight, T. N. and Potter-Perigo, S. (2011) 'The extracellular matrix: an active or passive player in fibrosis?', *American journal of physiology. Gastrointestinal and liver physiology*, 301(6).

Wilk, J. B., Djousse, L., Arnett, D. K., Rich, S. S., Province, M. A., Hunt, S. C., Crapo, R. O., Higgins, M. and Myers, R. H. (2000) 'Evidence for major genes influencing pulmonary function in the NHLBI Family Heart Study', *Genetic Epidemiology*, 19(1), pp. 81-94.

Williams, D. L., Ha, T., Li, C., Kalbfleisch, J. H., Schweitzer, J., Vogt, W. and Browder, I. W. (2003) 'Modulation of tissue Toll-like receptor 2 and 4 during the early phases of polymicrobial sepsis correlates with mortality', *Critical Care Medicine*, 31(6), pp. 1808-1818.

Williamson, J. D., Sadofsky, L. R. and Hart, S. P. (2015) 'The pathogenesis of bleomycin-induced lung injury in animals and its applicability to human idiopathic pulmonary fibrosis', *Experimental lung research*, 41(2), pp. 57-73.

Willis, B. C., Liebler, J. M., Luby-Phelps, K., Nicholson, A. G., Crandall, E. D., du Bois, R. M. and Borok, Z. (2005) 'Induction of Epithelial-Mesenchymal Transition in Alveolar Epithelial Cells by Transforming Growth Factor- β 1', *The American Journal of Pathology*, 166(5), pp. 1321-1332.

Willnow, T. E., Armstrong, S. A., HAMMERT, R. E., Herz, J., Goldstein, J. L., Rosahl, b. T. and Siidhof Howard, T. C. (1995) Functional expression of low density lipoprotein receptor-related protein is controlled by receptor-associated protein in vivo. [Online]. Available at: <https://www.pnas.org/content/pnas/92/10/4537.full.pdf>.

Willnow, T. E. and Herz, J. (1994) 'Genetic deficiency in low density lipoprotein receptor-related protein confers cellular resistance to Pseudomonas exotoxin A - Evidence that this protein is required for uptake and degradation of multiple ligands', *Journal of Cell Science*, 107(3), pp. 719-726.

- Wilson, M. S. and Wynn, T. A. (2009) 'Pulmonary fibrosis: pathogenesis, etiology and regulation', *Mucosal Immunology*, 2(2), pp. 103-121.
- Winkler, J., Abisoye-Ogunniyan, A., Metcalf, K. J. and Werb, Z. (2020) 'Concepts of extracellular matrix remodelling in tumour progression and metastasis', *Nature Communications* 2020 11:1, 11(1), pp. 1-19.
- Wirtz, H. R. and Dobbs, L. G. (2000) 'The effects of mechanical forces on lung functions', *Respiration Physiology*, 119(1), pp. 1-17.
- Wollin, L., Maillet, I., Quesniaux, V., Holweg, A. and Ryffel, B. (2014) 'Antifibrotic and Anti-inflammatory Activity of the Tyrosine Kinase Inhibitor Nintedanib in Experimental Models of Lung Fibrosis', *Journal of Pharmacology and Experimental Therapeutics*, 349(2), pp. 209-220.
- Wolters, P. J., Collard, H. R. and Jones, K. D. (2014) 'Pathogenesis of Idiopathic Pulmonary Fibrosis', *Annual Review of Pathology: Mechanisms of Disease*, 9(1), pp. 157-179.
- Won, J. H., Choi, J. S. and Jun, J.-I. (2022) 'CCN1 interacts with integrins to regulate intestinal stem cell proliferation and differentiation', *Nature Communications*, 13(1).
- Wu, A. and Song, H. (2020) 'Regulation of alveolar type 2 stem/progenitor cells in lung injury and regeneration', *Acta biochimica et biophysica Sinica*, 52(7), pp. 716-722.
- Wu, L. and Gonias, S. L. (2005) 'The low-density lipoprotein receptor-related protein-1 associates transiently with lipid rafts', *Journal of Cellular Biochemistry*, 96(5), pp. 1021-1033.
- Wygrecka, M., Wilhelm, J., Jablonska, E., Zakrzewicz, D., Preissner, K. T., Seeger, W., Guenther, A. and Markart, P. (2011) 'Shedding of low-density lipoprotein receptor-related protein-1 in acute respiratory distress syndrome', *American Journal of Respiratory and Critical Care Medicine*, 184(4), pp. 438-448.
- Wynn, T. A. and Barron, L. (2010) 'Macrophages: Master regulators of inflammation and fibrosis', *Seminars in Liver Disease*, 30(3), pp. 245-257.
- Xue, J., Schmidt, S. V., Sander, J., Draffehn, A., Krebs, W., Quester, I., DeNardo, D., Gohel, T. D., Emde, M., Schmidleithner, L., Ganesan, H., Nino-Castro, A., Mallmann, M. R., Labzin, L., Theis, H., Kraut, M., Beyer,

- M., Latz, E., Freeman, T. C., Ulas, T. and Schultze, J. L. (2014) 'Transcriptome-based network analysis reveals a spectrum model of human macrophage activation', *Immunity*, 40(2), pp. 274-288.
- Yamamoto, K., Owen, K., Parker, A. E., Scilabra, S. D., Dudhia, J., Strickland, D. K., Troeberg, L. and Nagase, H. (2014) 'Low Density Lipoprotein Receptor-related Protein 1 (LRP1)-mediated Endocytic Clearance of a Disintegrin and Metalloproteinase with Thrombospondin Motifs-4 (ADAMTS-4)', *Journal of Biological Chemistry*, 289(10), pp. 6462-6474.
- Yamamoto, K., Santamaria, S., Botkjaer, K. A., Dudhia, J., Troeberg, L., Itoh, Y., Murphy, G. and Nagase, H. (2017) 'Inhibition of Shedding of Low-Density Lipoprotein Receptor-Related Protein 1 Reverses Cartilage Matrix Degradation in Osteoarthritis', *Arthritis & rheumatology (Hoboken, N.J.)*, 69(6), pp. 1246-1256.
- Yamamoto, K., Scavenius, C., Meschis, M. M., Gremida, A. M. E., Mogensen, E. H., Thgersen, I. B., Bonelli, S., Scilabra, S. D., Jensen, A., Santamaria, S., Ahnström, J., Bou-Gharios, G., Enghild, J. J. and Nagase, H. (2022) 'A top-down approach to uncover the hidden ligandome of low-density lipoprotein receptor-related protein 1 in cartilage', *Matrix Biology*, 112, pp. 190-218.
- Yamine, S., Schmidt, A., Sutter, O., Fouzas, S., Singer, F., Frey, U. and Latzin, P. (2015) 'Functional evidence for continued alveolarisation in former preterms at school age?', *European Respiratory Journal*, 47(1), pp. 147-155.
- Yan, D. and Lin, X. (2009) 'Shaping morphogen gradients by proteoglycans', *Cold Spring Harbor perspectives in biology*, 1(3).
- Yoshimura, T., Kawano, Y., Arimura, N., Kawabata, S., Kikuchi, A. and Kaibuchi, K. (2005) 'GSK-3 β regulates phosphorylation of CRMP-2 and neuronal polarity', *Cell*, 120(1), pp. 137-149.
- Yue, X., Shan, B. and Lasky, J. A. (2010) 'TGF- β : Titan of Lung Fibrogenesis', *Current enzyme inhibition*, 6(2).
- Zakrzewicz, A., Kouri, F. M., Nejman, B., Kwapiszewska, G., Hecker, M., Sandu, R., Dony, E., Seeger, W., Schermuly, R. T., Eickelberg, O. and Morty, R. E. (2007) 'The transforming growth factor- β /Smad2,3 signalling

axis is impaired in experimental pulmonary hypertension', *European Respiratory Journal*, 29(6), pp. 1094-1104.

Zepp, J. A., Zacharias, W. J., Frank, D. B., Cavanaugh, C. A., Zhou, S., Morley, M. P. and Morrisey, E. E. (2017) 'Distinct Mesenchymal Lineages and Niches Promote Epithelial Self-Renewal and Myofibrogenesis in the Lung', *Cell*, 170(6), pp. 1134-1148.e10.

Zhang, D. and Newton, C. A. (2021) 'Familial Pulmonary Fibrosis', *Chest*, 160(5), pp. 1764-1773.

Zhao, J., Zhao, J. and Perlman, S. (2010) 'T Cell Responses Are Required for Protection from Clinical Disease and for Virus Clearance in Severe Acute Respiratory Syndrome Coronavirus-Infected Mice', *Journal of Virology*, 84(18), pp. 9318-9325.

Zilberberg, A., Yaniv, A. and Gazit, A. (2004) 'The Low Density Lipoprotein Receptor-1, LRP1, Interacts with the Human Frizzled-1 (HFz1) and Down-regulates the Canonical Wnt Signaling Pathway', *Journal of Biological Chemistry*, 279(17), pp. 17535-17542.

Zuo, F., Kaminski, N., Eugui, E., Allard, J., Yakhini, Z., Ben-Dor, A., Lollini, L., Morris, D., Kim, Y., DeLustro, B., Sheppard, D., Pardo, A., Selman, M. and Heller, R. A. (2002) 'Gene expression analysis reveals matrilysin as a key regulator of pulmonary fibrosis in mice and humans', *Proceedings of the National Academy of Sciences*, 99(9), pp. 6292-6297.

Zurhove, K., Nakajima, C., Herz, J., Bock, H. H. and May, P. (2008) 'S-Secretase Limits the Inflammatory Response Through the Processing of LRP1', *Science Signaling*, 1(47).